UNIVERSITY of RWANDA

DOCTORAL THESIS

Linear and Non-linear Waves in Multispecies Plasmas

by Mushinzimana Xavier

2022

UNIVERSITY of RWANDA

COLLEGE OF SCIENCE AND TECHNOLOGY

LINEAR AND NONLINEAR WAVES IN MULTISPECIES PLASMAS

Submitted by

Mushinzimana Xavier

Reg. number: 218014522

In fulfillment of the requirements of the degree of
Doctor of Philosophy in Physics,
School of Science,
College of Science and Technology,
University of Rwanda.

Supervisors:

Assoc. Prof. Lakhan Lal Yadav

Dr François Nsengiyumva

Kigali, July 2022

Dedication

Dedicated to my family ...

Declaration

I, Mushinzimana Xavier,
declare that the thesis entitled **Linear and nonlinear waves in multispecies plasmas** and submitted for the degree of Doctor of Philosophy to University of Rwanda is the result of my own work under supervision of Assoc. Prof. Lakhan Lal Yadav (Department of Mathematics,Science and Physical Education, University of Rwanda-College of Education, Rwanda) and Dr François Nsengiyumva (Civil Engineering department, Institut d'Enseignement Superieur de Ruhengeri, Rwanda). The work is original and has not been submitted for any other degree at UR or any other institution.

Wherever necessary other person's works have been acknowledged and appropriately cited in the text and referenced in the bibliography.

Mushinzimana Xavier

Assoc. Prof. Lakhan Lal Yadav

Dr François Nsengiyumva

Publications

Results in this thesis have been published and the publication references are following:

X. Mushinzimana, F. Nsengiyumva, L. L. Yadav and T. K. Baluku, *"Dust ion acoustic solitons and double layers in a dusty plasma with adiabatic positive dust, adiabatic positive ion species and Cairns-distributed electrons."* AIP Adv.**1**2, 015208 (2022).
https://doi.org/10.1063/5.0076894.

X. Mushinzimana, F. Nsengiyumva and L. L. Yadav, *"Large amplitude slow ion-acoustic solitons, supersolitons and double layers in a warm negative ion plasma with superthermal electrons."* AIP Adv.**1**1, 025325 (2021).
https://doi.org/10.1063/5.0039372.

X. Mushinzimana and F. Nsengiyumva, *"Large amplitude ion-acoustic solitary waves in a warm negative ion plasma with superthermal eletrons: The fast mode revisited."* AIP Adv.**1**0, 065305 (2020).
https://doi.org/10.1063/1.5127199.

Acknowledgement

This work would not have been layed out had it not been the invaluable guidance of my Supervisors, Assoc. Prof Lakhan Lal Yadav from the Department of Mathematics, Science and Physical Education, College of Education, University of Rwanda (UR), and Dr Nsengiyumva François from the Department of Civil Engineering, Institut d'Enseignement Superieur de Ruhengeri (INES Ruhengeri). May they find here the expression of my heart-felt gratitude and sincere thanks.

I take this opportunity to also address my sincere thanks to University of Rwanda and Rwanda Astrophysics, Space and Climate Science Research Group (RASC-SRG) for their financial support.

I will remain grateful to my family for its moral support, especially to my son *Dukunde Louis Maxime* for his untiring encouragement during this adventure towards the unknown.

Abstract

Space and laboratory plasmas are inherently multispecies with electrons, two or more positive and/or negative ion species, and possibly charged dust species. Nonthermal particle distributions have also been observed in many space, and astrophysical environments. In this thesis, we have investigated the propagation of the fast and slow ion acoustic modes in a negative ion plasma with heavier and cooler positive ion species and kappa distributed electrons, and the propagation of the dust ion acoustic wave in a dusty plasma with a positively charged dust and Cairns distributed electrons.

When the temperature of ion species is very small compare to the electron temperature, the fast mode in a negative ion plasma supports the propagation of both compressive and rarefactive solitons, and there exist a range of plasma parameter values in which the two types of structures coexist. When the ion temperature effects are important, it supports only rarefactive solitons and this effect is enhanced by the superthermal behavior of the electrons. If electrons are strongly nonthermal, the slow mode supports normal compressive solitons, supersolitons and double layers for high values of the negative ion density. The double layers occur under two different identities, first as the lower limit to the supersoliton existence range and, second, as the limiting factor for the propagation of normal solitons.

A dusty plasma with positively charged dust and strongly nonthermal electrons supports the coexistence of KdV (nonKdV) compressive solitons limited by the occurrence of the ion sonic point and nonKdV (KdV) rarefactive solitons limited by the occurrence of double layers. At a critical dust-to-ion density ratio, compres-

sive and rarefactive solitons coexist without a soliton with finite amplitude at the acoustic speed, contrary to earlier studies. This suggests that the existence of a soliton with finite amplitude at the acoustic speed is not always a pre-requisite for the coexistence of nonlinear structures of both polarities.

Contents

List of Figures

Chapter 1

General introduction

1.1 Introduction

1.1.1 The fourth state of matter

The main difference between the different states of matter is the distance between their constituents. At a fixed temperature and pressure, this distance depends on the strength of the attractive force between them and their kinetic energy. The atoms or molecules composing a solid are closely packed and vibrate about their position of equilibrium in a motion also called thermal motion, because it is due to the substance temperature. When the temperature of the solid is increased for example by heating it, its constituents kinetic energy increases. For some substances, this increase in thermal motion results in the constituents overcoming the intermolecular forces, and there is a transition from solid state to liquid state. Particles in a liquid move freely but the distances between them remains very small as in solids. That is why solids and liquids form the same family of condensed matter. If a liquid's temperature is continuously increased, its constituents move faster and faster as energy is supplied. Ultimately the liquid boils and transforms into a gas. In a gas, particles are far apart from each other, move randomly and do not interact. A further increase of the gas temperature increases its particles kinetic energy. When an electron in an atom or molecule of the gas gains enough kinetic energy, it escapes from the nuclear attraction, a process known as ionisation. As more and more energy is added to the gas, more and more atoms or molecules are ionised converting the gas into a mixture of neutral particles, electrons and positive ions. Such a mixture is called a plasma [1] and constitutes the fourth state of matter. Contrary to the normal gas made of neutral particles, a plasma can carry currents due the presence of free charges (electrons and ions) and is sensitive to electric and magnetic fields. A more rigorous definition of plasma is given by Chen [2]: *A plasma is a quasineutral gas of charged and neutral particles which exhibits collective behaviour*. The terms "quasineutral" and "collective behaviour" are explained in the following sections.

Plasma collective behaviour

In general, not any ionised gas is treated as a plasma. In a neutral gas, the motion of the particles is controlled by the collision among themselves and with the

walls of the container. As a result of these collisions, the particles of a neutral gas follow a random Brownian motion. In a plasma, contrary to the neutral gas, the interaction between charged particles is governed by the Coulomb force which is a long range force. Therefore each particle interacts with a big number of other particles and affects their motion even far away from its location. Thus elements of the plasma affect each other, giving the plasma its characteristic collective behaviour, which means that the macroscopic response to an external stimulus is the cooperative response of many plasma particles. Examples of plasma collective behaviour are Debye shielding, plasma sheath, plasma oscillations and ion-acoustic waves.

Debye shielding

The plasma as defined above is a gas with magnitude of positive charge equal to the magnitude of negative charge. When the plasma potential is perturbed at some location by for example introducing an extra positive charge Q, plasma charges redistribute themselves. The extra positive charge constitutes a perturbation that creates an electric field whose field lines radiate out. In this field, electrons are attracted toward the charge Q and form a cloud, whose electric field opposes that of the perturbation. This effect is also known as the Debye shielding of the plasma from the influence of the perturbation. The Debye length λ_D is a characteristic distance of a plasma, representing the distance at which the bulk of the plasma is shielded from the influence of the perturbation.

Assuming that the electrons and ions are in thermodynamic equilibrium, their number densities n_e and n_i respectively are given by the Boltzmann distribution

$$n_e = n_{e0} e^{\frac{e\varphi}{k_B T_e}} \tag{1.1}$$

and

$$n_i = n_{i0} e^{-\frac{e\varphi}{k_B T_e}}, \tag{1.2}$$

where φ is the electrostatic potential, n_{e0} and n_{i0} are the electron and ion equilibrium density far from the perturbation, where $n_{e0} = n_{i0} = n_0$ and electrostatic potential vanishes, T_e and T_i are the electron and ion temperature respectively, and k_B is the

Boltzmann constant ($k_B = 1.38 \times 10^{-23} J/K$ in SI units). The Poisson's equation then has the form

$$\nabla^2 \varphi = \frac{e}{\varepsilon_0}(n_e - n_i), \tag{1.3}$$

where e is the elementary charge $e = 1.6 \times 10^{-19} C$ and $\varepsilon_0 = 8.85 \times 10^{-12} C^2/Nm^2$ is the permittivity of free space. For small perturbations, $e\varphi/k_B T \ll 1$ and we can expand (1.1) and (1.2) in Taylor series up to the first order. We then replace these series in (1.3) and solve the resulting equation. The solution that decays to *zero* at large distance is given by

$$\phi = \frac{Q}{4\pi\varepsilon_0 r} e^{-\frac{r}{\lambda_D}}, \tag{1.4}$$

where the Debye length is given by

$$\lambda_D = \frac{\lambda_{D_e}\lambda_{D_i}}{\sqrt{\lambda_{D_e}^2 + \lambda_{D_i}^2}}. \tag{1.5}$$

The species Debye lengths λ_{D_e} (electron Debye length) and λ_{D_i} (ion Debye length) are given by

$$\lambda_{D_j} = \sqrt{\frac{\varepsilon_0 k_B T_j}{n_j e^2}}, \tag{1.6}$$

where $j = e, i$. Eq. (1.5) shows that the Debye length is mainly determined by the temperature of the cold species. In SI system of units, Eq. (1.6) can also be written as

$$\lambda_{D_j} = 7.4 \times 10^3 \sqrt{\frac{T_j(eV)}{n_j(m^{-3})}}[m]. \tag{1.7}$$

In Eq. (1.7), $T_j(eV)$ is the temperature of j^{th} species expressed in units of energy (see section 1.1.2), $n_j(m^{-3})$ is the density of the j^{th} species expressed in SI units (number of particles per meter cube) and the Debye length is expressed in meters.

A sphere of radius λ_D is called a Debye sphere. Equation (1.4) shows that for $r \ll \lambda_D$, the electrostatic potential in a plasma is the usual coulomb potential, but for $r > \lambda_D$ it exponentially falls off. Therefore the influence of the perturbation is felt inside the Debye sphere but is vanishingly small outside.

Plasma quasineutrality

A plasma is quasineutral if the Debye length λ_D is much smaller than the plasma dimensions L so that any perturbation is limited inside the Debye sphere but the bulk of the plasma remains neutral.

Plasma frequency

When the quasineutrality is disturbed at a point in a plasma, the more mobile electrons are accelerated to restore the charge neutrality. This motion results in a separation of charges and establishment of an electric field whose amplitude depends on the distance x between positive and negative clouds:

$$E = \frac{e}{\varepsilon_0} n_e x, \tag{1.8}$$

and the restoring force on the electrons is

$$F = eE = \frac{e^2}{\varepsilon_0} n_e x. \tag{1.9}$$

Under this restoring force, the equation of motion of an electron is

$$m_e \frac{d^2x}{dt^2} = \frac{e^2}{\varepsilon_0} n_e x. \tag{1.10}$$

where m_e is the mass of an electron. The electron therefore oscillates with angular frequency

$$\omega_{p_e} = \sqrt{\frac{n_e e^2}{\varepsilon_0 m_e}} [s^{-1}]. \tag{1.11}$$

called electron plasma frequency ω_{p_e}. In principle, there is a plasma frequency for each plasma component species, ions and electrons. But as the ion mass is much larger than the electron mass, the ion plasma frequency is much smaller than the electron plasma frequency so that when reference is made to plasma frequency it is meant the electron plasma frequency. An alternative form of the plasma frequency in SI units is given by

$$\omega_{p_e} \approx 2\pi \times 9 \times \sqrt{n(m^{-3})} [s^{-1}]. \tag{1.12}$$

If the plasma is partially ionised, oscillating electrons collide also with neutral particles. This interaction is characterised by the average time between two electron-neutral collisions τ_n.

Plasma existence criteria

With the parameters above, an ionised gas is characterised as being in plasma state if it satisfies the following conditions:

1. The Debye length λ_D must be very small compare to the dimensions of the plasma L:

   $$\lambda_D \ll L.$$

   This criterion means that there is enough space that a perturbation will be localised in a small region, while the bulk remains quasi neutral.

2. The Debye length depends on thermal motion of charged particles and is derived from statistical principles. Statistics assume averaging over a large number of particles. Thus we have to assume that in a Debye sphere, there is a large number of particles:

   $$N_D = n\frac{4\pi}{3}\lambda_D^3 \gg 1.$$

   As the density of particles n is inversely proportional to the cube of inter-particle distance, this criterion means that the Debye length is greater than the mean distance between two particles.

3. In a partially ionised plasma, oscillating electrons collide with neutral particles. If these collisions are too frequent, electron motion is controlled by ordinary hydrodynamic forces rather than by electromagnetic forces, thus cancelling the collective behaviour. For a gas to be considered as a plasma, the electron-neutral particles collision frequency must be small in comparison to the electron plasma oscillation:

   $$\omega_{pe}\tau_n \gg 1.$$

   This criterion means that the motion of charged particles in a plasma is controlled by electromagnetic forces rather than by hydrodynamic forces.

1.1.2 Basic plasma parameters

To characterise a plasma, three basic plasma parameters are used [3]: the charged particle density n (number of particles per cubic meter), the temperature T of each component of the plasma and the magnetic field.

From the point of view of classical mechanics, a plasma is a many particle system whose state is determined using the laws of motion of individual particles. Due to a large number of particles in the system, this is almost impossible to accomplish. Such a system is therefore studied using the statistical methods in which the distribution function plays a key role. The distribution function is rather a function from which average values of different physical macroscopic quantities are calculated. Charged particles in a plasma move with different velocities. In general for a gas in thermodynamic equilibrium, the distribution of particles in velocity space is given by the Maxwell-Boltzmann velocity distribution law:

$$F_M(v) = n_0 \left(\frac{m}{2\pi k_B T} \right)^{3/2} e^{-\frac{mv^2}{2k_B T}}, \tag{1.13}$$

where m is the mass of the particles, n_0 is the equilibrium density of particles, T is the thermodynamic temperature, $v^2 = v_x^2 + v_y^2 + v_z^2$ is the square of the speed of the particles and k_B is the Boltzmann constant.

The product $F_M(v)d^3v$ where $d^3v = dv_x dv_y dv_z$ is the number of particles in a unit volume and having velocity between $\vec{v}$ and $\vec{v} + d\vec{v}$. With this distribution function, the total number of particles in a unit volume is found by integrating (1.13) over the velocity space

$$n_0 = \int_{-\infty}^{+\infty} F_M(v) d^3v. \tag{1.14}$$

Similarly, we define the mean square velocity as

$$\bar{v^2} = \frac{1}{n_0} \int_{-\infty}^{+\infty} v^2 F_M(v) d^3v, \tag{1.15}$$

from which we get the average kinetic energy

$$\bar{E}_{av} = \frac{1}{2} m \bar{v^2} = \frac{3k_B T}{2}. \tag{1.16}$$

Due to this relation between average kinetic energy and temperature, in plasma physics the temperature is expressed in units of energy by virtue of the relation

$$T(eV) = k_B T(K), \tag{1.17}$$

where $T(eV)$ and $T(K)$ is the temperature expressed in electronvolts (unit of energy) and kelvin respectively. The temperature of $1eV$ corresponds to $11,600K$.

When a plasma is placed in external electric and magnetic fields, charged particles are subjected to the Lorentz force

$$\vec{F} = q\left(\vec{E} + \vec{v} \times \vec{B}\right), \tag{1.18}$$

where $\vec{F}$ is the force, q is the electric charge, $\vec{E}$ is the electric field, $\vec{v}$ is the charged particle velocity and $\vec{B}$ is the magnetic field vector. The first term of the right hand side of equation (1.18) is the electric force. It shows that the electric force on a charged particle is parallel to the electric field vector in the case of a positive charge, and anti-parallel in the case of a negative charge. This force does not depend on the velocity of the particle. The second term is the magnetic force. It shows that the magnetic force on a charged particle is perpendicular to the magnetic field vector, and depends on the velocity of the particle: if the particle velocity is zero or if it is in the same direction as the direction of the magnetic field vector, the magnetic force is zero.

Besides externally applied electric and magnetic fields, there are electric fields generated by each charged particle and magnetic fields resulting from motion of charged particles. This means that each particle moves in the microscopic fields of other particles, but at the same time it affects these fields by generating its own fields. As a consequence the dynamics of each particle has to self-consistently account for its self-generated fields during its motion. This makes the particle dynamics very complicated and almost untreatable. However some methods and approximation describing the dynamics in a plasma have been elaborated and are reviewed in Sec. 1.3.

1.1.3 Multispecies plasmas

A plasma made of electrons and one positive ion species is the simplest quasineutral plasma. In many situations a plasma consists of three or more charged species. Such a plasma is called multispecies or multicomponent plasma. In addition to negatively charged electrons, these plasmas contain ions or particles some of which are charged positively and possibly some others being negatively charged. Multispecies plasmas have been studied theoretically [5–10, 32] and experimentally [11–13].

Among the different multispecies plasmas, negative ion and dusty plasmas have got a particular attention due to their presence in space and laboratory environments. A negative ion plasma is a plasma made of electrons, positive ions and negative ions. They have been investigated theoretically by different authors including Tagare et al. [14], Kumar and Mishra [15], Rouhani et al. [1], El Labany et al. [16] and so on. They have been investigated experimentally by D'Angelo [17], Merlino and Loomis [18], Ichiki et al. [12, 19] and so on. The propagation of solitary waves in a negative ion plasma is studied in *chapters* 2 *and* 3.

Another class of multispecies plasma, that is interesting theoretically and experimentally, is the class of dusty plasmas, consisting of electrons, some positive ion species and one or more charged dust species. A dust is a micron or submicron sized particle [20] with a very large mass as compared to the mass of the plasma electrons and protons. Its charge can be as high as 10^4 elementary charge [21] and then if present, it can participate in the collective behaviour of the plasma. In many situations the dust is negatively charged after capturing the more mobile electrons, however it has been proven that light dust may be positively charged by photoionisation mechanism [22]. While the field of dusty plasma has gained a boost in the recent years, interest to them goes back to the beginning of plasma physics with Irving Langmuir, Lyman Spitzer, and Hannes Alfvén, three pioneers of plasma physics in the 20^{th} century [23]. A dusty plasma comprising electrons, positive ions and positively charged dust is studied in *Chapter* 4.

1.1.4 Plasma state in space, laboratory and industry

A common belief [20] is that 99% of matter in universe is in plasma state, only the remaining 1% being planets where the solid, liquid and gaseous states dominate. Plasma state is found throughout the solar system, interstellar and intergalactic medium, in laboratory conditions and in industrial applications.

The sun is a star in plasma state. It continuously emits a conducting plasma made of electrons, protons and alpha particles (Helium nuclei) from its surface and in all directions [24]. These emanations form the solar wind that travels to several hundred astronomical units ($1AU \approx 1.5 \times 10^{11} m$).

Like the earth, most of the solar system planets are magnetised. A magnetosphere of a planet is the region around that planet where it exerts magnetic effects on charged particles. In its path the solar wind interacts with the planets' magnetospheres, pushing the planetary magnetic field towards the planet on the day side and extending the magnetic field on the night side of the planet forming a magnetic tail. A similar interaction is also observed in case of comets having their own magnetic field like the comet Halley. Beyond the solar system, the interstellar medium is also filled with matter in plasma state with low temperature and low density.

Near the earth's surface at altitudes $\gtrsim 60km$ the solar ultraviolet rays ionise part of the neutral particles, resulting in a partially ionised plasma. This region, called the ionosphere [24] is the transition region from the neutral atmosphere at altitudes below $\lesssim 60km$ to the fully ionised magnetospheric plasma in the plasmasphere, extending to about $4R_E$ and Van Allen radiation belt at about $6R_E$, where $R_E = 6371km$ is the earth's radius. Lightning and auroras are natural phenomena in which the plasma state dominates.

On the earth's surface, man-made plasmas are produced for technological applications such as fluorescent tubes, plasma television screens, neon signs. Technological applications are numerous and their number increases day by day as a result of research.

1.2 Applications of plasmas

As it is for other states of matter, the plasma state has found different applications in our daily lives. We discuss some of them.

Perhaps the oldest application of plasma state is the use of the earth's ionosphere to reflect high frequency radio waves for the purpose of radio communications. When a radio signal arrives at the boundary of a plasma, it is refracted with index of refraction

$$n_r = \frac{c}{v_p}, \tag{1.19}$$

where n_r in the plasma index of refraction, c is the speed of light and v_p is the wave phase speed in the plasma. The ionospheric index of refraction is given by the Altar-Appleton-Hartree dispersion relation [25]. In case of a longitudinal wave (in direction of the magnetic field) and negligible loss (no wave damping), the Altar-Appleton-Hartree [25] dispersion relation reduces to

$$n_r = \sqrt{1 - \frac{\omega_{p_e}^2}{\omega^2}}, \tag{1.20}$$

where $\omega_{p_e} = (n_e e^2/\varepsilon_0 m_e)^{1/2}$ is the electron plasma frequency and ω is the frequency of the incident wave. Expression (1.20) shows that for a fixed frequency ω of the radio signal, the refractive index n_r decreases when the electron density n_e increases until it reaches a critical value n_{ec} at which $n_r = 0$. For larger values of n_e, n_r is complex number and the radio wave can no longer be propagated in the ionospheric plasma, rather it is reflected back to earth. In this context of reflection, the earth's ionospheric plasma has been used and continues to be used for long distance radio communication.

Another application of matter in plasma state of major technological importance is the production of energy from *controlled thermonuclear fusion*. Fusion is the process during which two light atoms combine to form a heavier atom with release

of energy. An example is the fusion of Deuterium and Tritium to give helium atom with release of $17.6MeV$ of energy. The reaction is as following:

$$^{2}_{1}D + ^{3}_{1}T \rightarrow ^{4}_{2}H_e + ^{1}_{0}n + 17.6MeV. \tag{1.21}$$

The combination of the two atoms is, however, subject to the condition that the two atoms must overcome the coulomb potential barrier to come as close as possible. This may be effectively done if the two atoms are moving at very high speeds. In classical mechanics, high speeds mean also high temperatures and high temperatures mean that atoms are ionised, and thus the gas is in the plasma state. Different thermonuclear fusion reactors of different types are being developed around the world. The biggest of them is the ITER, the *International Thermonuclear Experimental Reactor*.
Other operational nuclear fusion facilities include the Joint European Torus (JET) in UK, the Tokamak Fusion Test Reactor (TFTR) in USA, the T-15MD in Russia, the Experimental Advanced Superconducting Tokamak (EAST) in China, the Laser Mégajoule (LMJ) in France, JT-60 in Japan, the KSTAR (Korean Superconducting Tokamak Reactor) in South Korea etc.

Matter in plasma state is used for sterilisation of medical equipment [26]. The sterilisation efficiency is improved and the processing time is reduced in addition to less damage caused to medical devices by conventional techniques used in hospitals. Plasma based electric propulsion technology (plasma thrusters) is used for the keeping of spacecraft orbit and orbit topping [27]. In textile industry, low temperature plasmas are used to make textile hydrophobic, hydrophilic or dirt-repellent [28]. Plasma etching process is used in semiconductor industry for the removal of substrate material [29]. Plasma torches are used for the disposal of waste [30]. Plasma processing are now very important to many manufacturing industries including but not limited to aerospace, automotive, biomedicine, defence, optics, solar energy, paper and polymer industries [29]. These examples of plasmas in space, laboratory and industrial conditions and their applications underline the importance of learning and describing the behaviour of matter in the plasma state. A wide range of literature [2] provides this description.

1.3 Plasma dynamics

Like gases made of neutral particles, a plasma has neither definite shape, nor definite volume. In a gas of neutral particles, the interaction between two particles is by the contact collision. In a plasma, any charged particle generates electric and magnetic fields in which other particles move. This means that charged particles in a plasma interact by long range electromagnetic forces. In addition to internally-generated fields, a plasma may be also subjected to external electric and magnetic fields. Any theoretical description of the plasma behaviour has to account for all of these fields. Due to difficulty in integrating all these fields, different approximations can be used depending on the problem to be studied. There are mainly four approximations [2, 24]:

1.3.1 Single particle motion

In this approximation, one considers the motion of individual particles under the influence of externally applied electric and magnetic fields. It is assumed that the charged particles do not interact and the fields created by individual particles do not affect the externally applied fields. This means that this approximation can be applied if the charged particle density is low.

The motion of a charged particle in an electromagnetic field obeys Newton's second law

$$m\frac{d\vec{v}}{dt} = q\left(\vec{E} + \vec{v}\times\vec{B}\right), \tag{1.22}$$

where m, q and $\vec{v}$ is the particle mass, electric charge and velocity, respectively. In the absence of the electric field, this equation reduces to

$$m\frac{d\vec{v}}{dt} = q\vec{v}\times\vec{B}. \tag{1.23}$$

This last equation shows that the acceleration of a charged particle $\vec{a} = d\vec{v}/dt$ in a magnetic field is perpendicular to its velocity, *i.e.* it is a centripetal acceleration. This means that the magnitude of the particle velocity and its kinetic energy do not change under the action of the magnetic field, and the magnetic field does no work on the particle, but the particle moves in a circle around magnetic field lines with

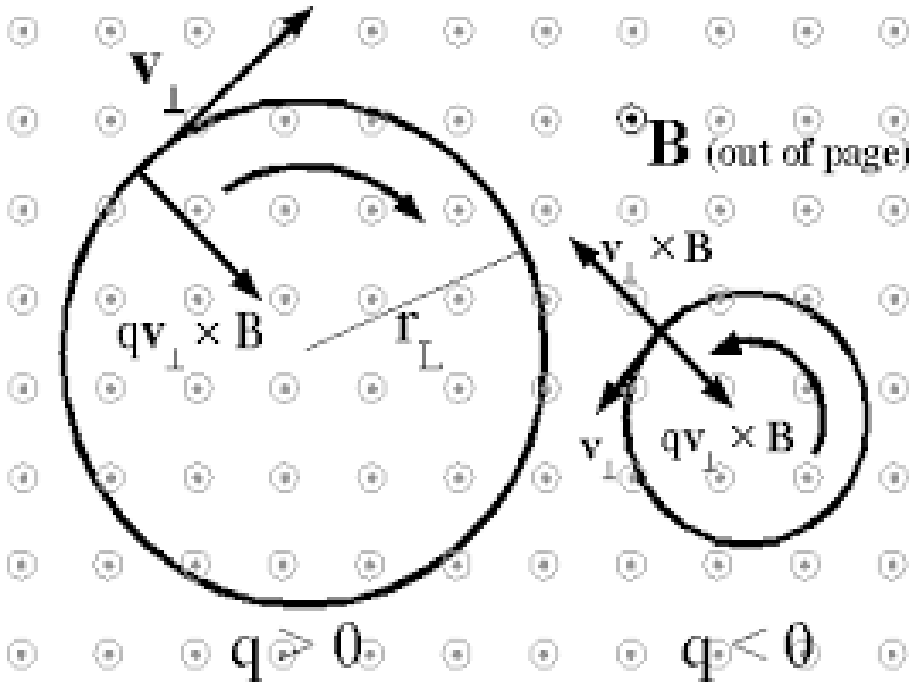

Figure 1.1: Gyration of a charged particle around a magnetic field line. Positively charged ($q > 0$) and negatively charged ($q < 0$) particles are initially moving with velocity $\vec{v_\perp}$ before falling in a region where there is a magnetic field directed out of the page.

gyration frequency (gyrofrequency or cyclotron frequency)

$$\omega_g = \frac{|q|B}{m}. \tag{1.24}$$

This is illustrated in Fig. 1.1. Positive and negative charges with parallel velocities gyrate in opposite directions. The radius of the circular orbit of the charge is given by

$$r_L = \frac{v_\perp}{\omega_g} = \frac{mv_\perp}{|q|B}, \tag{1.25}$$

where $v_\perp$ is the component of the particle velocity in the plane perpendicular to the magnetic field. The radius r_L is normally called the Larmor radius or gyroradius and its center is called the guiding center.

1.3.2 Kinetic theory

As discussed in Sec. 1.1.2, the dynamics of a charged particle in a plasma consisting of a large number of particles is very complicated because it has to self-consistently account for self generated fields and microscopic fields of all other particles. Rather than providing description of each particle individually as it is with the single particle theory, in kinetic theory description, the plasma is assumed to be a system of many strongly interacting particles. Each particle at position $\vec{r}(t)$ has velocity $\vec{v}(t)$ and both position and velocity are functions of time t, but are independent variables. They define a six-dimensional space with coordinate axes $(\vec{r},\vec{v})$ also called the phase space.

In this phase space, one defines the particle velocity distribution function $f(\vec{r},\vec{v},t)$ as the particle number density at position $\vec{r}$ and velocity $\vec{v}$ at time t. Thus $f(\vec{r},\vec{v},t)d\vec{r}d\vec{v}$ where $d\vec{r} = d^3r = dx.dy.dz$ and $d\vec{v} = d^3v = dv_x.dv_y.dv_z$ in Cartesian coordinates is the total number of particles having positions in the range between $\vec{r}$ and $\vec{r}+d\vec{r}$ and velocities in the range between $\vec{v}$ and $\vec{v}+d\vec{v}$ at time t.

In a plasma, each particle species has its own distribution function f_j. This distribution function is normalised such that its integral over the velocity space is equal to the species particle density $n_j(\vec{r},t)$ at position $\vec{r}$ at time t:

$$n_j(\vec{r},t) = \int f_j(\vec{r},\vec{v},t)d\vec{v}. \tag{1.26}$$

The kinetic theory is a formalism of study of a system of many particles by describing the microscopic properties of its constituents and their interactions, leading to observable macroscopic variables such as pressure, density and so on. This is achieved by solving a kinetic equation, which is an equation that describes the time evolution of the distribution function. If there are no particles added or lost to the plasma, the total number of particles is conserved and therefore the distribution function is constant, *i.e*

$$\frac{df_j}{dt} = 0. \tag{1.27}$$

This total time derivative evaluates the change of the distribution function f_j due to the change of the particle position in $(\vec{r},\vec{v})$ space, as well as the explicit time variation of f_j with time t. But both $\vec{r}$ and $\vec{v}$ are time dependent and using the differential

chain rule, the total time derivative takes the form of a convective derivative

$$\begin{aligned} \frac{d}{dt} &= \frac{\partial}{\partial t} + \frac{\partial}{\partial \vec{r}}\frac{\partial \vec{r}}{\partial t} + \frac{\partial}{\partial \vec{v}}\frac{\partial \vec{v}}{\partial t} \\ &= \frac{\partial}{\partial t} + \vec{v}.\nabla_{\vec{r}} + \frac{\partial \vec{v}}{\partial t}.\nabla_{\vec{v}}, \end{aligned} \tag{1.28}$$

where

$$\begin{aligned} \nabla_{\vec{r}} &= \vec{i}\frac{\partial}{\partial x} + \vec{j}\frac{\partial}{\partial y} + \vec{k}\frac{\partial}{\partial z}, \\ \nabla_{\vec{v}} &= \vec{i}\frac{\partial}{\partial v_x} + \vec{j}\frac{\partial}{\partial v_y} + \vec{k}\frac{\partial}{\partial v_z} \end{aligned} \tag{1.29}$$

and $\partial\vec{v}/\partial t = d\vec{v}/dt$ is the acceleration $\vec{a}_j$ of the particles. Then Eq. (1.27) takes the form

$$\frac{\partial f_j}{\partial t} + \vec{v}.\nabla_{\vec{r}} f_j + \vec{a}_j.\nabla_{\vec{v}} f_j = 0. \tag{1.30}$$

This is the Vlasov kinetic equation for the distribution function f_j. It states that along a particle's orbit in the phase space, the particle density $f_j(\vec{r},\vec{v},t)d^3v$ remains unchanged. This holds as long as particle collisions and correlations between particles and microscopic fields are negligible [24].

When collisions between plasma components are important, they cause a variation of the distribution function that is expressed by an additional term on the right hand side of equation (1.30). The resulting equation is called the Boltzmann equation

$$\frac{\partial f_j}{\partial t} + \vec{v}.\nabla_{\vec{r}} f_j + \frac{q_j}{m_j}\left(\vec{E} + \vec{v}\times\vec{B}\right).\nabla_{\vec{v}} f_j = \left(\frac{\partial f_j}{\partial t}\right)_{coll}. \tag{1.31}$$

The self-consistent electric $\vec{E}$ and magnetic $\vec{B}$ fields are determined from the Maxwell's equations:

$$\nabla.\vec{E} = \frac{1}{\varepsilon_0}\rho \quad \left(Gauss's\ law for\ electric\ field\right), \tag{1.32}$$

$$\nabla.\vec{B} = 0 \quad \left(Gauss's law\ for\ magnetic\ field\right), \tag{1.33}$$

$$\nabla\times\vec{E} = -\frac{\partial\vec{B}}{\partial t} \quad \left(Faraday's\ law\ of\ electromagnetic\ induction\right), \tag{1.34}$$

$$\nabla \times \vec{B} = \mu_0 \vec{J} + \mu_0 \varepsilon_0 \frac{\partial \vec{E}}{\partial t} \quad \left(Generalised\ Ampere's\ law\right), \tag{1.35}$$

where

$$\rho = \sum_j q_j n_j = \sum_j q_j \int f_j d^3v \tag{1.36}$$

is the net electric charge calculated over all charge species, and

$$\vec{J} = \sum_j q_j n_j \vec{v} = \sum_j q_j \int \vec{v} f_j d^3v \tag{1.37}$$

is the total current due to positive and negative charges.

The Vlasov equation is nonlinear in the six-dimensional phase space and is in general very difficult to solve. Due to this it is a normal practice to obtain information on the average behaviour of the plasma by finding the moments of the Vlasov equation. By definition, the k^{th} moment of the distribution function $f(\vec{r},\vec{v},t)$ is obtained by multiplying f by various powers of $\vec{v}$ and integrating over velocity space.

$$M_k(\vec{r},t) = \int v^k f_j(\vec{r},\vec{v},t) d^3v. \tag{1.38}$$

The distribution function is a function of position vector $\vec{r}$, velocity $\vec{v}$ and time t, but the average macroscopic variables like density, pressure and so on depend only on the position and time. The integration is therefore carried out on the entire velocity space. The zero-order moment yields the particle density n, the first moment is the particle flux $n\vec{v}$, the second moment is the stress tensor and so on.

1.3.3 Multifluid theory

In the multifluid description, each plasma component j is considered as a separate fluid and the plasma as an ensemble of interpenetrating charged fluids. Each individual fluid has its own distribution function obeying the Vlasov equation. Taking the moments of the entire Vlasov equation results in a set of partial differential equations in terms of means of macroscopic variables like particle density, particle velocity, plasma temperature and so on. The resulting equations are called fluid

equations and together with Maxwell's equations they describe in a good approximation the plasma behaviour.

The zero-order moment of the Vlasov equation has the form

$$\int \left[\frac{\partial f_j}{\partial t} + \vec{v}.\nabla_{\vec{r}} f_j + \frac{q_i}{m_j} \left(\vec{E} + \vec{v} \times \vec{B} \right) .\nabla_{\vec{v}} f_j \right] d^3v = 0. \tag{1.39}$$

Integrating over the entire velocity space yields the equation of continuity for each plasma species j

$$\frac{\partial n_j}{\partial t} + \nabla . \left(n_j \vec{u}_j \right) = 0, \tag{1.40}$$

where $\vec{u}_j$ is the species average flow velocity

$$\vec{u}_j = \frac{1}{n_j(\vec{r},t} \int_{-\infty}^{+\infty} \vec{v} f_j(\vec{r},\vec{v},t) d^3v, \tag{1.41}$$

and n_j is its density. This equation describes the conservation of matter: the number of particles in a test volume can change only if there is a flux of particles across the boundary of the volume.

The first-order moment obtained by multiplying the Vlasov equation by $\vec{v}^1 = \vec{v}$ and integrating over the velocity space is the momentum transport equation

$$m_j n_j \left[\frac{\partial \vec{u}_j}{\partial t} + \left(\vec{u}_j . \nabla \right) \vec{u}_j \right] = q_j n_j \left[\vec{E} + \vec{u}_j \times \vec{B} \right] - \nabla P_j. \tag{1.42}$$

Also known as the fluid equation of motion, the momentum transport equation describes the motion of a fluid element (the change in its momentum due to applied forces) in presence of Lorentz force and pressure gradient ∇P_j.

Integration of the zero-order moment (1.39) has introduced the first-order moment (1.41), and integration of the first-order moment has introduced the second-order moment, the pressure tensor P:

$$P_j(\vec{r},t) = \int_{-\infty}^{+\infty} m_j \vec{v'} \vec{v'} f_j(\vec{r},\vec{v'},t) d^3v', \tag{1.43}$$

where $\vec{v'} = \vec{v} - \vec{u}$ is the thermal velocity. In general, when we take the k^{th} moment of the Vlasov equation, we obtain an equation for that moment containing however a $(k+1)^{th}$ moment. This recurrence means that the system of equations obtained by calculating up to k^{th} moment is never closed. Instead of finding higher and higher moments, a common procedure is to truncate the process and assume an equation of state to close the system.

An equation of state relates the pressure of a gas and its density. Two extreme cases arise in the isothermal and adiabatic processes. In an isothermal process, temporal variations of the plasma variables are so slow that the plasma has enough time to redistribute energy and maintain a constant temperature. The relation between pressure and density is then the ideal gas law

$$P_j = n_j k_B T_j. \tag{1.44}$$

In the adiabatic case, the time variations are so fast that no heat exchange in the plasma is possible. The equation of state in this case has the form

$$P_j = P_{j0} \left(\frac{n_j}{n_{j0}} \right)^{\gamma}, \tag{1.45}$$

where the adiabatic index $\gamma = \frac{C_p}{C_v}$ is the ratio of the specific heat at constant pressure to the specific heat at constant volume. In both cases, the pressure gradient is such that

$$\frac{\nabla P_j}{P_j} = \gamma \frac{\nabla n_j}{n_j}, \tag{1.46}$$

where $\gamma = 1$ for the isothermal case. Generally, the adiabatic index is related to the number of degrees of freedom N by the relation $\gamma = (2+N)/N$ [2]. Thus for a one dimensional adiabatic compression of the j^{th} plasma species, γ takes the value 3, and it takes a value of $5/3$ for a three dimensional adiabatic compression. In addition to fluid equation and equation of state, each fluid component has to satisfy the Maxwell's equations, Eqs. (1.32) to (1.35).

1.3.4 Magnetohydrodynamic (Single fluid) theory

In the magnetohydrodynamic (MHD) model description, the plasma is considered as a single conducting fluid in which all the plasma constituents move with the

same velocity. This then reduces the number of variables to be considered. The magnetohydrodynamic equations can be derived from the multifluid equations by introducing the new variables

$$\begin{aligned} n &= \sum_j m_j n_j, & \vec{U} &= \frac{1}{n}\sum_j m_j n_j \vec{u}_j, \\ \rho &= \sum_j q_j n_j, & \vec{J} &= \sum_j q_j n_j \vec{u}_j. \\ P &= \sum_j P_j, \end{aligned} \tag{1.47}$$

In these variables, the MHD equations of continuity and momentum are

$$\frac{\partial n}{\partial t} + \nabla.\left(n\vec{U}\right) = 0 \tag{1.48}$$

and

$$n\left[\frac{\partial \vec{U}_j}{\partial t} + \left(\vec{U}.\nabla\right)\vec{U}\right] = \rho\vec{E} + \vec{j}\times\vec{B} - \nabla P. \tag{1.49}$$

Generally, the MHD is used to describe low frequency phenomena occuring at large spatial scales, where the plasma is neutral with charge density $\rho \approx 0$.

1.4 Velocity distributions

Particle densities play an important role in the study of the wave propagation [31] and they can be derived from the velocity distribution functions. Particle velocity distribution functions may have different forms depending on the particular conditions of existence of the plasma state. Some of the common particle velocity distributions are the Maxwellian distribution, the generalised Lorentz distribution (kappa distribution) and the Cairns distribution. The Maxwellian particle distribution has been used in Sec. 1.1.2 to define the three basic plasma parameters. In the study of plasma waves, the Maxwellian distribution has been used in different models of plasma configurations [8, 32–34].

1.4.1 Kappa distribution

As many other celestial bodies, the earth is surrounded by a magnetic field whose intensity at its surface is between $20\mu T$ and $60\mu T$ [35]. This field decreases with

increasing altitude. When the solar wind comes closer to the earth's magnetosphere, it is deflected by the earth's magnetic field, protecting the earth against possible hazardous effects of solar wind. This interaction of the earth's magnetic field and the solar wind results in the modification of the magnetosphere's magnetic field. The magnetic field of the dayside is compressed and that of the nightside is stretched resulting in a long tail.

While investigating the low – energy electron population in magnetosphere within the local time range 17:00 to 22:00 using data collected by OGO 1 and OGO 3 satellites, Vasyliunas [36] observed that "the plasma sheet electrons typically have a broad, quasi – thermal energy spectrum peaked anywhere between a few hundred eV and a few keV, with a non–Maxwellian energy tail". To fit these data with a velocity distribution function, he devised a non–Maxwellian distribution function that he called Kappa distribution function. Two factors guided him:

- The satellite data showed that electron fluxes were isotropic, and hence their velocity distribution function depends only on their speeds and not on velocity.
- Electron distribution in plasma sheet is broader than Maxwellian distribution and tends to power law at high energies.

The three dimensional kappa velocity distribution function is given by the expression [36–38]

$$F_\kappa(v) = \frac{n_0}{(\pi\kappa\theta^2)^{\frac{3}{2}}}\frac{\Gamma(\kappa+1)}{\Gamma(\kappa-1/2}\left(1+\frac{v^2}{\kappa\theta^2},\right)^{-(\kappa+1)}, \tag{1.50}$$

where $\Gamma(x)$ is the gamma function, n_0 and v are the particle number density and velocity respectively, κ is a parameter that indicates the deviation from Maxwellian distribution and gives the name to the function and θ is a characteristic velocity, related to the thermal speed $v_t^2 = k_B T/m$ by the relation

$$\theta = \sqrt{\frac{2\kappa-3}{\kappa}}v_t. \tag{1.51}$$

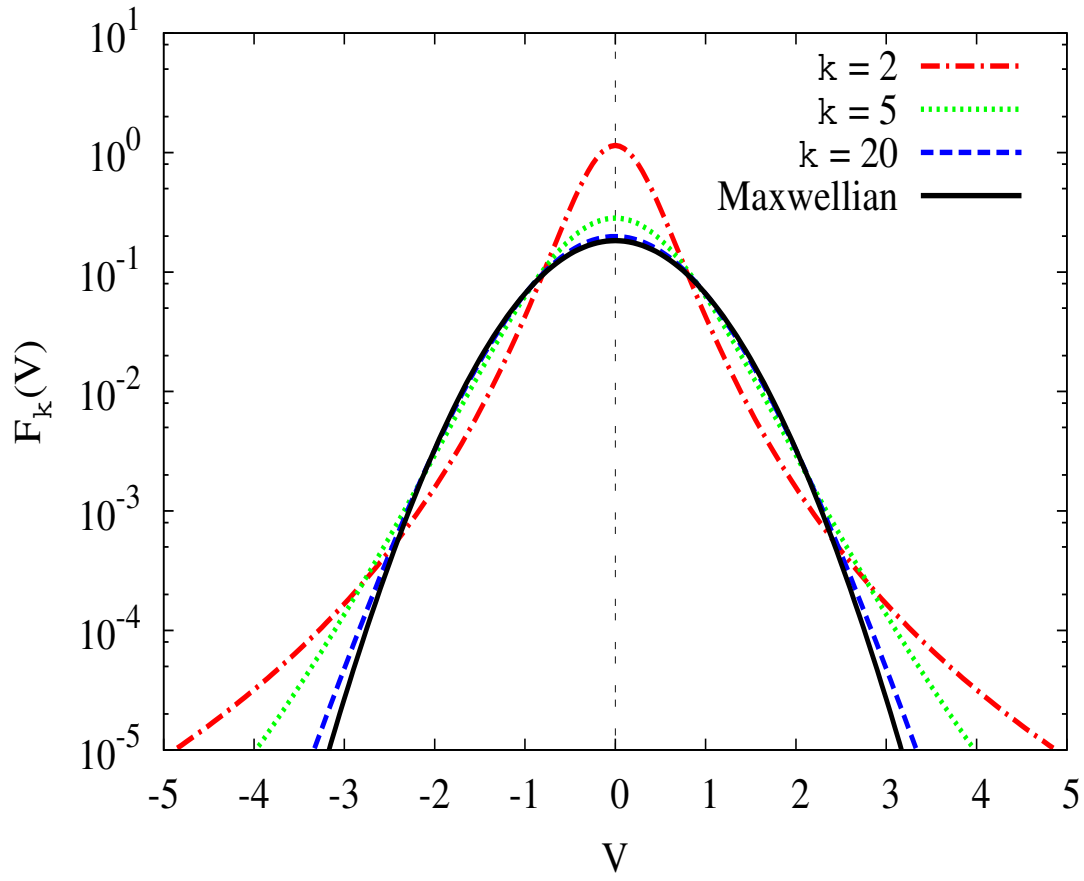

Figure 1.2: Kappa velocity distribution function for different values of the spectral index κ. The variable $V^2 = v^2/2v_t^2$ and the function is stretched by a factor of $(2\pi v_t^2)^{3/2}/n_0$. The black solid line represents a Maxwellian ($\kappa \to \infty$), the dashed blue line is plotted at $\kappa = 20$, the dotted green line is at $\kappa = 5$, and the red dot dashed line represents strongly non-Maxwellian distribution with $\kappa = 2$.

For θ to be a real valued function, it is required that the parameter κ takes values larger than $\kappa > 3/2$. A value of κ close to but larger than $3/2$, *e.g.* $\kappa = 2$ indicates that the plasma is strongly non-Maxwellian. While (1.50) is a power law, it however tends to the Maxwellian distribution as the parameter κ tends to infinity:

$$F_M(v) = \lim_{\kappa \to \infty} F_\kappa(v). \tag{1.52}$$

Figure 1.2 shows the kappa 3-dimensional isotropic speed distribution function as a function of $v^2/2v_t^2$ and stretched by a factor of $(2\pi v_t^2)^{3/2}/n_0$ for various values of the spectral index, $\kappa = 2$ (red dot dashed line), $\kappa = 5$ (green dotted line), $\kappa = 20$ (blue dashed line) and $\kappa \to \infty$ (black solid line). As it can be seen, the kappa distribution for $\kappa = 20$ (blue dashed curve) is much closer to Maxwellian distribution than are distributions for $\kappa = 5$ and $\kappa = 2$. It is also seen that at high speeds, i.e. high energies, the Maxwellian tends to zero quicker than the kappa, justifying the use of kappa to model systems with long tails in the high energy domains. Low values of κ correspond to longer tails and as κ increases, tails decrease also approaching the Maxwellian distribution at larger values of κ.

In the presence of a potential ϕ, we replace v^2 by $v^2 + 2q\phi/m$ where q is the species charge and m is the mass of one particle. The presence of a potential modifies the density distribution of the particles and the zero moment gives the new distribution as a function of the potential and equilibrium density n_0 as

$$n = n_0 \left(1 + \frac{2q\phi}{(2\kappa - 3)K_B T}\right)^{(\kappa - 1/2)}. \tag{1.53}$$

Particles with kappa distribution have been found in different space [39–42] and laboratory [43] environments. Subsequently different studies have used the kappa distribution to model particle distribution with long tails [1, 15, 16, 44–46].

1.4.2 Cairns distribution

Another distribution that has been used is the Cairns distribution [47].

Cairns distribution was introduced by Cairns et al. [47] in 1995 to explain density depletions, observed by FREJA satellite in the upper ionosphere. Density depletion was not expected since the KdV theory predicts the existence of solitons

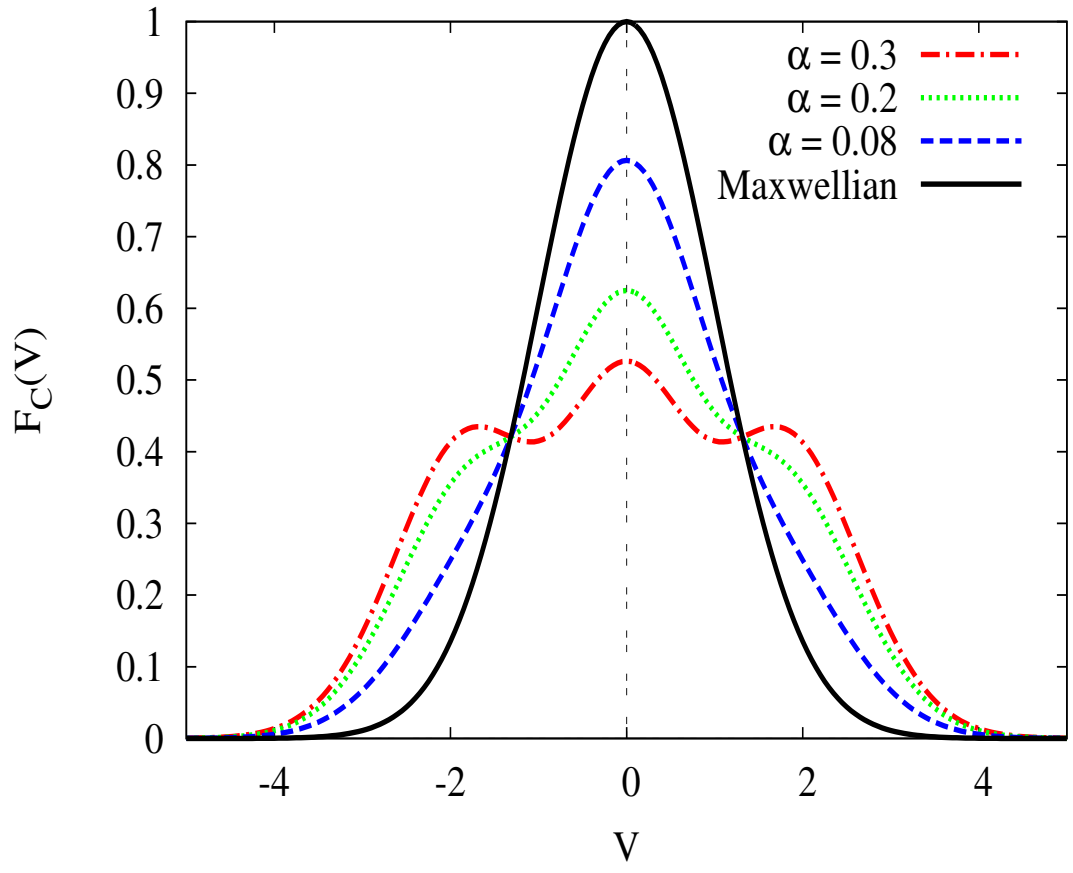

Figure 1.3: Cairns distribution as a function of $V = v/v_t$ and stretched by $\sqrt{2\pi v_t^2}$ for different values of the nonthermal parameter α. The black solid line is plotted at $\alpha = 0$, and corresponds to a Maxwellian. The blue dashed line is plotted at $\alpha = 0.08$ and the distribution is slightly non Maxwellian. The green dotted line is plotted at $\alpha = 0.2$ at which the distribution is strongly non-Maxwellian. The red dot dashed line plotted at $\alpha = 0.3$ ($\beta \simeq 0.63$) presents wings and the corresponding value of α is beyond the acceptable range.

with density enhancement instead of density depletion. Cairns et al. [47] were able to show that the nature of the ion acoustic soliton can change to the opposite if the electron distribution is non-thermal with excess energetic particles in the tail of the distribution, like the counterstreaming electrons observed by Viking and AMPTE satellites. The one dimensional Cairns distribution has the following form [47]

$$F_C(v) = \frac{n_0}{(3\alpha+1)\sqrt{2\pi v_t^2}} \left(1 + \frac{\alpha v^4}{v_t^4}\right) e^{-\frac{v^2}{2v_t^2}}, \tag{1.54}$$

where α determines the population of nonthermal particles and varies in the interval $0 < \alpha < \infty$. For $\alpha = 0$, we obtain the Maxwellian distribution and therefore the nonthermality increases with increasing α. Fig. 1.3 shows the function $F_C(v)$ for different values of α. In the presence of a non-zero electrostatic potential, integration of the resulting distribution over the velocity space gives the charge density

$$n = n_0 \left(1 + q\beta\varphi + q^2\beta\varphi^2\right) e^{-q\varphi}, \tag{1.55}$$

where $\beta = 4\alpha/(1+3\alpha)$. The parameter β is bounded by 0 on the lower side and $4/3$ on the upper side for very large α. However as is shown by the red dot dashed line in Fig. 1.3 plotted for $\alpha = 0.3$ ($\beta = 12/19$), as α increases, the distribution develops wings and becomes unstable [48]. Therefore the acceptable values of α are in the range $0 \leqslant \alpha < 0.25$ or $0 \leqslant \beta < 4/7$.

There have been several studies on the ion acoustic solitons in plasmas with Cairns distributed particles [48–52, 54, 69]. It has been shown that the presence of Cairns distributed plasma component modifies the soliton structure as compared to the Maxwellian distribution.

1.5 Waves in plasmas

1.5.1 Definition

The equilibrium state of a plasma is characterised by uniform density of positively and negatively charged particles and absence of charge concentration that would lead to the presence of an electric field. When the equilibrium is perturbed, this

perturbation can propagate. A wave is a moving disturbance in space and time, transferring energy from one point to another. In this kind of motion, there is no displacement of particles, but they oscillate about their position of equilibrium. Plasmas support both longitudinal and transverse waves. A wave is longitudinal when the particles oscillate in the direction of wave propagation. When the particles oscillate in direction perpendicular to the direction of wave propagation, the wave is transverse. Waves in plasmas are further classified as electromagnetic or electrostatic according to whether or not there is an oscillating magnetic field component. Electrostatic waves are longitudinal waves in which there is no oscillating magnetic field, and the electric field perturbation associated with the wave is parallel to the wave propagation direction. Such waves are accompanied with density and potential fluctuations. Electromagnetic waves are transverse waves and their electric and magnetic fields oscillate in a plane perpendicular to the direction of the wave propagation.

1.5.2 Mathematical description of waves

Let u be the waving quantity. This may be the height of a plucked string, the electric and/or the magnetic fields and so on. In absence of external forces, a wave propagating with constant speed c can be described by a second order partial differential equation

$$\nabla^2 u - \frac{1}{c^2}\frac{\partial^2 u}{\partial t^2} = 0, \tag{1.56}$$

where

$$\nabla^2 = \frac{\partial^2}{\partial x^2} + \frac{\partial^2}{\partial y^2} + \frac{\partial^2}{\partial z^2} \tag{1.57}$$

is the Laplacian. For a one dimensional wave moving in x direction this equation is written as

$$\frac{\partial^2 u}{\partial x^2} - \frac{1}{c^2}\frac{\partial^2 u}{\partial t^2} = 0, \tag{1.58}$$

Introducing the simplified notations $u_{tt} = \partial^2 u/\partial t^2$ and $u_{xx} = \partial^2 u/\partial x^2$, this equation takes the form

$$u_{tt} - c^2 u_{xx} = 0, \tag{1.59}$$

The general solution to (1.59) is called the D'Alembert's solution:

$$u(x,t) = f(x-ct) + g(x+ct). \tag{1.60}$$

where f and g are arbitrary functions and each of them represents a solution to Eq. (1.59). The solutions $f(x-ct)$ and $g(x+ct)$ represent a wave moving to the right and to the left, respectively, with speed c without change of shape. The wave equation (1.59) can then be split into two first order partial differential equations

$$\begin{cases} u_t + cu_x = & 0 \\ u_t - cu_x = & 0 \end{cases} \tag{1.61}$$

The first equation describes the wave motion to the right, while the second equation describes the wave motion to the left. In the next sections we consider only the equation for the left to right moving one dimensional wave.

1.5.3 Linear waves

An equation or a system of equations is linear if the linear combination of any two or more of its solutions is also a solution: u_1, u_2, ... u_n are solutions, so $\sum u_i$ is also a solution.

The advection equation

The one dimensional linear advection equation is the equation of the form

$$u_t + cu_x = 0, \tag{1.62}$$

where $u = u(x,t)$, and c is constant. It describes the transport of a scalar field $u(x,t)$ by a fluid flow of constant speed c. For example, this equation can describe the transport of oil dropped in a river flowing with speed c. In this case, $u(x,t)$ is the concentration of oil at position x at time t. The advection equation is a linear evolution partial differential equation whose general solution is of the form $u(x,t) = f(x-ct)$ where f is an arbitrary function. One characteristic of this solution is that it represents a perturbation that moves without deformation along the x-axis: the value of the perturbation at point x is the same as its value at previous

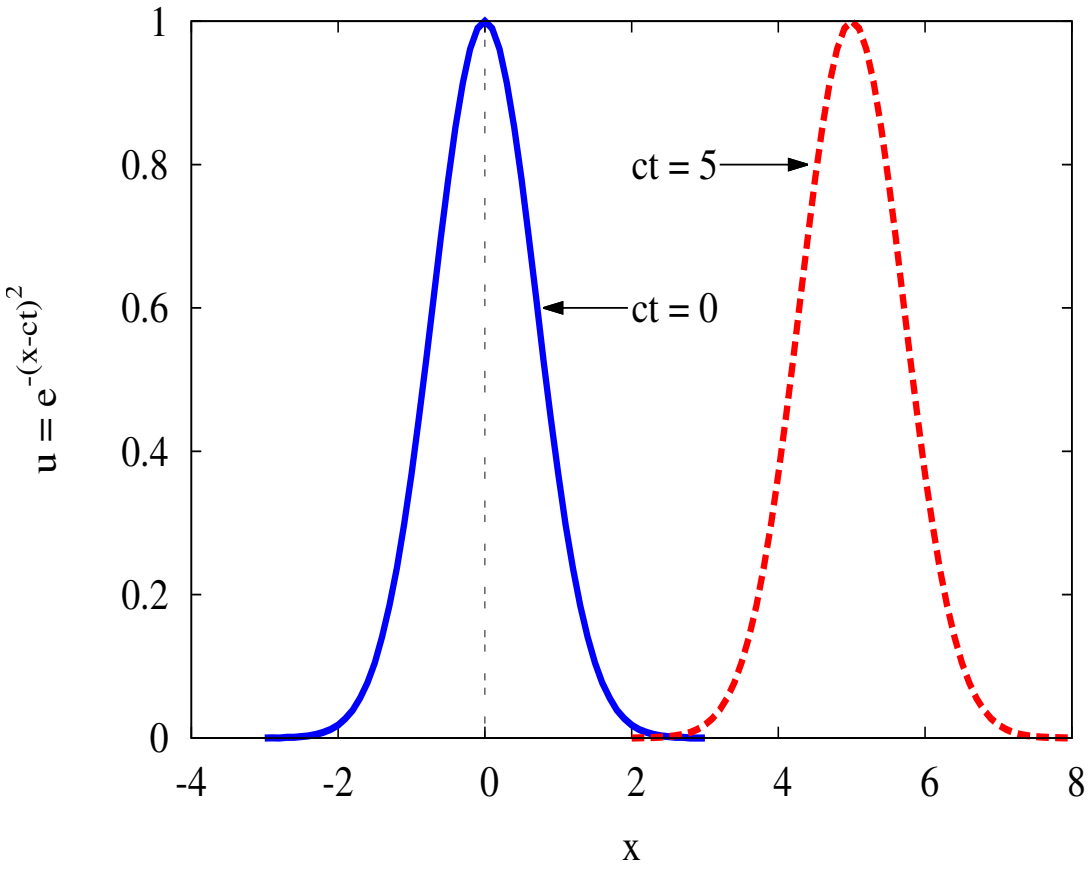

Figure 1.4: The solution $u(x,t) = f(x-ct) = e^{-(x-ct)^2}$ represents a perturbation that moves along x axis without change of its shape. The solution is plotted at $ct = 0$ and $ct = 5$.

position $x - \triangle x$ at earlier time such that $\triangle x = ct$. Fig. 1.4 shows a Gaussian plotted at two values of ct, 0 (blue solid curve) and 5 (red dashed curve). This figure shows that the red curve is the same as the blue curve displaced to the right by $\triangle x = 5$ in arbitrary units.

Among the different forms of the function $f(x-ct)$, two are interesting :

1. Plane wave solution: A plane wave solution to the equation (1.62) is the

solution of the form

$$u(x,t) = Ae^{i(kx-\omega t)}, \tag{1.63}$$

where A is the wave amplitude, k is its wave number, and ω is its angular frequency. The ratio $k/2\pi = 1/\lambda$, where λ is the wave wavelength, is the number of waves per unit length, and $\omega/2\pi = f$, where f is the wave frequency, is the number of waves per unit time. Such a wave is localised in the whole space. Differentiating (1.63) with respect to time coordinate t and space coordinate x and replacing in (1.62), we get a condition that the angular frequency ω and the wave number k have to satisfy for (1.63) to be a solution:

$$\omega = ck. \tag{1.64}$$

This relation between ω and k is called the dispersion relation. The dispersion relation is the functional dependence of the wave phase velocity on the wave number k: $\omega = \omega(k)$.

Because c is constant, this relation tells us that the plane wave is a solution to the advection equation if the wave angular frequency is a linear function of the the wave number k. The solution to equation (1.62) is then a travelling wave with wave speed c:

$$u(x,t) = Ae^{ik(x-ct)}. \tag{1.65}$$

Using the relation (1.64), we define the wave phase velocity and the wave group velocity. The wave phase velocity is defined as

$$v_{ph} = \frac{\omega}{k}. \tag{1.66}$$

It is the velocity of motion of a point of constant phase. The wave group velocity is defined as

$$v_{gp} = \frac{\partial \omega}{\partial k}, \tag{1.67}$$

and represents the velocity at which energy is transferred by the wave. For advection equation (1.62), we see that the phase and group velocity are equal to each other. In general, when ω is a linear function of k, the wave phase speed and group speed are equal to each other and we say that the wave is non dispersive. An initial

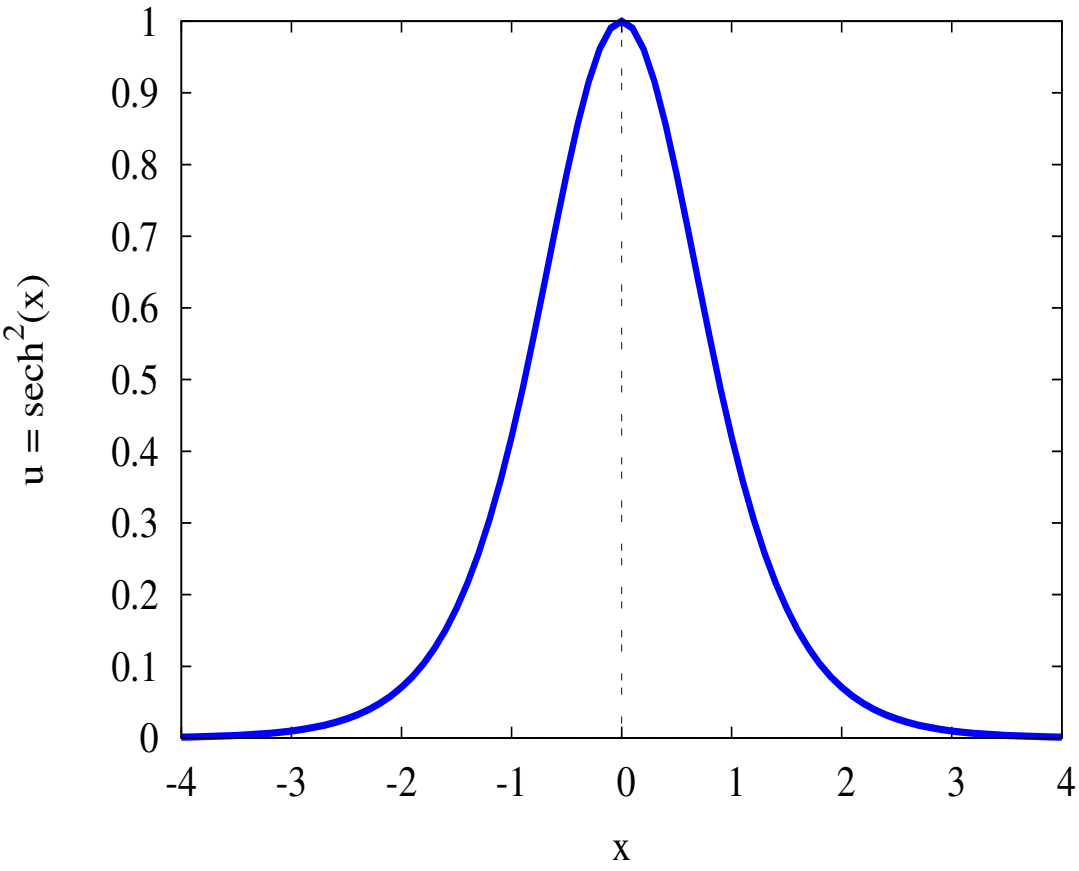

Figure 1.5: Soliton solution. The soliton amplitude $A = 1$ and the wave is plotted at $ct = 0$.

perturbation of the form $F(x)$ can be decomposed in Fourier components with different wave numbers and the general solution of Eq. (1.62) is a linear superposition of all Fourier components. Because for a nondispersive medium all Fourier components move at the same phase speed, the wave retains the same shape over time.

2. Solitary wave solution: Another class of solutions to the equation (1.62) is the solitary wave solution, commonly known as soliton solution. Analytically, this solution has the form

$$u(x,t) = A\,sech^2(x-ct), \tag{1.68}$$

where A is the wave amplitude. A soliton is a travelling wave having the following

properties:

1. It retains its shape;
2. It is localised in space;
3. Solitons pass through each other unchanged (particle like property).

We will see that soliton solutions exist for some other partial differential equations, and particularly for some nonlinear partial differential equations. A wave that moves undeformed in space and time is however almost hypothetical. In general waves arising naturally are damped or disperse. Dispersion means that the different Fourier components move with different phase speeds and the wave is destroyed, and damping means that the wave amplitude decreases and finally gets to zero. Equation (1.62) is not able to describe such behaviour which requires to include terms with higher derivatives.

Linear dissipative waves

Equation (1.62) describes the transport of the scalar field u due to flow of the fluid with speed c. In natural phenomena, the transport of u is accompanied by its diffusion. Diffusion is a process of motion of a physical property (concentration, heat, etc.) as a result of the presence of a gradient of that property in the considered medium. Examples of diffusion processes include the heat conduction (heat moves from hot to cold places) and transport of matter from high concentration to low concentration. Therefore the diffusion tends to smooth out differences in a physical property. The 1-D equation combining transport and diffusion is called the advection-diffusion equation and has the form

$$u_t + cu_x - Du_{xx} = 0, \tag{1.69}$$

where D is a positive constant called the coefficient of diffusion and represents the dissipative effect of the scalar field u. Replacing the plane wave ansatz in (1.69) we get the dispersion relation $\omega = ck - iDk^2$ and the plane wave solution has the form

$$u(x,t) = Ae^{-Dk^2t}e^{ik(x-ct)}. \tag{1.70}$$

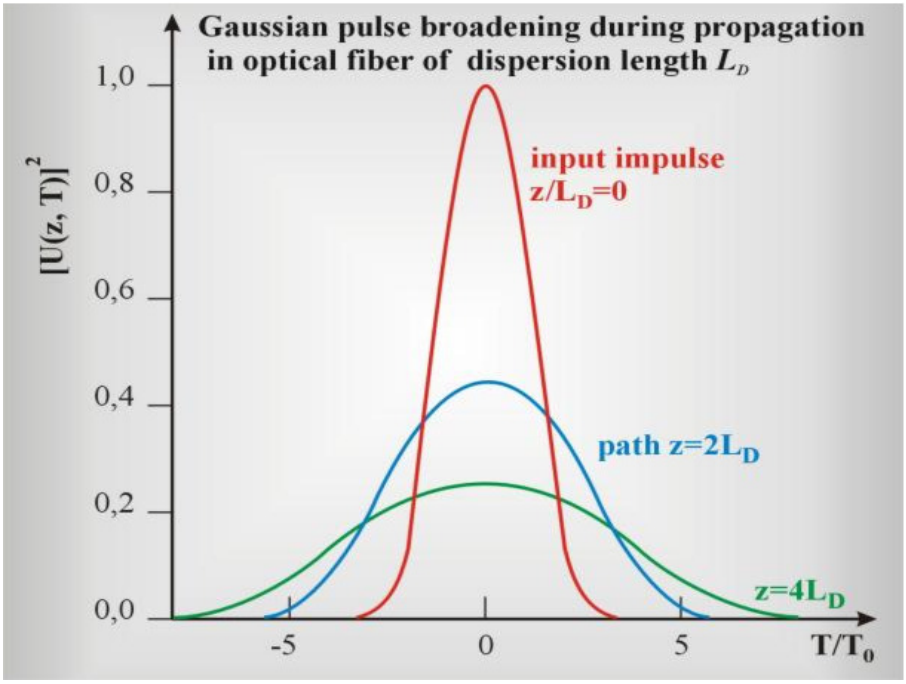

Figure 1.6: Effect of dispersion. Image taken from internet at `https://www.semanticscholar.org`.

This is a plane wave solution whose amplitude decays exponentially with time. As the energy transported by a wave is proportional to the square of its amplitude, then the energy of a dissipative wave decreases with time.

Linear dispersive waves

The dispersion is another physical phenomenon that tends to reduce the oscillation in a system. In a dispersive medium, waves with different frequencies move with different phase speeds. To model the wave dispersion we add to (1.62) a third order spatial derivative and get

$$u_t + cu_x + \beta u_{xxx} = 0 \tag{1.71}$$

Consideration of the plane wave solution leads to the dispersion relation $\omega = ck - \beta k^3$. From this relation, the phase speed is given by

$$v_p = c - \beta k^2, \tag{1.72}$$

and the group speed is

$$v_g = c - 3\beta k^2. \tag{1.73}$$

For positive β, the wave phase speed is larger than the group speed and both are quadratic functions of the wave number k. Hence the low frequency (longer wavelength) components travel with larger phase velocities than high frequency (shorter wavelength) components. The wave spreads out and its width increases with time. This effect is shown in Fig. 1.6.

1.5.4 Nonlinear waves

The terms describing the dissipation and dispersion have shown to be not enough to describe natural phenomena, most of which can be described by nonlinear equations. A nonlinear differential equation is an equation combining the function and its derivative to an order higher than one. In this case, if two or more solutions of that equation are known, we cannot apply the principle of superposition to find another solution.

Inviscid Burgers equation

To understand the effects of nonlinearity, we consider a nonlinear equation in which the wave speed c is a linear function of the wave amplitude. In the simplest case the function $c(u) = u$ is an increasing function of u and the wave speed increases with the wave amplitude. Parts of the wave with larger displacement move faster than those with smaller displacement and overtake them. Equation with such nonlinearity is called the Burgers equation:

$$u_t + uu_x = 0. \tag{1.74}$$

The disturbance u depends on both time t and space x coordinates and the space coordinate x is also a function of time $x = x(t)$. A solution to Eq. (1.74) with initial condition $u(x,0) = u_0(x)$ (Cauchy problem) is

$$u(x,t) = u_0(x - u(x,t)t). \tag{1.75}$$

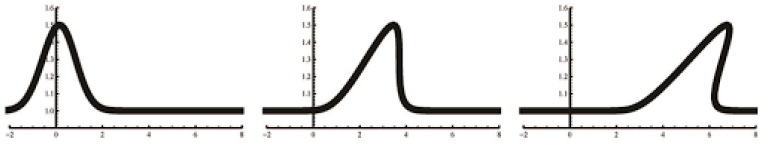

Figure 1.7: Effect of nonlinearity

The gradient of function $u(x,t)$ is

$$u_x = \frac{u_0'}{1+u_0't}, \tag{1.76}$$

where $u_0' = \frac{\partial u_0}{\partial x}$. For the parts of the initial disturbance for which $u_0' > 0$, i.e. the propagation speed is an increasing function of x, $1+u_0't$ increases with time. The slope u_x decreases with time and the wave profile flattens. For the parts of the initial disturbance for which $u_0' < 0$, $1+u_0't$ decreases with time, the slope u_x increases with time and the wave profile steepens. This is shown in Fig. 1.7. In this figure, the curve to the left is the initial profile $u_0(x)$, a Gaussian pulse moving to the right with $u_0' > 0$ at the trailing edge and $u_0' < 0$ at the leading edge. The curve in the middle represents the same profile at time $t > 0$. It shows that the trailing edge is flatter while the leading edge is steeper than at $t = 0$. With time this deformation continues until the slope u_x on the disturbance parts with initial negative gradient becomes infinitely large, when $1+u_0't$ approaches zero at time

$$t_b = -\frac{1}{min\{u_0'\}}. \tag{1.77}$$

This time is also called the breaking time. At $t = t_b$, the function $u(x,t)$ has an infinite slope in $\{x,u\}$ space and the solution $u(x,t)$ coincides with the $u-$axis, becoming infinitely multivalued. This discontinuity is called a *shock*. For all $t > t_b$ the solution $u(x,t)$ is multivalued. Physically, multiple valued function would mean that a physical quantity like density, pressure, velocity etc. has two or more values at the same position. Because this is not possible, the equation (1.74) fails to describe the physical phenomenon.

While mathematically this inconsistency can be solved by assuming a weak solution at $t > t_b$, i.e. a solution that is not necessarily a differentiable nor continuous

function, on the physical point of view, we go back to the problem under study and improve the model equation (1.74). Eq. (1.74) describes the motion of a non-viscous incompressible fluid and ignores the fluid viscosity. When the slope u_x becomes important, it is no longer possible to neglect the viscosity and including a viscosity related term to Eq. (1.74) improves the model, leading to the viscid Burgers equation whose solution does not break.

Nonlinear dissipative waves: the viscid Burgers' equation

The viscid Burgers equation is an equation that associates nonlinearity and dissipation. It is of the form

$$u_t + uu_x = \nu u_{xx}. \tag{1.78}$$

where ν, the viscosity of the compressible fluid is a positive constant. When the right hand side term is negligible ($\nu \to 0$), we recover equation Eq. (1.74). For small amplitude solutions, the nonlinear term can be neglected and the remaining equation is the diffusion equation whose solution dies out as time increases. For large amplitude solutions, the nonlinear term first dominates and the solution tends to the shock wave. However near the breaking point, the viscosity term grows much faster than the nonlinear term and starts playing a role of preventing the breakdown. This way, the solution u remains smooth owe to the presence of viscosity, but the amplitude of the solution reduces progressively and the wave dies out after some time. Therefore the combination of nonlinearity and dissipation does not lead to a permanent shape structure.

Nonlinear dispersive waves: KdV equation

It is thus obvious that nonlinear nondispersive wave equation (inviscid Burgers equation) does not admit a soliton solution, rather the leading edge of the wave profile steepens due to the nonlinearity. On the other side, the solution to the linear dispersive wave equation spreads out with time as a result of dispersion of different components of the wave. Although nonlinearity and dispersion have each of them the tendency to break the wave profile, it has been proven that an equation that combines them appropriately can result in a stable solution. This happens when the

nonlinear steepening effects balance the dispersive spreading effects. An equation with such a balance is called the Korteweg de Vries (KdV) equation. The KdV equation was first derived by Diederik Johannes Korteweg together with his PhD student Gustav de Vries while studying shallow-water gravity waves. In a fixed frame of reference, the KdV equation has the form

$$u_t + cu_x + Auu_x + Bu_{xxx} = 0, \tag{1.79}$$

where $u(x,t)$ is the height of the water's surface above its quiescent position and c is the speed of small amplitude waves. A is the nonlinear coefficient and B is the dispersion coefficient.

Later, it was found that the KdV equation is also appropriate to describe internal waves in oceans and atmosphere, the propagation of nonlinear acoustic waves in liquids with gas bubbles [55, 56], to model arterial pulse pressure waves and cardiac hemodynamics [57], to describe the propagation of ion acoustic waves in plasmas [58] etc.

The second term on the left hand side is eliminated by performing the transformation

$$\begin{cases} x' = & x - ct \\ t' = & t \end{cases} \tag{1.80}$$

and the observer is now in a reference frame moving with velocity c. Dropping the primes on the coordinates, the KdV equation in this moving reference frame has the form

$$u_t + Auu_x + Bu_{xxx} = 0. \tag{1.81}$$

The first term u_t characterises the time evolution of the wave. That is why Eq. (1.81) is referred to as an evolution equation. The second nonlinear term arises from the convective derivative in the Navier-Stokes equation and describes the wave steepening, while the third term expresses the dispersion of the wave.

The KdV equation admits three types of solution, the soliton solution, the nonlinear periodic wave solution and the multiple soliton solution. While in general

nonlinear partial differential equations have no exact analytical solutions, the KdV equation is one of the rare nonlinear partial differential equations having an exact analytical solution. Some other nonlinear partial differential equations having soliton as an exact solution include
Nonlinear Schrödinger equation (NLS equation):

$$iu_t + \nu|u|^2 u + \delta u_{xx} = 0, \tag{1.82}$$

where $i^2 = -1$ is the imaginary number, $\delta > 0$ is the dissipation coefficient and ν is the nonlinearity coefficient. The NLS equation describes the wave propagation and nonlinear effects in nonlinear media like in optical fibers and also in plasmas.
Nonlinear Sine-Gordon equation (NLSG equation):

$$u_{tt} - u_{xx} + sin(u) = 0. \tag{1.83}$$

The Sine-Gordon equation is used in different areas of research, in mechanical transmission lines for example where $u(x,t)$ represents an angle of rotation of the pendulums.

1.6 Some nonlinear wave structures

The plasma fluid model is the simplest model for a qualitative and quantitative description of plasma behaviour. A plasma is a nonlinear medium, affected by electric and magnetic fields through the Lorentz force. This complex medium of particles and fields supports a large variety of collective wave phenomena. Identifying these waves is useful for understanding their effects on human life and environment, either directly or indirectly. This then justifies why the formation and propagation of nonlinear wave structures has become one of the principal research areas in Physics of Plasmas. Examples of such nonlinear structures are solitary waves, double layers, shocks, sheaths and vortices.

1.6.1 Solitary waves

A solitary wave was observed and studied for the first time by a Scottish naval architect John Scott Russell in 1834 on the Union Canal in Scotland. He later described

his observation in these words [59]: *I was observing the motion of a boat which was rapidly drawn along a narrow channel by a pair of horses, when the boat suddenly stopped—not so the mass of water in the channel which it had put in motion; it accumulated round the prow of the vessel in a state of violent agitation; then suddenly leaving it behind, rolled forward with great velocity, assuming the form of a large solitary elevation, a rounded, smooth and well defined heap of water, which continued its course along the channel apparently without change of form or diminution of speed. I followed it on horseback, and overtook it still rolling on at a rate of some eight or nine miles an hour, preserving its original figure some thirty feet long and a foot to foot and half in height. Its height gradually diminished, and after a chase of one or two miles I lost it in the windings of the channel. Such, in the month of August,* 1834*, was my first chance interview with that singular and beautiful phenomenon which I have called the Wave of Translation*.

After this discovery, Russel spent time reproducing the solitary wave phenomenon in laboratory experiments. However most of his contemporary scientists, including Sir George Gabriel Stokes and George Biddell Airy did not believe in Russel's discovery, arguing that waves of permanent form could not exist. The doubt persisted until, in 1895, Korteweg and de Vries published their paper in which the nonlinear partial differential KdV equation (1.79) was derived. Washimi andTaniuti [58] have shown that KdV equation also describes a weakly nonlinear one dimensional ion sound wave distubances in a plasma, traveling the ion sound speed.

After the publication of the paper by Korteweg and De Vries, the theory of nonlinear waves was stored in cupboards by the mathematical community until, in 1965, Zabusky and Kruskal [60] published a seminal paper in which they showed that when two solitary waves with different amplitudes collide, they emerge unchanged from the collision. This is the particle property of the solitary waves that they renamed as *Solitons*. The paper by Zabusky and Kruskal revived the interest in the field of nonlinear wave theory and nowadays, generation, formation and propagation of solitons is a major experimental and theoretical research area in several branches of science, including but not limited to nonlinear optics [61], oceanography [62], atmospheric science [63], bioscience [64, 65], plasma science etc.

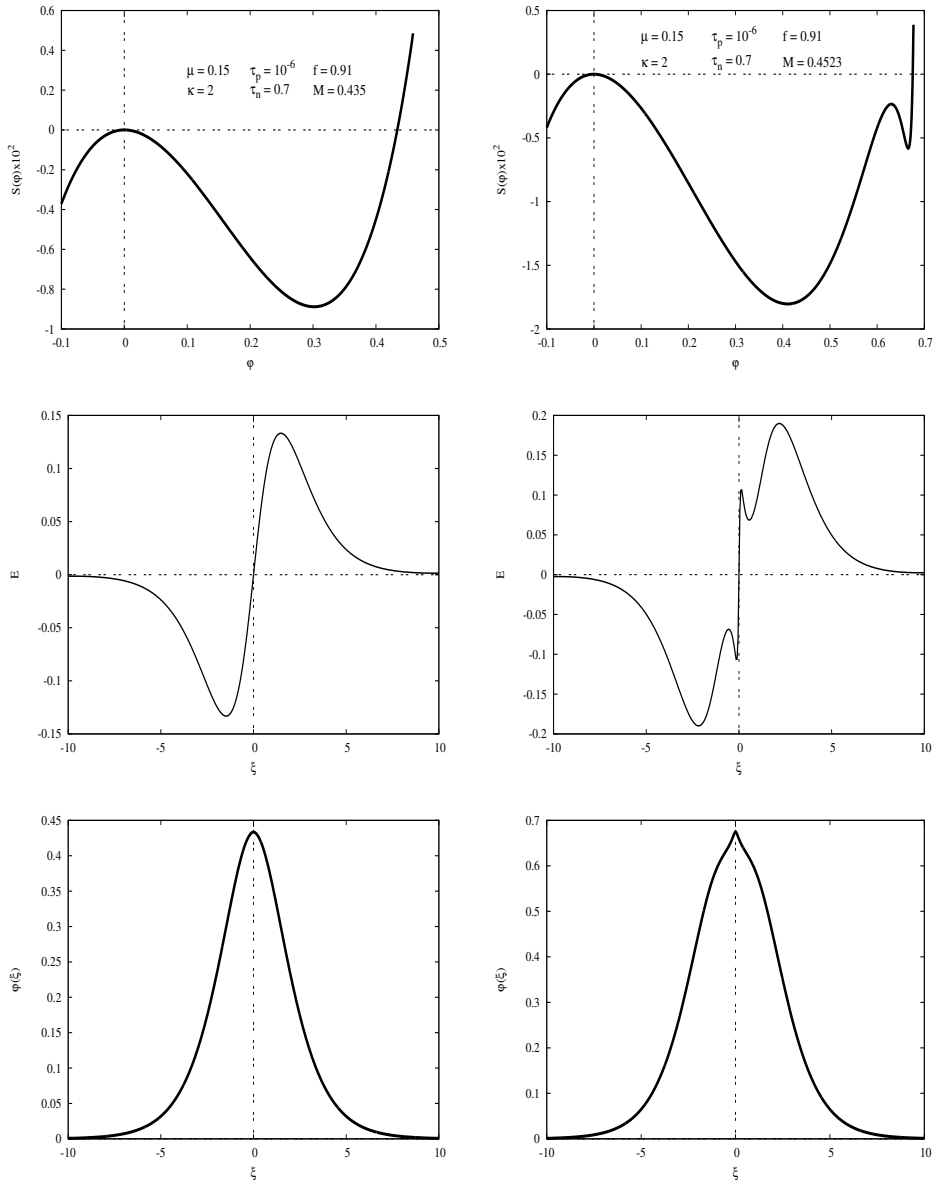

Figure 1.8: The upper panels present the potential well of a standard soliton (upper left panel) and supersoliton (upper right panel). The middle panels present the corresponding electric field signatures and the lower panels their profiles. The presence of supplementary wings on the electric signature of a supersoliton is well displayed. As a consequence the supersoliton profile does not present a bell-shaped profile as it is in the case of a standard soliton.

In plasma science, electrostatic solitons have been observed in space as bipolar electric pulses in the direction of magnetic field as shown in Fig. 1.8 middle left panel. The upper left panel shows the potential well of a standard positive potential soliton, and the middle and lower panels show the corresponding bipolar electric field and soliton profiles respectively.

More complicated pulses have been observed however [66]. A supersoliton is a nonlinear structure characterised by the presence of supplementary maxima on the wings of the bipolar structure of a soliton [67]. Fig. 1.8 right panels illustrates the supersoliton potential well (upper right panel), the corresponding electric field with two auxilliary maxima superimposed on the bipolar structure (middle right panel) and the supersoliton profile (lower right panel). Supersolitons have been introduced by Dubinov [6] in 2012 and since then they have been found to propagate in different plasma configurations [68–70].

1.6.2 Double layer

Double layers constitute another class of nonlinear structures that can be described by KdV like equations. A double layer is a structure in a plasma consisting of two layers with equal in magnitude but opposite electric charges. There is therefore an abrupt change of the electric potential from one layer to another with a subsequent electric field between the two layers directed from the positive layer to the negative layer, while outside the double layer the plasma remains neutral.

Double layers are classified as strong and weak depending on the thermal energy of the plasma components. A double layer is strong when the potential drop across the double layer is larger than the thermal potential $k_B T/e$ of the plasma components. A positively charged particle entering the double layer region from the higher potential will be accelerated through the DL. If it is a negatively charged particle that enters the DL from the higher potential, it will be decelerated, and for many particles, when their kinetic energy is less than the potential energy across the DL, they will be reflected without crossing the DL. For particles entering the DL region from the lower potential it is the negatively charged particles that are

accelerated while positively charged particles are reflected.

A double layer is weak when the potential drop across the double layer is smaller than the thermal potential of the plasma components.

On the mathematical point of view, small amplitude double layers are described by a KdV equation with a higher order nonlinearity. Such equation is also called mixed modified KdV equation (Eq. (1.96) in Sec. 1.7.1) and its double layer solution has the form

$$\varphi = \frac{\varphi_m}{2}\left[1 \pm tanh\left(\frac{\zeta}{\Lambda}\right)\right] \tag{1.84}$$

where the double layer amplitude φ_m is given by

$$\varphi_m = -\frac{A}{C} \tag{1.85}$$

and the double layer width

$$\Lambda = \left[\frac{\varphi_m}{2}\sqrt{\frac{-C}{6B}}\right]^{-1}. \tag{1.86}$$

Double layers have been observed in space plasma as monopolar pulses [71, 72].

1.7 Nonlinear methods

1.7.1 Reductive perturbation method

Many natural systems are modelled by nonlinear partial differential equations. The pendulum and fluid flow are elementary examples. Nonlinear partial differential equations describe wave phenomena in fluid mechanics, plasma physics, biophysics, neurology, optics etc. However it is not trivial to find an exact solution to a nonlinear partial differential equation (NL PDE). Often the non solvable NL PDE under study is linearised and replaced by a solvable linear equation. But in this process information contained in the nonlinearity is lost and cannot be captured by the solution of the linear equation. The linearisation of continuity, momentum and Poisson's equations is developed in appendix *A*. To account for nonlinearity, some approximations have to be used. The reductive perturbation technique (RPM) is one of

the techniques used to determine approximate solutions to NL PDE for which exact analytical solutions cannot be obtained. This method applies for weakly nonlinear phenomena. It considers small deviations from equilibrium and reduces non solvable NL PDE to solvable NL equations such as Burgers equation, KdV equation and NLS equation.

In the study of electrostatic waves in a plasma, the magnetic field is static. Consequently the Faraday's law of electromagnetic induction shows that the electric field is electrostatic also and therefore it is a gradient of the scalar electric potential field. Equations relevant for the wave propagation are therefore
the continuity equation:

$$\frac{\partial n_j}{\partial t} + \nabla.\left(n_j \vec{u}_j\right) = 0, \tag{1.87}$$

the momentum equation:

$$m_j n_j \left[\frac{\partial \vec{u}_j}{\partial t} + \left(\vec{u}_j.\nabla\right)\vec{u}_j\right] = q_j n_j \left[\vec{E} + \vec{u}_j \times \vec{B}\right] - \nabla P_j, \tag{1.88}$$

where pressure P_j and density n_j of the j^{th} plasma component species are related by an equation of state, and the system is closed by Poisson's equation

$$\nabla.\vec{E} = \frac{1}{\varepsilon_0}\rho, \tag{1.89}$$

where the net electric charge ρ is given by

$$\rho = \sum_j q_j n_j. \tag{1.90}$$

and the electrostatic field vector $\vec{E}$ is given by

$$\vec{E} = -\nabla.\varphi \tag{1.91}$$

where φ is the electrostatic potential. Eqs. (1.87) and (1.88) are nonlinear. To convert them into a tractable nonlinear partial differential equation, we use the procedure initiated by Gardner and Morikawa [73]. In a pioneering research paper, Gardner and Morikawa have shown that it is possible to reduce a system of hydromagnetic equations to a KdV equation by applying the stretched coordinates. Later

washimi and Taniuti [58] used the same technique to reduce a system of equations similar to (1.87) and (1.88) to a KdV equation.

Following Washimi and Taniuti [58], we introduce the following stretched coordinates

$$\xi = \varepsilon^{1/2}(x - vt), \tau = \varepsilon^{3/2}t \tag{1.92}$$

that transform the fluid equations to a reference frame moving with velocity v. The variable ε is a small parameter.

Next, we let a function f represents any of the system variables, plasma component density n, its velocity u, the electrostatic potential φ, etc. Considering small deviations from the equilibrium, the variable f is given as a power series of ε

$$f = f_0 + \varepsilon f_1 + \varepsilon^2 f_2 + \varepsilon^3 f_3 + ..., \tag{1.93}$$

where the coefficients f_j are functions of the plasma parameters. For a plasma at equilibrium far from the perturbation, $f_0 = 0$ if f represents the electrostatic potential or the flow velocity of a plasma component. Expansion (1.93) is valid provided a small perturbation produces a small change of $f(x,t)$.

Then substituting expansion (1.93) in Eqs. (1.87) to (1.89) along with space-time stretched coordinates (1.92) and comparing coefficients of various powers of ε results in a system of partial differential equations [74].

Coefficients under the *zeroth* power (ε^0) yields the equilibrium condition (charge neutrality) with equality between positive and negative charges.

Under the first nonzero power of the small parameter ε, we get the dispersion relation that determines the spectrum of possible values for the speed v. The speed v is found to coincide with the phase speed of the linear acoustic wave, also obtained by the linearisation method.

The coefficients under the next nonzero power of ε yield the KdV equation. For the electrostatic potential, this equation has the form

$$\frac{\partial \varphi_1}{\partial \tau} + A\varphi_1 \frac{\partial \varphi_1}{\partial \xi} + B\frac{\partial^3 \varphi_1}{\partial \xi^3} = 0, \tag{1.94}$$

where the coefficients A and B are functions of plasma parameters. For some combinations of plasma parameter values, the nonlinear coefficient A and the dispersion coefficient B can balance so that a solution to the KdV equation yields a stable nonlinear structure. In the laboratory frame, that solution has the form

$$\varphi(x,t) = \frac{3\delta M}{A} sech^2 \left[\sqrt{\frac{\delta M}{4B}} (x - Mt) \right], \tag{1.95}$$

where $M = v + \delta M$ is the wave phase speed in the laboratory frame and δM is the wave phase speed as viewed from the frame, moving with velocity v. As the dispersion constant B is a positive constant, $\delta M > 0$ for a real function $\varphi(x,t)$. Therefore solitary waves are super acoustic structures, meaning that they move at speeds higher than the sound speed. and their amplitudes vanish when $M = v$ or $\delta M = 0$. Such solitary waves described by a KdV equation are called KdV solitary waves[75]. However in recent years it has been shown that in some plasma configurations solitary waves with finite amplitude at sound speed are possible [75, 76]. These cannot be described by KdV equation and consequently are called non-KdV solitary waves.

From Eq. (1.95) the amplitude of the solitary wave is proportional to the solitary wave speed and inversely proportional to the nonlinear coefficient in the KdV equation. Therefore the taller the solitary waves are, the faster they move. Their polarity is always given by the sign of the nonlinear coefficient. As the soliton width is inversely proportional to the square root of the solitary wave speed, taller solitary waves are thinner. The details of the derivation of KdV equation for the fast mode in a negative ion plasma and its solution (1.95) are given in appendix B.

There may be plasma compositions under which the nonlinear coefficient A vanishes $(A = 0)$. In such situations we say that the plasma composition is critical and the KdV equation fails to describe the balance between nonlinearity and dispersion. To solve this problem we consider the next order which yields a modified KdV

equation (mKdV) [77]

$$\frac{\partial \varphi}{\partial \tau} + C\varphi^2 \frac{\partial \varphi}{\partial \xi} + B\frac{\partial^3 \varphi}{\partial \xi^3} = 0 \tag{1.96}$$

whose solution is also a solitary wave, when C is positive and a double layer when C is negative.

For near critical composition, the coefficient A is very small but not *zero* and instead of the mKdV, we obtain a mixed modified KdV equation

$$\frac{\partial \varphi}{\partial \tau} + A\varphi\frac{\partial \varphi}{\partial \xi} + C\varphi^2 \frac{\partial \varphi}{\partial \xi} + B\frac{\partial^3 \varphi}{\partial \xi^3} = 0. \tag{1.97}$$

For localised structures, Eq. (1.97) has soliton solutions with both polarities and double layer solutions depending on the relative strengths of the coefficients A, B and C. Solutions to modified and mixed modified KdV equations are also given in appendix B.

1.7.2 Pseudopotential method

When the wave amplitude is large, the RPM is no longer a valid approximation. The arbitrary large amplitude method, also called the Sagdeev pseudopotential [78] method, uses the multifluid equations and reduces them to a single equation in which the soliton is compared to a particle in a potential well. For such a particle oscillating along the x axis, the one dimensional equation has the form

$$m\frac{d^2x}{dt^2} + \frac{dV}{dx} = 0, \tag{1.98}$$

where V is the potential well and the one dimensional force applied on the particle is found as $F = -\frac{dV}{dx}$. The equation for the soliton electrostatic potential has thus the form

$$\frac{d^2\varphi}{dx^2} + \frac{dS}{d\varphi} = 0. \tag{1.99}$$

This equation can be transformed into an energy-like equation

$$\frac{1}{2}\left(\frac{d\varphi}{dx}\right)^2 + S(\varphi) = 0 \tag{1.100}$$

where the function $S(\varphi)$ is called the Sagdeev pseudopotential. This function depends on all plasma parameters but it is analysed as a function of the electrostatic potential.

For analogy, Eq. (1.100) describes the oscillation of a pseudo-particle with unit mass, coordinate φ and time x in a potential well $S(\varphi)$. Thus if the function $S(\varphi)$ is known, it is analysed for soliton existence domain the same way the potential V is analysed for the existence of various states of the particle.

Soliton existence conditions

The conditions fulfilled by the function $S(\varphi)$ for the Eq. (1.100) to yield soliton solution are [32]:

1. $S(0,M) = S'(0,M) = 0$;
2. $S''(0,M) \leqslant 0$, the origin is unstable;
3. $S(\varphi_m, M) = 0$ for some M in the soliton existence domain and $\varphi_m \neq 0$;
4. $S(\varphi, M) < 0$ for $0 < |\varphi| < |\varphi_m|$; and
5. For double layers, $S'(\varphi_m, M) = 0$ for some M in addition to $1-4$.

Here primes designate the derivatives of the Sagdeev potential relative to the electrostatic potential. The soliton amplitude φ_m is such that there is no other root between $\varphi = 0$ and $\varphi = \varphi_m$.

1.8 Motivation

Although solitons were first investigated in the context of shallow water waves, solitons occur in many other branches of science like molecular biology [64, 65], nonlinear optics [61, 79, 80], ocean and planetary atmospheres [81–85].

Space, astrophysical and laboratory plasmas are on the forefront of the list of medium in which nonlinear structures have been observed. The observations in situ

have been made possible by the use of man made space crafts and satellites orbiting the earth at different altitudes from the earth's center.

Solitary waves and double layers in space plasmas were reported for the first time by Temerin et al. [86] after analysing waveform data taken by $S3-3$ polar-orbiting satellite in the auroral acceleration region at $6,000$ to $8,000km$ of altitude. The electric field of these structures were parallel to the background magnetic field and were thus of electrostatic nature. Fast solitary waves travelling antiearthward were also observed by FAST satellite in the mid altitude auroral zone [87].

Analysing also the waveform data obtained by Plasma Wave Instrument (PWI) onboard Geotail spacecraft, Matsumoto et al. [88] reported the presence of electrostatic solitary waves in the Plasma Sheet Boundary Layer (PSBL) during the broadband electrostatic noise (BEN). They showed that most of the BEN in the PSBL is made of electrostatic solitary waves characterised by bipolar electric field aligned with the background magnetic field. Both Geotail and CLOUSTER satellites have recorded electrostatic solitary waves associated with reconnection near the diffusion region and along PSBL [90]. Recorded data have shown that the BEN waves are not random noises, but are a series of large amplitude electric bipolar and offset bipolar pulses.

In the outer Van Allen belts, electrostatic and electromagnetic solitary waves and double layers have been detected by the Van Allen Probes [89]. These nonlinear structures represent the dominant element of wave activity in the Van Allen radiation belts.

In the unperturbed solar wind at $200R_E$, the spacecraft WIND observed and recorded the presence of a continuous electrostatic activity, appearing to be a mixture of wave packets and weak double layers [91].

Nonlinear structures have also been found in many other space and astrophysical plasmas, in the earth's magnetosheath [92], in the earth's magnetopause [93] and in the planetary magnetospheres [94].

In laboratory plasmas, fast mode ion acoustic solitary waves have been observed in a negative ion plasma using a single ended Q machine. The plasma composition, K^+ positive ions, SF_6^- negative ions and electrons was chosen as the fast mode has a negligible damping when the ratio of negative ion mass to positive ion mass is large. Conversely, Ichiki et al. [12] have shown that when the ratio of negative ion mass to positive ion mass is small it is the slow mode that can be observed. The slow mode in a negative ion plasma has been observed by Ichiki et al. [12] in a $X_e^+ - F^-$ and by Handique et al. [11] in a $A_r^+ - F^-$. Merlino et al. [95] have shown experimentally that electrostatic ion acoustic solitary waves can easily be excited in a dusty plasma with negatively charged grains.

Double layers have been also observed experimentally in a negative ion plasma by Merlino et al. [18] in a triple-plasma device, Stenzel et al. [96, 97] in a double plasma device.

In situ, ground-based and laboratory observations of nonlinear structures in space and laboratory plasmas are numerous and various. This omnipresence questions about the role these waves play in the dynamics of space and laboratory plasmas. Observations from FAST satellite have shown field-aligned up-going electron fluxes [87]. As solitary waves are capable of trapping charged particles, it is assumed that solitary waves directed out of the ionosphere transport charged particles to the outer magnetosphere [98]. This transport mechanism constitutes a mechanism for charged particle loss in the radiation belts, protecting the earth from energetic solar wind radiations [89]. Solitary waves and other wave modes play an important role in the dynamics of magnetic reconnection [90]. They have been shown to cause stochastic heating in the solar corona [99, 100]. In the polar regions, double layers have been identified in regions where electric field is parallel to the magnetic field [86]. These double layers are responsible for acceleration of electrons that produce visible aurora.

These and many other applications of the solitary waves motivated us to undertake research whose results are presented in this thesis.

1.9 Problem statement

Nonlinear processes is an area of research that is expanding. Different aspects related to solitary waves such as generation, formation and propagation mechanisms in different plasma configurations are not yet fully understood. In this study we have focused on the study of the existence and propagation of linear and nonlinear electrostatic solitary waves in some multispecies plasmas as encountered in space, astrophysical and laboratory plasmas.

1.10 Contributions to the body knowledge

The base for the thesis is a collection of published papers. These papers are presented in their full length in *Chapters* 2, 3 and 4 respectively. In this section, we present a summary of the results obtained in our investigations. These results constitute our contributions to the body knowledge in the area of nonlinear processes in Physics of plasmas.

1.10.1 Summary of the results of paper $N^o 1$

In chapter 2, we have investigated in details the fast mode in a negative ion plasma. A common result for the fast mode in a negative ion plasma is that only positive (compressive) solitons are supported at low values of negative ion density and only negative (rarefactive) solitons are supported at high values of negative ion density. At the intermediate values of negative ion density both positive and negative solitons coexist. Coexistence of compressive and rarefactive solitons in this context means that one possibility occurs at time depending on the initial conditions. After confirming earlier results [1, 15], we have found some new results, most of which have been published as **"Large amplitude ion-acoustic solitary waves in a warm negative ion plasma with superthermal electrons: The fast mode revisited", AIP Advances, 10, 065305 (2020).**
https://doi.org/10.1063/1.5127199 [101].

In the plasma model under investigation, the adiabatic positive ion species was treated as the cooler ion species and the adiabatic negative ions as the hotter ion species. The mass of the two ion species was expressed through the negative-to-positive ion mass ratio $\mu = m_n/m_p$. We have assumed that the mass of the cooler ion species is larger than the mass of hotter ion species. Therefore the value of the parameter μ was fixed to 0.5.

For the purpose of comparison of our results with those obtained for a two positive ion plasma model, we have introduced a parameter z that models the charge on the lighter ion species. It takes a value of $z = -1$ for a negative ion plasma and $z = 1$ for a two positive ion plasma. We have first studied a negative ion plasma with $z = -1$ and then revisited the existence of the stop bands as reported by Nsengiyumva et al. [8] in a two-positive ion plasma with $z = 1$. Both ion species are dynamic and we have retained their inertia in the fluid equations.

The parameters $\sigma_j = T_j/T_e$ $(j = n, p)$ express the ion-to-electron temperature ratio. They vary from very low values (we have used numerical value of 10^{-4}) for cold ions to values close to 1 assuming that light electrons remain hotter than ions. In the analysis of ion thermal effects in a negative ion plasma, we have taken the same values for ion-to-electron temperature $\sigma_p = \sigma_n = \sigma$ but used different values while analysing the thermal effects in a two-positive ion plasma.

The other plasma variables are the equilibrium negative-to-positive ion density ratio $\alpha = n_{n0}/n_{p0}$ whose values are in the range $0 < \alpha < 1$ avoiding the extreme values which would result in the breaching of the model.

1. In the linear approximation, we have derived the dispersion relation and have shown that the superthermal behaviour of the electrons increases the plasma shielding by reducing the electron Debye length. The linear approximation has also shown that the ion acoustic speed decreases when the electro superthermality increases. In the long wavelengths limit, the phase wave and the group wave speeds are equal to each other. For large wave vectors, only standing oscillations are possible.

2. Using the reductive perturbation method, we have derived the KdV equation and found its solitary wave solution. It was found that the soliton amplitude is of the order of the small expansion parameter ε while its width is inversely proportional to the square root of ε. As a result the soliton width is larger for smaller amplitudes, which justifies the balance between nonlinear steepening and dispersion spreading [58].

3. Using the Sagdeev pseudopotential method, we have first considered the soliton existence domain in $\{\alpha, M\}$ space where M is the soliton Mach number when electrons are Maxwellian ($\kappa = 1000$) and ions are cold (their temperature $\sigma_p = \sigma_n = 10^{-4}$ is very small compare to the temperature of electrons). A common result for all studies of the fast mode is that a negative ion plasma supports the propagation of only positive ion acoustic solitons at low values of negative ion density; only negative solitons at high values of negative ion density and both polarity solitons coexist for the intermediate values of negative ion density [1]. This translates in $\{\alpha, M\}$ space by the existence of a cutoff density α_p on high values for positive solitons and a cutoff density α_n on low values for negative solitons. This result is confirmed for Maxwellian electrons and cold ion species. Under these plasma parameter values, the positive soliton cutoff occurs at $\alpha_p \simeq 0.45$ and only negative solitons exist for $\alpha > 0.45$; the negative soliton cutoff occurs at $\alpha_n \simeq 0.028$ and only positive solitons exist for $\alpha < 0.028$. Both polarity solitons coexist for $0.028 < \alpha < 0.45$. On the lower side both positive and negative soliton Mach number ranges are limited by the acoustic Mach number which is the minimum Mach number, solitons being acoustic or superacoustic [102]. On the upper side positive and negative soliton Mach number ranges are limited by their maximum Mach numbers resulting from the occurrence of their respective sonic points.

4. When the electron superthermality increases, there is a shift of the minimum and maximum Mach numbers to lower values. At the same time the cutoff density ratios α_p and α_n also change with a significant decrease of α_p towards lower values. As a result the coexistence region in $\{\alpha, M\}$ space narrows with increase of the electron superthermality.

5. For a given value of density ratio α, when the ion temperature expressed through σ increases and ions are warmer, the minimum Mach numbers are shifted to higher values but the maximum Mach numbers due to the occurrence of the positive ion sonic point are shifted to lower values, resulting in a significant decrease of the range in Mach numbers of positive solitons. For enough large values of σ, positive solitons, and hence the coexistence domain, disappear and only negative solitons survive. Alternatively, when the ion thermal effects are significant, a negative ion plasma supports negative solitons only.

6. The ion and electron superthermal effects on the maximum speed soliton characteristics have been also explored. When the ion temperature increases the amplitude of the soliton of either polarity decreased, while the soliton width increased. Furthermore, it was observed that an increase of the electron superthermality also leads to a decrease of the soliton amplitude and increase of soliton width. Therefore, the ion thermal and electron superthermal effects enhance each other, and when they are combined, only small amplitude solitons can propagate in a negative ion plasma. Such solitons can well be described by the KdV theory.

7. Rearranging our analytical work so as to get a two-positive ion plasma, our results show the presence of stopbands in the soliton existence domains. Stop bands were obtained as a result of different temperature of the two positive ion species, with the more massive species being hotter than the lighter species. We have therefore used here as indicative values $\sigma_c = 10^{-6}$ for the temperature ratio of the cooler ion species and $\sigma_h = 0.12$ for the temperature ratio of hotter ion species, where subscripts c and h refer to the cool and hot ion species, respectively, avoiding the assumption $\sigma_c = \sigma_h$. With these parameter values, we recover the stopbands reported by Nsengiyumva et al. [8]. Increasing the electron superthermality by reducing the value of κ has an effect to shift the stopbands to higher values of density ratio α. Considering low values of κ, typically $1.5 < \kappa \lesssim 10$, we do not find stopbands. Similarly reducing the gap between the two ion-to-electron temperature ratios by increasing the value of σ_c while keeping a high value of κ (Maxwellian electrons) causes the stopbands to disappear. This is in agreement with the findings of Maharaj and Bharuthram [103].

1.10.2 Summary of the results of paper $N^o 2$

In chapter three we have analysed the slow mode in a negative ion plasma. The results in this chapter have been published under the title **"Large amplitude slow ion-acoustic solitons, supersoltons and double layers in a warm negative ion plasma with superthermal electrons", AIP Advances,11, 025325 (2021).** https://doi.org/10.1063/5.0039372 [104].

The slow mode exists provided at least one of the ion species has a finite temperature. In our model with adiabatic positive and negative ion species, that requirement translates to having a cooler and a hotter ion species with the terms "cool" and "hot" related to the thermal speeds and not to the kinetic temperature. For this mode, we have taken advantage of the results obtained by Ichiki et al. [12] according to which the slow mode can be observed experimentally if the mass of the negative ion species is smaller than the mass of the positive ion species. For this reason, we have used a value of $\mu = m_n/m_p = 0.15$ for the negative to positive ion mass ratio. Then the heavier positive ion species has been considered as the cooler ion species and the negative ion species to be the hotter ion species. The other plasma parameters were varied: the electron superthermal index was varied from high value ($\kappa = 1000$) appropriate for Maxwellian distribution to low value ($\kappa = 2$) for strongly nonthermal electrons. The values of the ratio of negative to positive ion equilibrium density $f = n_{n0}/n_{p0}$ were between 0 and 1 but the extreme values were excluded as they reduce the negative ion plasma to a two component plasma, namely to an ion-electron plasma if $f = 0$ (no negative ions) or to a plasma consisting of positive and negative ions without electrons if $f = 1$. The positive to negative ion temperature ratio τ_p and the negative ion to electron temperature ratio τ_n were varied from very low values (10^{-4}) (cold ions) up to values close to 1 (warm ions).

After a detailed analysis, we have found the following results:

1. For strongly non-Maxwellian electrons ($\kappa = 2$), cold positive ions ($\sigma_p = 10^{-4}$) and warm negative ions ($\sigma_n = 0.7$), the negative ion plasma supports the propagation of slow mode standard solitons and positive supersolitons for a narrow

range of negative-to-positive ion density ratio f.

2. The soliton Mach number range is limited, on the lower side by the ion acoustic Mach number and, on the upper side by the occurrence of positive ion sonic point for low to intermediate values of density ratio f, while the limiting factor is a double layer for higher values of f.

3. Supersolitons are limited, on the lower side, either by the double layer or the coalescence of two consecutive extrema, and on the upper side, by the coalescence of two consecutive extrema or the occurrence of positive ion sonic point.

4. When the double layer acts as the lower limit to the supersoliton existence range, there is a jump in the soliton amplitude between double layer amplitude and supersoliton amplitudes as was reported for the first time by Baluku et al. [75]. In other words there is a range of electrostatic potentials that are not accessible from the undisturbed conditions [105]. But when the coalescence is the lower limit, the supersoliton amplitude varies continuously.

5. The range of density ratio supporting the propagation of supersolitons ends when a double layer occurs at the positive ion sonic point.

We note here that these results differ qualitatively with those obtained for Maxwellian electrons while for the fast mode [101] they were qualitatively the same. This breaks down a common belief, according to which kappa distribution does not bring any new qualitative differences from the results with Maxwellian distribution [106].

6. For Maxwellian electrons ($\kappa = 1000$), cold positive ions ($\sigma_p = 10^{-4}$) and warm negative ions ($\sigma_n = 0.7$), the plasma supports the propagation of normal positive solitons only, limited on the upper side by the occurrence of positive ion sonic point for the whole range of density ratio f.

7. As the relative temperature of the two ion species is reduced (τ_p is increased) with fixed spectral index κ, the range of negative-to-positive ion density ratio f,

supporting the propagation of double layers as the upper limit to the soliton amplitude shifts to higher values of f, increasing at the same time the density range supporting solitons, limited by the occurrence of positive ion sonic point. This means that at high density ratio, the soliton upper limit is the double layer when positive ions are cold, but changes to the positive ion sonic point when positive ions are warm. Ultimately, with a further increase of τ_p, double layers disappear as the negative ion density, necessary to support them tends to be larger than the limiting value of $f = 1$ and from then solitons are limited by sonic point for the whole range of f.

8. When it is the electron superthermality that increases (by virtue of decreasing the spectral index κ) under fixed τ_p, the density range supporting double layers extends to lower values of f, decreasing at the same time the density range supporting solitons, limited by the occurrence of positive ion sonic point. There is, at intermediate values of f the transition from the positive ion sonic point as the soliton upper limit to double layers as the soliton limiting factor.

9. While the amplitudes of the maximum speed solitons and supersolitons decrease with a decrease of the relative temperature of the two ion species, an effect that is enhanced by the superthermal behavior of the electrons, it is found that the amplitudes of the double layers increase with a decrease of the relative temperature of the two ion species but decrease with an increase of the electron superthermality.

1.10.3 Summary of the results of paper $N^o 3$

Chapter four of this thesis was devoted to the study of the existence and propagation of solitons and double layers in a dusty plasma with adiabatic positive dust, adiabatic positive ion species and Cairns distributed electrons. The study was motivated by the existence of dust in many space, astrophysical and laboratory plasmas. Nonthermal particle distributions have also been observed in different plasma environments. A dust in a plasma environment may be charged either by collecting electrons from the plasma in which case it is negatively charged or by photoelectron

and secondary electron emission in which case it is positively charged. Charged dust become part of the plasma and modifies its collective behaviour. The existence and experimental observation [107] of dust ion acoustic and dust acoustic wave modes are examples of such modifications. In this chapter we have investigated the dust ion acoustic wave mode and the results have been published under the title **"Dust ion acoustic solitons and double layers in a dusty plasma with adiabatic positive dust, adiabatic positive ions and Cairns distributed electrons", AIP Advances 12, 015208 (2022).**
https://doi.org/10.1063/5.0076894 [108].

The plasma parameters in this study were the dust to ion equilibrium density ratio $f = z_d n_{d0}/z_i n_{i0}$, where $z_j (j = i,d)$ is the charge residing on the j^{th} species, the dust-to-ion charge-to-mass ratio $\mu = z_d m_i/z_i m_d$, the dust to electron temperature ratio $\tau_d = T_d/z_d T_e$, the ion to electron temperature ratio $\tau_i = T_i/z_i T_e$ and the electron superthermality $\beta = 4\alpha/(1+3\alpha)$ where α is the Cairns nonthermal parameter. The density ratio is bounded by $0 < f < 1$, the temperature ratios are also in the range $0 \leqslant \tau_{d,i} < 1$ and the electron superthermality values are in the interval $0 \leqslant \beta \leqslant 4/7$, where $\beta = 0$ corresponds to Maxwellian distribution.

The mass of a dust embedded in a plasma is normally very large compare to its charge and its charge-to-mass ratio is very small compared to the same ratio for positive ions. As a consequence we have kept the parameter μ to a low value, *viz.* $\mu = 10^{-4}$ throughout this chapter. Furthermore, the dust to electron temperature ratio τ_d enters the Sagdeev potential through the normalised dust thermal speed $\mu\tau_d$. Due to the small value of μ, the normalised dust thermal speed $\mu\tau_d$ remains very small even for large values of τ_d and the temperature of the dust does not change the results for a large range of τ_d. Thus we have kept a constant value of $\tau_d = 10^{-4}$. The other parameters were allowed to take all possible values in their respective ranges.

After a detailed analysis, we have found the following results:

1. When electrons are Maxwellian $(\beta = 0)$, the model supports the propagation

of positive solitons for all values of ion temperature and density ratio. This result is reminiscent of that obtained by Baluku et al. [75, 109].

2. When electrons are strongly nonthermal ($\beta = 0.5$), in addition to positive solitons the model supports also the propagation of negative solitons for low to intermediate values of the ion to electron temperature ratio but supports only positive solitons at high values of τ_i.
On the lower side positive and negative soliton Mach numbers are limited by the ion sound speed. On the upper side the positive ion Mach number range is limited by the occurrence of the ion sonic point while that of the negative solitons is limited by the occurrence of negative double layer.

3. When electrons are strongly nonthermal ($\beta = 0.5$) and positive ions are cold ($\tau_i = 10^{-4}$) positive solitons exist for the whole range of density ratio f but negative solitons exist at low values of f up to $f_n \approx 0.408$ at which they disappear. This means that positive and negative solitons coexist for density ratio in the range $0 < f \lesssim 0.408$.

4. In the coexistence region in $\{f, M\}$ space, positive solitons are non KdV in nature for $f \lesssim f_c = 0.333$. This means that in this range there exist a soliton with finite amplitude at the acoustic Mach number. Such soliton cannot be described by the KdV equation which predicts only superacoustic nonlinear structures. In the range $f \lesssim f_c = 0.333$, negative solitons are superacoustic and therefore are of KdV nature.

5. For values of f larger than the value f_c but smaller than the value $f_n = 0.408$ at which negative solitons disappear, there exist a negative soliton at the acoustic speed, suggesting that negative solitons in the range $f_c < f < f_n$ are non KdV in nature, while positive solitons are KdV. There is thus a change of polarity for both KdV and non KdV at density ratio f_c. This special point has been named a critical point.

6. At the critical point $f_c \approx 0.333$, the third derivative of the Sagdeev poten-

tial vanishes and its sign changes from negative to positive. At point f_c, there is no soliton at acoustic speed, but for Mach number slightly larger than the acoustic Mach number , solitons of both polarities exist. These solitons are therefore of KdV nature. This then shows that the existence of a soliton at acoustic speed is not a prerequisite for the existence of a coexistence region, as was suggested by Verheest et al. [110].

7. For $0 < f < f_c$, the amplitude of positive solitons at the acoustic speed decreases with increasing f until they vanish at $f = f_c$. For $f_c < f < f_n$ the amplitude of negative solitons at the acoustic speed increases with increasing f until at f_n there is cutoff of negative solitons when a double layer occurs at the acoustic speed. For values larger than f_n the plasma supports only positive KdV solitons irrespective of the ion temperature.

8. When the ion temperature increases, the critical point f_c shifts to lower values of f until it vanishes. The shift of f_c to lower values when the ion temperature increases is accompanied with the shift of the whole coexistence domain to lower values of f. Therefore upon increase of τ_i, there may be change of soliton polarity at a fixed density ratio f. Thus, while there is cutoff of negative solitons at $f_n \approx 0.408$ when $\tau_i = 10^{-4}$, it occurs at $f_n \approx 0.33$ when τ_i is 0.1 and at $f_n \approx 0.12$ when $\tau_i = 0.5$.

9. For values of density ratio smaller than the critical value f_c, $f = 0.1$ *e.g.*, there is switch of polarity from positive to negative when the ion temperature increases from $\tau_i = 10^{-4}$ to a critical ion temperature $\tau_{ic} \approx 0.28$. For larger values of $\tau_i > \tau_{ic}$ negative solitons appear at the acoustic speed with amplitudes increasing with increase of ion temperature until the negative soliton cutoff at $\tau_{in} \approx 0.56$ when a negative polarity double layer occurs at the acoustic speed. For $\tau_i > \tau_{in}$ only positive solitons are supported for $f = 0.1$. Therefore $\tau_{in} \approx 0.56$ terminates the range of ion temperature supporting the coexistence of solitons of both polarities. A similar behaviour is observed for larger values of f, *e.g.* at $f = 0.25$ but now both τ_{ic} and τ_{in} occur at lower values, 0.08 and 0.22, respectively.

10. When the density ratio is higher than the critical density ratio f_c, $f = 0.37$

e.g., the amplitude of the negative soliton at the acoustic speed increases with increasing temperature until at $\tau_{in} \approx 0.043$ a double layer occurs at the acoustic speed terminating the range of ion temperature supporting non KdV solitons at $f = 0.37$. At this value, there is no switch of polarity but there is disappearance of solitons at acoustic speed as the ion temperature increases.

1.11 References

[1] M. R. Rouhani and Z. E. Abbasi, Phys. Plasmas **1**9, 112307 (2012).

[2] F. F. Chen, *Introduction to Plasma Physics and Controlled Fusion*, 2nd ed. New York: Plenum press, 1984, vol. 1.

[3] Paul M. Bellan, *Fundamentals of Plasma Physics*, London: Cambridge University Press, 2012, https://doi.org/10.1017/CBO9780511807183.

[4] S. Baboolal, R. Bharuthram, and M. A. Hellberg, J. Plasma Phys. **4**4, 1 (1990).

[5] G. S. Lakhina, S. V. Singh, and A. P. Kakad, Phys. Plasmas **2**1, 062311 (2014).

[6] A. E. Dubinov and D. Yu. Kolotkov, IEEE Trans. Plasma Sci. **4**0, 1429 (2012).

[7] L. L. Yadav, S. R. Sharma, and R. S. Tiwari Phys. Plasmas **1**, 559 (1994).

[8] F. Nsengiyumva, M. A. Hellberg, F. Verheest, and R. L. Mace, Phys. Plasmas **2**1, 102301 (2014).

[9] F. Nsengiyumva, M. A. Hellberg, and R. L. Mace, Phys. Plasmas **2**2, 092304 (2015).

[10] F. Verheest, M. A. Hellberg, and I. Kourakis, Phys. Plasmas **1**5, 112309 (2008).

[11] B. Handique, H. Bailung, G. C. Das and J. Chutia, Phys. Plasmas **6**, 1636 (1999).

[12] R. Ichiki, S. Yoshimura, T. Watanabe, Y. Nakamura, and Y. Kawai, Phys. Plasmas **9**, 4481 (2002).

[13] B. Song, N. D'Angelo, and R. L. Merlino, Phys. Fluids B **3**, 284 (1991).

[14] S. G. Tagare, J. Plasma Physics **3**8, 301 (1986).

[15] K. Kumar and M. K. Mishra, AIP Advances **7**, 115114 (2017).

[16] S. K. El-labany, R. Sabry, E. F. El-shamy, and D. M. Khedr, J. Plasma Physics **7**9, 613 (2013).

[17] N. D'Angelo, S. V. Goeler, and T. Ohe, Phys. Fluids **9**, 1605 (1966).

[18] R. L. Merlino and J. J. Loomis, Phys. Fluids B **2**, 2865 (1990).

[19] R. Ichiki, M. Shindo, S. Yoshimura, T. Watanabe, and Y. Kawai, Phys. Plasmas **8**, 4275 (2001).

[20] P. K. Shukla and A. A. Mamum, *Introduction to Dusty Plasma Physics*, London: IOP Press, 2002.

[21] N.Ya. Kotsarenko, S.V. Koshevaya, and A. N. Kotsarenko, Geofísica Internacional **3**7, 71 (1998).

[22] W. F. El-Taibany and M. WadatiN, Phys. Plasmas **1**4, 103703 (2007).

[23] R. L. Merlino and J. A. Goree, Phys. Today**5**7(7), 32 (2004).

[24] W. Baumjohann and R. A. Treumann, Basic space plasma physics, London: Imperial College Press, 1999.

[25] T. H. Stix, Waves in Plasmas, New York: Springer-Verlag, 1999.

[26] N. Vichiansan, N. Kaai, K. Leksakul, S. Lumyong and J. G. Han, Chiang Mai J. Sci. **4**5(4), 1811 (2018).

[27] S. Singh, S. Kumar, S. K. Meena, and S. K. Saini, *Introduction to Plasma Based Propulsion System: Hall Thrusters*. http://dx.doi.org/10.5772/intechopen.96916.

[28] R. Abd Jelil, J. Mater. Sci. **5**0, 5913 (2015).

[29] J. Proud et al., *Plasma processing of materials: scientific opportunities and Technological challenges*, Washington, D.C.:The National Academies Press, 1991.

[30] X. Cai and C. Du, Plasma Chemistry and Plasma Processing **4**1, 1 (2021).

[31] T. S. Gill, P. Bala, H. Kaur, N. S. Saini, S. Bansal, and J. Kaur, Eur. Phys. J. D **3**1, 91 (2004).

[32] S. Baboolal, R. Bharuthram, and M. A. Hellberg, Phys. Plasmas **3**, 4446 (1996).

[33] M. K. Mishra and R. S. Chhabra, J. Plasma Phys. **4**4, 1 (1996).

[34] T. K. Baluku, M. A. Hellberg, and F. Verheest, Europhys. Lett. **9**1, 15001 (2010).

[35] F. J. Pavón-Carrasco and A. De Santis, Front. Earth Sci. **4**, 40 (2016).

[36] V. M. Vasyliunas, J. Geophys. Res. **7**3, 2839 (1968).

[37] D. Summers and R. M. Thorne, Phys. Fluids B **3**, 1835 (1991).

[38] M. A. Hellberg, R. L. Mace, T. K. Baluku, I. Kourakis, and N. S. Saini, Phys. Plasmas **1**6, 094701 (2009).

[39] M. Maksimovic, V. Pierrard, and P. Riley, Geophys. Res. Lett. **2**4, 1151 (1997).

[40] P. Schippers, M. Blanc, N. Andre, I. Dandouras, G. R. Lewis, L. K. Gilbert, A. M. Persoon, N. Krupp, D. A. Gurnett, A. J. Coates, S. M. Krimigis, D. T. Young, and M. K. Dougherty, J. Geophys. Res. **1**13, A07208 (2008).

[41] V. De La Haye, J. H. Waite Jr., R. E. Johnson, R. V. Yelle, T. E. Cravens, J. G. Luhmann, W. T. Kasprzak, D. A. Gell, B. Magee, F. Leblanc, M. Michael, S. Jurac, and I. P. Robertson, J. Geophys. Res. **1**12, A07309 (2007).

[42] V. Pierrard and M. Lazar, Sol. Phys. **2**67, 153 (2010).

[43] E. Fourkal, V. Yu. Bychenkov, W. Rozmus, R. Sydora, C. Kirkby, C. E. Capjack, S. H. Glenzer, and H. A. Baldis Phys. Plasmas **8**, 550 (2001).

[44] S. Hussain, N. Akhtar, and S. Mahmood, Astrophys Space Sci **3**38, 265 (2012).

[45] S. Ali Shan and N. Akhtar, Astrophys Space Sci **3**46, 367 (2013).

[46] M. Mehdipoor, Astrophys Space Sci **3**48, 115 (2013).

[47] R.A. Cairns, A.A. Mamum, R. Bingham, R. Boström, R.O. Dendy, C.M.C. Nairn, and P.K. Shukla, Geophys. Res. Lett. **2**2, 2709 (1995).

[48] F. Verheest and S. R. Pillay, Phys. Plasmas **1**5, 013703 (2008).

[49] R. Sabry, W. M. Moslem, and P. K. Shukla, Phys. Plasmas **1**6, 032302 (2009).

[50] T. K. Baluku and M. A. Hellberg, Plasma Physics and Controlled Fusion **5**3, 095007 (2011).

[51] F. Verheest and M. A. Hellberg, Phys. Plasmas **2**2, 012301 (2015).

[52] I. Habumugisha, S. K. Anguma E. Jurua, and N. Noreen, International Journal of Astronomy and Astrophysics **6**, 72 (2016).

[53] F. Verheest and C. P. Olivier, Phys. Plasmas **2**4, 113708 (2017).

[54] D. Debnath and A. Bandyopadhyay, Astrophysics and Space Science **3**65, 72 (2020).

[55] D. G. Crighton, Acta Applicandae Mathematicae **3**9, 39 (1995).

[56] G. A. El, *Solitary waves in fluids, Advances in fluid mechanics*, Vol 47, WIT Press, UK (2007). www.witpress.com.

[57] M. R. Alfonso, R. L. Armentano, L. J. Cymberknop, A. R. Ghigo, F. M. Pessana, and W. E. Legnani, Journal of Healthcare Engineering **2**018, Article ID 1364185, 9 pages (2017).

[58] H. Washimi and T. Taniuti, Phys. Rev. Lett. **1**7, 996 (1966).

[59] P. G. Drazin and R. S. Johnson, *Solitons: an introduction*, London: Cambridge University Press, 2012, https://doi.org/10.1017/CBO9781139172059.

[60] N. J. Zabusky and M. D. Kruskal, Phys. Rev. Lett. **1**5, 240 (1965).

[61] A. Hasegawa and F. Tappert, Appl. Phys. Lett. **2**3, 142 (1973).

[62] J. R. Apel, L. A. Ostrovsky, Y. A. Stepany, and J. F. Lynch, J. Acoust. Soc. Am. **1**21, 695 (2007).

[63] S. E. Koch, C. Flamant, J. W. Wilson, B. M. Gentry, and B. D. Jamison, J. Atmos. Ocean. Technol. **2**5, 1267 (2008).

[64] A. S. Davydov, Phys. Scripta **2**0, 387 (1979).

[65] T. Heimburg and A. D. JacksonA, PNAS **1**02, 9790 (2005).

[66] J. S. Pickett, L.-J. Chen, S. W. Kahler, O. Santolik, D. A. Gurnett, B. T. Tsurutani, and A. Balogh, Ann. Geophys. **2**2, 2515 (2004).

[67] F. Verheest, M. A. Hellberg, and I. Kourakis, Phys. Plasmas **2**0, 012302 (2013).

[68] A. Paul and A. Bandyopadhyay, Indian J. Phys. **9**2, 1187 (2018).

[69] F. Verheest and C. P. Olivier, Phys. Plasmas **2**4, 113708 (2017).

[70] S. V. Steffy and S. S. Ghosh, Phys. Plasmas **2**4, 102111 (2017).

[71] S. V. Steffy and S. S. Ghosh, arXiv:2107.1048 V1 [physics.plasm-ph], (2021).

[72] G. S. Lakhina, S. V. Singh, R. Rubia, and S. Devanandhan, Plasma **2**021, 681 (2021).

[73] C. S. Gardner and G. K. Morikawa, *Similarity in the asymptotic behavior of collision-free hydromagnetic waves and water waves. Report MF-2, NYO-9080*, Courant Institute of Mathematical Sciences, New York University, 1960.

[74] P. K. Kythe, P. Puri, and M. R. Schäferkotter, *Partial Differential equations and boundary value problems with Mathematica*, 2nd ed. Boca Raton: Chapman & Hall/CRC, 2003

[75] T. K. Baluku, M. A. Hellberg, I. Kourakis, and N. S. Saini, Phys. Plasmas **1**7, 053702 (2010).

[76] M. A. Hellberg, T. K. Baluku, and F. Verheest, AIP Conference Proceedings **1**306, 50 (2010).

[77] T. Cattaert, *Large amplitude solitary waves in space plasmas*[Doctoral thesis, Universiteit Gent]. https://biblio.ugent.be/publication/472050.

[78] R. Z. Sagdeev, Rev. Plasma Phys. **4**, 23 (1966).

[79] M. J. Ablowitz, G. Biondini, and L. A. OstrovskyS, Chaos **1**0, 471 (2000).

[80] V. C. Kuriakose and K. Porsezian, Resonance, 643 (2010).

[81] D. Bourgault, P. S. Galbraith, and C. Chavanne, Nature Communications **7**, 13606 (2016).

[82] E. Pelinovsky, O. Polukhina, A. Slunyaev, and T. Talipova, *Transactions on State of the Art in Science and Engineering*, Vol 9, WIT Press, UK (2007). www.witpress.com.

[83] W. Hereman, arXiv:1308.5383 V1 [nlin.SI], (2013).

[84] J. W. Rottman and F. Einaudi, J. Atmos. Sci. **5**0, 2116 (1993).

[85] L. Chen and L. Yang, Complexity **2**020, Article ID 7609582, 16 pages (2020).

[86] M. Temerin, K. Cerny, W. Lotko, and F. S. Mozer, Phys. Rev. Lett. **4**8, 1175 (1982).

[87] R. E. Ergun, C. W. Carlson, J. P. McFadden, F. S. Mozer, G. T. Delory, W. Peria, C. C. Chaston, M. Temerin, I. Roth, L. Muschietti, R. Elphic, R. Strangeway, R. Pfaff, C. A. Cattel, D. Klumpar, E. Shelley, W. Peterson, E. Moebius, and L. Kistler, Geophys. Res. Lett. **2**5, 2041 (1998).

[88] H. Matsumoto, H. Kojima, T. Miyatake et al., Geophys. Res. Lett. **2**1, 2915 (1994).

[89] X.H. Deng a, R.X. Tang, H. Matsumoto, J. S. Pickett, A. N. Fazakerley, H. Kojima, W. Baumjohann, A. Coates, R. Nakamura, D. A. Gurnett, and Z. X. Liu, Adv. Space Res. **3**7, 1373 (2006).

[90] F. S. Mozer, O. V. Agapitov, A. Artemyev, J. F. Drake, V. Krasnoselskikh, S. Lejosnend, and I. Vasko, Geophy. Res.Lett. **4**2, 3627 (2015).

[91] A. Mangeney, C. Salem, C. Lacombe, J.-L. Bougeret, C. Perche, R. Manning, P. J. Kellogg, K. Goetz, S. J. Monson, and J.-M. Bosqued, Annales Geophysicae **1**7, 307 (1999).

[92] J. S. Pickett, L.-J. Chen, R. L. Mutel, I. W. Christopher, O. Santolík, G. S. Lakhina, S. V. Singh, R. V. Reddy, D. A. Gurnett, B. T. Tsurutani, E. Lucek, and B. Lavraud, Adv. Space Res. **4**1, 1666 (2008).

[93] D. B. Graham, Yu. V. Khotyaintse, A. Vaivads, and M. André, J. Geophys. Res. Space Physics **1**21, (2016).

[94] J. S. Pickett, W. S. Kurth, D. A. Gurnett, R. L. Huff, J. B. Faden, T. F. Averkamp, D. Píša, and G. H. Jon, J. Geophys. Res. Space Physics **1**20, 6569 (2015).

[95] R. L. Merlino, A. Barkan, C. Thompson, and N. D'Angelo, Phys. Plasmas **5**, 1607 (1998).

[96] R. L. Stenzel, M. Ooyama, and Y. Nakamura, Phys. Rev. Lett **4**5, 1498 (1980).

[97] R. L. Stenzel, M. Ooyama, and Y. Nakamura, Phys. Fluids **2**4, 708 (1981).

[98] L.-J. Chen and G. K. Parks, Nonlinear Process. Geophys. **9**, 111 (2009).

[99] J. Vranjes, A and A **5**54, A90 (2013).

[100] N. P. Abraham,S. Sebastian, G. Sreekala, R. Jayapal, C. P. Anilkumar, and V.Chandu, J. Astrophys. **2**013, Article ID 838534, 7 pages (2013).

[101] X. Mushinzimana and F. Nsengiyumva, AIP Advances **1**0, 065305 (2020).

[102] F. Verheest and M. A. Hellberg, Phys. Plasmas **1**7, 023701 (2010).

[103] S. K. Maharaj and R. Bharuthram, Phys. Plasmas **2**6, 052302 (2019).

[104] M. Xavier, F. Nsengiyumva, and L. L. Yadav, AIP Adv. **1**1, 025325 (2021).

[105] F. Verheest, M. A. Hellberg, and I. Kourakis, Phys. Rev. E **8**7, 043107 (2013).

[106] F. Verheest and M. A. Hellberg, Phys. Plasmas **1**7, 102312 (2010).

[107] A. Barkan, N. D'Angelo, and R. L. Merlino, Planet. Space Sci. **4**4, 239 (1996).

[108] X. Mushinzimana, F. Nsengiyumva, L. L. Yadav, and T. K. Baluku, AIP Advances **1**2, 015208 (2022).

[109] T. K. Baluku, M. A. Hellberg, and R. L. Mace, Phys. Plasmas **1**5, 033701 (2008).

[110] F. Verheest, M. A. Hellberg, and T. K. BalukuI, Phys. Plasmas **1**9, 032305 (2012).

Chapter 2

Large amplitude fast ion-acoustic solitary waves in a warm negative ion plasma with superthermal electrons: The fast mode revisited

Large amplitude fast ion-acoustic solitary waves in a warm negative ion plasma with superthermal electrons: The fast mode revisited

X. Mushinzimana[1, a)] , and F. Nsengiyumva[2,b)]

[1] *Department of Physics, University of Rwanda*

College of Science and Technology

P. O. Box 3900 Kigali, Rwanda

[2] *Department of Civil Engineering*

Institut d'Enseignement Superieur de Ruhengeri

P. O. Box 155 Musanze, Rwanda

[a)] Author to whom correspondence should be addressed: muxavier2000@yahoo.fr

[b)] Email: franco.nseng@gmail.com

Abstract

Large amplitude ion-acoustic fast mode solitary waves in a negative ion plasma with superthermal electrons are revisited, using the Sagdeev pseudopotential approach. As is well known, this plasma supports the propagation of both compressive and rarefactive solitons, and there exists a range of parameter values in which the two type of structures coexist. This is confirmed by the present study, which is based on well-established soliton existence domains. After investigating the existence of solitons in terms of the lower and upper Mach number limits for broader regions in parameter space, we have found that as a result of the ion thermal effects, the range in the allowed Mach numbers is reduced and only small amplitude rarefactive solitons propagate in this plasma, an effect that is enhanced by the superthermal behavior of the electrons. Rearranging our analytical work so as to get a two-positive ion plasma, our results show the presence of stopbands in the soliton existence domains, as reported by Nsengiyumva et al. [Phys. Plasmas **2**1, 102301 (2014)] despite the use of different normalization and different parameter space. This suggests that the observed stopbands are a real phenomenon, which needs consideration when studying plasma waves.

2.1 Introduction

Negative ion plasmas have been observed in numerous physical systems [1–15]. These observations have motivated several studies of solitary waves propagating in a negative ion plasma [16–27]. From these studies, with further knowledge from related studies [28–42], it is well known that a negative ion plasma with finite temperature of at least one of the two ion species supports the propagation of two mode waves with different phase speeds. This result holds irrespective of the electron velocity distribution.

Traditionally, a Maxwellian velocity distribution has been the basis of many studies of plasma waves. However, under some circumstances, a Maxwellian distribution may fail to model appropriately the velocities of plasma particles,

and therefore a kappa velocity distribution, a model distribution function that generalizes the Maxwellian and approaches a power law at high energies, has been introduced [43]. This distribution has been found to be a good fit for plasma particle velocities in various space environments [44–49]. The three dimensional kappa velocity distribution is given by [43, 50, 51]

$$f(v) = N\left(\pi\kappa\theta^2\right)^{-3/2} \frac{\Gamma(\kappa+1)}{\Gamma\left(\kappa-\frac{1}{2}\right)} \left(1+\frac{v^2}{\kappa\theta^2}\right)^{-(\kappa+1)}, \qquad (2.1)$$

where N is the number density, Γ is the gamma function, v is the particle speed, and the most probable speed, θ (which may be regarded as an effective thermal speed), is related to the usual thermal speed, v_t, by
$\theta = [(2\kappa-3)/\kappa]^{1/2} v_t$, requiring that the spectral index $\kappa > 3/2$.
To date, most studies of solitary waves supported by a negative ion plasma have focused on cases of small amplitude KdV solitons [17–24] or large amplitude Sagdeev cases in which the two ion species are cold [25, 26]. Very little [27] is known about the ion thermal effects on large amplitude solitary waves propagation characteristics. The main result, that is common to all studies of the fast mode, is that a negative ion plasma supports the propagation of both compressive (positive) and rarefactive (negative) fast mode solitons, which also coexist for some parameter values. Compressive solitons are supported by low negative ion densities, while rarefactive solitons occur at high negative ion densities. The two type of structures coexist in an intermediate range of negative ion densities.

We recall that the slow mode wave exists only when at least one of the two ion species has finite temperature. When the two ion species are cold, the slow mode disappears and the fast mode reduces to the well-known ion-acoustic wave [52]. With this in mind, the results of Rouhani and Abbasi [25] retrieve the main feature of the fast mode solitary waves supported by warm negative ion plasmas, namely, the coexistence of compressive and rarefactive solitons, as discussed earlier. We recall that Rouhani and Abbasi [25] considered cold negative and positive ion species with superthermal (kappa) electrons and studied small and large amplitude solitary waves supported by

this plasma, using the KdV and Sagdeev pseudopotential approaches.

An attempt to extend the work of Rouhani and Abbasi [25], by incorporating the ion thermal effects, was reported recently by Kumar and Mishra [27]. These authors considered a plasma consisting of warm negative and positive ion species and superthermal electrons to study large amplitude ion-acoustic solitons supported by that plasma. Some of their results are consistent with earlier findings [25], for example, the coexistence of compressive and rarefactive solitons and show that an increase in the ion temperature leads to a decrease in the amplitude of solitons of either polarity.

However, we note that there are significant gaps in the work reported by Kumar and Mishra [27]. As discussed in detail by Verheest et al. [34], the density of an adiabatic species involves the $\pm$ signs, where the upper sign must be used when the slow mode is considered and the lower sign corresponds to the fast mode. However, Kumar and Mishra [27] do not take account of this very well known fact. Instead, after solving their quadratic equations (Eqs. (12) and (13)), they consider the $+$ sign (in their Eqs. (14) and (15)) for the subsequent discussion of solitary waves, without mentioning that that sign corresponds to the fast mode and do not make any comment on the existence of the slow mode.

Furthermore, as discussed in detail in earlier studies [34, 36, 38, 39, 53, 54], the upper limit in Mach numbers of solitons supported by the plasma under consideration is obtained when the flow speed of the adiabatic species coincides with a sonic point [34, 53, 54]. This corresponds to cases in which the density of the adiabatic species ceases to be real. At that point, the species' flow is choked, hence limiting the amplitude of the wave [53, 54]. Thus, the sonic points play an important role in the determination of the soliton existence domains.

From the work of Kumar and Mishra [27], one then expects the maximum Mach numbers due to the occurrence of the negative ion sonic point and the maximum Mach numbers due to the occurrence of the positive ion sonic point [34, 36, 38, 39]. However, Kumar and Mishra [27] consider the upper limit due to the positive ions only (their Eqs. (22)-(24)), and subsequently

do not find the well-known region [25] of coexistence of compressive and rarefactive solitons during their numerical study of soliton existence domains (their Figs. 1 and 2). The authors [27] discuss the compressive and rarefactive solitons as well as their coexistence by numerical trial and error of the Sagdeev pseudopotential plots (their Figs. $3-12$), rather than basing the investigation on soliton existence domains.

In the study of solitary waves, soliton existence domains play an important role because when they are well established, further study of solitary waves is done based on a well-known parameter space, rather than relying on numerical trial and error of Sagdeev pseudopotential plots. Until recently [38], it was known that the range of Mach numbers between the lower and the upper limits is always a passband. Surprisingly, in a recent study [38] of a plasma composed of cold and adiabatic positive ion species with Boltzmann electrons, Nsengiyumva et al. [38] showed that a stopband may exist between the lower and the upper limits in soliton speeds. We recall that a stopband means a range of Mach numbers, between two passbands of a soliton existence domain, over which solitons do not propagate. This novel phenomenon has been investigated further and confirmed by Maharaj and Bharuthram [41, 42], who extended the work of Nsengiyumva et al. [38] by incorporating the superthermal effects of the electrons [41] and the thermal effects of the cooler ion species [42]. We note that Maharaj and Bharuthram [41, 42] used the normalization of Nsengiyumva et al. [38]. This then leads to a further open question. Would one find the stopbands reported by Nsengiyumva et al. [38] by using a different normalization?

The significant gaps in the work of Kumar and Mishra [27] in conjuction with the open question associated with stopbands in the soliton existence domains, as mentioned above, motivate us to reconsider the study of large amplitude fast and slow mode solitary waves supported by a negative ion plasma with superthermal electrons. Such plasmas are numerous in space environments [1, 2, 55–58]). While a comprehensive study of the slow mode will be reported elsewhere, here we report on the fast mode. We show that

there are significant new results which have never been reported before. Inter alia, we show that when the ion thermal effects are significant, the domain of coexistence of compressive and rarefactive solitons reported in earlier studies [25] disappears and only rarefactive solitons propagate. This effect is enhanced by the electron superthermal effects. Rearranging our analytical work in order to get the two-positive ion plasma studied by Nsengiyumva et al. [38], we are able to find the stopbands in the soliton existence domains reported by Nsengiyumva et al. [38], despite the use of different normalization and different parameter space, hence supporting earlier findings [38, 41, 42]. However, no stopbands are found in the existence domains of solitons propagating in a negative ion plasma.

The work is organized as follows. After this introduction, we derive, in Sec. II, an analytical expression of the Sagdeev pseudopotential for the plasma model under consideration, which is the basis for further soliton study in Sec. III. Section IV revisits the stopbands reported by Nsengiyumva et al. [38], and our findings are summarized in Sec. V.

2.2 Plasma densities and Sagdeev pseudopotential

We consider a non-relativistic, unmagnetized, collisionless, plasma composed of kappa-distributed electrons and warm negative and positive ion species that are singly charged. Assuming one dimensional motion of all species, the dimensionless basic equations governing the dynamics of this plasma model are, respectively, the momentum and continuity equations for the positive (p) and negative (n) ion species

$$\frac{\partial u_p}{\partial t} + u_p \frac{\partial u_p}{\partial x} = -\frac{1}{\beta}\frac{\partial \varphi}{\partial x} - \frac{3\sigma_p}{\beta} n_p \frac{\partial n_p}{\partial x}, \tag{2.2}$$

$$\frac{\partial n_p}{\partial t} + \frac{\partial \left(n_p u_p\right)}{\partial x} = 0, \tag{2.3}$$

$$\frac{\partial u_n}{\partial t} + u_n \frac{\partial u_n}{\partial x} = -\frac{z}{\mu\beta}\frac{\partial \varphi}{\partial x} - \frac{3\sigma_n}{\mu\beta} n_n \frac{\partial n_n}{\partial x}, \tag{2.4}$$

$$\frac{\partial n_n}{\partial t} + \frac{\partial (n_n u_n)}{\partial x} = 0, \tag{2.5}$$

and the dimensionless Poisson's equation

$$\frac{\partial^2 \varphi}{\partial x^2} = n_e - \frac{\alpha z}{1+\alpha z} n_n - \frac{1}{1+\alpha z} n_p, \tag{2.6}$$

where n_e is the dimensionless density of kappa-distributed electrons [59]

$$n_e = \left[1 - \frac{2\varphi}{2\kappa - 3}\right]^{-\kappa+\frac{1}{2}}, \tag{2.7}$$

n_p (u_p) and n_n (u_n) are the densities (velocities) of the positive and negative ion species, respectively, φ is the electrostatic potential, x is the space coordinate, t is the time, $\mu = m_n/m_p$ is the negative to the positive ion mass ratio, $\sigma_j = T_j/T_e$ is the ion to electron temperature ratio ($j = n, p$), and $\alpha = n_{n0}/n_{p0}$ is the equilibrium negative to positive ion density ratio, which must be within the range $0 < \alpha < 1$, so as to satisfy the equilibrium charge neutrality condition. In Eqs. (2.2) and (2.4), we have used the adiabatic-pressure-density relation [34, 54] with polytropic index $\gamma = 3$, that is,

$$p_j n_j^{-3} = p_{j0} n_{j0}^{-3} = constant, \tag{2.8}$$

where the unperturbed pressure of the j^{th} adiabatic species is defined as [60] $p_{j0} = n_{j0} T_j$.

Furthermore, for ease of comparison of our work with that of Kumar and Mishra [27], we assume that the negative ion species are lighter. This assumption is based on the fact that Kumar and Mishra [27] used values of μ in the range $0 < \mu < 1$, in their numerical investigation. With this assumption, and for the purpose of the organization of the work in this paper, we have introduced in Eqs. (2.4) and (2.6) a parameter z that defines the sign of the charge on the lighter ion species. Introducing this parameter is particularly useful for our discussion in Sec. IV. More explicitly, we first consider a case in which the lighter ion species are negatively charged ($z = -1$) and study a negative ion plasma following Kumar and Mishra [27],

then, in Sec. IV, we will consider a case in which the lighter ion species are also positively charged ($z = +1$) and revisit the investigation of the presence of stopbands in the existence domains of solitons supported by the two positive ion plasma studied by [38, 41, 42].

The normalization of variables in Eqs. (2.2−2.7) has been done following [27], as follows: The space coordinate x has been normalized by the electron Debye length $\lambda_{De} = (\varepsilon_0 T_e/n_{e0}e^2)^{\frac{1}{2}}$; the time has been normalized by the inverse of the effective ion plasma frequency $\omega_{pi} = (n_{e0}e^2\beta/\varepsilon_0 m_p)^{\frac{1}{2}}$, where $\beta = \frac{\mu+\alpha z^2}{\mu(1+\alpha z)}$; the velocities have been normalized by the ion sound velocity in the mixture $c_s \equiv \omega_{pi}\lambda_{De} = (T_e\beta/m_p)^{\frac{1}{2}}$; the electrostatic potential has been normalized by T_e/e, the densities n_n, n_p, and n_e have been normalized by their respective equilibrium densities n_{n0}, n_{p0}, and n_{e0}.
With this normalization, Eqs. (2.2−2.7) are reminiscent of Eqs. $(1)-(6)$ of Kumar and Mishra [27], noting that there is a typographical error in the first terms of the left hand side of their Eqs. (2) and (4). It should also be noted that, since we are considering singly charged ions, we have not introduced the charge multiplicity ε_z ($\varepsilon_z = +1$), as in Kumar and Mishra [27]; instead, we have introduced the parameter z, discussed earlier. We follow Kumar and Mishra [27] to obtain the density of the ion species, by assuming that all the dependent variables depend on a single independent variable

$$\xi = x - Mt, \tag{2.9}$$

where the Mach number $M = V/c_s$ is the speed of the solitary wave, as seen in an inertial frame, normalized by the ion sound speed, c_s. Using the transformation (2.9), Eqs. (2.2)-(2.6) become, respectively,

$$-M\frac{\partial u_p}{\partial \xi} + u_p\frac{\partial u_p}{\partial \xi} = -\frac{1}{\beta}\frac{\partial \varphi}{\partial \xi} - \frac{3\sigma_p}{\beta}n_p\frac{\partial n_p}{\partial \xi}, \tag{2.10}$$

$$-M\frac{\partial n_p}{\partial \xi} + \frac{\partial (n_p u_p)}{\partial \xi} = 0, \tag{2.11}$$

$$-M\frac{\partial u_n}{\partial \xi} + u_n\frac{\partial u_n}{\partial \xi} = -\frac{z}{\mu\beta}\frac{\partial \varphi}{\partial \xi} - \frac{3\sigma_n}{\mu\beta}n_n\frac{\partial n_n}{\partial \xi}, \tag{2.12}$$

$$-M\frac{\partial n_n}{\partial \xi}+\frac{\partial\left(n_n u_n\right)}{\partial \xi}=0, \tag{2.13}$$

$$\frac{\partial^2 \varphi}{\partial \xi^2}=n_e-\frac{\alpha z}{1+\alpha z}n_n-\frac{1}{1+\alpha z}n_p. \tag{2.14}$$

Integrating Eqs. (2.10)-(2.13), using the usual boundary conditions far away from the solitary wave where the plasma is undisturbed, i.e., $n_p=1$, $n_n=1$, $u_p=0$, $u_n=0$, $\varphi=0$, results in biquadratic equations [27] in n_p and n_n, as

$$\frac{3\sigma_p}{\beta}n_p^4-\left(M^2-\frac{2\varphi}{\beta}+\frac{3\sigma_p}{\beta}\right)n_p^2+M^2=0 \tag{2.15}$$

and

$$\frac{3\sigma_n}{\mu\beta}n_n^4-\left(M^2-\frac{2z\varphi}{\mu\beta}+\frac{3\sigma_n}{\mu\beta}\right)n_n^2+M^2=0, \tag{2.16}$$

whose solutions are, respectively,

$$n_p^2=\frac{\beta}{6\sigma_p}\left[M^2+\frac{3\sigma_p}{\beta}-\frac{2\varphi}{\beta}\pm\sqrt{\left(M^2+\frac{3\sigma_p}{\beta}-\frac{2\varphi}{\beta}\right)^2-\frac{12M^2\sigma_p}{\beta}}\right], \tag{2.17}$$

and

$$n_n^2=\frac{\mu\beta}{6\sigma_n}\left[M^2+\frac{3\sigma_n}{\mu\beta}-\frac{2z\varphi}{\mu\beta}\pm\sqrt{\left(M^2+\frac{3\sigma_n}{\mu\beta}-\frac{2z\varphi}{\mu\beta}\right)^2-\frac{12M^2\sigma_n}{\mu\beta}}\right]. \tag{2.18}$$

Equations (2.17) and (2.18) can be rewritten in an alternative form as [27]

$$n_p=\frac{\sqrt{2}M}{\left\{M^2-\frac{2\varphi}{\beta}+\frac{3\sigma_p}{\beta}\mp\sqrt{\left(M^2-\frac{2\varphi}{\beta}+\frac{3\sigma_p}{\beta}\right)^2-\frac{12\sigma_pM^2}{\beta}}\right\}^{\frac{1}{2}}}, \tag{2.19}$$

and

$$n_n=\frac{\sqrt{2}M}{\left\{M^2-\frac{2z\varphi}{\mu\beta}+\frac{3\sigma_n}{\mu\beta}\mp\sqrt{\left(M^2-\frac{2z\varphi}{\mu\beta}+\frac{3\sigma_n}{\mu\beta}\right)^2-\frac{12\sigma_nM^2}{\mu\beta}}\right\}^{\frac{1}{2}}}. \tag{2.20}$$

Equations (2.19) and (2.20) are reminiscent of Eqs. (14) and (15) of Kumar and Mishra [27]. The $\mp$ signs in front of the square root contain interesting information about the slow and fast mode waves supported by the plasma model under consideration [34]. As discussed in detail by Verheest et al. [34], for a closely related plasma model, the upper sign has to be used for a subsonic species ($V < v_{tj}$) and the lower sign for a supersonic one ($V > v_{tj}$) ($j = p, n$), so that far away from the solitary wave where the plasma is undisturbed, $\varphi = 0$, the correct limit n_{j0} is obtained, and the ordering [33, 39]

$$v_{tc} < V_{slow} < v_{th} < V_{fast} < v_{te}, \tag{2.21}$$

which can be rewritten in dimensionless form as

$$\sqrt{\frac{3\sigma_p}{\beta}} < M_{slow} < \sqrt{\frac{3\sigma_n}{\mu\beta}} < M_{fast} < \frac{v_{te}}{c_s}, \tag{2.22}$$

is satisfied, where we assume, as indicative guideline, that the lighter ions are hotter. In Eq. (2.21), v_{tc}, v_{th} and v_{te} are, respectively, the thermal speeds of cooler (c) ions, hotter (h) ions and electrons, and V_{slow} and V_{fast} are the phase speeds of the slow and the fast mode waves, respectively. Perhaps the most interesting feature of Eq. (2.22) is that the Mach numbers of the slow and fast mode waves must satisfy $M < \sqrt{3\sigma_n/\mu\beta}$ and $M > \sqrt{3\sigma_n/\mu\beta}$, respectively. From Eqs. (14) and (15) of Kumar and Mishra [27], it is clear that these authors did not take account of the upper sign, which contains important information about the existence of the slow mode wave, and considered the lower sign only without any comment on either of the two mode waves.

Unlike the approach of Kumar and Mishra [27], which leads to complicated density expressions, Eqs. $(2.19) - (2.20)$, we follow the approach of Ghosh et al. [61], and rewrite Eqs. (2.17) and (2.18) in the form

$$n_j = c_j \left[\sqrt{a} \pm \sqrt{b}\right], \tag{2.23}$$

which results in simpler expressions for densities, where c_j $(j = n, p)$ are $\sqrt{\mu\beta/6\sigma_n}$ and $\sqrt{\beta/6\sigma_p}$, respectively, a and b are unknowns which must be determined by substituting (2.23) in (2.17) and (2.18). In this way, Eqs.

(2.17) and (2.18) are expressed as

$$n_p = \frac{1}{2}\sqrt{\frac{\beta}{3\sigma_p}}\left[\sqrt{\left(M+\sqrt{\frac{3\sigma_p}{\beta}}\right)^2-\frac{2\varphi}{\beta}} \pm\sqrt{\left(M-\sqrt{\frac{3\sigma_p}{\beta}}\right)^2-\frac{2\varphi}{\beta}}\right], \tag{2.24}$$

and

$$n_n = \frac{1}{2}\sqrt{\frac{\mu\beta}{3\sigma_n}}\left[\sqrt{\left(M+\sqrt{\frac{3\sigma_n}{\mu\beta}}\right)^2-\frac{2z\varphi}{\mu\beta}} \pm\sqrt{\left(M-\sqrt{\frac{3\sigma_n}{\mu\beta}}\right)^2-\frac{2z\varphi}{\mu\beta}}\right], \tag{2.25}$$

respectively. Since in this paper we are interested in the fast mode only, in Eqs. (2.24) and (2.25), we consider the lower sign $(-)$ for the subsequent discussion.

Having obtained all density expressions, Eqs. (2.7), (2.24), and (2.25), we introduce their coupling in Poisson's equation, Eq. (2.14). Multiplying by $d\varphi/d\xi$ and integrating once, with the usual boundary conditions, results in the usual energy-like equation

$$\frac{1}{2}\left(\frac{d\varphi}{d\xi}\right)^2 + S(\varphi,M) = 0, \tag{2.26}$$

where

$$\begin{aligned} S(\varphi,M) \;=\; & 1-\left(1-\tfrac{2\varphi}{2\kappa-3}\right)^{-\kappa+3/2} \\ & +\tfrac{\alpha\mu\beta}{6(1+\alpha z)}\sqrt{\tfrac{\mu\beta}{3\sigma_n}}\left\{2\left(\tfrac{3\sigma_n}{\mu\beta}\right)^{3/2}+6M^2\left(\tfrac{3\sigma_n}{\mu\beta}\right)^{1/2}\right. \\ & \left.-\left[\left(M+\sqrt{\tfrac{3\sigma_n}{\mu\beta}}\right)^2-\tfrac{2z\varphi}{\mu\beta}\right]^{3/2}+\left[\left(M-\sqrt{\tfrac{3\sigma_n}{\mu\beta}}\right)^2-\tfrac{2z\varphi}{\mu\beta}\right]^{3/2}\right\} \\ & +\tfrac{\beta}{6(1+\alpha z)}\sqrt{\tfrac{\beta}{3\sigma_p}}\left\{2\left(\tfrac{3\sigma_p}{\beta}\right)^{3/2}+6M^2\left(\tfrac{3\sigma_p}{\beta}\right)^{1/2}\right. \\ & \left.-\left[\left(M+\sqrt{\tfrac{3\sigma_p}{\beta}}\right)^2-\tfrac{2\varphi}{\beta}\right]^{3/2}+\left[\left(M-\sqrt{\tfrac{3\sigma_p}{\beta}}\right)^2-\tfrac{2\varphi}{\beta}\right]^{3/2}\right\}. \end{aligned} \tag{2.27}$$

is the Sagdeev pseudopotential for the fast mode solitary waves supported by the plasma model under consideration. In the limits $\alpha \to 0$, i.e. in cases where the number of negative ions is negligible, and $\sigma_p \to 0$ (cold positive ions), Eq. (2.27) reduces to Eq. (19) of Saini et al. [62], who studied a two component plasma composed of kappa-distributed electrons and cold positive ions.

2.3 General considerations of fast mode solitary waves in warm negative ion plasmas

2.3.1 The minimum and maximum Mach numbers

From the theory of the Sagdeev pseudopotential, it is well known that $S(0) = 0$ and $\partial S(0,M)/\partial\varphi = 0$, i.e. the origin must be unstable for a soliton solution to Eq. (2.26) to exist. This is generally expressed as

$$\left.\frac{\partial^2 S(\varphi,M)}{\partial\varphi^2}\right|_{\varphi=0} \leqslant 0, \tag{2.28}$$

often called the soliton condition, and it is verified that this is satisfied by the pseudopotential in (2.27). It is well known that the M value determined from

$$\left.\frac{\partial^2 S(\varphi,M)}{\partial\varphi^2}\right|_{\varphi=0} = 0, \tag{2.29}$$

is the acoustic speed, M_s, which is the minimum soliton speed, for the plasma model under consideration. Using (2.27), we obtain

$$-\frac{2\kappa-1}{2\kappa-3}+\frac{\alpha z^2}{\mu\beta(1+\alpha z)}\frac{1}{M_s^2-3\sigma_n/\mu\beta}+\frac{1}{\beta(1+\alpha z)}\frac{1}{M_s^2-3\sigma_p/\beta}=0. \tag{2.30}$$

Since we are investigating the fast mode structures for which the Mach numbers must satisfy $M > \sqrt{3\sigma_n/\mu\beta}$, from Eq. (2.30) the root $M_s > \sqrt{3\sigma_n/\mu\beta}$ must be chosen. This yields

$$\begin{aligned} M_s^2 \;=\; & \tfrac{3\sigma_p}{2\beta}+\tfrac{3\sigma_n}{2\mu\beta}+\tfrac{2\kappa-3}{2(2\kappa-1)}+\tfrac{2\kappa-3}{2(2\kappa-1)}\left\{\left[\tfrac{2\kappa-1}{2\kappa-3}\left(\tfrac{3\sigma_p}{\beta}+\tfrac{3\sigma_n}{\mu\beta}\right)+1\right]^2\right. \\ & \left.-4\tfrac{2\kappa-1}{2\kappa-3}\left[\tfrac{2\kappa-1}{2\kappa-3}\tfrac{9\sigma_p\sigma_n}{\mu\beta^2}+\tfrac{3(\alpha z^2\sigma_p+\sigma_n)}{\mu\beta^2(1+\alpha z)}\right]\right\}^{1/2}, \end{aligned} \tag{2.31}$$

whose Taylor series expansion to the zeroth order leads to

$$M_s^2 \approx \frac{3\sigma_p}{\beta} + \frac{3\sigma_n}{\mu\beta} + \frac{2\kappa - 3}{2\kappa - 1}. \tag{2.32}$$

It is clear from Eq. (2.32) that M_s is strictly greater than $\sqrt{3\sigma_n/\mu\beta}$, the thermal speed of the lighter ions, as predicted by the ordering (2.22). We also note that an increase in the temperature (expressed through σ_p and σ_n) of either ion species results in the increased acoustic speed, M_s. The third term of the right hand side of Eq. (2.32) reveals interesting electron superthermal effect, which will be explored numerically later considering the full expression of M_s, Eq. (2.31). A decrease in the value of κ, i.e. an increase in the electron superthermal effect, leads to a decrease in M_s; alternatively, the superthermal behavior of the electrons shifts the acoustic speed to lower values.

We recall, from earlier studies [34, 36, 38, 39, 53, 54], that the upper limit in Mach numbers of solitons supported by the plasma model under consideration is obtained when the flow of the adiabatic species coincides with a sonic point [34, 53, 54]. This corresponds to cases in which the density of the adiabatic species ceases to be real. From Eq. (2.24), the positive ion density ceases to be real when the electrostatic potential exceeds

$$\varphi_{lp} = \frac{\beta}{2}\left(M_{lp} - \sqrt{\frac{3\sigma_p}{\beta}}\right)^2, \tag{2.33}$$

and in that case

$$S(\varphi_{lp}, M) = 0, \tag{2.34}$$

where M_{lp} is the maximum/limiting (l) Mach number associated with the occurrence of the positive (p) ion sonic point. We use Eq. (2.34) to determine a relation between M_{lp} and α (ion density ratio), which we write as

$$(\lambda_p + z\delta_p)\,\alpha + \delta_p + \gamma_p = 0, \tag{2.35}$$

where

$$\begin{aligned}
\lambda_p &= \frac{\mu\beta}{6}\sqrt{\frac{\mu\beta}{3\sigma_n}}\left\{2\left(\frac{3\sigma_n}{\mu\beta}\right)^{3/2}+6M_{lp}^2\left(\frac{3\sigma_n}{\mu\beta}\right)^{1/2}\right. \\
&\quad -\left[\left(M_{lp}+\sqrt{\frac{3\sigma_n}{\mu\beta}}\right)^2-\frac{z}{\mu}\left(M_{lp}-\sqrt{\frac{3\sigma_p}{\beta}}\right)^2\right]^{3/2} \\
&\quad \left.+\left[\left(M_{lp}-\sqrt{\frac{3\sigma_n}{\mu\beta}}\right)^2-\frac{z}{\mu}\left(M_{lp}-\sqrt{\frac{3\sigma_p}{\beta}}\right)^2\right]^{\frac{3}{2}}\right\}, \\
\delta_p &= 1-\left[1-\frac{\beta}{2\kappa-3}\left(M_{lp}-\sqrt{\frac{3\sigma_p}{\beta}}\right)^2\right]^{-\kappa+3/2}, \\
\gamma_p &= \frac{\beta}{6}\sqrt{\frac{\beta}{3\sigma_p}}\left\{2\left(\frac{3\sigma_p}{\beta}\right)^{3/2}+6M_{lp}^2\left(\frac{3\sigma_p}{\beta}\right)^{1/2}-\left(4M_{lp}\sqrt{\frac{3\sigma_p}{\beta}}\right)^{\frac{3}{2}}\right\}.
\end{aligned}$$

Similarly, from Eq. (2.25) the negative ion density becomes complex beyond

$$\varphi_{ln}=\frac{\mu\beta}{2z}\left(M_{ln}-\sqrt{\frac{3\sigma_n}{\mu\beta}}\right)^2, \tag{2.36}$$

satisfying

$$S(\varphi_{ln},M)=0, \tag{2.37}$$

from which we get a relation between the maximum/limiting Mach number (M_{ln}) due to the occurrence of the negative ion sonic point and α as

$$(\lambda_n+z\delta_n)\,\alpha+\delta_n+\gamma_n=0, \tag{2.38}$$

where

$$\lambda_n = \frac{\mu\beta}{6}\sqrt{\frac{\mu\beta}{3\sigma_n}}\left\{2\left(\frac{3\sigma_n}{\mu\beta}\right)^{3/2}+6M_{ln}^2\left(\frac{3\sigma_n}{\mu\beta}\right)^{1/2}-\left(4M_{ln}\sqrt{\frac{3\sigma_n}{\mu\beta}}\right)^{\frac{3}{2}}\right\},$$

$$\delta_n = 1-\left[1-\frac{\mu\beta}{z(2\kappa-3)}\left(M_{ln}-\sqrt{\frac{3\sigma_n}{\mu\beta}}\right)^2\right]^{-\kappa+3/2},$$

$$\gamma_n = \frac{\beta}{6}\sqrt{\frac{\beta}{3\sigma_p}}\left\{2\left(\frac{3\sigma_p}{\beta}\right)^{3/2}+6M_{ln}^2\left(\frac{3\sigma_p}{\beta}\right)^{1/2}\right.$$
$$-\left[\left(M_{ln}+\sqrt{\frac{3\sigma_p}{\beta}}\right)^2-\frac{\mu}{z}\left(M_{ln}-\sqrt{\frac{3\sigma_n}{\mu\beta}}\right)^2\right]^{\frac{3}{2}}$$
$$\left.+\left[\left(M_{ln}-\sqrt{\frac{3\sigma_p}{\beta}}\right)^2-\frac{\mu}{z}\left(M_{ln}-\sqrt{\frac{3\sigma_n}{\mu\beta}}\right)^2\right]^{\frac{3}{2}}\right\}.$$

Equations (2.31), (2.35) and (2.38) will be used for the numerical determination of the soliton existence domains in $\{\alpha, M\}$ space, for fixed values of other plasma parameters. While (2.31) will correspond to the minimum Mach number for solitons to exist, (2.35) and (2.38) will provide the maximum Mach numbers due to the occurrence of the positive and negative ion sonic points, respectively. Comparing this with Eqs. $(21)-(24)$ of Kumar and Mishra [27], it is clear that Kumar and Mishra [27] did not derive an expression for the maximum Mach numbers associated with the negative ions. In what follows, we numerically determine the soliton existence domains for the plasma model under consideration, with emphasis on the ion thermal and the electron superthermal effects on the soliton Mach number (speed). Considering parameter values from well-established soliton existence domains, we then investigate the ion thermal and the electron superthermal effects on the soliton amplitude and width. In our numerical investigation, we will assume $\sigma_p = \sigma_n \equiv \sigma$ for the ion-to-electron temperature ratio, since our aim is to get insights regarding the ion thermal effects on the solitary waves propagation characteristics.

2.3.2 The ion thermal and electron superthermal effects on the soliton existence domains

To start our discussion, we recall that this plasma model is well known to support both compressive (positive) and rarefactive (negative) solitons, which also, for some parameter values, coexist [17–21, 24–27]. Here, we first show that our calculations are able to reproduce the well-known results [25, 27], then proceed to demonstrate that there are significant new results which have never been reported before.

Figure 2.1 shows the soliton existence domains in $\{\alpha, M\}$ space for $\mu = 0.5$, $\kappa = 1000$ (left panels) and $\kappa = 1.8$ (right panels). The value $\mu = 0.5$ means that the mass of the positive ion species is two times that of the negative ion species, and has been chosen for comparison of our results with those of Kumar and Mishra [27], who used values of μ in the range $0 < \mu < 1$. The value $\kappa = 1000$ means that the electrons are Maxwellian-distributed. We recall, from studies of plasma waves based on kappa velocity distribution, [50] that quasi-Maxwellian behavior is already obtained for values of κ as low as 20. We have used $\kappa = 1000$ as extreme case in which the Maxwellian behavior for the electrons would be fully recovered. The value $\kappa = 1.8$ represents a case in which the electrons are strongly non-Maxwellian, a case which is common in many space environments [44–49], recalling that acceptable values of κ must be strictly greater than 1.5. For each of these values of κ, the effect of increasing the value of σ is shown.

The upper left panel shows the results obtained for $\sigma = 0.0001$. This value of σ means that the ions are effectively cold. This case has been investigated in Rouhani and Abbasi [25]. The solid line corresponds to the minimum Mach number for solitons to exist, dot-dashes correspond to the maximum Mach number due to the occurrence of the negative ion sonic point, whereas dashes represent the maximum Mach number due to the occurrence of the positive ion sonic point. The allowed Mach numbers are those between the minimum and maximum Mach numbers. The same linestyle applies to all other panels of this figure. The results presented in the upper left panel show that compressive solitons occur at low values of the negative-to-positive ion density ratio

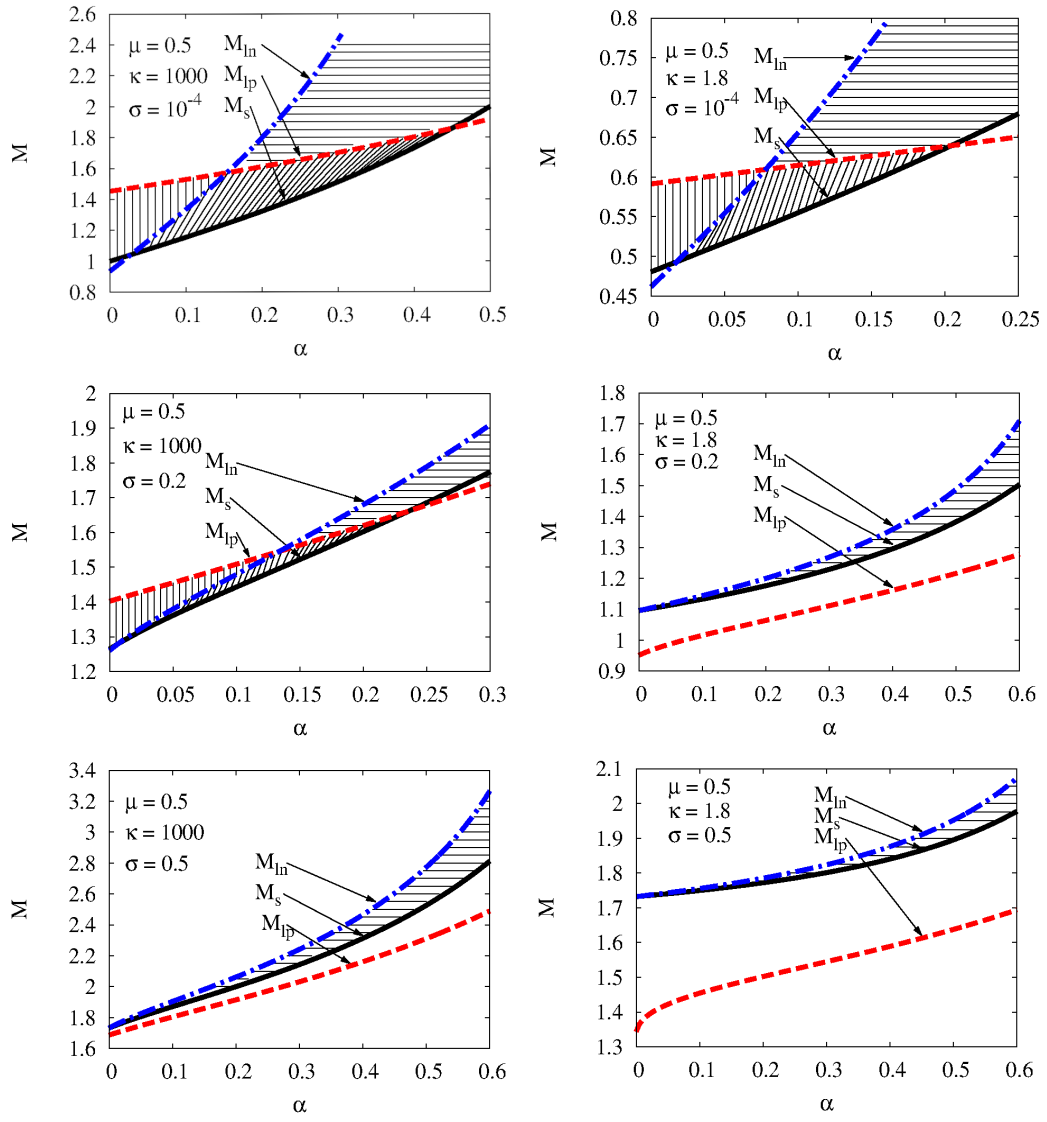

Figure 2.1: (Colour online) Soliton existence domains in $\{\alpha, M\}$ space for $\kappa = 1000$ (left panels) and $\kappa = 1.8$ (right panels), showing the ion thermal effects, expressed through σ. The upper panels are for $\sigma = 0.0001$, the middle panels are for $\sigma = 0.2$, and the lower panels are for $\sigma = 0.5$. The value of the negative-to-positive ion mass ratio used in all panels is $\mu = 0.5$. In each panel, the solid line corresponds to the minimum Mach number (M_s) for solitons to exist, dot-dashes correspond to the maximum Mach number (M_{ln}) due to the occurrence of the negative ion sonic point, whereas dashes represent the maximum Mach number (M_{lp}) associated with the positive ion sonic point. The allowed Mach numbers are those between the minimum and maximum Mach numbers, shaded as explained in the text.

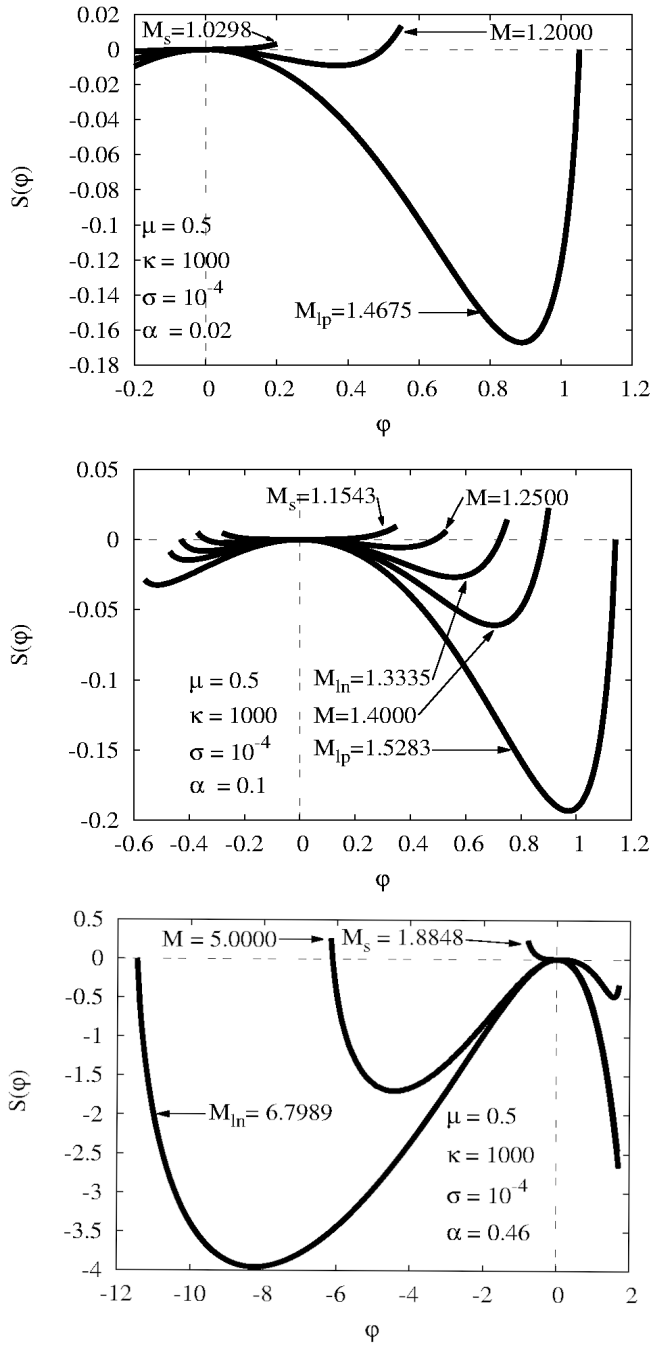

Figure 2.2: (Colour online) Sagdeev pseudopotentials, based on the soliton existence domain presented in the upper left panel of Fig. 2.1, showing that compressive solitons occur at low values of α (upper panel), while high values of α support rarefactive solitons (lower panel), and the two type of structures coexist [25] in the intermediate range of α values (middle panels).

(vertically-shaded domain) whereas rarefactive solitons occur at high values of α (horizontally-shaded domain). We observe, further, that intermediate values of α (obliquely-shaded domain) support the coexistence of compressive and rarefactive solitons. Confirmation of this result is illustrated in Fig. 2.2, in which we present the Sagdeev pseudopotential plots for $\alpha = 0.02$ (upper panel), $\alpha = 0.1$ (middle panel), and $\alpha = 0.46$ (lower panel). This result confirms earlier results. [25]

In the middle left panel, we show the effect of increasing the value of σ to 0.2. The value $\sigma = 0.2$ means that the electrons are 5 times hotter than the ions. This is physically meaningful because the inertialess electrons are expected to be hotter than the ions for which we have retained the inertia. It should be noted that we have plotted the results presented in this panel considering a smaller range of values of α than that for the results in the upper left panel for visibility of the domain in which compressive and rarefactive solitons coexist, which reduces significantly as a result of an increase in the ion thermal effects. We observe that as a result of this increase of σ to 0.2, the domain in which solitons exist is reduced, and this is particularly so for the domain that supports compressive solitons. This result will be explored in greater detail later.

For high values of σ, the upper limiting curve associated with the positive ion sonic point falls below the lower limit. This is illustrated in the lower left panel for $\sigma = 0.5$. In this case, compressive solitons, hence the coexistence domain, disappear and only rarefactive solitons survive. Alternatively, when the ion thermal effects are significant, a negative ion plasma supports the propagation of rarefactive solitons only. This result is important and was not reported in the recent work of Kumar and Mishra. [27]

In the right panels of Fig. 2.1, we show the effect of reducing the value of κ from 1000 to 1.8, i.e. increasing the electron superthermal effect. The results presented in the upper right panel for $\sigma = 0.0001$ show features of the trend illustrated in the upper left panel when $\kappa = 1000$. The plasma still supports both compressive and rarefactive solitons, which also coexist in the intermediate values of α. However, it is observed that, as a result of this decrease of κ, both the minimum and maximum Mach numbers are shifted to lower

values. This is consistent with Eq. (2.32) from which we have found that M_s decreases with decreasing κ. Furthermore, the range in α that supports the coexistence of compressive and rarefactive solitons is narrower than for the case $\kappa = 1000$ (upper left panel), due to the fact that the maximum Mach numbers associated with positive ions are more significantly shifted to lower values than the minimum Mach numbers and therefore the crossover point of these two limiting curves is shifted to lower values of α.

These electron superthermal effects are enhanced as the value of σ is increased. For values of σ as high as 0.2 (middle right panel), the limiting curve associated with positive ions falls below the lower limiting curve, hence the coexistence domain disappears completely and only rarefactive solitons remain. Results of similar trend are obtained for higher values of σ (lower right panel). Overall, it is observed that the ion thermal effects on the soliton existence domains, as presented in the left panels for $\kappa = 1000$, are enhanced by the electron superthermal effects.

As mentioned briefly earlier, the range of Mach numbers which supports the existence of solitons diminishes with increasing ion-to-electron temperature ratio, σ. We explore this result in greater detail in Fig. 2.3, in which we present plots of the minimum Mach numbers (M_s), maximum Mach numbers due to the occurrence of the positive ion sonic point (M_{lp}) and maximum Mach numbers due to the occurrence of the negative ion sonic point (M_{ln}) against σ, for $\kappa = 1000$ (upper panel) and $\kappa = 1.8$ (lower panel). It is observed that, for a given value of κ, M_s increases with σ for all values of σ, as predicted by Eq. (2.32), whereas M_{lp} and M_{ln} first decrease with σ for low values of σ, attaining minimum values from which they increase with σ. Considering the range of σ in which the curves $M_{lp}(\sigma)$ and $M_{ln}(\sigma)$ have positive slopes, it is observed that the increase in the lower Mach number limit is more rapid, which explains why the lower Mach number limiting curve is entirely above the curve corresponding to the positive ion sonic point, resulting in the disappearance of positive solitons for large σ.

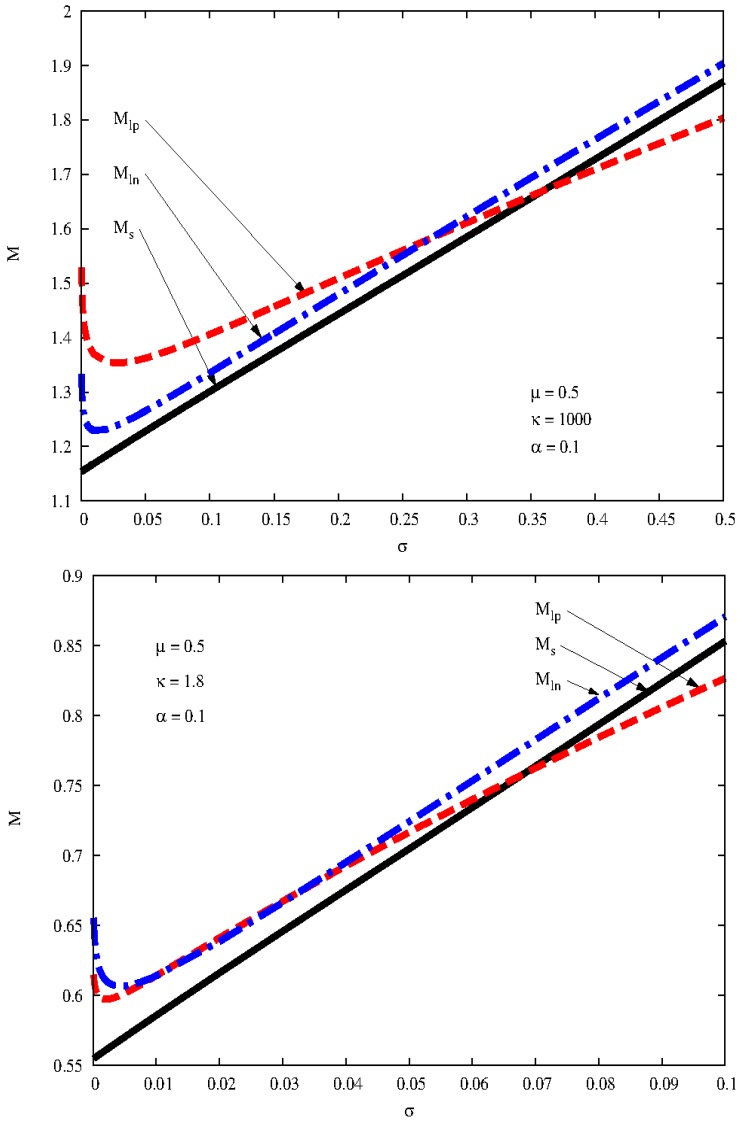

Figure 2.3: (Colour online) Illustration of the ion thermal effects, expressed through σ, on the minimum Mach numbers (solid line), maximum Mach numbers due to the occurrence of the positive ion sonic point (dashed line), and maximum Mach numbers due to the occurrence of the negative ion sonic point (dot-dashes), for $\kappa = 1000$ (upper panel) and $\kappa = 1.8$ (lower panel). The values $\mu = 0.5$ and $\alpha = 0.1$ have been used to obtain the results presented in both panels.

2.3.3 The ion thermal and electron superthermal effects on the soliton amplitude and width

The importance of the soliton existence domains is that when they are well established, further study of solitary waves is done based on a well-known parameter space. In what follows, we consider parameter values from the soliton existence domains presented in Fig. 2.1 for numerical investigation of the ion thermal and electron superthermal effects on the soliton amplitude and width. Figure 2.4 presents the Sagdeev pseudopotentials, in which the ion thermal effects (upper to lower panels) and the electron superthermal effects (left to right panels) on the soliton amplitude and width are shown. In all panels of this figure, the values of μ and α are fixed to 0.5 and 0.3, respectively. We then investigate the effect of increasing the value of σ from 0.0001 to 0.2 for $\kappa = 1000$ (left panels) and for $\kappa = 1.8$ (right panels), considering the Mach numbers ranging from the lower to the upper limit, obtained from the respective soliton existence domains presented in Fig. 2.1.

The upper left panel shows the results obtained when the ions are cold ($\sigma = 0.0001$) and the electrons are Maxwellian ($\kappa = 1000$). In this case, compressive and rarefactive solitons exist together. The amplitude of a compressive soliton with maximum speed ($M_{lp} = 1.7011$) is $\varphi_{lp} \approx 1.42$ and the amplitude of a rarefactive soliton with maximum speed ($M_{ln} = 2.4273$) is $\varphi_{ln} \approx -1.44$. As a result of the increase of the value of σ to 0.2 (lower left panel), the amplitude of a rarefactive soliton with maximum speed decreases from $\varphi_{ln} \approx -1.44$ to $\varphi_{ln} \approx -0.17$, recalling that in this case there are no compressive solitons at $\alpha = 0.3$, since the domain that supports compressive solitons is shifted to lower values of α as σ is increased.

The upper right panel shows the results obtained when the ions are cold ($\sigma = 0.0001$) and the electrons are strongly non-Maxwellian ($\kappa = 1.8$). We recall from Fig. 2.1 that $\kappa = 1.8$ supports rarefactive solitons only at $\alpha = 0.3$, since the domain that supports compressive solitons is shifted to lower values of α as the value of κ is decreased. As a result of this decrease of the value of κ, the amplitude of a rarefactive soliton with maximum speed decreases from $\varphi_{ln} \approx -1.44$ to $\varphi_{ln} \approx -0.40$. Increasing the value of σ to 0.2 (lower

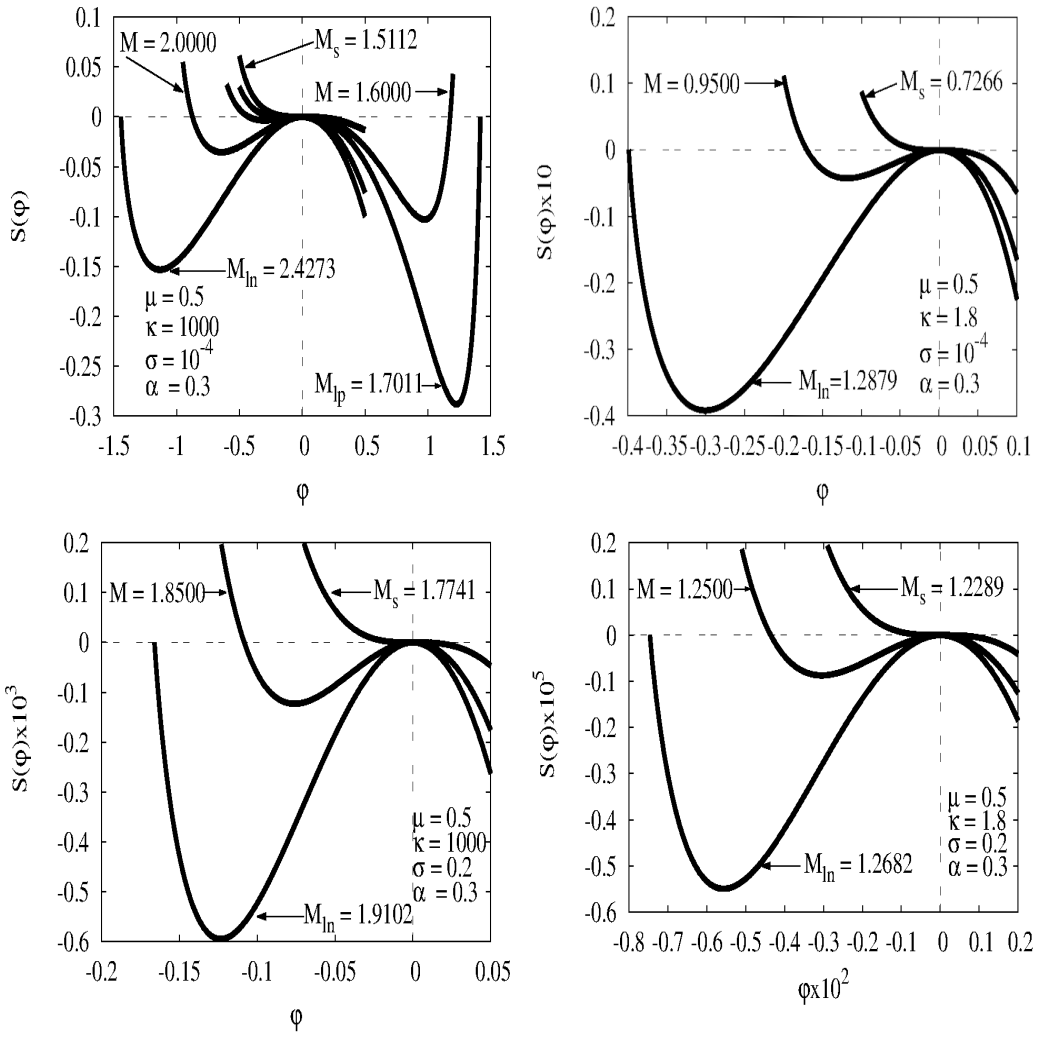

Figure 2.4: (Colour online) Sagdeev pseudopotentials, showing the ion thermal effect (upper to lower panels) and the electron superthermal effect (left to right panels) on the soliton amplitude and width. The effect of increasing the value of σ from 0.0001 (upper panels) to 0.2 (lower panels) is clearly shown. The electron superthermal effect is shown by decreasing the value of κ from 1000 (left panels) to 1.8 (right panels). The two effects are combined in the lower right panel. In all panels, the values of α and μ are fixed to 0.3 and 0.5, respectively.

right panel) results in a significant decrease of the amplitude of a rarefactive soliton with maximum speed, from $\varphi_{ln} \approx -0.40$ to $\varphi_{ln} \approx -0.007$. This means that when combined ion thermal and electron superthermal effects are significant, only small amplitude rarefactive solitons can propagate in a negative ion plasma. Such solitons can well be described by the KdV theory.

We note, from our numerical results presented in Figs. 2.2 and 2.4, that Sagdeev pseudopotential curves for larger M always lie below those for smaller M, and do not cross, outside the common point $\varphi = 0$, where $S(0,M) = 0$ for all M. This is not only a numerical result, but a fact that has also been proved analytically [60, 63, 64]. Indeed, these authors [60, 63, 64] have shown, analytically, that for given compositional parameters, $\partial S/\partial M < 0$. Thus, basing our investigation on a standard approach [60, 63, 64] makes it easier to compare our results with those of Kumar and Mishra [27].

Insights about the ion thermal and electron superthermal effects on the soliton width can be deduced from the energy equation, Eq. (4.14). This equation predicts that when $S(\varphi,M)$ is vanishingly small (i.e. $S(\varphi,M) \to 0$), the steepness of a soliton profile ($d\varphi/d\xi$) is also vanishingly small (i.e. $d\varphi/d\xi \to 0$), implying an increased soliton width. From Fig. 2.4, we observe that when the value of σ is increased to 0.2 (upper to lower left panels), the depth of the pseudopotential well decreases significantly. This decrease in the depth of the pseudopotential well is enhanced when the value of κ is reduced to 1.8 (right panels), suggesting an enhanced increase in the soliton width.

This result is explored, more explicitly, in Fig. 2.5 in which we present the profiles of compressive and rarefactive solitons with maximum speeds for $\mu = 0.5$. The upper panel presents the results obtained for $\alpha = 0.02$, a value which supports compressive solitons only, showing the effect of increasing the value of σ from 0.0001 (solid line) to 0.2 (dashed line) for $\kappa = 1000$. It is clear that this increase in the value of σ results in a significant decrease in the soliton amplitude, but an increased soliton width. The lower panel presents the profile of a rarefactive soliton for $\alpha = 0.3$, showing the combined ion thermal and electron superthermal effects on the soliton amplitude and width,

by reducing the value of κ from 1000 (solid line) to 1.8 (dashed line), keeping the ions warm ($\sigma = 0.2$). Clearly, these combined effects lead to an enhanced decrease in the soliton amplitude, but an enhanced increase in the soliton width.

Up to this point, we have good information that, as a result of the ion thermal effect, the soliton amplitude is decreased while the soliton width is increased, and we know that this effect is enhanced by the superthermal behavior of the electrons. For completeness, it is more informative to explore this result considering a wider range of α. We present in Fig. 2.6 profiles of compressive and rarefactive solitons with maximum speeds for $\alpha = 0.1$, where the two type of structures coexist, and show the effect of reducing the value of κ from 1000 (solid line) to 1.8 (dashed line). Clearly, this decrease in the value of κ leads to a significant decrease in the soliton amplitude, but an increase in the soliton width, confirming our earlier results.
The effect of κ on the soliton amplitude, as shown in Figs. 2.4, 2.5 and 2.6, contradicts the findings of Kumar and Mishra [27]. These authors reported that an increase in the superthermal behavior of the electrons results in an increased soliton amplitude. We note that their investigation of the effect of κ on the soliton amplitude was done for fixed value of the Mach number (soliton speed). This approach is physically incorrect because a variation of κ has effect on the soliton speed, amplitude and width at the same time. For physical reasons, in this work, we fix α and investigate the effect of varying κ on all solitary wave propagation characteristics (speed, amplitude, and width), at the same time. Furthermore, to be more specific, we consider a soliton with maximum Mach number (maximum speed). In this way, Figs. 2.1, 2.4, 2.5, and 2.6 clearly show that decreasing the value of κ decreases the soliton Mach number and amplitude, but increases the soliton width, and this is so for both compressive and rarefactive solitons. For completeness, we have also investigated the effect of κ on the soliton amplitude by following the approach of Kumar and Mishra [27], and the results obtained are presented in Appendix A (Fig. 2.9). We then observe that our results in Appendix A agree qualitatively with those of Kumar and Mishra, i.e., a decrease in the

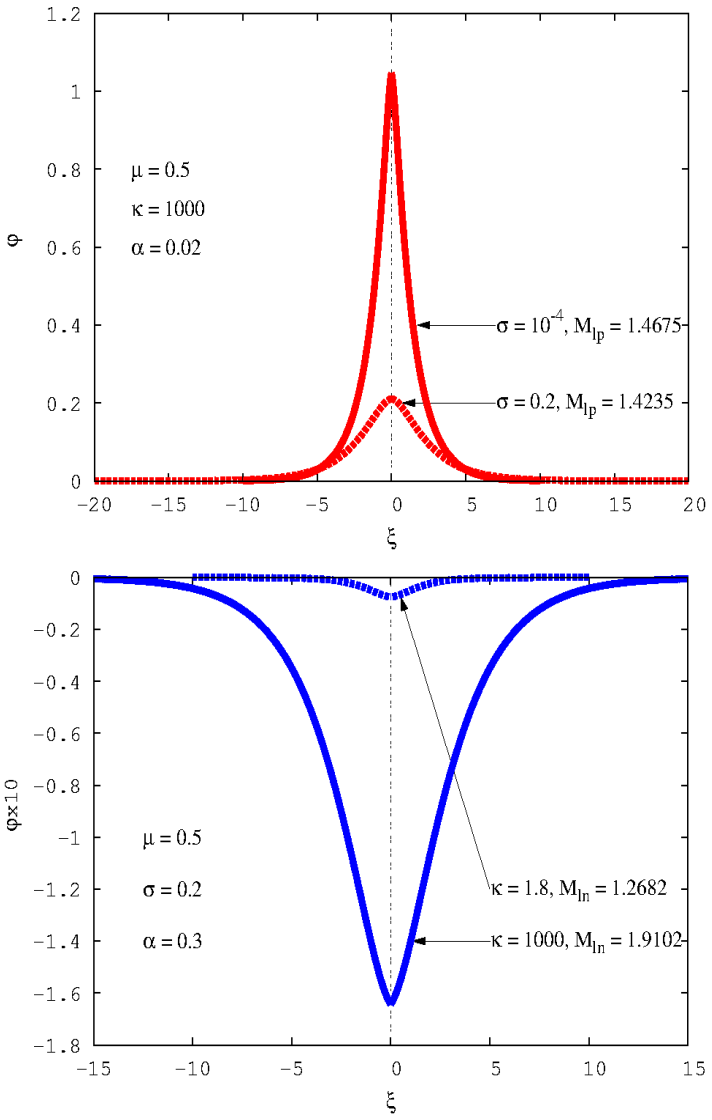

Figure 2.5: (Colour online) Profiles of solitons with maximum speeds, showing the ion thermal effect on compressive solitons at $\alpha = 0.02$ (upper panel) as well as combined ion thermal and electron superthermal effects on rarefactive solitons at $\alpha = 0.3$ (lower panel). The value $\mu = 0.5$ is used in both panels. The interpretation of linestyles is clarified in the figure.

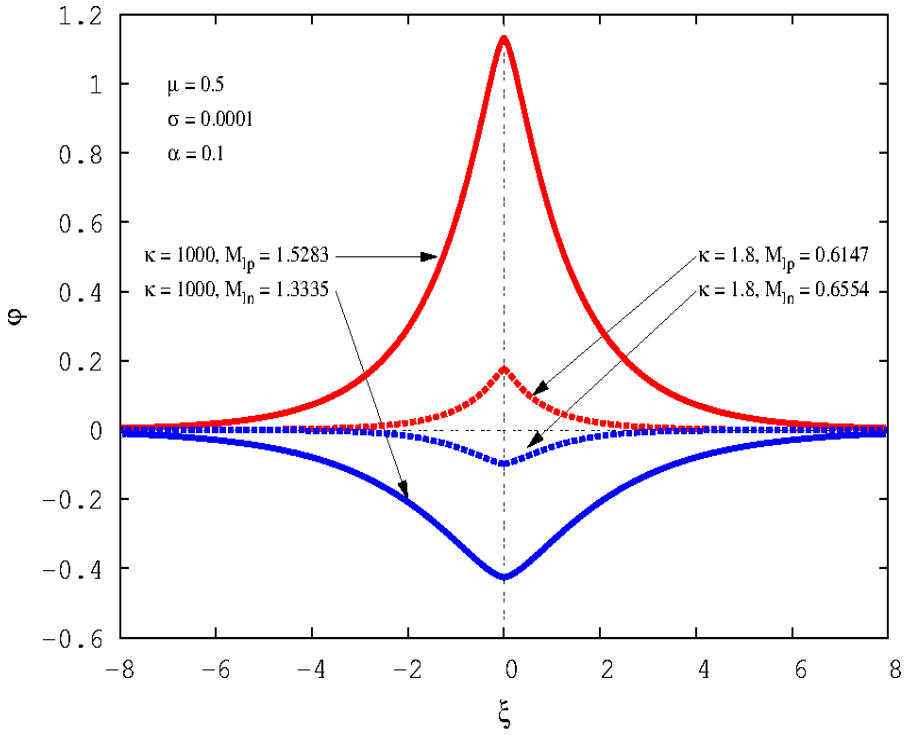

Figure 2.6: (Colour online) Profiles of compressive and rarefactive solitons with maximum speeds at $\alpha = 0.1$ where they coexist, showing the effect of reducing the value of κ from 1000 (solid line) to 1.8 (dashed line), keeping the ions cold ($\sigma = 0.0001$).

value of κ leads to an increase in the soliton amplitude. We also note that the same misconception appears in other papers [25, 62].

It is perhaps worth mentioning that although our discussion of the ion thermal effects on the solitary wave propagation characteristics is done here assuming that $\sigma_p = \sigma_n$, our numerical investigation shows that the conclusions reached remain, qualitatively, unchanged if one varies σ_p for fixed σ_n or vice-versa.

2.4 Stopbands in soliton existence domains

The results presented in Fig. 2.1 show that, for a given value of α, the range of Mach numbers from the lower to the upper limit is a continuous passband,

and this has been known to be the general trend of the soliton existence domains until the recent report by Nsengiyumva et al. [38]. These authors studied a plasma composed of cold and adiabatic positive ion species as well as Boltzmann electrons and reported on the presence of stopbands in the soliton existence domains.

Due to the novel nature of this result in the soliton study, it is important to carry out further work to check whether the observed phenomenon may exist in plasma models other than the one studied by Nsengiyumva et al. [38]. This has motivated the recent work by Maharaj and Bharuthram [41, 42], who have confirmed the presence of stopbands in the soliton existence domain reported by Nsengiyumva et al. [38]. We note that Maharaj and Bharuthram [41, 42] were extending the work of Nsengiyumva et al. [38], by incorporating the electron superthermal effects [41] and the cool ion thermal effects [42], using the same normalization, recalling that the authors [38, 41, 42] normalized all variables with respect to the characteristics of the hot ion species. Would Maharaj and Bharuthram [41, 42] have found the stopbands reported by Nsengiyumva et al. [38] had they used a different normalization?

This is investigated in the present paper, which is based on a different but closely related plasma model. As mentioned previously, the motivation for this paper is based on the significant gaps found in the work of Kumar and Mishra [27]. For this reason, we have used the normalization of Kumar and Mishra [27] for ease of the comparison of our results with theirs. Our analytical work is organized in a way that allows one to recover a plasma with two positive ion species in which stopbands have been observed [38, 41, 42]. This is achieved by varying the parameter z appearing in Eqs. (2.4) and (2.6), setting it to -1 to get a negative ion plasma [27] and to $+1$ to get a two positive ion plasma [38, 41, 42]. Thus, instead of using the subscripts p and n to refer to the positive and negative (lighter) ion species, in this section we use c and h to refer to the cool and hot ion species, respectively, avoiding the assumption $\sigma_p = \sigma_n$ made in Sec. 2.3, since stopbands [38] were found when the temperatures of the two ion species were different. Based on the equi-

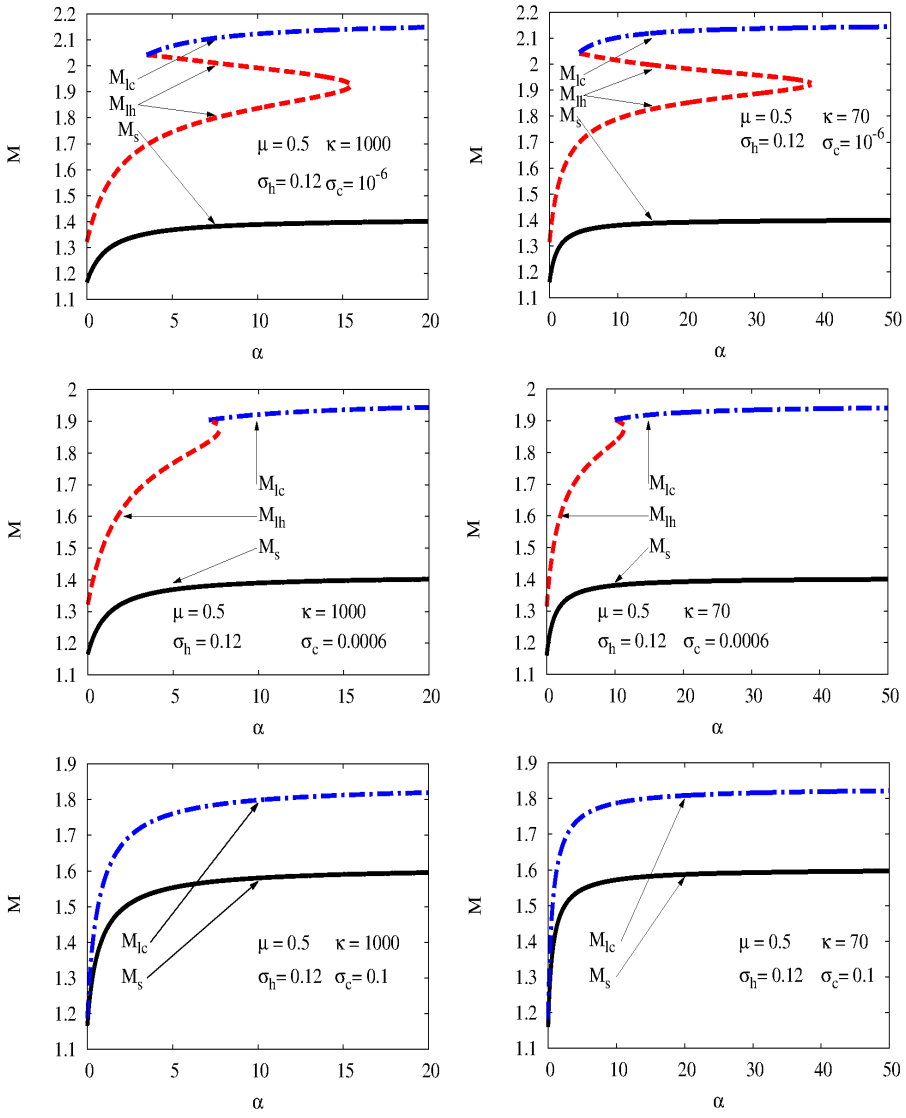

Figure 2.7: (Colour online) Soliton existence domains for $z = +1$, $\kappa = 1000$ (left panels) and $\kappa = 70$ (right panels), showing the presence of stopbands [38] in the upper panels and the effect of reducing the gap between the two ion-to-electron temperature ratios [42]), by increasing the value of σ_c (middle to lower panels). The value $\mu = 0.5$ is used in all panels.

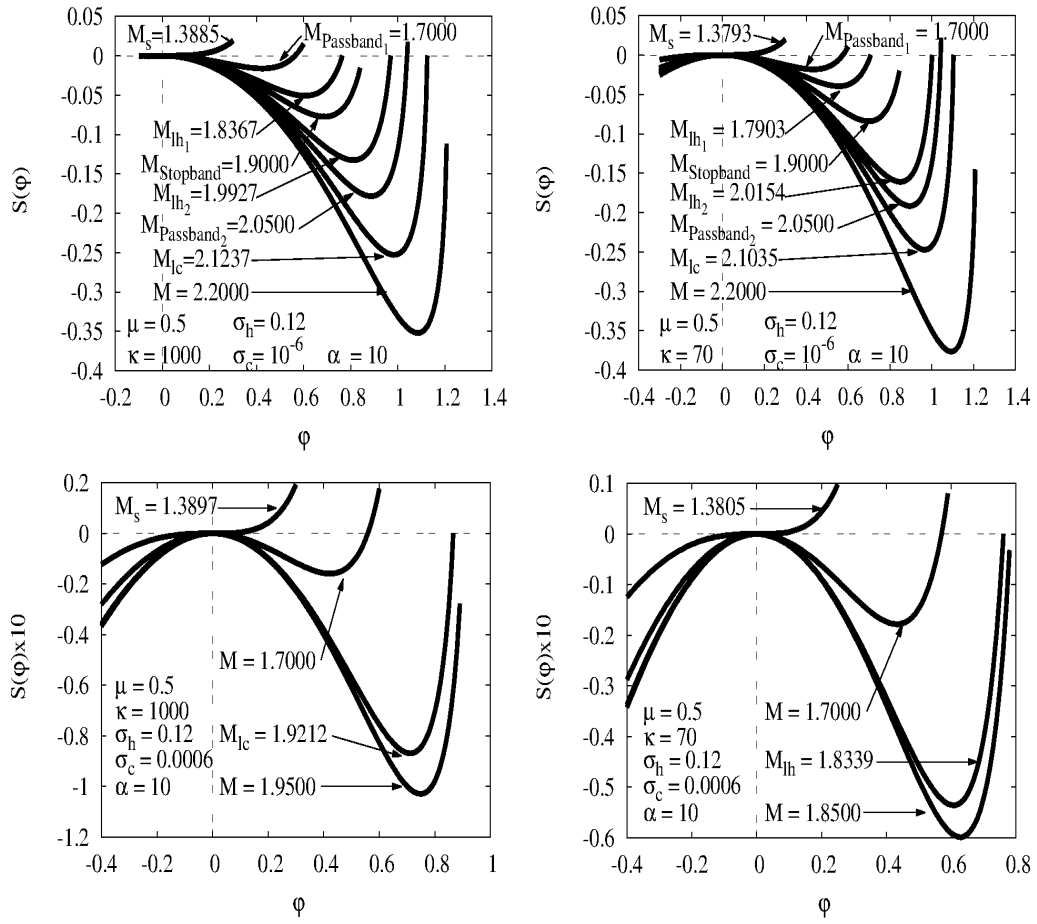

Figure 2.8: (Colour online) Sagdeev pseudopotentials obtained based on parameter values from the soliton existence domains presented in the upper and middle panels of Fig. 2.7, respectively, showing the effect of increasing the Mach number from the acoustic speed, M_s, for $\alpha = 10$.

librium charge neutrality condition, we note that when both ion constituents are positively charged, the equilibrium hot-to-cool ion density ratio, α, can exceed 1.

Figure 2.7 illustrates the soliton existence domains obtained for $\kappa = 1000$ (left panels) and $\kappa = 70$ (right panels). In the upper left panel, we show the results obtained for $\sigma_c = 10^{-6}$ (cold ions) and $\sigma_h = 0.12$ (hot ions). The value $\sigma_h = 0.12$ has been chosen for numerical reasons, and another value could have been used without changing the insights. With these parameter

values, we recover the stopbands reported by Nsengiyumva et al. [38]. In the upper right panel, we show the effect of reducing the value of κ from 1000 to 70. In this case, we still observe stopbands, but these are shifted to high values of α. Considering low values of κ, typically $1.5 < \kappa \lesssim 10$, we do not find stopbands. This is in agreement with the findings of Maharaj and Bharuthram [41].

Reducing the gap between the two ion-to-electron temperature ratios by increasing the value of σ_c from 10^{-6} to 0.006 for $\kappa = 1000$ (middle left panel) results in a significant decrease in the range of α that supports stopbands. Results of similar trend are obtained when the value of κ is reduced to 70 (middle right panel). The soliton existence domains obtained for $\sigma_c = 10^{-2}$ (not shown here) do not show any stopbands, but the maximum Mach numbers are still associated with both limiting factors (hot and cool ion sonic points) with the maximum Mach numbers associated with the hot ion sonic point shifted to very low values of α. The results presented in the lower panels, obtained for $\sigma_c = 0.1$, illustrate a typical case in which the upper limiting curve is entirely associated with the cool ion sonic point. This is in agreement with the recent result of Maharaj and Bharuthram [42], who reported that the observed stopbands [38] are very sensitive to the cool ion temperature.

A simple way to check whether a soliton existence domain is accurate is to plot the Sagdeev pseudopotentials for Mach numbers ranging from the lower to the upper limit. We present in Fig. 2.8 the pseudopotential plots for $\alpha = 10$, based on the soliton existence domains presented in the upper and middle panels of Fig. 2.7, respectively, showing the effect of increasing the Mach number. The results presented in the upper left panel are reminiscent of Fig. 3 of Nsengiyumva et al. (2014), which is discussed in detail in that paper. Similar results are, qualitatively, obtained for $\kappa = 70$ (upper right panel). The point of the present discussion is that we are able to find the stopbands reported by Nsengiyumva et al. [38] using different normalization and different parameter space, hence supporting earlier findings.

On the other hand, it is clear from the pseudopotential plots presented in the

lower panels for the same value of α (i.e. $\alpha = 10$) that the findings are real positive solitons, with a continuous range of Mach numbers, from the acoustic speed (lower limit) to the upper limit, because stopbands are significantly shifted to lower values of α as σ_c is slightly increased to a higher value. Pseudopotential plots (not shown here) of similar trend are obtained based on the soliton existence domains presented in the lower panels of Fig. 2.7. This supports the recent results of Maharaj and Bharuthram [42].

2.5 Summary and conclusions

In this paper, we have revisited the study of large amplitude ion-acoustic fast mode solitary waves in a negative ion plasma with superthermal electrons, using the Sagdeev pseudopotential approach. The overall objective of the study was to investigate the ion thermal and electron superthermal effects on fast mode solitary wave propagation characteristics, closing the gaps found in earlier results [27].

The study was done based on well-established soliton existence domains, which recover the well-known three regions [25, 27] of parameter space that support solitary waves propagating in this plasma. Low values of the negative-to-positive ion density ratio, α, support compressive solitons, whereas high values of α support rarefactive solitons. The two type of structures coexist in the intermediate range of α values [25, 27]). After confirming the earlier findings [25, 27] and closing the observed gaps [27], we have found that there are significant new results, as follows.

1. As a result of the ion thermal effects, expressed through σ, the range in the allowed Mach numbers is reduced, for a given value of α. For large values of σ, compressive solitons, hence the coexistence domain, disappear and only rarefactive solitons survive. Alternatively, when the ion thermal effects are significant, a negative ion plasma supports rarefactive solitons only, and this effect is enhanced by the superthermal behavior of the electrons. This result is important and was not reported in the recent work of Kumar and Mishra [27].

2. For a fixed value of σ, increasing electron superthermal effect shifts the Mach numbers to lower values.

3. Due to the ion thermal effects, the soliton amplitude is decreased, while the soliton width is increased, and this is enhanced by the superthermal behavior of the electrons. When combined ion thermal and electron superthermal effects are significant, only small amplitude rarefactive solitons can propagate in a negative ion plasma. Such solitons can well be described by the KdV theory.

4. Rearranging our analytical work so as to get a two-positive ion plasma, our results show the presence of stopbands in the soliton existence domains, as reported by Nsengiyumva et al. [38], despite the use of different normalization and different parameter space. This suggests that the observed stopbands are a real phenomenon, which needs consideration when studying plasma waves.

Acknowledgements

Partial financial support from the Swedish International Development Cooperation Agency (SIDA) through the International Science Programme (ISP) to the University of Rwanda (UR) through the Rwanda Astrophysics, Space and Climate Science Research Group is gratefully acknowledged. Further financial support from the World Academy of Sciences (TWAS) for the Advancement of Science in developing countries, Grant No. $19-123$ RG/PHYS/AF/AC_I$-$FR3240310162, through the Institut d'Enseignement Superieur de Ruhengeri (INES-Ruhengeri) is also acknowledged.

2.6 References

[1] V. Vuitton, P. Lavvas, R. V. Yelle, M. Galand, A. Wellbrock, G. R. Lewis, A. J. Coates, and J.-E. Wahlund, Planet. Space Sci. **5**7, 1558 (2009).

[2] A. J. Coates, A. Wellbrock, G. R. Lewis, G. H. Jones, D. T. Young, F. J. Crary, J. H. Waite, R. E. Johnson, T. W. Hill, and E. C. Sittler Jr., The Royal Society of Chemistry **1**47, 293 (2010).

[3] A. J. Coates, G. H. Jones, G. R. Lewis, A. Wellbrock, D. T. Young, F. J. Crary, R. E. Johnson, T. A. Cassidy, and T. W. Hill, Elsevier **2**06, 618 (2010).

[4] P. Chaizy, H. Reme, J. A. Sauvaud, C. d'Uston, R. P. Lin, D. E. Larson, D. L. Mitchell, K. A. Anderson, C. W. Carlson, A. Korth, and D. A. Mendis, Nature **3**49, 393 (1991).

[5] K. Agren, N. J. T. Edberg, and J.-E. Wahlund, Geophys. Res. Lett. **3**9, L10201 (2012).

[6] A. J. Coates, A. Wellbrock, G. R. Lewis, G. H. Jones, D. T. Young, F. J. Crary, and J. H. Waite Jr., Planet. Space Sci. **5**7, 1866 (2009).

[7] S. von Goeler, T. Ohe, and N. D'Angelo, J. Appl. Phys. **3**7, 2519 (1966).

[8] A. Y. Wong, D. L. Mamas, and D. Amush, Phys. Fluids **1**8, 1489 (1975).

[9] D. P. Sheehan and N. Rynn, Rev. Sci. Instrum. **5**9, 1369 (1988).

[10] B. Song, D. Suszcynsky, N. D'Angelo, and R. L. Merlino, Phys. Fluids B **1**, 2316 (1989).

[11] J. Jacquinot, B. D. McVey, and J. E. Scharer, Phys. Rev. Lett. **3**9, 88 (1977).

[12] Y. Nakamura, T. Odagiri, and I. Tsukabayashi, Plasma Phys. Contr. F. **3**9, 115004 (2001).

[13] A. Weingarten, R. Arad, Y. Maron, and A. Fruchtman, Phys. Rev. Lett. **8**7, 115004 (2001).

[14] R. A. Gottscho and C. E. Gaebe, IEEE Trans. Plasma Sci. **1**4, 92 (1986).

[15] M. Bacal and G. W. Hamilton, Phys. Rev. Lett. **4**2, 1538 (1979).

[16] R. Sabry, W. M. Moslem, and P. K. Shukla, Phys. Plasmas **1**6, 032302 (2009).

[17] S. G. Tagare, J. Plasma Phys. **3**8, 301 (1986).

[18] M. K. Mishra and R. S. Chhabra, Phys. Plasmas **3**, 4446 (1996).

[19] T. S. Gill, P. Bala, H. Kaur, N. S. Saini, S. Bansal, and J. J. Kaur, Eur. Phys. J. D **3**1, 91 (2004).

[20] M. K. Mishra, R. S. Tiwari, and J. K. Chawla, Phys. Plasmas **1**9, 062303 (2012).

[21] S. Hussain, N. Akhtar, and S. Mahmood, Astrophys. Space Sci. **3**38, 265 (2012).

[22] K. Jilani, A. M. Mirza, and T. A. Khan, Astrophys. Space Sci. **3**44, 135 (2013).

[23] S. Ali Shan and N. Akhtar, Astrophys. Space Sci. **3**46, 367 (2013).

[24] M. Mehdipoor, Astrophys. Space Sci. **3**48, 115 (2013).

[25] M. R. Rouhani and Z. E. Abbasi, Phys. Plasmas **1**9, 112307 (2012).

[26] S. K. El-labany, R. Sabry, E. F. El-shamy, and D. M. Khedr, J. Plasma Phys. **7**9, 613 (2013).

[27] K. Kumar and M. K. Mishra, AIP Advances **7**, 115114 (2017).

[28] B. D. Fried, R. B. White, and T. K. Samec, Phys. Fluids **1**4, 2388 (1971).

[29] I. M. A. Gledhill and M. A. Hellberg, J. Plasma Phys. **3**6, 75 (1986).

[30] Y. Nakamura, M. Nakamura, and T. Itoh, Phys. Rev. Lett. **3**7, 209 (1976).

[31] M. Q. Tran, Phys. Plasmas **1**6, 1167 (1974).

[32] M. Q. Tran and S. Coquerand, Phys. Rev. A **1**4, 2301 (1976).

[33] F. Verheest, M. A. Hellberg, and G. S. Lakhina, Astrophys. Space Sci. Trans. **3**, 15 (2007).

[34] F. Verheest, M. A. Hellberg, and I. Kourakis, Phys. Plasmas **1**5, 112309 (2008).

[35] A. E. Dubinov, Plasma Phys. Rep. **3**5, 991 (2009).

[36] F. Verheest, M. A. Hellberg, N. S. Saini, and I. Kourakis, Phys. Plasmas **1**8, 042309 (2011).

[37] G. S. Lakhina, S. V. Singh, and A. P. Kakad, Phys. Plasmas **2**1, 062311 (2014).

[38] F. Nsengiyumva, M. A. Hellberg, F. Verheest, and R. L. Mace, Phys. Plasmas **2**1, 102301 (2014).

[39] F. Nsengiyumva, M. A. Hellberg, and R. L. Mace, Phys. Plasmas **2**2, 092304 (2015).

[40] S. K. Maharaj, R. Bharuthram, S. V. Singh, and G. S. Lakhina, Phys. Plasmas **2**2, 032313 (2015).

[41] S. K. Maharaj and R. Bharuthram, Phys. Plasmas **2**4, 022305 (2017).

[42] S. K. Maharaj and R. Bharuthram, Phys. Plasmas **2**6, 052302 (2019).

[43] V. M. Vasyliunas, J. Geophys. Res. **7**3, 2839 (1968).

[44] E. T. Sarris, S. M. Krimigis, A. T. Y. Lui, K. L. Ackerson, L. A. Frank, and D. J. Williams, Geophys. Res. Lett. **8**, 349 (1981).

[45] T. E. Eastman, L. A. Frank, W. K. Peterson, and W. Lennartsson, J. Geophys. Res. **8**9, 1553 (1984).

[46] S. P. Christon, D. G. Mitchell, D. J. Williams, L. A. Frank, C. Y. Huang, and T. E. Eastman, J. Geophys. Res. **9**3, 2562 (1988).

[47] S. P. Christon, D. J. Williams, D. G. Mitchell, L. A. Frank, and C. Y. Huang, J. Geophys. Res. **9**41, 13409 (1989).

[48] N. Divine and H. B. Garrett, J. Geophys. Res. **8**8, 6889 (1983).

[49] S. M. Krimigis, J. F. Carbary, E. P. Keath, T. P. Armstrong, L. J. Lanzerotti, and G. Gloeckler, J. Geophys. Res. **8**8, 8633 (1983).

[50] D. Summers and R. M. Thorne, Phys. Fluids B **3**, 1835 (1991).

[51] M. A. Hellberg, R. L. Mace, T. K. Baluku, I. Kourakis, and N. S. Saini, Phys. Plasmas **1**6, 094701 (2009).

[52] S. G. Tagare, Plasma Physics **1**5, 1247 (1973).

[53] J. F. McKenzie, Phys. Plasmas **9**, 800 (2002).

[54] F. Verheest, T. Cattaert, G. S. Lakhina, and S. V. Singh, J. Plasma Phys. **7**0, 237 (2004).

[55] A. J. Coates, F. J. Crary, G. R. Lewis, D. T. Young, J. H. Waite Jr. and E. C. Sittler Jr., Geophys. Res. Lett. **3**4, L22103 (2007).

[56] V. Mukundan and A. Bhardwaj, The Astrophysical Journal **8**56, 168 (2018).

[57] P. Schippers, M. Blanc, N. Ande, I. Dandouras, G. R. Lewis, L. K. Gilbert, A. M. Anderson, N. Krupp, D. A. Gurnett, J. A. Coates, S. M. Krimigis, D. T. Young and M. K. Dougherty, J. Geophys. Res. **1**13, A07208(2008).

[58] P. Lavvas, R. V. Yelle, T. Koskinen, A. Bazin, V. Vuitton, E. Vigren, M. Galand, A. Wellbrock, A. J. Coates, J. Wahlund, F. J. Crary and D. Snowden, PNAS **1**10, 2729(2013).

[59] T. K. Baluku and M. A. Hellberg, Phys. Plasmas **1**5, 123705 (2008).

[60] F. Verheest and M. A. Hellberg, J. Plasma Phys. **7**6, 277 (2010).

[61] S. S. Ghosh, K. K. Ghosh, and A. N. Sekar Iyengar, Phys. Plasmas **3**, 3939 (1996).

[62] N. S. Saini, I. Kourakis, and M.A. Hellberg, Phys. Plasmas **1**6, 062903(2009).

[63] F. Verheest and M. A. Hellberg, Phys. Plasmas **1**7, 023701 (2010).

[64] F. Verheest, Phys. Plasmas **1**7, 062302 (2010).

Appendix: The electron superthermal effect on the soliton amplitude for $M = 1.18$

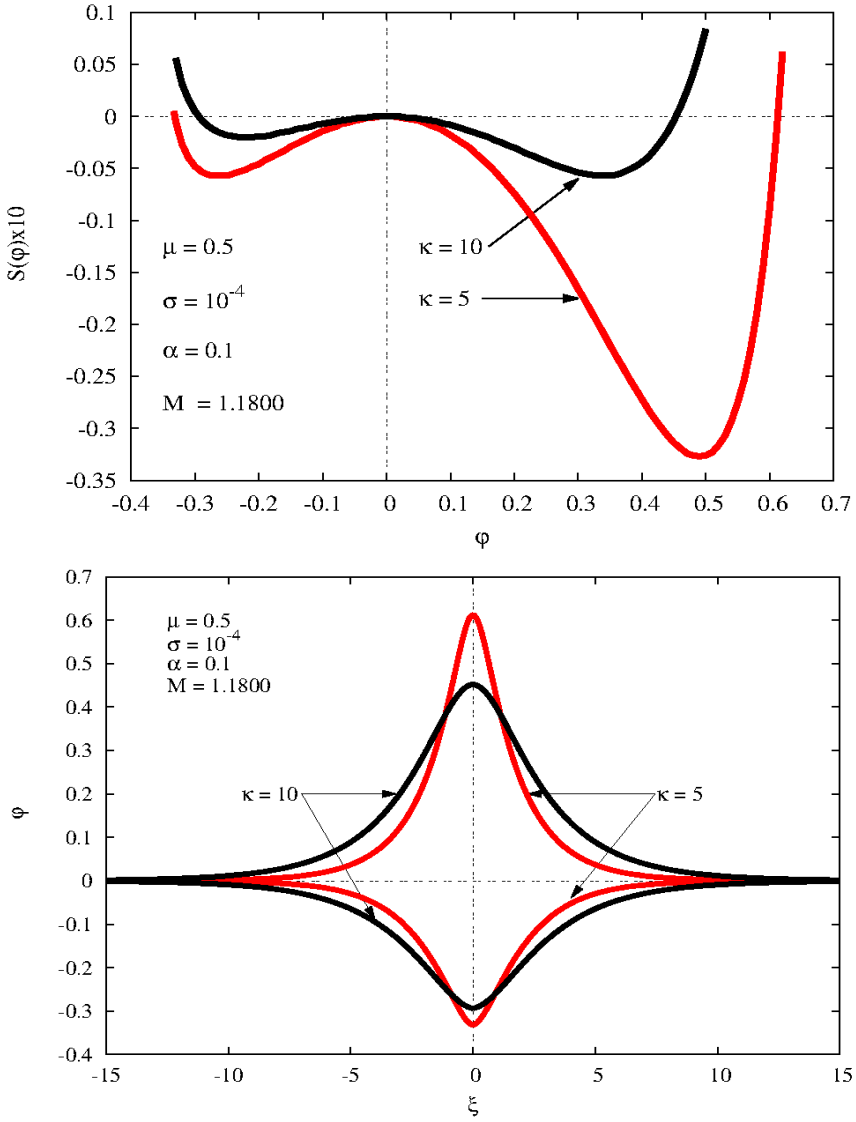

Figure 2.9: (Colour online) Sagdeev pseudopotential (upper panel) and the corresponding soliton profile (lower panel) for $\mu = 0.5$, $\alpha = 0.1$, and $\sigma = 10^{-4}$, showing the effect of reducing the value of κ from 10 to 5 on the soliton amplitude and width, when the Mach number M is fixed to 1.18 [27].

Chapter 3

Large amplitude slow ion-acoustic solitons, supersolitons, and double layers in a warm negative ion plasma with superthermal electrons

Large amplitude slow ion-acoustic solitons, supersolitons, and double layers in a warm negative ion plasma with superthermal electrons

X. Mushinzimana[1, a)] , F. Nsengiyumva[2,b)] , and L. L. Yadav[2,c)]

[1] *Department of Physics, University of Rwanda*

College of Science and Technology

P. O. Box 3900 Kigali, Rwanda

[2] *Department of Civil Engineering*

Institut d'Enseignement Superieur de Ruhengeri

P. O. Box 155 Musanze, Rwanda

[3] *Department of Mathematics, Science and Physical Education,*

University of Rwanda- College of Education,

P. O. Box 55 Rwamagana, Rwanda.

[a)] Author to whom correspondence should be addressed: muxavier2000@yahoo.fr

[b)] Email: franco.nseng@gmail.com

[c)] Email: yadavll@yahoo.com

Abstract

The pseudopotential approach is used to investigate the ion thermal and electron superthermal effects on the slow mode solitary wave propagation characteristics in a negative ion plasma, comprising warm positive and negative ions and kappa-distributed electrons. The Sagdeev pseudopotential for the plasma model is derived and analysed in a systematic way. While it is well known that a negative ion plasma supports the propagation of the fast mode normal solitons, it is found that it supports, in addition to the slow mode normal solitons, the propagation of the slow mode supersolitons and double layers for high values of the negative ion density. The double layers occur as the lower limit to the supersoliton existence range and as the limiting factor for the propagation of normal solitons. When the relative temperature of the two ion species decreases, it is found that the Mach number range supporting the propagation of the nonlinear structures reduces, while the amplitudes of solitons and supersolitons decrease, and these effects are enhanced by the superthermal behaviour of the electrons. The amplitudes of the double layers increase with a decrease in the relative temperature of the two ion species but decrease with an increase in the electron superthermality.

3.1 Introduction

Theoretical and experimental investigations of the propagation of electrostatic waves in negative ion plasmas have been of interest in the recent years. The interest in negative ion plasmas has been motivated, on one hand, by observations of negative ions in naturally occurring space plasmas. They have been observed in D and F regions of the Earth's ionosphere [1], in Halley's cometary comae [2], in the interstellar medium [3, 4], and in the solar wind [5]. Recently, negative ions have been found in the ionosphere of Saturn's moons Titan [6–11], and Enceladus [8] by the electron spectrometer on board Cassini spacecraft. On the other hand, these investigations were motivated by the importance of negative ions in human made technology.

The neutral beam injection based on negative ion sources is one of the most promising heating system for plasma heating in fusion reactors [12], and negative ion plasmas are used in the area of material processing such as plasma surface etching and ion implantation [13] to cite only a few examples.

Experimental [14–18] and theoretical [19–34] studies have revealed that in any two ion species plasma with finite temperature of at least one of the ion species, two wave modes with different phase speeds propagate, the fast mode and the slow mode. The differentiation between these two modes is made on the basis of the range of their phase speeds [35] vis à vis the ion thermal speeds, *viz.*,

$$v_{tc} < v_{slow} < v_{th} < v_{fast} < v_{te}, \tag{3.1}$$

where v_{tc}, v_{th}, v_{te} are the thermal speeds of colder ion species, hotter ion species and electrons, v_{slow} and v_{fast} being the phase speeds of the slow and the fast wave modes, respectively.

An important parameter in the study of negative ion plasmas is the ratio of negative-to-positive ion density that shows the percentage of the negative ions in the plasma. Theoretical [36] and experimental [16] investigations have shown that as the negative-to-positive density ratio increases, the slow mode increasingly damps, while the fast mode is less and less damped, making it the dominant mode. However, in a numerical analysis of the dispersion relation, Ichiki et al. [37] have shown that the slow mode dominates the fast mode whenever the negative ion species is much lighter than the positive ion species. Subsequently, Ichiki et al. [18] observed, in the low temperature regime, the slow mode in $X_e^+ - F^- - e$ negative ion plasma, having negative-to-positive ion mass ratio $\mu = 0.15$. The propagation of the slow mode waves has also been observed experimentally by Handique et al. [17] in an experiment with $A_r^+ - F^- - e$ plasma. In space plasmas, the propagation of the slow mode waves has been observed in the Earth's plasma sheet boundary layer (PSBL) by the Cluster multispacecraft as reported by

Norgren et al. [38] and Kakad et al. [39].

Most of the theoretical studies on the slow mode have focused on the small amplitude solitons based on the KdV theory [21, 25–28, 40–43]. However, it is well known that negative ion plasmas can support nonlinear structures which cannot be described by KdV theory [44, 45]. An example of such a structure is the supersoliton [46]. A supersoliton is a nonlinear structure, characterised by its unusual Sagdeev potential and distorted electric field [47, 48]. Such distorted electric fields have already been observed in space plasmas [49]. Supersolitons have been predicted in multi-component plasmas [46, 47, 50–54]. A two component plasma cannot, however, support supersolitons as has been shown by Verheest et al. [55]. We note here that Sagdeev pseudopotentials yielding supersolitons had been reported [56, 57] before the name supersoliton was coined by Dubinov and Kolotkov [46], but they were not recognised as new nonlinear structures.

In most cases [21, 41, 43], studies of the propagation of the slow mode electrostatic solitary waves supported by negative ion plasmas was based on a Maxwellian distribution of electrons. However, observations and measurements by satellites in different space environments have shown the presence of particle distributions with a high energy tail, following a power law instead of the Maxwellian distribution [58]. Among non-Maxwellian distribution functions that have been utilised to model such particles, the so-called generalised Lorentzian or kappa distribution [58] has been found to be appropriate in many cases. The three-dimensional isotropic kappa velocity distribution function $f_\kappa(v)$ for any particle species is given by [59]

$$f_\kappa(v) = \frac{N}{(\pi\kappa\theta^2)^{3/2}} \frac{\Gamma(\kappa+1)}{\Gamma\left(\kappa-\frac{1}{2}\right)} \left(1+\frac{v^2}{\kappa\theta^2}\right)^{-(\kappa+1)}, \tag{3.2}$$

where κ is a parameter showing the departure from the Maxwellian distribution and is called the spectral index, v is the particle speed, N is the species particle density, Γ is the gamma function and θ is the effective thermal speed modified by the spectral index and is related to the normal thermal speed,

v_t, by $\theta = [(2\kappa - 3)/\kappa]^{1/2} v_t$, provided that the spectral index $\kappa > 3/2$. For large values of κ ($\kappa \to \infty$), the function $f_\kappa(v)$ approaches the Maxwellian distribution while low values of κ indicate the presence of a large fraction of particles with speeds greater than the thermal speed. Kappa-distributed particles with $2 < \kappa < 6$ have been observed in the solar wind [60], Saturn's magnetosphere [61] and in Titan's upper atmosphere [62]. A more complete review of regions in space environments where kappa-distributed particles are present can be found in Pierrard and Lazar [63].

Based on the kappa velocity distribution for the electrons and the fluid theory for both ion species, we, inter alia, show that a negative ion plasma supports the propagation of the slow mode supersolitons and double layers. The paper is organised as follows. After this introductory section, we derive from the fluid equations an expression for the Sagdeev pseudopotential in Sec. II. We then discuss in this same section the lower and upper limits of the soliton existence domain in terms of Mach number range. Sec. III specialises to the ion thermal and electron superthermal effects on the soliton existence domain, amplitude and width for low-to-intermediate values of negative-to-positive ion density ratio. These same effects are also discussed in Sec. IV for higher values of the negative-to-positive ion density ratio, for which the plasma supports the propagation of slow mode supersolitons and double layers. A summary of the results is presented in Sec. V.

3.2 Basic formalism

3.2.1 Plasma densities and Sagdeev pseudopotential

We consider a one dimensional, collisionless, unmagnetized negative ion plasma comprising singly charged adiabatic positive (label p) and negative (label n) ion species, as well as nonthermal electrons (label e), distributed according to kappa distribution, and investigate the slow mode arbitrary amplitude ion-acoustic electrostatic waves using the Sagdeev pseudopotential method. In light of Eq. (3.1), the slow mode exists provided the thermal

speeds of the ion species are different. Accordingly, we treat the positive ion species to be the colder component and the negative ion species to be the hotter component. Both ion species are dynamic and the nonlinear behavior of the ion acoustic waves obeys the following set of normalised partial differential equations in the fluid description

$$\frac{\partial n_p}{\partial t} + \frac{\partial \left(n_p u_p\right)}{\partial x} = 0, \tag{3.3}$$

$$\frac{\partial u_p}{\partial t} + u_p \frac{\partial u_p}{\partial x} = -\mu \frac{\partial \varphi}{\partial x} - f^2 \mu \tau_p n_p \frac{\partial n_p}{\partial x}, \tag{3.4}$$

$$\frac{\partial n_n}{\partial t} + \frac{\partial \left(n_n u_n\right)}{\partial x} = 0, \tag{3.5}$$

$$\frac{\partial u_n}{\partial t} + u_n \frac{\partial u_n}{\partial x} = \frac{\partial \varphi}{\partial x} - n_n \frac{\partial n_n}{\partial x}, \tag{3.6}$$

where x is the space coordinate, t is the time coordinate, φ is the electrostatic potential, n_p, u_p and n_n, u_n are the densities and fluid flow velocities of positive and negative ion species, respectively. The parameter $\mu = m_n/m_p$ is the negative to positive ion mass ratio, $\tau_p = T_p/T_n$ is the positive to negative ion temperature ratio and $\tau_n = T_n/T_e$ is the ratio of the negative ion temperature to the electron temperature. The variable $f = n_{n0}/n_{p0}$ is the ratio of negative ion equilibrium density n_{n0} to positive ion species equilibrium density n_{p0} and expresses the percentage of the negative ions in the plasma. Its values are in the range $0 < f < 1$, where $f = 0$ corresponds to the absence of negative ions and $f = 1$ corresponds to the absence of electrons. We will skip these extreme values in our analysis. Positive ion, negative ion and electron densities are coupled through the Poisson's equation

$$\frac{\partial^2 \varphi}{\partial x^2} = n_e + n_n - n_p, \tag{3.7}$$

where the density of the inertialess electrons n_e in an electrostatic potential φ, obtained by integrating expression (3.2) over velocity space is given by

$$n_e = \frac{1-f}{f}\left(1 - \frac{2\tau_n \varphi}{2\kappa - 3}\right)^{-\kappa+1/2}. \tag{3.8}$$

The system is closed by the equation of state. We have assumed the ion flow to be adiabatic with the relation between the j^{th} $(j = p,n)$ ion species pressure and its density to be

$$p_j n_j^{-\gamma} = constant, \tag{3.9}$$

where $\gamma = 3$ is the polytropic index and the unperturbed pressure of the j^{th} adiabatic species is defined as [64] $p_{j0} = n_{j0}T_j/3$. The variables have been normalized as following: the space coordinate x is normalised by $\lambda_{Dn} = (\varepsilon_0 T_n/n_{n0}e^2)^{1/2}$, the time by the inverse of $\omega_{pn} = (n_{n0}e^2/\varepsilon_0 m_n)^{1/2}$, the flow velocities by the negative ion species thermal velocity $v_{tn} = (T_n/m_n)^{1/2}$, the electrostatic potential by the thermal potential T_e/e and densities are normalised by the negative ion species equilibrium density. With this normalization, the thermal speeds of positive and negative ions are $\mu\tau_p$ and 1, respectively, and the boundary conditions far away from the perturbation, where the plasma is undisturbed, are

$$\begin{aligned} &n_p(\infty) = \tfrac{1}{f}, && n_n(\infty) = 1, \\ &u_p(\infty) = 0, && u_n(\infty) = 0, \\ &\varphi(\infty) = \tfrac{d\varphi}{d\xi}(\infty) = \tfrac{d^2\varphi}{d\xi^2}(\infty) = 0. \end{aligned} \tag{3.10}$$

To find the ion densities n_p and n_n in Eq. (3.7), the fluid Eqs. (3.3)-(3.6) are written in a frame where the nonlinear structure is stationary, by assuming that all dependent variables depend on a single independent variable $\xi = x - Mt$, where the Mach number $M = V/v_{tn}$ is the speed V of the nonlinear structure in the inertial frame, normalized by the negative ion thermal speed. Using this transformation and going through the necessary algebra, Eqs. (3.3)-(3.7) become

$$-M\frac{dn_p}{d\xi} + \frac{d(n_p u_p)}{d\xi} = 0, \tag{3.11}$$

$$-M\frac{du_p}{d\xi} + u_p\frac{du_p}{d\xi} = -\mu\frac{d\varphi}{d\xi} - f^2\mu\tau_p n_p\frac{dn_p}{d\xi}, \tag{3.12}$$

$$-M\frac{dn_n}{d\xi} + \frac{d(n_n u_n)}{d\xi} = 0, \tag{3.13}$$

$$-M\frac{du_n}{d\xi}+u_n\frac{du_n}{d\xi}=-\frac{d\varphi}{d\xi}-n_n\frac{dn_n}{d\xi}, \tag{3.14}$$

$$\frac{d^2\varphi}{d\xi^2}=n_e+n_n-n_p. \tag{3.15}$$

After integrating the pairs of equations (3.11) and (3.12) and (3.13) and (3.14) with the boundary conditions (3.10), we get a biquadratic equation for each of the ion species density,

$$\mu\tau_p f^4 n_p^4-\left(M^2-2\mu\varphi+\mu\tau_p\right)f^2n_p^2+M^2=0, \tag{3.16}$$

for the positive ion density and

$$n_n^4-\left(M^2+2\varphi+1\right)n_n^2+M^2=0, \tag{3.17}$$

for the negative ion density. The solutions to these equations are, respectively,

$$n_p^2=\frac{1}{2f^2\mu\tau_p}\left[M^2-2\mu\varphi+\mu\tau_p\pm\sqrt{\left(M^2-2\mu\varphi+\mu\tau_p\right)^2-4M^2\mu\tau_p}\right], \tag{3.18}$$

and

$$n_n^2=\frac{1}{2}\left[M^2+2\varphi+1\pm\sqrt{\left(M^2+2\varphi+1\right)^2-4M^2}\right]. \tag{3.19}$$

According to Eq. (3.1), the colder positive ion species is supersonic and $V>v_{tp}$ or $M>\sqrt{\mu\tau_p}$ in normalized variables. Therefore, far from the perturbation, where $\varphi=0$, $\sqrt{(M^2-\mu\tau_p)^2}=M^2-\mu\tau_p$ and we choose the negative sign in front of the square root of Eq. (3.18) to get the correct limit $n_p(\infty)=1/f$. For similar reason, we have to choose the positive sign in front of the square root in Eq. (3.19) for the hotter subsonic negative ion species ($V<v_{tn}$). With this choice of signs, Eqs. (3.18) and (3.19) can be rewritten following the approach of Ghosh et al. [65] as

$$n_j=c_j\left[\sqrt{a}\pm\sqrt{b}\right], \tag{3.20}$$

where c_j ($j=p,n$) are $c_p=1/2f\sqrt{\mu\tau_p}$ and $c_n=1/2$, a and b are unknowns which are determined by substituting (3.20) in (3.18) and (3.19). This results in the simplified expressions for the ion densities as

$$n_p=\frac{1}{2f\sqrt{\mu\tau_p}}\left[\sqrt{\left(M+\sqrt{\mu\tau_p}\right)^2-2\mu\varphi}-\sqrt{\left(M-\sqrt{\mu\tau_p}\right)^2-2\mu\varphi}\right], \tag{3.21}$$

for the positive ion species and

$$n_n = \frac{1}{2}\left[\sqrt{(1+M)^2+2\varphi}+\sqrt{(1-M)^2+2\varphi}\right], \tag{3.22}$$

for the negative ion species. After introducing density expressions (3.8), (3.21) and (3.22) in Poisson's equation (3.7), we multiply it by $d\varphi/d\xi$ and integrate with the boundary conditions (3.10) and get an energy-like equation

$$\frac{1}{2}\left(\frac{d\varphi}{d\xi}\right)^2 + S(\varphi) = 0, \tag{3.23}$$

where $-d\varphi/d\xi$ is the electric field associated with the electrostatic potential φ and

$$\begin{aligned} S(\varphi,M) \;=\; & \tfrac{1-f}{f\tau_n}\left[1-\left(1-\tfrac{2\tau_n\varphi}{2\kappa-3}\right)^{-\kappa+3/2}\right] \\ & +\tfrac{\tau_p}{6f(\mu\tau_p)^{3/2}}\left\{2(\mu\tau_p)^{3/2}+6M^2(\mu\tau_p)^{1/2}\right. \\ & \left.-\left[\left(M+\sqrt{\mu\tau_p}\right)^2-2\mu\varphi\right]^{3/2}+\left[\left(M-\sqrt{\mu\tau_p}\right)^2-2\mu\varphi\right]^{3/2}\right\} \\ & +\tfrac{1}{6}\left\{2+6M^2-\left[(1+M)^2+2\varphi\right]^{3/2}-\left[(1-M)^2+2\varphi\right]^{3/2}\right\} \end{aligned} \tag{3.24}$$

is the Sagdeev pseudopotential.

As is well known, Eq. (3.23) has solitary wave solutions if the Sagdeev pseudopotential satisfies the following conditions [66]

(i) $S(0,M) = S'(0,M) = 0$;

(ii) $S''(0,M) \leqslant 0$, the origin is unstable;

(iii) $S(\varphi_m,M) = 0$ for some M in the soliton existence domain and $\varphi_m \neq 0$;

(iv) $S(\varphi,M) < 0$ for $0 < |\varphi| < |\varphi_m|$; and

(v) For double layers, $S(\varphi_m,M) = S'(\varphi_m,M) = 0$ for some M in addition to $(i)-(iv)$.

Here primes denote the derivatives of the Sagdeev pseudopotential with respect to the electrostatic potential and φ_m is the soliton amplitude.

3.2.2 Minimum and maximum Mach numbers

One of the advantages of using the Sagdeev pseudopotential method is that the function $S(\varphi, M)$, and its derivatives determine the conditions under which nonlinear structures exist in the plasma model it represents, going as far as determining the minimum and the maximum Mach numbers of these structures. Generally, the slow mode Mach number is constrained by Eq. (3.1), which fixes the smallest Mach number to the thermal speed of the colder ion species (positive ion species in our case), and the largest Mach number to the thermal speed of the hotter ion species (negative ion species in our case). Normalising Eq. (3.1) by the negative ion thermal speed v_{tn}, and considering the interval containing only the slow mode Mach number M_{slow}, it is found that

$$\sqrt{\mu\tau_p} < M_{slow} < 1. \tag{3.25}$$

These limits do not account for other physical constraints that may bring in some modifications, such as an ion species reaching its sonic point or the occurrence of a double layer. These supplementary constraints reduce further the interval (3.25) of admissible Mach numbers, making it narrower. A closer look shows that the Sagdeev pseudopotential (3.24) already satisfies conditions (i). Application of condition (ii), often referred to as the soliton condition yields the constraint

$$-\frac{(1-f)(2\kappa-1)\tau_n}{2\kappa-3} + \frac{f}{M^2-1} + \frac{\mu}{M^2-\mu\tau_p} \leqslant 0, \tag{3.26}$$

where the equality has been addressed by [64] and [44]. Physically, the constraint (3.26) means that the nonlinear structures corresponding to $S(\varphi, M)$ are acoustic or super-acoustic [64], by fixing the minimum Mach number M_s

for their existence, *viz.*,

$$M^2 \geqslant M_s^2 = \frac{2\kappa-3}{2(1-f)(2\kappa-1)\tau_n}\left\{\frac{(1-f)(2\kappa-1)\tau_n}{2\kappa-3}(1+\mu\tau_p)+f+\mu \pm\left[\left(\frac{(1-f)(2\kappa-1)\tau_n}{2\kappa-3}(1-\mu\tau_p)+f-\mu\right)^2+4f\mu\right]^{1/2}\right\}, \tag{3.27}$$

where M_s is the ion acoustic speed, normalised by the negative ion thermal speed v_{tn} and satisfies the equation $S''(0,M_s)=0$. The $+$ and $-$ signs in Eq. (3.27) correspond to the fast and the slow wave modes, respectively, and for our study of the slow mode, we choose the negative sign. For most of plasma parameter values, the second term under the square root is much smaller than the first and we can expand (3.27) in Taylor series, resulting in an approximate value of the slow mode acoustic speed as

$$M_s^2 \approx \mu\tau_p + \frac{\mu(2\kappa-3)}{(1-f)(2\kappa-1)\tau_n}. \tag{3.28}$$

This equation shows that $M_s > \sqrt{\mu\tau_p}$ as required by (3.25). Furthermore, Eq. (3.28) shows that the ion acoustic speed of the slow mode waves increases with increasing colder-to-hotter temperature ratio τ_p, or, in other words, M_s increases when the relative temperature of the two ion species decreases. As of the dependence of M_s on the electron superthermality, Eq. (3.28) shows that when the electron superthermality increases (the spectral index decreases) with other plasma parameters fixed, M_s decreases.

Having found the soliton minimum mach number from the physical constraint that the origin be unstable, the maximum Mach number is found from the constraint that the ion densities remain real valued functions. As is well known [21–23], the polarity of the slow mode soliton in any two ion species plasma is the same as the sign of the charge of the colder ion species. As a consequence only positive solitons are encountered in the model with colder positive ion species under study. This means that the negative ion species density (see Eq. (3.22)) remains real for all possible values of the electrostatic potential φ. But to remain real valued function, the positive ion species

density (see Eq. (3.21)) requires that

$$\varphi \leqslant \varphi_{lp} = \frac{1}{2\mu}\left(M - \sqrt{\mu\tau_p}\right)^2, \tag{3.29}$$

where φ_{lp} is the limiting electrostatic potential. Putting this limiting value of φ_{lp} in $S(\varphi_{lp}, M) = 0$, we find the solution of this equation which gives $M = M_{lp}$. This allows us to determine a relation between M_{lp} and the negative-to-positive density ratio f in the form

$$(\alpha - \beta)f + \beta + \delta = 0, \tag{3.30}$$

where

$$\begin{aligned}
\alpha &= \frac{1}{6}\left\{2 + 6M_{lp}^2 - \left[(1+M_{lp})^2 + \frac{1}{\mu}(M_{lp} - \sqrt{\mu\tau_p})^2\right]^{3/2}\right. \\
&\quad \left. - \left[(1-M_{lp})^2 + \frac{1}{\mu}(M_{lp} - \sqrt{\mu\tau_p})^2\right]^{3/2}\right\}, \\
\beta &= \frac{1}{\tau_n}\left[1 - \left(1 - \frac{\tau_n(M_{lp} - \sqrt{\mu\tau_p})^2}{\mu(2\kappa - 3)}\right)^{-\kappa+3/2}\right],
\end{aligned}$$

and

$$\delta = \frac{\tau_p}{6(\mu\tau_p)^{3/2}}\left[2(\mu\tau_p)^{3/2} + 6M_{lp}^2(\mu\tau_p)^{1/2} - \left(4M_{lp}\sqrt{\mu\tau_p}\right)^{3/2}\right].$$

The solution to Eq. (3.30), M_{lp} as a function of f is the Mach number of the slow mode if it satisfies simultaneously the conditions (3.25) and (3.27). Because the positive ion density becomes complex valued for electrostatic potentials larger than φ_{lp}, φ_{lp} is the largest real root of Eq. (3.30). When this root is accessible from the undisturbed condition $\varphi = 0$, the corresponding Mach number M_{lp} is the upper limit to the soliton Mach number range for corresponding plasma parameter values. There are situations in which the root φ_{lp} is not accessible from the undisturbed condition $\varphi = 0$ because there is another root or more in between [67]. In this case, it is a double layer that occurs as a limiting factor to the soliton amplitude before the sonic point is

reached, and the corresponding Mach number is the upper limit to the soliton Mach number range. We recall here that the double layer Mach number and corresponding amplitude are calculated from the system of equations [23]

$$\begin{cases} S(\varphi, M) & = 0 \\ S'(\varphi, M) & = 0. \end{cases} \tag{3.31}$$

In addition to the occurrence of double layers as the limiting factor to the soliton Mach number range, double layers have been shown also to occur as the lower limit to a set of supersolitons in different plasma models [45, 47, 48, 57, 68]. As is now known [47], the supersoliton existence domain in Mach number range and in compositional parameter space is limited, on the lower side, either by double layers, if they exist, or by other boundaries, arising from the merging of consecutive extrema. This will be illustrated in Sec. 3.4.2.

Anticipating our results, we have found that standard slow mode solitons are found to propagate at low to intermediate values of negative-to-positive density ratio, while supersolitons and double layers are possible at higher values. For a complete analysis, we consider each region separately, starting by the region of low to intermediate values of f.

3.3 Solitary waves supported by low to intermediate values of the negative-to-positive ion density ratio

3.3.1 Soliton existence domains

In negative ion plasmas, the replacement of light electrons by heavy negative ions reduces the electron shielding effect, an effect that increases with increase of negative-to-positive ion density ratio f [69]. This implies that the negative-to-positive ion density ratio plays an important role in the study of negative ion plasmas. In the following analysis, we use Eq. (3.27) and

solve numerically Eqs. (3.30) and (3.31) for different plasma parameter values to delineate the soliton existence domains in $\{f, M\}$ space, where M is the soliton Mach number. The soliton existence domains are depicted in Fig. 3.1 for different plasma parameter values. In this figure, we show the ion thermal effects on the soliton existence domains from the upper to lower panels and the electron superthermal effects are shown from left to right panels. To study the effects of the relative temperature of the two ion species, we fix the ratio of the negative ion species temperature to electron temperature to $\tau_n = 0.7$ and vary τ_p. With fixed τ_n, an increase of τ_p implies the increase of the positive ion temperature at fixed negative ion temperature, which means that the ions relative temperature decreases with increasing values of τ_p. The negative-to-positive mass ratio is also fixed to a value of $\mu = 0.15$, corresponding to a $X_e^+ - F^- - e$ plasma used by Ichiki et al. [18] in their experiments.

In the upper left panel, the positive-to-negative ion temperature $\tau_p = 10^{-6}$ models effectively cold positive ions, whereas the spectral index value $\kappa = 1000$ shows that electrons are Maxwellian. For these parameter values, the slow mode supersonic limit is $\approx 0.4 \times 10^{-3}$ while the subsonic limit is 1. The solid line (black colour online) represents the minimum Mach number M_s for the existence of solitons. It lies well above the supersonic limit for the whole range of the negative-to-positive ion density ratio f. The dashed line (red colour online) represents the upper limit M_{lp} due to occurrence of positive ion sonic point, where M_{lp} is determined numerically from Eq. (3.30).
We see that this limit remains well below the subsonic limit 1. Solitons may propagate if their Mach numbers are between the minimum M_s and the maximum M_{lp}. Therefore, for the plasma parameter values in the upper left panel, positive solitons, limited by the occurrence of positive ion sonic point exist for all values of the negative-to-positive ion density ratio f.

The lower left panel presents the soliton existence domain when τ_p is increased to 0.7, shifting the supersonic limit to ≈ 0.32. As a result of this increase, the minimum Mach number M_s at a fixed density ratio f also

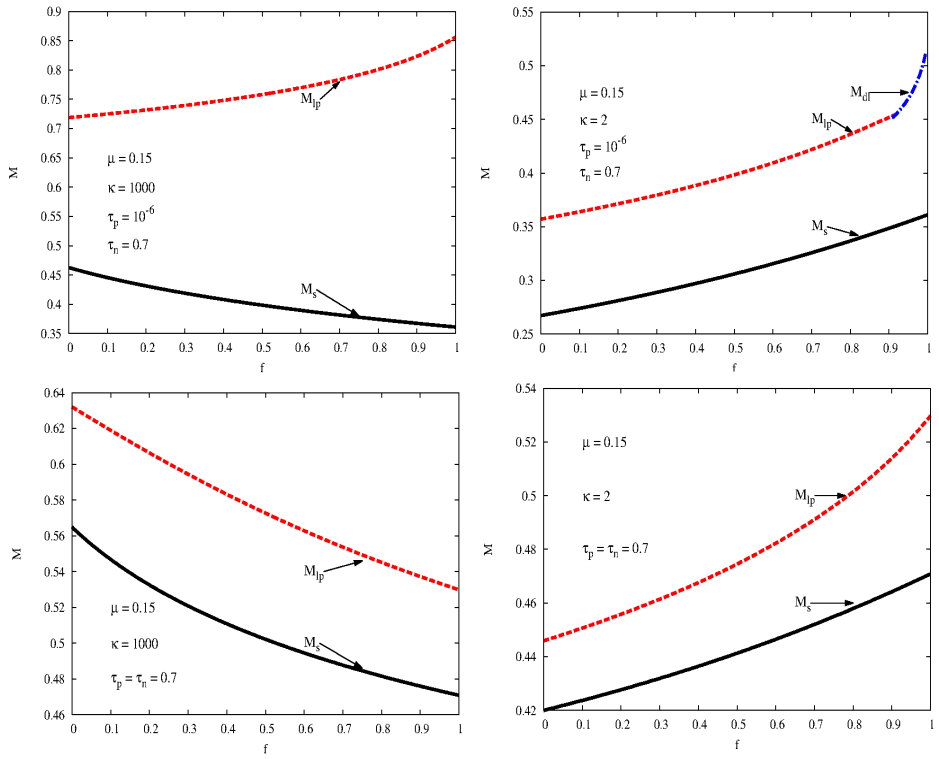

Figure 3.1: (Colour online) Existence domain of ion acoustic solitary waves and double layers in $\{f, M\}$ space. The left panels show the effects of increasing the positive ion temperature when electrons are Maxwellian ($\kappa = 1000$) and the right panels show the same effects when electrons are strongly non-Maxwellian ($\kappa = 2$). The fixed plasma parameters are $\mu = 0.15$ and $\tau_n = 0.7$.

increases to a higher value. This result is consistent with Eq. (3.28) which shows that M_s increases with increasing τ_p. The maximum Mach number M_{lp} has a different behaviour when τ_p is increased. At low values of τ_p, M_{lp} decreases very quickly with an increase of τ_p and the Mach number range supporting the propagation of solitary waves narrows. With further increase of τ_p, the values of M_{lp} go through a minimum before they start increasing with increasing τ_p, but the soliton Mach number range continues to narrow due to a faster growing of the acoustic Mach number. This result is shown in detail in Fig. 3.2, where the Mach number difference $\delta M = M_{lp} - M_s$, calculated at a fixed value of negative-to-positive ion density ratio $f = 0.5$, is plotted as a function of τ_p for two values of the spectral index, $\kappa = 1000$

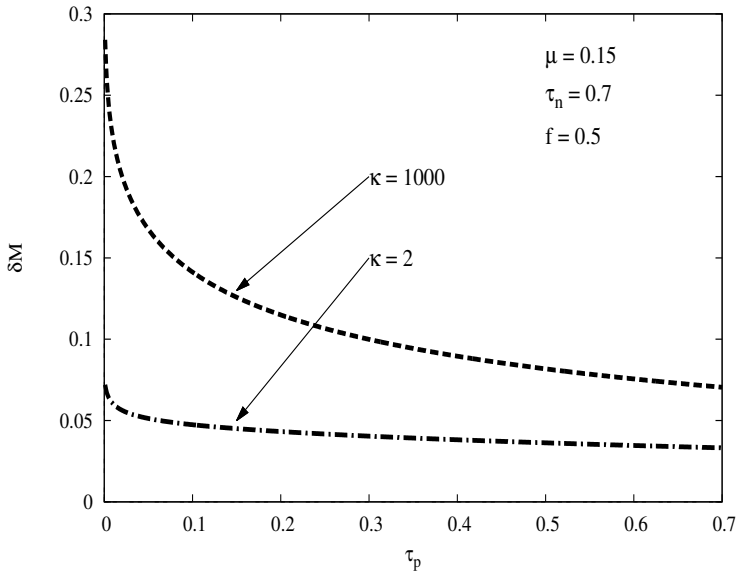

Figure 3.2: Soliton existence domain in $\{\tau_p, \delta M\}$ space, where $\delta M = M_{lp} - M_s$ at density ratio $f = 0.5$ for $\kappa = 1000$ (dashed line) and $\kappa = 2$ (dash-dotted line). In both cases, the soliton Mach number range δM, supporting the propagation of solitons, decreases with increasing τ_p.

(Maxwellian electrons) and $\kappa = 2$ (strongly non-Maxwellian electrons). This figure shows clearly that δM decreases with increasing τ_p, meaning that the values of M_s and M_{lp} get closer as τ_p increases. We recall that with the adopted normalisation by hotter negative ion characteristics, increasing τ_p means that the temperature of the colder positive ion species is increased and the supersonic limit moves towards the subsonic limit, therefore reducing the possible slow mode Mach number range as given by (3.25). A continuous increase of τ_p moves the supersonic limit to higher values towards the subsonic limit so that at $\tau_p \approx 6.7$, both limits coincide. At values of $\tau_p \gtrsim 6.7$, the colder (positive) ion thermal speed $\sqrt{\mu\tau_p}$ is larger than the hotter (negative) ion thermal speed 1 and the inequality (3.25) is breached.

The right panels of Fig. 3.1 shed light on the effects of increasing the electron superthermality by reducing the spectral index κ from 1000 to 2. In the upper right panel, positive ions are still cold with negative-to-positive

ion temperature ratio $\tau_p = 10^{-6}$. Comparison with the upper left panel shows that an increase of the electron superthermality causes both the minimum M_s and the maximum M_{lp} Mach numbers to shift to lower values, but M_{lp} undergoes a more significant shift. As a result, the Mach number range supporting the soliton propagation at a fixed density ratio f narrows with an increase of the superthermal behavior of the electron. This result, obtained by considering extreme values of the parameter κ, is also valid for intermediate values. The decrease of M_s as κ decreases is also consistent with Eq. (3.28).

Fig. 3.1 upper right panel also shows that there are two other effects on the soliton existence domain which arise due to the increase of the electron superthermality. On one hand, it is observed that when the spectral index decreases from $\kappa = 1000$ to $\kappa = 2$, the upper limit to the soliton Mach number range is still the maximum Mach number M_{lp} at low-to-intermediate values of density ratio, but at higher values of f, double layers arise as the limiting factor. Double layers are discussed further in the next section.
On the other hand, while the minimum Mach numbers decrease with increasing negative-to-positive density ratio f when electrons are Maxwellian $(\kappa = 1000)$ (left panels), they increase when electrons are strongly non-Maxwellian $(\kappa = 2)$ (right panels). This means that when κ is varied with other parameters held fixed, there is a critical value κ_c of the spectral index at which the acoustic Mach number M_s is constant for all values of the density ratio f, κ_c being a function of other plasma parameters. The M_s curve as a function of the density ratio f decreases for values of $\kappa > \kappa_c$ and increases when $\kappa < \kappa_c$. When μ, τ_n and/or τ_p are changed, the value of κ_c follows. As an example, for fixed values of $\mu = 0.15$ and $\tau_n = 0.7$, numerical simulations have shown that the values of κ_c are between $\kappa_c \approx 3.1$ when $\tau_p = 10^{-6}$ and $\kappa_c \approx 2.57$ when $\tau_p = 1$. This explains why, e. g., the minimum Mach number M_s decreases as a function of density ratio f in the upper left panel, where the spectral index $\kappa = 1000$ is larger than the critical value $\kappa_c = 3.1$, while in the upper right panel, where $\kappa = 2$ is smaller than the critical value $\kappa_c = 3.1$ and M_s is an increasing function f.

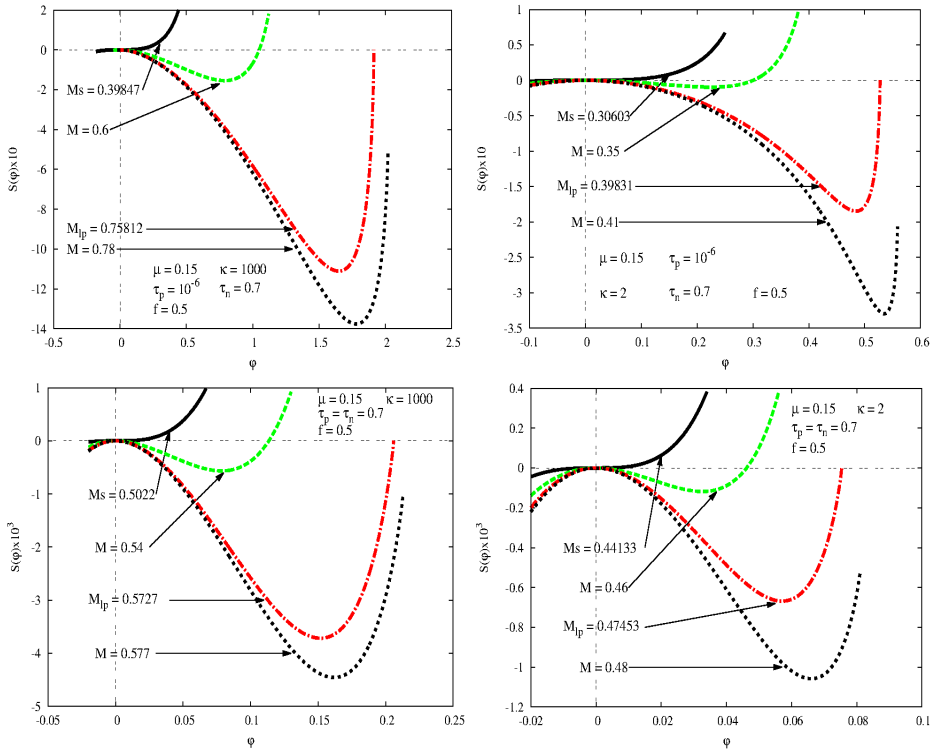

Figure 3.3: (Colour online) Sagdeev pseudopotentials with parameter values taken in the soliton existence domain. Fixed plasma parameters are $f = 0.5$, $\mu = 0.15$, $\tau_n = 0.7$. The upper to lower panels show the ion thermal effects, while the left to right panels show the electron superthermal effects on the soliton amplitude and width.

Fig. 3.1 lower right panel shows a combined effect of reducing the relative ion temperature by increasing τ_p and increasing the superthermal behavior of the electrons by decreasing the spectral index κ. In this panel, $\tau_p = 0.7$ and $\kappa = 2$. As a result of increasing τ_p and decreasing κ, the soliton Mach number range is significantly reduced. This means that the superthermal behavior of the electrons and the ion thermal effect enhance each other.

3.3.2 The ion thermal and electron superthermal effects on the soliton amplitude and width

For low-to-intermediate values of negative-to-positive density ratio f, we take an indicative value of $f = 0.5$. At this value of f, we present in Fig. 3.3 the pseudopotentials for parameter values taken from the soliton existence domains presented in Fig. 3.1. From the upper to lower panel, we show the effects of reducing the relative ion temperature for Maxwellian electrons ($\kappa = 1000$) (left panels) , and strongly non-Maxwellian electrons ($\kappa = 2$) (right panels). The effects of increasing the electron superthermality are presented from left to right panels.

In the upper left panel, positive ions are cold with $\tau_p = 10^{-6}$ and electrons are Maxwell-distributed with $\kappa = 1000$. With these plasma parameter values, the plasma supports slow mode normal solitons, propagating with Mach numbers in the range $M_s < M \leqslant M_{lp}$, where $M_s = 0.39847$ and $M_{lp} = 0.75812$. The amplitude of the maximum speed soliton (dash-dotted line, red colour online) is $\varphi_{lp} \approx 1.91$. As τ_p increases, the amplitude of the positive solitons with maximum speed decreases and, at $\tau_i = 0.7$ (lower left panel), $\varphi_{lp} \approx 0.21$. This decrease in amplitude is all the more important as the electron superthermality is higher. So, in the lower right panel with other plasma parameters set to the same values, the maximum speed soliton amplitude decreases from $\varphi_{lp} \approx 0.21$ for $\kappa = 1000$ (lower left panel) to $\varphi_{lp} \approx 0.07$ (lower right panel). Therefore, reducing the relative ion temperature has an effect of decreasing the maximum speed soliton amplitude, and this effect is enhanced by the electron superthermality. When the relative ion temperature increases to such a value that the ion thermal speeds of both ion species are equal, the slow mode vanishes.

This result is presented more explicitly in Fig. 3.4, in which we have plotted the soliton profiles for plasma parameters as considered in Fig. 3.3. Moreover, this figure shows that when the soliton amplitude decreases, its width increases.

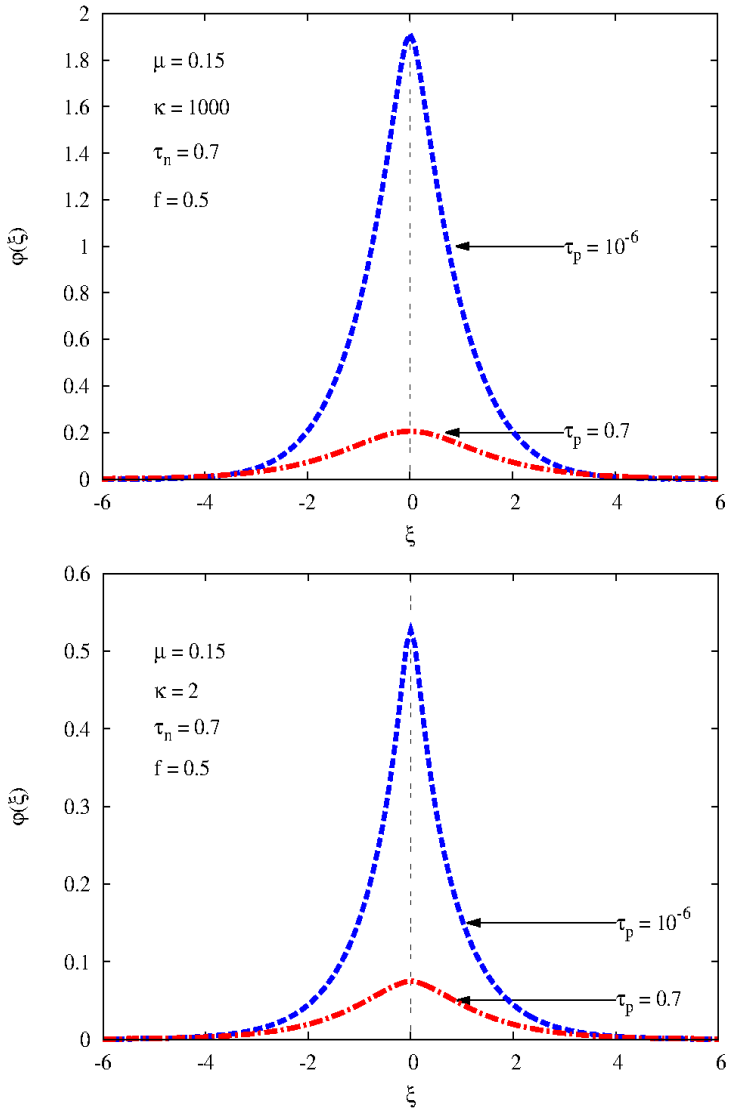

Figure 3.4: (Colour online) Profiles of solitons with maximum speeds, showing the effects of positive ion thermal effects on the soliton amplitude and width for Maxwellian ($\kappa = 1000$) (upper panel) and strongly non-Maxwellian ($\kappa = 2$) (lower panel). In both panels, $\mu = 0.15$, $\tau_n = 0.7$, $f = 0.5$.

3.4 Solitary waves supported by high values of the negative-to-positive ion density ratio

In Fig. 3.1 upper panels, positive ions are effectively cold with $\tau_p = 10^{-6}$. While in the left upper panel the soliton wave amplitude is limited by the occurrence of the positive ion sonic point for the whole density ratio range $0 < f < 1$, in the right panel, in which electrons are strongly non-Maxwellian, the occurrence of positive ion sonic point acts as the upper limit to soliton amplitude for low to intermediate values of f, but at higher values of f, the limiting factor is a double layer. The soliton existence domain at high values of f has been blown up and replotted in Fig. 3.5, omitting the curve for the acoustic Mach numbers for clarity. The dashed line (red colour online) represents the occurrence of positive ion sonic point as found from Eq. (3.30) and the dash-dotted line (blue colour online) represents the double layer as solution to the set of Eqs. (3.31). Fig. 3.5 shows that the double layer and positive ion sonic point curves cross over at a critical density ratio $f_c \approx 0.918$ with the same Mach number $M_{dl} = M_{lp} = 0.45459$.

For $f < f_c$, there is a range of ion density ratio values $0.88 \lesssim f \lesssim 0.92$ supporting the existence of double layers, that do not represent the soliton upper limit, but occur as the lower limit to a set of supersolitons, with the positive ion sonic point as the upper limiting factor. For this range, the limiting electrostatic potential φ_{lp} is the largest solution to Eq. (3.30), and there is no other solution between $\varphi = 0$ and $\varphi = \varphi_{lp}$.
The double layer curve for this case lies below the positive ion sonic point curve. The region of $\{f, M\}$ space admitting supersolitons with double layer as the lower limit is shaded horizontally in Fig. 3.5. Starting from f_c, double layers occur as the upper limiting factor to the soliton amplitude, and the corresponding curve in $\{f, M\}$ space lies above the positive ion sonic point curve. For this range, the limiting electrostatic potential φ_{lp} is also the largest solution to Eq. (3.30), but there are other solutions between $\varphi = 0$ and $\varphi = \varphi_{lp}$ so that φ_{lp} is not accessible from the origin. This region, plotted between

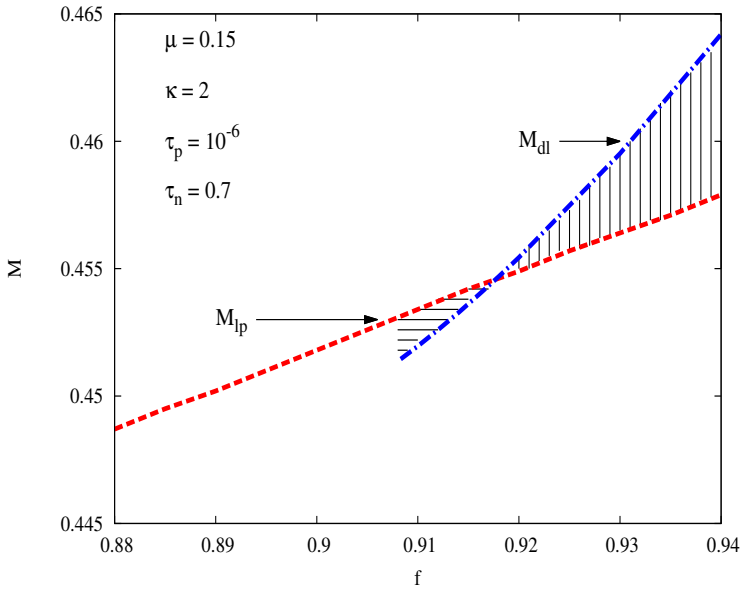

Figure 3.5: (Colour online) Double layer and supersoliton existence domains in $\{f, M\}$ space: Blow up of Fig. 3.1 upper right panel at high values of f. Supersolitons with double layers as the lower limit exist in the region shaded horizontally. In the region shaded vertically, normal solitons exist with Mach number larger than M_{lp} and double layer as the upper limit.

M_{lp} and M_{dl} curves up to $f = 0.94$ for clarity is shaded vertically. In the following discussion, we analyse the nonlinear structures characteristics in each region separately.

3.4.1 Existence domain of double layers as the soliton limiting factor

We start our discussion by first considering the range of density ratio f, supporting the occurrence of double layer as the upper limit to the soliton Mach number range. The pseudopotential at the critical negative-to-positive density ratio f_c, at which a double layer occurs at the positive ion sonic point with Mach number $M_{dl} = M_{lp} = 0.45459$ is shown in Fig. 3.6 upper panel. At this point, the double layer with amplitude $\varphi_{dl} \approx 0.63$ signals the end of the soliton Mach number range before the sonic point with limiting

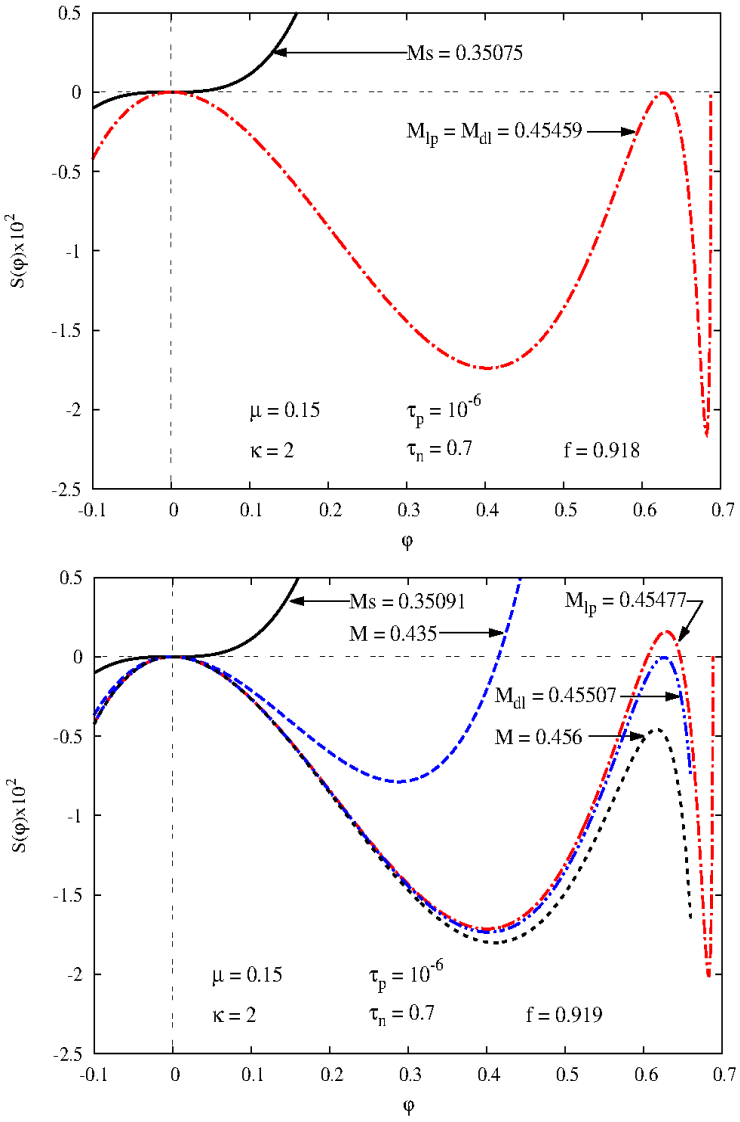

Figure 3.6: (Colour online) Upper panel: The pseudopotentials plotted at the critical negative-to-positive density ratio $f_c = 0.918$. A double layer exists at the positive ion sonic point. Lower panel: the pseudopotentials are plotted at a slightly higher value $f = 0.919$. The positive ion sonic curve presents two roots before the limiting potential is reached. In both panels, other plasma parameters are $\mu = 0.15, \tau_n = 0.7, \tau_p = 10^{-6}$ and $\kappa = 2$.

electrostatic potential $\varphi_{lp} \approx 0.68$ is reached [23].

In Fig. 3.6 lower panel, the pseudopotential curves are plotted at negative-to-positive density ratio $f = 0.919$, slightly larger than f_c, from the minimum Mach number M_s. At Mach number $M_{lp} = 0.45477$ corresponding to the sonic point, the pseudopotential curve (dash-dotted line, red colour online) presents 2 roots, $\varphi_1 \approx 0.60$ and $\varphi_2 \approx 0.65$ before the maximum root $\varphi_{lp} \approx 0.69$ is reached. Therefore φ_{lp} is not accessible from the undisturbed condition $\varphi = 0$, and only the first encountered root φ_1 yields a normal soliton. Because φ_1 is smaller than φ_{lp}, the positive ion density is a real valued function at φ_1. It is thus possible to increase the Mach number M beyond the value of M_{lp} without rendering the positive ion density a complex valued function. Therefore, the occurrence at M_{lp} of the two roots before the sonic point opens a window beyond M_{lp}, in which ordinary solitons exist with Mach numbers $M > M_{lp}$, but with amplitudes, smaller than the limiting amplitude φ_{lp}. A continuous increase of Mach number M beyond M_{lp} yields normal solitons with increasing amplitudes until, at $M_{dl} = 0.45507 > M_{lp}$, a double layer occurs with amplitude $\varphi_{dl} \approx 0.62$, also smaller than the limiting amplitude φ_{lp}. No solitons are found to exist for Mach numbers M larger than M_{dl}, which means that the soliton Mach number range is terminated by the occurrence of the double layer. This situation repeats itself for all values of $f > 0.918$ but less than the limiting value $f = 1$, at which the model breaks down.

3.4.2 Existence domain of supersolitons

Fig. 3.5 shows that double layers exist also in a narrow range of values of f, smaller than f_c, but in this case they do not signal the end of the soliton Mach number range, rather they signal the lower boundary of a set of supersolitons that terminates when the sonic point is reached (horizontally shaded region). In the region below f_c, the double layer curve lies below the positive ion sonic point curve in $\{f, M\}$ space and the Mach number M_{lp} corresponding to the maximum amplitude φ_{lp} is still the limiting Mach number to the soliton

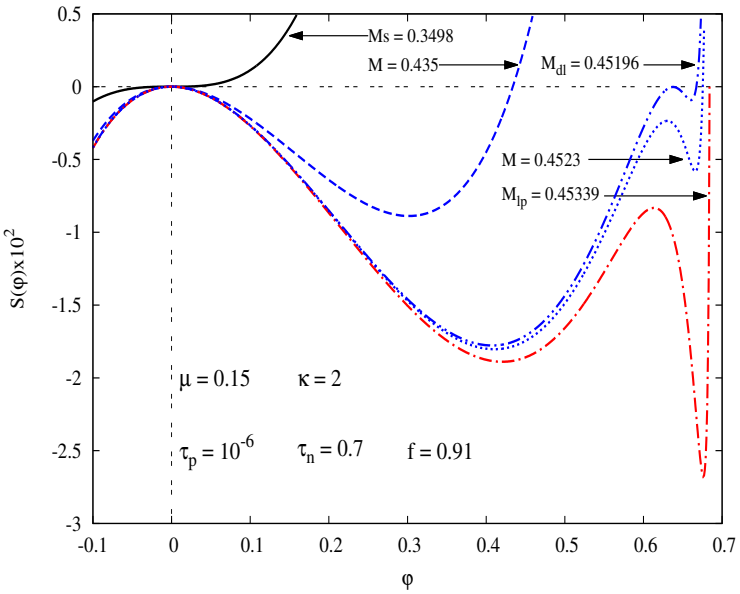

Figure 3.7: (Colour online) Pseudopotentials plotted at $f = 0.91$ from the minimum M_s up to the maximum M_{lp}. The dashed line (blue colour online) represents a normal soliton , the dash-double-dotted line (blue colour online) represents a double layer and both the dotted (blue colour online) and dash-dotted (red colour online) lines represent supersolitons. Other plasma parameters are $\mu = 0.15$, $\kappa = 2, \tau_i = 10^{-6}$, $\tau_e = 0.7$.

Mach number range.

Figure. 3.7 is a plot of the pseudopotentials at $f = 0.91$, slightly smaller than f_c, for different values of Mach number M, ranging from the acoustic speed $M_s = 0.3498$ up to the maximum Mach number $M_{lp} = 0.45339$ due to occurrence of positive ion sonic point. The dashed line (blue colour online) is plotted at $M = 0.435$ and represents the normal soliton pseudopotential curve. The dash-double-dotted line (blue colour online) is plotted at $M = 0.45196$ and represents a double layer. The pseudopotential curve plotted at a slightly larger Mach number $M = 0.4523$ (dotted line, blue colour online) presents three subsidiary extrema between the undisturbed conditions $\varphi = 0$ and the nonlinear structure amplitude. As is well known, such curve with two subwells represents a supersoliton [48]. When the Mach number is increased further, we observe that the corresponding pseudopotentials represent super-

solitons even at the maximum Mach number due to the occurrence of the positive ion sonic point (dash-dotted line, red colour online). At Mach numbers greater than the maximum, no more supersolitons exist in the plasma as is the case for normal solitons.

Supersolitons found in this case are part of a set of solitons and the transition route from normal soliton to supersoliton is through the occurrence of a double layer. Normal solitons exist for Mach numbers between M_s and M_{dl} while supersolitons are encountered for Mach numbers between M_{dl} and M_{lp}. The double layer is thus the lower boundary to this set of supersolitons. Double layers also occur as the lower boundary for the supersoliton sets for other values of f, ranging from ~ 0.908 up to ~ 0.918. At $f = 0.918$, the lower limit (double layer) and the upper limit (sonic point) occur with the same Mach number, signalling the end of the supersoliton domain on the high value of f. This range and corresponding upper limits form a region in $\{f, M\}$ space that is shaded horizontally in Fig. 3.5.

For values of f lower than 0.908, supersolitons exist with different limitations, arising from the merging of consecutive extrema. This case is illustrated in Fig. 3.8. In both panels, the three subsidiary extrema are labeled A, B, and C.
The upper panel is plotted at $f = 0.894$. The pseudopotential curve representing a supersoliton (dashed line, blue colour online) is found between two pseudopotential curves, the solid line (black colour online) and the dash-dotted line (red colour online). The dash-dotted line is plotted at the maximum Mach number M_{lp} and corresponds to the maximum speed supersoliton. The solid line (black colour online), plotted at Mach number $M = 0.44905$ results from the merging of rightmost extrema B and C so that it has a single well, appropriate for a normal soliton. Verheest et al. [47] used the terminology "coalescence" to designate the merging between two consecutive extrema, and the corresponding curve is designed as the curve of coalescence or the curve of inflection [51, 52], because it is defined such that it has a point of inflection between the undisturbed conditions. To find

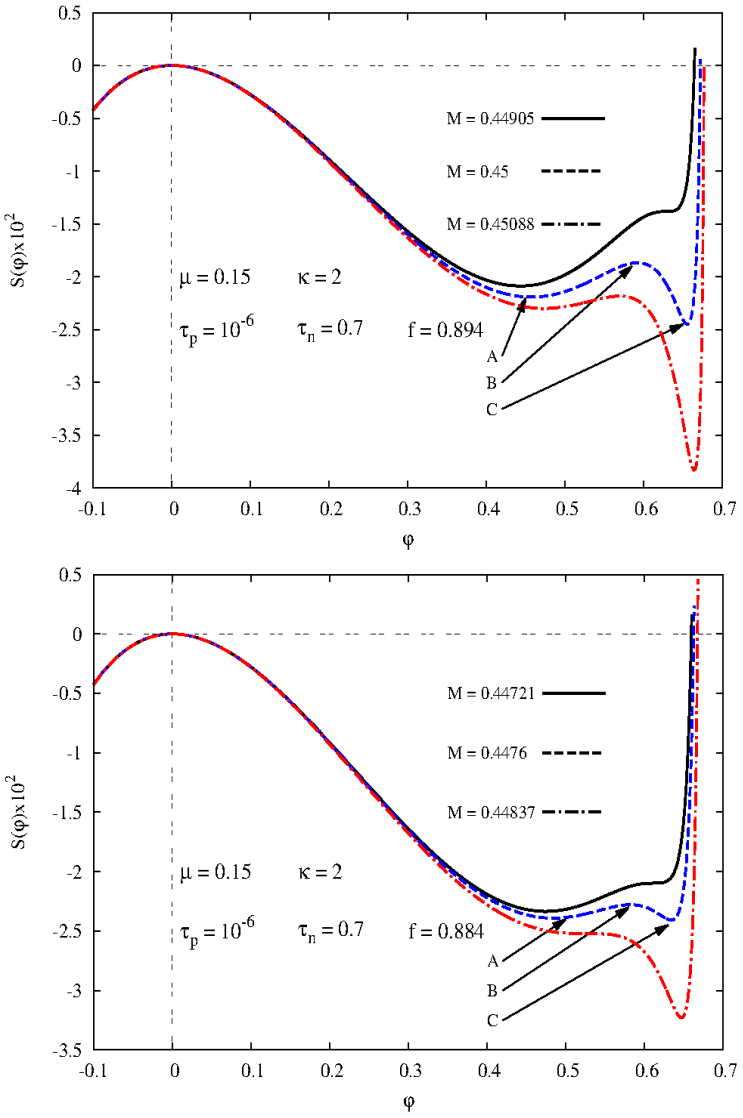

Figure 3.8: (Colour online) Upper panel: Pseudopotentials yielding supersolitons with the coalescence of rightmost extrema B and C as the lower limit to the supersoliton Mach number range and a supersoliton occuring at the sonic point. Lower panel: Pseudopotentials yielding supersolitons lying between two normal solitons, resulting from the coalescence of the two rightmost extrema B and C (solid line) and the two leftmost extrema A and B (dash-dotted line).

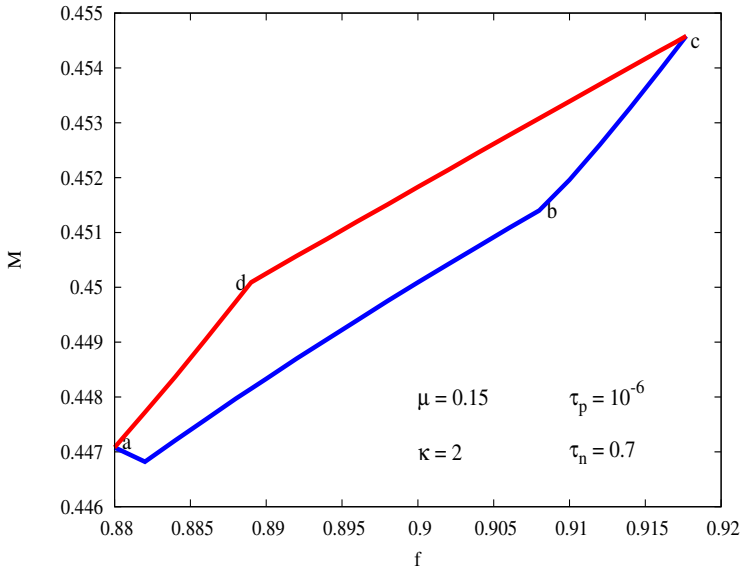

Figure 3.9: (Colour online) Supersoliton existence domain. Plasma parameter values are $\mu = 0.15$, $\kappa = 2$, $\tau_p = 10^{-6}$, $\tau_n = 0.7$. At a fixed density ratio f, supersolitons exist for Mach numbers between the lower and the upper curves. From a to b, supersoliton lower limit is a coalescence and from b to c it is a double layer. On the upper side, the supersoliton Mach number ends by the coalescence between a and d and by the positive ion sonic point between d and c.

the Mach number and the corresponding potential at which a coalescence occurs, one has to solve the system of equations $S'(\varphi) = S''(\varphi) = 0$. [47] Supersolitons limited on the lower side by the coalescence of two subsidiary extrema and the sonic point on the upper side are found in the interval $0.889 \lesssim f \lesssim 0.908$.

Fig. 3.8 lower panel is plotted at $f = 0.884$. For this case, the supersoliton is sandwiched between two normal solitons resulting from the coalescence of the two rightmost extrema B and C (solid line, black color online) and the two leftmost A and B (dash-dotted line, red color online). Such supersolitons are found in the interval $0.88 \lesssim f \lesssim 0.889$. At $f \approx 0.88$, the upper and lower limits coincide, signalling the end of the supersoliton existence domain on the lower side of f. The supersoliton domain in $\{f, M\}$ space is plotted in Fig. 3.9.

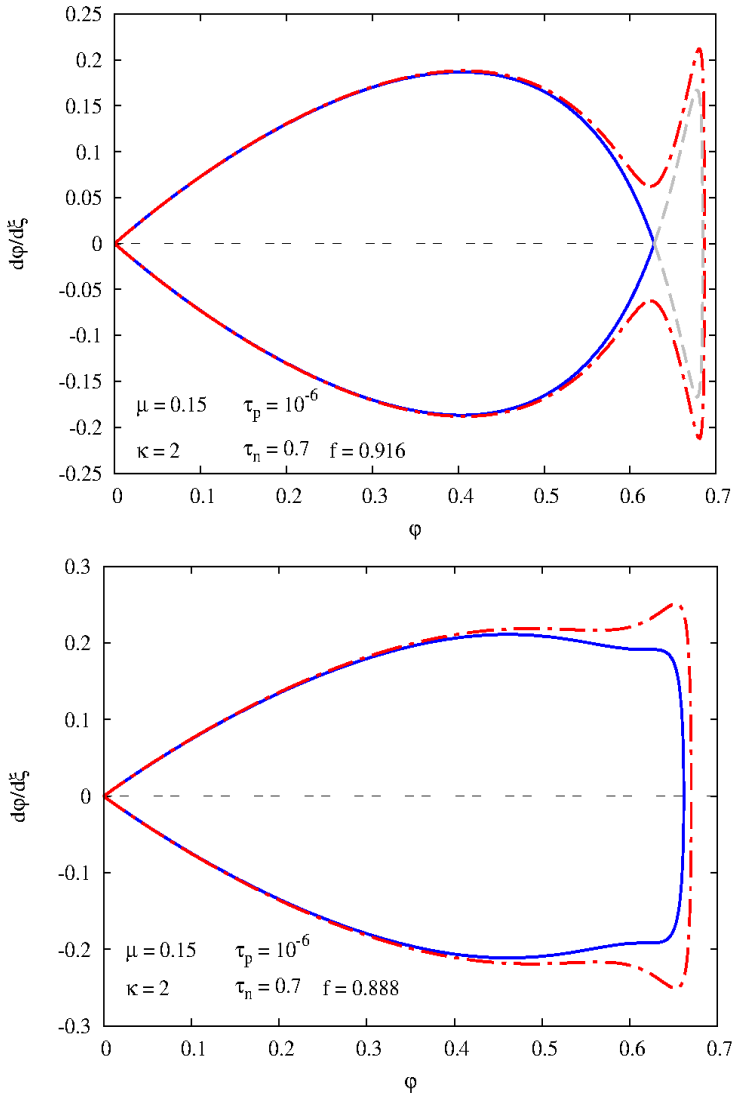

Figure 3.10: (Colour online) Phase diagrams, plotting $d\varphi/d\xi$ as a function of φ. The upper panel is plotted at $f = 0.916$ at which the lower boundary to the set of supersolitons is a double layer. The dashed grey curve delineates the potential range,which is not accessible from the undisturbed condition. The lower panel is plotted at $f = 0.888$ at which the lower boundary to the set of supersolitons is the coalescence of two consecutive extrema. Other parameter values are $\mu = 0.15, \tau_n = 0.7, \tau_p = 10^{-6}$ and $\kappa = 2$.

Based on the lower limit to the supersoliton set, Steffy and Ghosh [51, 52] classified as Type I supersolitons with a double layer as the lower limit, and as Type II those for which the lower limit is the coalescence of two subsidiary extrema. While in principle there is no difference between these two types, they can however be identified based on the variation of the amplitude when there is transition from normal soliton to supersoliton. This identification is easily seen from Fig. 3.10 showing the phase diagrams for the two routes. While the Type I transition (upper panel) is accompanied by the existence of a range of electrostatic potentials that are not accessible from the undisturbed conditions (the range limited by the dashed curve, grey colour online) [48], the amplitude varies continuously from soliton to supersoliton for Type II transition (lower panel).

3.4.3 Ion thermal and electron superthermal effects on the range of the density ratio f, supporting supersolitons and double layers

In Secs. 3.4.1 and 3.4.2, it was observed that supersolitons and double layers exist when the negative ion density is high (low density of electrons). Thus in Fig. 3.1 upper right panel, when the positive to negative ion temperature ratio is $\tau_p = 10^{-6}$ and the spectral index $\kappa = 2$, the negative-to-positive density ratio range supporting supersolitons extends from $f \approx 0.88$ up to $f \approx 0.918$, and the double layers as the limiting factor to the soliton propagation occur for $f \gtrsim 0.918$. When the relative ion temperature is reduced, or, equivalently when τ_p is increased, these two ranges shift to higher values of f and at the same time narrow. So, at $\tau_p = 2 \times 10^{-3}$ e.g., supersolitons exist for density ratio ranging from $f \approx 0.926$ up to $f \approx 0.931$, while double layers occur for $f \gtrsim 0.931$. When τ_p is continuously increased further, these ranges narrow more and shift to higher values of f until they vanish at $\tau_p \approx 0.2$. For larger values of τ_p, only positive ion sonic point occurs as the limiting factor to the soliton amplitude for all values of negative-to-positive density ratio f. Fig.

3.1 lower right panel which is plotted at $\tau_p = 0.7$ larger than 0.2 shows that only normal solitons limited by the occurrence of positive ion sonic point exist for the whole range of f.

Keeping τ_p fixed at 10^{-6} and reducing the spectral index (increasing the superthermal behavior of electrons), it is found that the negative-to-positive ion density ranges supporting the supersolitons and double layers shift to lower values of f, and become larger. For example, if the spectral index decreases from 2 to 1.8, these ranges shift from $0.88 \lesssim f \lesssim 0.918$ and $0.918 \lesssim f \lesssim 1$ to $0.77 \lesssim f \lesssim 0.813$ and $0.813 \lesssim f \lesssim 1$, respectively. When, on the contrary, the spectral index is increased (decreasing the superthermal behavior of electrons), the density ratio ranges supporting supersolitons and double layers propagation shift to higher values of f, and become narrower. For values of $\kappa \gtrsim 2.5$, supersolitons and double layers disappear and only normal solitons, limited by positive ion sonic points are encountered. This analysis shows that in the model under study, supersolitons and double layers exist when the gap between the ion temperatures is large and electrons are strongly non-Maxwellian.

3.4.4 The ion thermal and electron superthermal effects on the double layer amplitude and width

Fig. 3.11 shows the ion thermal effects (left panels) and electron superthermal effects (right panels) on the double layer amplitude and width. The plasma parameter values $\mu = 0.15$, $\tau_n = 0.7$ and $f = 0.95$ are the same for all panels in this figure. The value of the density ratio $f = 0.95$ has been chosen so that the soliton upper limiting factor is a double layer when $\tau_p = 10^{-6}$ and $\kappa = 2$. The left panels show the effects of increasing the negative to positive ion temperature from $\tau_p = 10^{-6}$ to $\tau_p = 5 \times 10^{-3}$ when the spectral index value is $\kappa = 2$. As a result of this increase, the double layer amplitude increases from $\varphi_{dl} \approx 0.62$ (solid line, blue colour online) to $\varphi_{dl} \approx 0.64$ (dash-dotted line, red colour online) and its width decreases as is seen in the lower left

panel. At the same time, the range of the density ratio supporting the double layers as the upper limit to the soliton amplitude shifts to higher values of f as discussed in Sec. 3.4.3. This means that with sufficiently high value of τ_p, the double layer gives way to the occurrence of sonic point as the upper limiting factor. This is what happens when τ_p increases to $\tau_p = 7 \times 10^{-3}$. At this value, the soliton upper limit is a normal soliton with soliton amplitude $\varphi_{lp} = 0.65$, occurring at the positive ion sonic point. With this new limit, a further increase of τ_p leads to the decrease of the soliton amplitude as it was observed for a plasma with low-to-intermediate values of f.

The electron superthermal effects on the double layer amplitude and width are shown in Fig. 3.11 right panels, where positive to negative ion temperature ratio is $\tau_p = 10^{-6}$. The double layer amplitude, which is $\varphi_{dl} \approx 0.62$ when the spectral index $\kappa = 2$ (solid line, blue colour online) decreases to $\varphi_{dl} \approx 0.33$ when κ decreases to 1.8 (dash-dotted line, red color online). Therefore, when the electron superthermality increases, the double layer amplitude decreases and its width increases. We have shown in Sec. 3.3.1 that for Maxwellian electrons, only normal solitons are found. This means that as the spectral index increases, the upper limit changes. Thus while the upper limit is the double layer when $\kappa = 2$, at $\kappa = 2.2$ the upper limit is a supersoliton and it is a normal soliton when κ exceedes a value of 2.3.

3.4.5 The ion thermal and electron superthermal effects on the supersoliton amplitude and width

For some plasma parameter values, supersolitons occur at the positive ion sonic point with maximum speed. For a fixed density ratio f, the amplitude and width of a maximum speed supersoliton vary similar to the same characteristics of the maximum speed normal soliton when the relative temperature of the two ion species is reduced by increasing τ_p, and when the electron superthermality is increased by decreasing the value of the

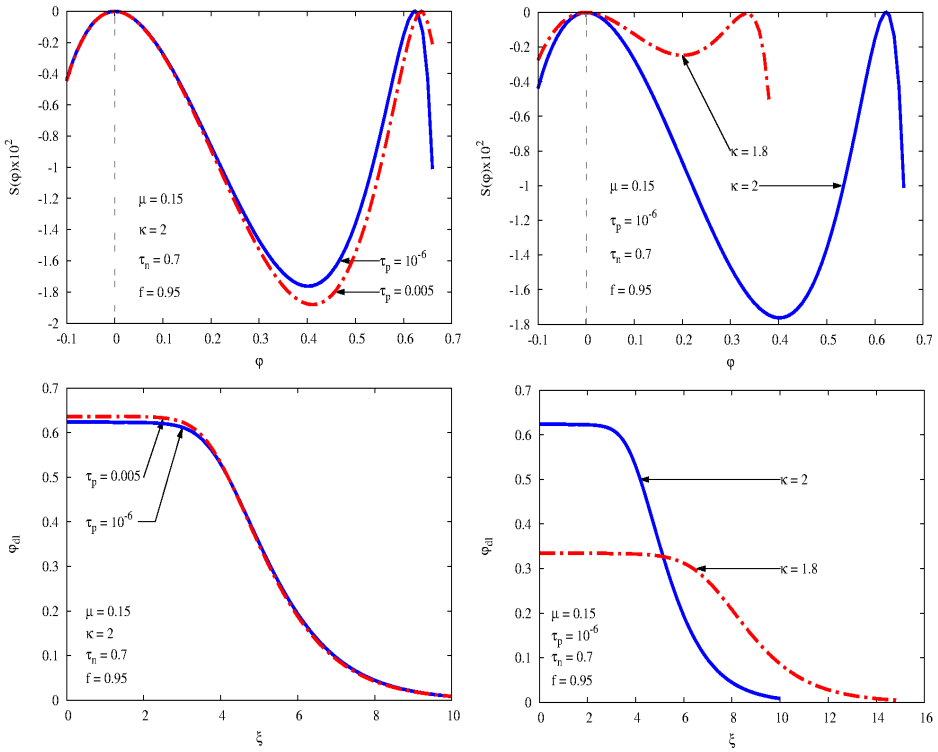

Figure 3.11: (Colour online) The ion thermal effects (left panels) and electron superthermal behavior effects (right panels) on the double layer amplitude and width. The fixed parameter values taken in the double layer existence domain are $\mu = 0.15$, $\tau_n = 0.7$ and $f = 0.95$. The left panels are plotted at $\tau_p = 10^{-6}$ (solid line, blue colour online) and 5×10^{-3} (dash-dotted line, red colour online) at fixed spectral index $\kappa = 2$. The right panels are plotted at $\kappa = 2$ (solid line, blue colour online) and 1.8 (dash-dotted line, red colour online) at fixed $\tau_p = 10^{-6}$.

spectral index κ. Namely, the supersoliton amplitude decreases and its width increases with an increase of τ_p and this effect is enhanced by the electron superthermality. However, it is important to emphasise that a continuous increase of τ_p and a continuous decrease of κ lead, ultimately, to the change of the soliton amplitude upper limit. This transition is shown in Fig. 3.12 in which we have plotted the pseudopotentials (upper panels) of the maximum amplitude structures and the corresponding profiles (lower panels). The values of the plasma parameters $\mu = 0.15$, $\tau_n = 0.7$ and $f = 0.91$ are the same for all panels. The left panels, where the spectral index $\kappa = 2$, show

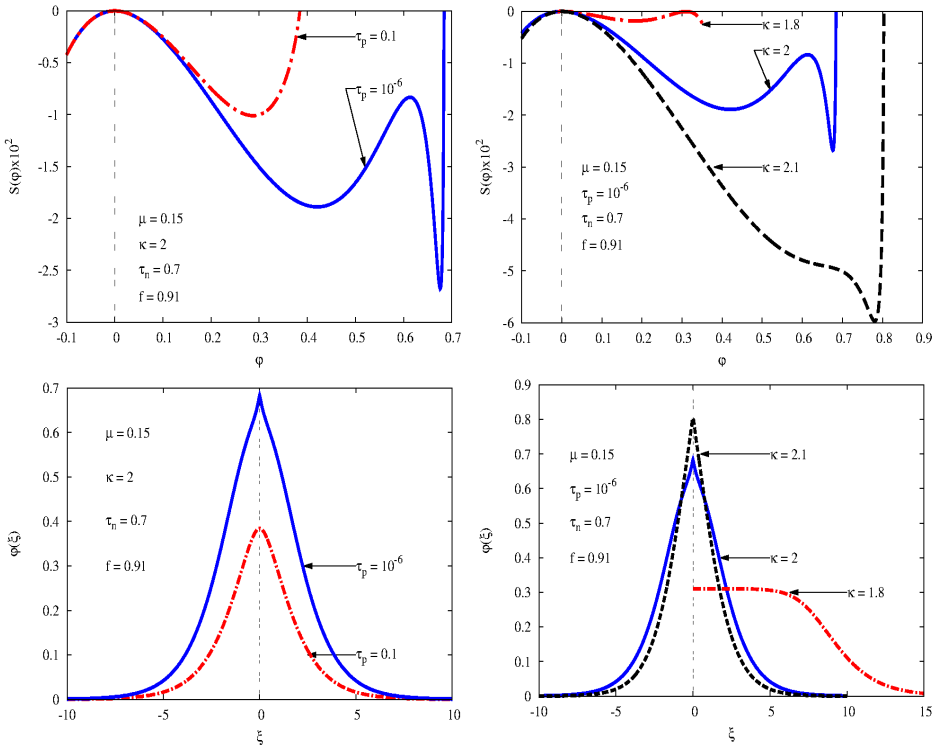

Figure 3.12: (Colour online) The transition from a supersoliton to a normal soliton as the positive ion temperature increases (left panels) and to a double layer as the superthermal behavior of electrons increases (right panels). The fixed parameter values parameter values taken from the supersoliton existence domain are $\mu = 0.15, \tau_n = 0.7$ and $f = 0.91$. The left panels are plotted at $\tau_p = 10^{-6}$ (solid line, blue colour online) and 0.1 (dash-dotted line, red colour online) at fixed spectral index $\kappa = 2$. The right panels are plotted at $\kappa = 2$ (solid line, blue colour online), 1.8 (dash-dotted line, red colour online) and 2.1 (dashed line, black online) at fixed $\tau_p = 10^{-6}$.

the ion thermal effect on the soliton upper limit transition. As is shown in both upper and lower left panels, when $\tau_p = 10^{-6}$ (solid blue line), the soliton upper limit to the soliton range is a supersoliton, occurring at the positive ion sonic point with amplitude $\varphi_{lp} = 0.68$. When the relative temperature of the two ion species decreases to $\tau_p = 0.1$ (dashed red line), the negative-to-positive density ratio range supporting the propagation of supersolitons shifts to higher values as discussed in Sec. 3.4.3, and there is transition from supersoliton upper limit to normal soliton upper limit with lower amplitude $\varphi_{lp} = 0.35$.

In the upper right panels we show the transition process when the electron superthermality is increased by decreasing the spectral index κ while keeping the positive to negative ion temperature fixed to $\tau_p = 10^{-6}$. In this case, the negative-to-positive ion density ratio range supporting the propagation of supersolitons shifts to lower values of f with an extension of the double layer existence range to lower values of f. It is thus possible that the supersoliton upper limit gives way to a double layer upper limit if the decrease of κ is sufficiently large. Thus in Fig. 3.12 right panels where $\kappa = 2$ (solid line, blue colour online), the soliton upper limit is the occurrence of a supersoliton with amplitude $\varphi_{lp} = 0.68$. When the spectral index decreases to $\kappa = 1.8$ (dash-dotted line, red colour online), there is transition of the upper limit to a double layer with a lower amplitude $\varphi_{dl} = 0.31$. On the other side, for a sufficiently large increase of the parameter κ, there is transition of the upper limit to a normal soliton in agreement with Fig. 3.1 upper panels. This transition is clear in Fig. 3.12 upper right panel, in which the dashed line (black line online) has been plotted at $\kappa = 2.1$. This curve has one potential well and represents a normal soliton as is confirmed by the corresponding soliton profile in the lower right panel. For values of $\kappa > 2.1$, only normal solitons limited by the occurrence of positive ion sonic points occur. We note here that, despite the transition, the amplitude of the limiting structure decreases continuously whether the relative ion temperature is continuously decreased or the electron superthermality is continuously increased.

3.5 Summary and conclusions

In this paper, we have used the Sagdeev pseudopotential method to investigate the ion thermal and electron superthermal effects on the slow mode ion-acoustic nonlinear waves in a negative ion plasma, comprising adiabatic positive and negative ions and kappa-distributed electrons. It is well known that in a two ion component plasma, the slow mode exists provided the thermal speeds of both ion species are different, with the polarity of the slow mode nonlinear structures being determined by the sign of the colder ion species [23]. In the present study, we have considered positive ion species to be colder, and negative ion species to be hotter and only positive potential nonlinear structures were found. The ion thermal effects are investigated through the parameter $\tau_p = T_p/T_n$, the positive to negative ion temperature ratio at fixed $\tau_n = T_n/T_e$, the negative ion temperature to electron temperature ratio. Thus increasing τ_p signifies increasing the temperature of positive ions at fixed temperature of negative ions, and the relative temperature of the two ion species is reduced. Having normalised the flow and nonlinear structures speeds by the negative ion thermal speed v_{tn}, the values of τ_p are limited by the condition $\mu\tau_p < 1$, where μ is the negative to positive ion mass ratio. The electron superthermal effects, on the other hand, are studied by considering different values of the spectral index κ of the kappa distributed electrons. The main results from this study are summarised as follows:

1. For Maxwellian electrons, cold positive ions and warm negative ions, the plasma supports the propagation of normal positive solitons, limited on the upper side by the occurrence of positive ion sonic point. As τ_p increases, i.e. as the relative temperature between the two ion species reduces, the range of the allowed Mach numbers also reduces, but shifts to higher values. This result differs significantly from that obtained for the fast mode, [34] *viz*. that at low temperature, a negative ion plasma supports both negative and positive potential fast mode solitary waves, and at high temperature, only negative fast mode solitons are found. The increase of τ_p is not however arbitrary, being limited by the slow mode Mach number range $\sqrt{\mu\tau_p} < M_{slow} < 1$.

2. When the electron superthermality increases with other plasma parameters held fixed, the soliton Mach number shifts to lower value and the Mach number range supporting the soliton propagation narrows. For strongly non-Maxwellian electrons, cold positive ions and warm negative ions, the plasma support, in addition to normal solitons, the propagation of slow mode positive supersolitons for a narrow range of negative-to-positive ion density ratio f. The soliton amplitude is limited, on the upper side, by the occurrence of positive ion sonic point for low to intermediate values of density ratio f, while the limiting factor is a double layer for higher values of f. As for the supersolitons, they are limited, on the lower side, either by the double layer or the coalescence of two consecutive extrema, and on the upper side, by the coalescence of two consecutive extrema or the occurrence of positive ion sonic point. When the double layer acts as the lower limit to the supersoliton existence range, there is a range of electrostatic potentials that are not accessible from the undisturbed conditions as was reported for the first time by Baluku et al. [57]; But when the coalescence is the lower limit, the supersoliton amplitude varies continuously. We note here that these results differ qualitatively with those obtained for Maxwellian electrons while for the fast mode [34] they were qualitatively the same. This breaks down a common belief, according to which kappa distribution does not bring any new qualitative differences from the results with Maxwellian distribution [64].

3. As the relative temperature of the two ion species is reduced (τ_p is increased) with fixed spectral index kappa, the range of negative-to-positive ion density ratio f supporting the propagation of double layers as the upper limit to the soliton amplitude shifts to higher values of f, increasing at the same time the density range supporting solitons limited by the occurrence of positive ion sonic point. This means that at high density ratio, the soliton upper limit is the double layer when positive ions are cold, but changes to the positive ion sonic point when positive ions are warm. Ultimately, with a further increase of τ_p double layers disappear as the negative ion

density, necessary to support them tend to be larger than the limiting value of $f = 1$ and from then solitons are limited by sonic point for the whole range of f. When it is the electron superthermality that increases (by virtue of decreasing the spectral index κ) under fixed τ_p, the density range supporting double layers extends to lower values of f, decreasing at the same time the density range supporting solitons limited by the occurrence of positive ion sonic point. There is, at intermediate values of f the transition from the positive ion sonic point as the soliton upper limit to double layer as the soliton limiting factor.

4. The range of negative-to-positive ion density ratio f supporting the propagation of double layers is preceded by a range supporting the propagation of supersolitons, the two being separated at point where a positive potential double layer occurs at the positive ion sonic point. Similar to the range supporting the propagation of double layers, the density range supporting the propagation of supersolitons shifts to higher values of f and narrows as the relative temperature of the two ions is reduced (τ_p is increased), and it shifts to lower values of f and becomes larger when it is the electron superthermality that increases (decreasing the spectral index κ). It is thus obvious that in the case under study, the existence of supersolitons and double layers is favoured by a combination of cold positive ions, warm negative ions and strongly non-Maxwellian electrons.

5. While the amplitudes of solitons and supersolitons decrease with a decrease of the relative temperature of the two ion species, an effect that is enhanced by the superthermal behavior of the electrons, it is found that the amplitudes of the double layers increase with a decrease of the relative temperature of the two ion species but decrease with an increase of the electron superthermality.

Acknowledgements

Partial financial support from the Swedish International Development Cooperation Agency (SIDA) through the International Science Programme (ISP) to University of Rwanda (UR) through the Rwanda Astrophysics, Space and Climate Science Research Group, Grant No. ISP/RWA : 01 is gratefully acknowledged. Further financial support from The World Academy of Sciences (TWAS) for the advancement of science in developing countries, Grant No. $19-123RG/PHYS/AF/AC_I-FR3240310162$, through the Institut d'Enseignement Superieur de Ruhengeri (INES-Ruhengeri) is also acknowledged.

Data availability

The data that support the findings of this study are available within the article.

3.6 References

[1] R. Sabry, W. M. Moslem, and P. K. Shukla, Phys. Plasmas **1**6, 032302 (2009).

[2] P. Chaizy, H. Reme, J. A. Sauvaud, C. d'Uston, R. P. Lin, D. E. Larson, D. L. Mitchell, K. A. Anderson, C. W. Carlson, A. Korth, and D. A. Mendis, Chem. Rev. **1**17(3), 393 (1991)

[3] T. J. Millar, C. Walsh and T. A. Field, Nature **3**49, 1765 (2017)

[4] M. Larsson, W. D. Geppert and G. Nyman, Rep. Prog. Phys. **7**5, 066901 (2012)

[5] J. L. Burch, T. E. Cravens, K. Llera, R. Goldstein, P. Mokashi, C. -Y. Tzou and T. Broiles, Geophys. Res. Lett. **4**2, 5125 (2015)

[6] A. J. Coates, A. Wellbrock, G. R. Lewis, G. H. Jones, D. T. Young, F. J. Crary, and J. H. Waite Jr., Planetary and Space Science **5**7, 1866 (2009).

[7] V. Vuitton, P. Lavvas, R. V. Yelle, M. Galand, A. Wellbrock, G. R. Lewis, A. J. Coates, and J.-E. Wahlund, Planetary and Space Science **5**7, 1558 (2009).

[8] A. J. Coates, A. Wellbrock, G. R. Lewis, G. H. Jones, D. T. Young, F. J. Crary, J. H. Waite, R. E. Johnson, T. W. Hill, and E. C. Sittler Jr., The Royal Society of Chemistry **1**47, 293 (2010).

[9] A. J. Coates, G. H. Jones, G. R. Lewis, A. Wellbrock, D. T. Young, F. J. Crary, R. E. Johnson, T. A. Cassidy, and T. W. Hill, Elsevier **2**06, 618 (2010).

[10] K. Agren, N. J. T. Edberg, and J.-E. Wahlund, Geophys. Res. Lett. **3**9, L10201 (2012).

[11] A. Wellbrock, A. J. Coates, G. H. Jones, G. R. Lewis and J. H. Waite, Geophys. Res. Lett **4**0, 4481 (2013).

[12] M. J. Singh, D. Boilson, A. R. Polevoi, T. Oikawa and R. Mitteau, New J. Phys. **1**9, 055004 (2017).

[13] K. Fujiwara, M. Endo, Y. Ikeda and H. Shindo, IEEE Conference Record - Abstracts. 2005 IEEE International Conference on Plasma Science, 150 (2005)

[14] G. O. Ludwig, J. L. Ferreira and Y. Nakamura, Phys. Rev. Lett. **5**2(4), 275 (1984).

[15] R. L. Merlino and J. J. Loomis, Phys. Fluids B **2**, 2865 (1990).

[16] B. Song, N. D'Angelo and R. L. Merlino, Phys. Fluids B **3**, 284 (1991).

[17] B. Handique, H. Bailung, G. C. Das and J. Chutia, Phys. Plasmas **6**, 1636 (1999).

[18] R. Ichiki, S. Yoshimura, T. Watanabe, Y. Nakamura and Y. Kawai, Phys. Plasmas **9**, 4481 (2002).

[19] S. G. Tagare, J. Plasma Physics **3**6, 301 (1986).

[20] L. L. Yadav, S. R. Sharma and R. S. Tiwari Phys. Plasmas **1**, 559 (1994).

[21] M. K. Mishra and R. S. Chhabra, Phys. Plasmas **3**, 4446 (1996).

[22] T. S. Gill, P. Bala, H. Kaur, N. S. Saini, S. Bansal, and J. J. Kaur, Eur. Phys. J. D **3**1, 91 (2004).

[23] F. Verheest, M. A. Hellberg, and I. Kourakis, Phys. Plasmas **1**5, 112309 (2008).

[24] M. K. Mishra, R. S. Tiwari, and J. K. Chawla, Phys. Plasmas **1**9, 062303 (2012).

[25] S. Hussain, N. Akhtar, and S. Mahmood, Astrophys Space Sci **3**38, 265 (2012).

[26] K. Jilani, A. M. Mirza, and T. A. Khan, Astrophys Space Sci **3**44, 135 (2013).

[27] S. Ali Shan and N. Akhtar, Astrophys Space Sci **3**46, 367 (2013).

[28] M. Mehdipoor, Astrophys Space Sci **3**48, 115 (2013).

[29] M. R. Rouhani and Z. E. Abbasi, Phys. Plasmas **1**9, 112307 (2012).

[30] S. K. El-labany, R. Sabry, E. F. El-shamy, and D. M. Khedr, J. Plasma Physics **7**9, 613 (2013).

[31] F. Nsengiyumva, M. A. Hellberg, F. Verheest, and R. L. Mace, Phys. Plasmas **2**1, 102301 (2014).

[32] F. Nsengiyumva, M. A. Hellberg, and R. L. Mace, Phys. Plasmas **2**2, 092304 (2015).

[33] K. Kumar and M. K. Mishra, AIP Advances **7**, 115114 (2017).

[34] X. Mushinzimana and F. Nsengiyumva, AIP Advances **1**0, 065305 (2020).

[35] F. Verheest, M. A. Hellberg, and G. S. Lakhina, Astrophys. Space Sci. Trans. **3**, 15 (2007).

[36] N. D'Angelo, S. V. Goeler and T. Ohe, Phys. Fluids **9**, 1605 (1966).

[37] R. Ichiki and M. Shindo and S. Yoshimura and T. Watanabe and Y. Kawai, Phys. Plasmas **8**, 4275 (2001).

[38] C. Norgren, M. André, A.Vaivads and Y. V. Khotyaintsev, Geophys. Res. Lett. **4**2, 1654 (2015).

[39] A. Kakad and B. Kakad and C. Anekallu and G. Lakhina and Y. Omura and A. Fazakerley, J. Geophys. Res. Space Physics **1**21, 4452 (2016).

[40] S. A. Shan and N. Imtiaz, Phys. Plasmas **2**4, 062101 (2017).

[41] S. Mahmood and H. Ur-Rehman, J. Phys. Soc. Jpn. **8**2, 074501 (2013).

[42] N. Akhtar, W. F. El-Taibany and S. Mahmood, Phys. Lett. A **3**77, 1282 (2013).

[43] A. E. Mowafy and W. M. Moslem, J. King Saud Univ. Eng. Sci. **2**4, 343 (2012).

[44] T. K. Baluku, M. A. Hellberg, I. Kourakis and N. S. Saini, Phys. Plasmas **1**7, 053702 (2010).

[45] F. Verheest, M. A. Hellberg and I. Kourakis, Phys. Plasmas **2**0, 082309 (2013).

[46] A. E. Dubinov and D. Y. Kolotkov, IEEE Trans. Plasma Sci. **4**0, 1429 (2012).

[47] F. Verheest, M. A. Hellberg and I. Kourakis, Phys. Plasmas **2**0, 012301 (2013).

[48] F. Verheest, M. A. Hellberg and I. Kourakis, Phys. Plasmas **8**7, 043107 (2013).

[49] J. S. Pickett and L. -J. Chen and S. W. Kahler and O. Santolik and D. A. Gurnett and B. T. Tsurutani and A. Balogh, Ann. Geophys. **2**2, 2515 (2004).

[50] F. Verheest and C. P. Olivier, Phys. Plasmas **2**4, 113708 (2017).

[51] S. V. Steffy and S. S. Ghosh, Phys. Plasmas **2**4, 102111 (2017).

[52] S. V. Steffy and S. S. Ghosh, Phys. Plasmas **2**3, 082304 (2016).

[53] A. Paul and A. Bandyopadhyay, Indian J. Phys. **9**2, 1187 (2018).

[54] D. -N. Gao, J. Zhang, Y. Yang and W. -S. Duan, Plasma Phys. Rep. **4**3, 833 (2017).

[55] F. Verheest, G. S. Lakhina and M. A. Hellberg, J. Plasma Phys. **2**1(6), (2014).

[56] F. Verheest, Phys. Plasmas **1**6, 013704 (2009).

[57] T. K. Baluku and M. A. Hellberg and F. Verheest, Europhys. Lett. **9**1, 15001 (2010).

[58] V. M. Vasyliunas, J. Geophys. Res. **7**3, 2839 (1968).

[59] D. Summers and R. M. Thorne, Phys. Fluids B **3**, 1835 (1991).

[60] M. Maksimovic, V. Pierrard and P. Riley, Geophys. Res. Lett. **2**4, 1151 (1997).

[61] P. Schippers, M. Blanc, N. Andre, I. Dandouras, G. R. Lewis, L. K. Gilbert, A. M. Persoon, N. Krupp, D. A. Gurnett, A. J. Coates, S. M. Krimigis, D. T. Young and M. K. Dougherty, J. Geophys. Res. **1**13, A07208 (2008).

[62] V. De La Haye, J. H. Waite Jr., R. E. Johnson, R. V. Yelle, T. E. Cravens, J. G. Luhmann, W. T. Kasprzak, D. A. Gell, B. Magee, F. Leblanc, M. Michael, S. Jurac, and I. P. Robertson, J. Geophys. Res. **1**12, A07309 (2007).

[63] V. Pierrard and M. Lazar, Sol. Phys. **2**67, 153 (2010).

[64] F. Verheest and M. A. Hellberg, Phys. Plasmas **1**7, 102312 (2010).

[65] S. S. Ghosh, K. K. Ghosh, and A. N. Sekar Iyengar, Phys. Plasmas **3**, 3939 (1996).

[66] S. Baboolal, R. Bharuthram and M. A. Hellberg, J. Plasma Phys.Phys. **4**4, 1 (1990).

[67] F. Verheest and M. A. Hellberg and N. S. Saini and I. Kourakis, Phys. Plasmas **1**8, 042309 (2011).

[68] S. K. Maharaj, R. Bharuthram, S. V. Singh and G. S. Lakhina, Phys. Plasmas **2**0, 083705 (2013).

[69] A. Y. Wong, D. L. Mamas, and D. Arnush, Phys. Fluids **1**8, 1489 (1975).

Chapter 4

Dust ion acoustic solitary waves in a dusty plasma with adiabatic positively charged dust, adiabatic positive ions and non-thermal electrons

Dust ion acoustic solitons and double layers in a dusty plasma with positive dust, adiabatic positive ion species, and Cairns distributed electrons

X. Mushinzimana[1, a)] , F. Nsengiyumva[2,b)] , L. L. Yadav[3,c)] and T. K. Baluku[4,d)]

[1] *Department of Physics, University of Rwanda*

College of Science and Technology

P. O. Box 3900 Kigali, Rwanda

[2] *Department of Civil Engineering*

Institut d'Enseignement Superieur de Ruhengeri

P. O. Box 155 Musanze, Rwanda

[3] *Department of Mathematics, Science and Physical Education,*

University of Rwanda- College of Education,

P. O. Box 55 Rwamagana, Rwanda

[4] *Department of Physics, Pwani University,*

P. O. Box 195-80108, Kilifi, Kenya.

[a)] Author to whom correspondence should be addressed: muxavier2000@yahoo.fr

[b)] Email: franco.nseng@gmail.com

[c)] Email: yadavll@yahoo.com

[d)] Email: balukuthomas@yahoo.co.uk

Abstract

The propagation of dust ion acoustic solitary waves and double layers is studied in a dusty plasma with heavy adiabatic positively charged dust grains and lighter adiabatic positive ions with Cairns-distributed electrons, using the arbitrary amplitude Sagdeev pseudopotential approach. The analysis of the Sagdeev pseudopotential shows that this plasma model supports the propagation of positive solitons limited by the occurrence of the ion sonic point and negative solitons limited by the occurrence of double layers. Solitons of both polarities coexist for a range of some plasma parameters. We have shown that at a critical dust-to-ion density ratio, f, at which the third derivative of the Sagdeev pseudopotential vanishes, positive and negative solitons coexist without a soliton with finite amplitude at the acoustic speed, contrary to an earlier study. This suggests that the existence of a soliton with finite amplitude at the acoustic speed is not always a pre-requisite for the coexistence of nonlinear structures of both polarities. Positive and negative solitons coexist when the electrons are strongly nonthermal, with moderate ion thermal effects. Increasing ion thermal effect shifts the coexistence region to lower values of f and when the ion thermal effects become important negative solitons disappear and only positive solitons survive. The effects of different plasma parameters on the characteristics of the nonlinear structures have also been discussed in detail.

4.1 Introduction

The propagation of nonlinear waves in plasmas containing dust grains in addition to positive ions and electrons has been an important research focus in recent years. [1–27] Dust particles embedded in a plasma are charged via different mechanisms and acquire a negative and/or a positive charge. [17, 18, 28, 29] Specifically a dust may be charged by collecting electrons and ions from the plasma. Due to the difference in the electron and ion speeds it becomes negatively charged. [11, 30] For less dense

plasma as observed in most astrophysical plasmas, photoelectron and secondary electron emissions are the dominant charging processes leading to positively charged dust. [15, 31–36] When charged dust grains become part of the plasma, they modify its collective behaviour. [28] Studies of dusty plasmas are motivated by the existence of charged dust in many space and astrophysical plasmas such as Earth's ionosphere and mesosphere, cometary tails, planetary rings and interstellar clouds, [1, 8, 9, 14, 18, 28] as well as in laboratory plasma experiments and industrial plasma processing units. [11, 14, 33, 35]

Theoretical [2, 3] and experimental [4–6] studies have shown that the presence of charged dust in a plasma not only modifies the propagation properties of the existing plasma wave modes, but also introduces new modes. Shukla and Silin [3] predicted the existence of a modified ion acoustic mode, called the dust ion acoustic (DIA) wave mode which was observed later by Barkan et al.[5] and Merlino et al.. [6] Rao et al. [2] predicted the existence of a new mode arising from the collective motion of negatively charged dust in a background of positive ions and electrons in thermodynamic equilibrium. This new mode was named as the dust acoustic (DA) wave mode and was observed later by Barkan et al. [4]

The DIA waves have been investigated in different plasma configurations. [3, 21, 22, 37, 38] The reductive perturbation method [21, 38] was used to derive the KdV equation, a nonlinear differential equation that describes the propagation of small amplitude solitary waves. These small amplitude waves are always found to be superacoustic with amplitude vanishing when the wave speed approaches the acoustic speed. Solitary waves with amplitudes vanishing at the acoustic speed are also termed KdV-like [39] solitons. The Sagdeev pseudopotential method [40] was used to describe the arbitrary amplitude solitary wave propagation. [15, 21, 22] In this method, the fluid equations are reduced to an energy-like equation involving a pseudopotential energy function, the Sagdeev pseudopotential, which is analysed in the same manner as the analysis of the potential energy for an oscillating particle in

classical mechanics. With this method, nonKdV [39] solitary waves with finite amplitude at the acoustic speed have been found in different plasma models. [21, 22, 39, 41]

Baluku et al. [21] have investigated the propagation of the dust ion acoustic solitons in a plasma with kappa-distributed electrons, positive ions and negatively or positively charged dust using both KdV and Sagdeev pseudopotential methods. They showed that when the dust is positively charged, only positive solitons are supported. Existence of only positive solitons was also confirmed by Baluku et al. [19] in an investigation of the existence of solitons in dusty plasma with positive dust grains using the fluid dynamics method.

Verheest et al. [41] investigated a model involving two cold positive ion species and Cairns-distributed [42] electrons. In this model, both positive and negative dust ion acoustic solitons have been found to coexist for a large range of parameter values. Verheest et al. [41] pointed out that the occurrence of solitons with finite amplitudes at the acoustic speed is a necessary and sufficient condition for the nonlinear structures of both polarities to coexist. In this paper, we investigate the existence of dust ion acoustic solitons and double layers in a dusty plasma consisting of adiabatic positively charged dust, adiabatic positive ions and Cairns distributed electrons, and present a case in which nonlinear structures of both polarities coexist without having a soliton with finite amplitude at the acoustic speed. This suggests that the conclusion reached by Verheest et al. [41] is not applicable to all plasma models and ranges of parameter values. The paper is organised as follows. After this introductory section, we derive, from the fluid equations, an expression for the Sagdeev pseudopotential in Sec. II, which we use to discuss the nonlinear structures in Sec. III. A summary of the results is presented in Sec. IV.

4.2 Model equations and Sagdeev pseudopotential

The propagation of the low frequency dust ion acoustic (DIA) wave mode in a dusty plasma with positively charged adiabatic dust, adiabatic positive ions and Cairns-distributed electrons is considered. The dust is more massive than the ion species but both dust and ions are supersonic (cool) in the sense that the speed of the nonlinear structures being investigated is larger than the thermal speed of either species. The number of charges residing on the dust and the ions is respectively z_d and z_i. To compare our results with those obtained elsewhere, [22] we introduce a variable s with value $s = 1$ when the dust is positively charged as is the case in the present study while $s = -1$ when the dust is negatively charged. After integrating the Cairns distribution function in phase space over velocity space, the density of inertialess electrons is found as [42]

$$n_e = n_{e0}\left(1 - \beta\varphi + \beta\varphi^2\right)\exp(\varphi), \tag{4.1}$$

where n_{eo} is the equilibrium electron density, φ is the electrostatic potential and the variable $\beta = 4\alpha/(1+3\alpha)$, where α is the Cairns nonthermal parameter, showing the departure of the Cairns distribution from the Maxwellian. For $\alpha = 0$ the Maxwell distribution is recovered and α increases to ∞ as the degree of nonthermality increases. The values of β are then in the interval $[0, 4/3]$, but it is normally limited to $4/7$ on the upper side to avoid the range in which the distribution develops beam instabilities. [22] For the dust and ion species, we retain the inertia of each of them and the dynamics of the electrostatic perturbation is governed by the fluid continuity and momentum equations for both species as

$$\frac{\partial n_d}{\partial t} + \frac{\partial\left(n_d u_d\right)}{\partial x} = 0, \tag{4.2}$$

$$\frac{\partial u_d}{\partial t} + u_d\frac{\partial u_d}{\partial x} = -s\mu\frac{\partial\varphi}{\partial x} - \mu\tau_d n_d\frac{\partial n_d}{\partial x}, \tag{4.3}$$

$$\frac{\partial n_i}{\partial t} + \frac{\partial\left(n_i u_i\right)}{\partial x} = 0, \tag{4.4}$$

$$\frac{\partial u_i}{\partial t} + u_i \frac{\partial u_i}{\partial x} = -\frac{\partial \varphi}{\partial x} - \tau_i n_i \frac{\partial n_i}{\partial x}. \tag{4.5}$$

where $n_d(u_d)$ and $n_i(u_i)$ are the densities (velocities) of the dust and ion species, respectively, x is the space coordinate and t is the time coordinate. The parameter $\mu = z_d m_i / z_i m_d$ is the dust to ion charge-to-mass ratio, $\tau_d = T_d / z_d T_e$ is the dust to electron temperature ratio and $\tau_i = T_i / z_i T_e$ is the ratio of the ion temperature to the electron temperature. The plasma component densities are coupled by Poisson's equation

$$\frac{\partial^2 \varphi}{\partial x^2} = (1 + sf) n_e - sf n_d - n_i, \tag{4.6}$$

where the variable $f = z_d n_{d0} / z_i n_{i0}$ is the ratio of the dust equilibrium charge density $z_d n_{d0}$ to ion species equilibrium charge density $z_i n_{i0}$. Without loss of generality, we will consider $f < 1$. The system of equations is closed by the Poisson's equation. In this study we have assumed the dust and ion species to be adiabatic with polytropic index $\gamma = 3$, and the unperturbed pressure of the j^{th} adiabatic species is defined as $p_{j0} = n_{j0} T_j / 3$. [43]
In Equations (4.2) to (4.6), the space coordinate x is normalised by $\lambda_{Di} = (\varepsilon_0 T_e / n_{i0} z_i e^2)^{1/2}$, the time by the inverse of $\omega_i = (n_{i0} z_i^2 e^2 / \varepsilon_0 m_i)^{1/2}$, the flow velocities by $c_{ti} = (z_i T_e / m_i)^{1/2}$, the electrostatic potential by the electron thermal potential T_e / e and the densities are normalised by their equilibrium values. With this normalisation, the thermal speeds of ion and dust speciers are $\sqrt{\tau_i}$ and $\sqrt{\mu \tau_d}$, respectively.

Equations (4.2) to (4.6) are used to describe the propagation of a perturbation in a plasma otherwise at rest. A commonly used frame to describe this propagation is the comoving frame in which the wave structure is stationary, introduced via the transformation $\xi = x - Mt$ where M is the velocity V of the wave normalised by c_{ti} and is yet to be determined. This transformation converts the partial differential equations (4.2) to (4.6) into ordinary differential equations in ξ as

$$-M \frac{dn_d}{d\xi} + \frac{d(n_d u_d)}{d\xi} = 0, \tag{4.7}$$

$$-M\frac{du_d}{d\xi}+u_d\frac{du_d}{d\xi}=-s\mu\frac{d\varphi}{d\xi}-\mu\tau_d n_d\frac{dn_d}{d\xi}, \tag{4.8}$$

$$-M\frac{dn_i}{d\xi}+\frac{d\left(n_i u_i\right)}{d\xi}=0, \tag{4.9}$$

$$-M\frac{du_i}{d\xi}+u_i\frac{du_i}{d\xi}=-\frac{d\varphi}{d\xi}-\tau_i n_i\frac{dn_i}{d\xi}. \tag{4.10}$$

$$\frac{d^2\varphi}{d\xi^2}=(1+sf)n_e-sfn_d-n_i, \tag{4.11}$$

This system can be integrated with appropriate boundary conditions. The boundary conditions are born in the nature of the solution in view, a localised solution in our case. Thus far from the perturbation where the plasma is undisturbed $n_d=1, n_i=1, u_d=0, u_i=0$ and $\varphi=0$. With these boundary conditions, integration of Eqs. (4.7) and (4.8) yields the dust density as

$$n_d=\frac{1}{2\sqrt{\mu\tau_d}}\left[\sqrt{\left(M+\sqrt{\mu\tau_d}\right)^2-2s\mu\varphi}\pm\sqrt{\left(M-\sqrt{\mu\tau_d}\right)^2-2s\mu\varphi}\right], \tag{4.12}$$

and integration of Eqs. (4.9) and (4.10) yields the ion density as

$$n_i=\frac{1}{2\sqrt{\tau_i}}\left[\sqrt{\left(M+\sqrt{\tau_i}\right)^2-2\varphi}\pm\sqrt{\left(M-\sqrt{\tau_i}\right)^2-2\varphi}\right]. \tag{4.13}$$

The $\pm$ signs in expressions (4.12) and (4.13) serve to differentiate between the dust ion acoustic mode and the dust acoustic mode. In the DIA mode, both dust and ion species are supersonic (cool) and therefore their thermal speeds are smaller than the speeds of the nonlinear structures being investigated. This means that for this case $\sqrt{\left(M-\sqrt{\mu\tau_d}\right)^2}=M-\sqrt{\mu\tau_d}$ and $\sqrt{\left(M-\sqrt{\tau_i}\right)^2}=M-\sqrt{\tau_i}$ and the lower signs are to be used in order to satisfy the boundary conditions. The upper signs would be used when investigating the DA mode for which one inertial species is supersonic while the other is subsonic *i.e.* its thermal speed is larger than the nonlinear structure speed. For the subsonic species we would then choose the upper sign to satisfy the boundary conditions as in this case $\sqrt{\left(M-\sqrt{\tau_j}\right)^2}=\sqrt{\tau_j}-M$.

After substituting density expressions (4.1), (4.12) and (4.13) in Eq. (4.11) and multiplying it by $d\varphi/d\xi$, it can be integrated with the boundary conditions, a process that results in an energy-like equation

$$\frac{1}{2}\left(\frac{d\varphi}{d\xi}\right)^2 + S(\varphi) = 0 \tag{4.14}$$

similar to the energy equation for a particle oscillating in a potential well, where

$$\begin{aligned} S(\varphi,M) &= (1+sf)\left[1+3\beta-(1+3\beta-3\beta\varphi+\beta\varphi^2)e^{\varphi}\right] \\ &\quad + \tfrac{f}{6\mu\sqrt{\mu\tau_d}}\left\{2\left(\mu\tau_d\right)^{3/2}+6M^2\left(\mu\tau_d\right)^{1/2}\right. \\ &\quad \left. -\left[\left(M+\sqrt{\mu\tau_d}\right)^2-2s\mu\varphi\right]^{3/2}+\left[\left(M-\sqrt{\mu\tau_d}\right)^2-2s\mu\varphi\right]^{3/2}\right\} \\ &\quad + \tfrac{1}{6\sqrt{\tau_i}}\left\{2\left(\tau_i\right)^{3/2}+6M^2\left(\tau_i\right)^{1/2}\right. \\ &\quad \left. -\left[\left(M+\sqrt{\tau_i}\right)^2-2\varphi\right]^{3/2}+\left[\left(M-\sqrt{\tau_i}\right)^2-2\varphi\right]^{3/2}\right\} \end{aligned} \tag{4.15}$$

is the Sagdeev pseudopotential. The first term of $S(\varphi,M)$ is the electron contribution. The second term is the contribution of the dust in the Sagdeev pseudopotential. When the dust is negatively charged $(s=-1)$ and cold as considered by Verheest et al., [22] it reduces to the second term in their Eq. (9). If, in addition, the dust is much heavier than the ion, it reduces to the second term in their Eq. (5). Similarly, the third term which is the contribution of the ions reduces to their third term when the ions are cold.

The Sagdeev pseudopotential can be analysed by finding plasma parameter ranges, supporting the existence and propagation of solitons and double layers, the same way the potential energy function is analysed in the case of an oscillating particle by plotting the curve $S(\varphi)$ as a function of φ for different plasma parameter values. We have chosen, however, not to follow this trial and error method, rather we will first determine the existence domain for

nonlinear structures before plotting the curve for well known parameter values in the existence domain. This way, the Sagdeev potential curves serve to show that the function S satisfies the necessary conditions to represent a nonlinear structure. Such conditions for the existence of the nonlinear structures are [39, 44]

1. $S(0,M) = S'(0,M) = 0$;
2. $S''(0,M) \leqslant 0$, the origin is unstable;
3. $S(\varphi_m, M) = 0$ for some M in the soliton existence domain and $\varphi_m \neq 0$;
4. $S(\varphi, M) < 0$ for $0 < |\varphi| < |\varphi_m|$; and
5. For double layers, $S(\varphi_m, M) = S'(\varphi_m, M) = 0$ for some M in addition to $(i) - (iv)$.

Here primes denote the derivatives of the Sagdeev pseudopotential with respect to the electrostatic potential, and φ_m is the amplitude of the nonlinear structure.

4.3 Solitary waves and double layers

4.3.1 Existence domains for solitons and double layers

The model under discussion involves $s, \mu, \tau_d, \tau_i, \beta$ and the density ratio f as plasma parameters that can be varied to study their effects on the solitary wave propagation characteristics. In the remainder of the discussion, we consider positively charged dust, therefore the value of the parameter s is fixed to 1. The charge to mass ratio of the dust is normally very small as compared to the same ratio for positive ions. [31] This means that the value of μ has to be kept very small. In our numerical analysis, we will use a value of $\mu = 10^{-4}$. Furthermore, Eq. (4.19) shows that when either the dust temperature or the ion temperature increases, the acoustic speed also increases. However, due to the small value of μ, the contribution of the dust remains insignificant even at a high value of τ_d. Subsequently, we will keep a constant value of $\tau_d = 10^{-4}$ throughout the remaining

sections. We remain with three parameters to be varied, the positive ion temperature ratio τ_i, the electron nonthermal parameter β and the density ratio f.

A direct verification shows that the function (4.15) satisfies the condition (i) for any wave speed M. The condition (ii) often referred to as the soliton condition leads to the inequality

$$M \geqslant M_s, \tag{4.16}$$

where M_s satisfies the equation

$$\frac{d^2 S(\varphi)}{d\varphi^2} = 0, \tag{4.17}$$

and is given by

$$\begin{aligned} M_s^2 &= \frac{1}{2\delta}\{\delta(\tau_i+\mu\tau_d)+1+f\mu \\ &\quad \pm\sqrt{[\delta(\tau_i+\mu\tau_d)+1+f\mu]^2-4\delta\,[\delta\mu\tau_i\tau_d+\mu\tau_d+f\tau_i]}\Big\}, \end{aligned} \tag{4.18}$$

where $\delta = (1+f)(1-\beta)$. It is well known that the solution of Eq. (4.17) yields the minimum Mach number for solitons to exist. The condition (4.16) expresses then the fact that nonlinear structures are acoustic or superacoustic in nature. [45]

We are investigating the existence of nonlinear structures when both dust and ion species are supersonic, a condition that is satisfied if we choose the positive sign in front of the square root in expression $(B.28)$. This can be verified by expanding $(B.28)$ in Taylor series up to the zeroth order. This gives

$$M_s^2 \approx \tau_i + \mu\tau_d + \frac{1+s^2 f\mu}{(1+sf)(1-\beta)}, \tag{4.19}$$

showing that the DIA Mach number M_s is larger than the thermal speeds of both dust and ion species, $\sqrt{\mu\tau_d}$ and $\sqrt{\tau_i}$, respectively as expected. Furthermore, Eq. (4.19) shows that when either the dust temperature or the

ion temperature increases, the acoustic speed also increases.

While the condition (ii) determines the lower limit in Mach number M_s for solitary waves to exist, the condition (iii) determines the upper limit. Indeed the condition (iii) means that Eq. (4.14) has solitary wave solutions only if the Sagdeev pseudopotential $S(\varphi, M)$ admits at least one root $\varphi = \varphi_m$ different from the root $\varphi = 0$ for some $M \geqslant M_s$. However, the constraint that the dust and ion densities remain real-valued functions of the electrostatic potential puts a limit to the possible highest value of φ_m, which is the amplitude of the nonlinear structure. For the model at hand, the ion and dust densities become complex-valued when the electrostatic potential φ exceeds the ion and dust sonic points

$$\begin{cases} \varphi_{li} = & \frac{(M-\sqrt{\tau_i})^2}{2}, \\ \varphi_{ld} = & \frac{(M-\sqrt{\mu\tau_d})^2}{2\mu}. \end{cases} \tag{4.20}$$

Both of them are positive and represent the upper limit to the positive potential electrostatic structure amplitudes. This means that for compatibility, the positive potential solitons are limited by the electrostatic potential with the smallest value among φ_{li} and φ_{ld}. For very small values of μ as considered here, $\varphi_{ld} \gg \varphi_{li}$ and the positive solitons are limited by the positive ion sonic point.

On the negative side of the electrostatic potential, the Sagdeev pseudopotential function $S(\varphi) \to -\infty$ for $\varphi \to -\infty$. This means that negative roots can exist in pairs with a double root counted as two roots. This then predicts the possible existence of negative solitons whose upper limit is the occurrence of a double layer. This prediction can be further refined by analysing the third derivative calculated at the acoustic speed

$$S'''(0, M_s) = -(1+f) + f\mu^2 \frac{3M_s^2 + \mu\tau_d}{(M_s^2 - \mu\tau_d)^3} + \frac{3M_s^2 + \tau_i}{(M_s^2 - \tau_i)^3}. \tag{4.21}$$

The sign of $S'''(\varphi)$ determines the sign of the KdV-like solitons, that is to say, solitons whose amplitudes vanish at the acoustic speed. Positive

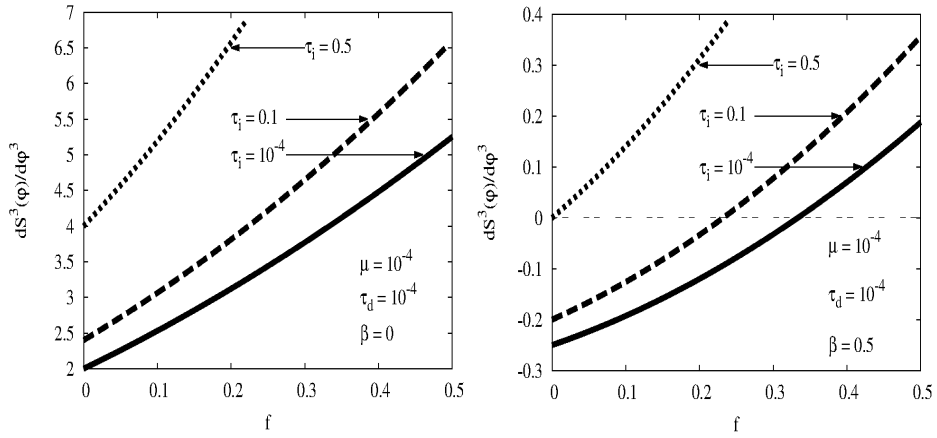

Figure 4.1: (Color online) The third derivative of the Sagdeev potential plotted against the density ratio f for different values of the ion temperature τ_i when electrons are Maxwellian with $\beta = 0$ (left panel) and when they are strongly non-Maxwellian with $\beta = 0.5$ (right panel). The other plasma parameter values are $\mu = 10^{-4}$ and $\tau_d = 10^{-4}$.

(negative) solitons are supported when $S'''(\varphi) > (<)0$.[21]

There is also the possibility of the existence of nonKdV-like solitons, which are solitons with finite amplitude at the acoustic speed, having the sign opposite to the sign of the KdV-like solitons for a fixed set of plasma parameter values. The existence of nonKdV-like solitons is not predicted by the third derivative of the pseudopotential, but if they are present a coexistence region may also exist. [41] By coexistence region we mean a set of plasma parameter values that admits solitons with either polarity depending on the initial conditions. This can be determined by a proper plot of the Sagdeev potential for these plasma parameter values.

Fig. 4.1 is a plot of $S'''(\varphi)$ as a function of the density ratio f. In the left panel, electrons are Maxwellian with the parameter β taking a value of 0. The ion temperature ratio is varied with $\tau_i = 10^{-4}$ (solid line), $\tau_i = 0.1$ (dashed line) and $\tau_i = 0.5$ (dotted line). For all these values, the third derivative remains positive, suggesting that for these plasma parameter

values, the model supports KdV-like positive solitons whose amplitude is limited by the occurrence of the ion sonic point.

The right panel of Fig. 4.1 shows a plot of the third derivative of the pseudopotential for strongly nonthermal electrons with nonthermal parameter $\beta = 0.5$ and the same values of τ_i as in the left panel. The third derivative of the pseudopotential takes now negative and positive values depending on the combination of density ratio f and ion temperature τ_i. For $\tau_i = 10^{-4}$, $S'''(\varphi)$ is negative for low values of f up to a critical value $f = f_c \approx 0.333$, but changes sign and becomes positive for $f > f_c$. Negative KdV-like solitons are supported for $f < f_c$ and positive KdV solitons are supported for $f > f_c$.

To understand better this configuration, we have plotted the soliton existence domain in $\{f, M\}$ space in Fig. 4.2. Electrons are Maxwellian ($\beta = 0$) in the left panels $(a), (c)$ and (e) and strongly nonthermal ($\beta = 0.5$) in the right panels $(b), (d)$ and (f). We have limited the plots at $f = 0.5$ for clarity but the trend of the curves remains the same for $f > 0.5$. In each panel of this figure, the blue solid line represents the minimum Mach number for solitons to exist. The dot-dashed red line represents the upper limit in Mach number due to the occurrence of the positive ion sonic point. Positive solitons may propagate if their Mach number is between M_s and M_{li} for a fixed density ratio, f. Panels $(a), (c)$ and (e) clearly show that when the electrons are Maxwellian, only positive solitons are supported by the model irrespective of the ion temperature. This result is reminiscent of that obtained by Baluku et al. [19, 21]

When the electrons are strongly nonthermal (panels (b) and (d)) negative solitons are also supported in addition to the existence of positive solitons. But in the absence of any physical fluid limit, their ranges are limited by the occurrence of negative double layers. The dashed green line in panels (b) and (d) represents such a limit. Panel (b) shows that negative solitons are supported for low density ratio up to $f = f_n \approx 0.408$ at which value there is a cutoff of negative solitons whereas positive solitons exist for even

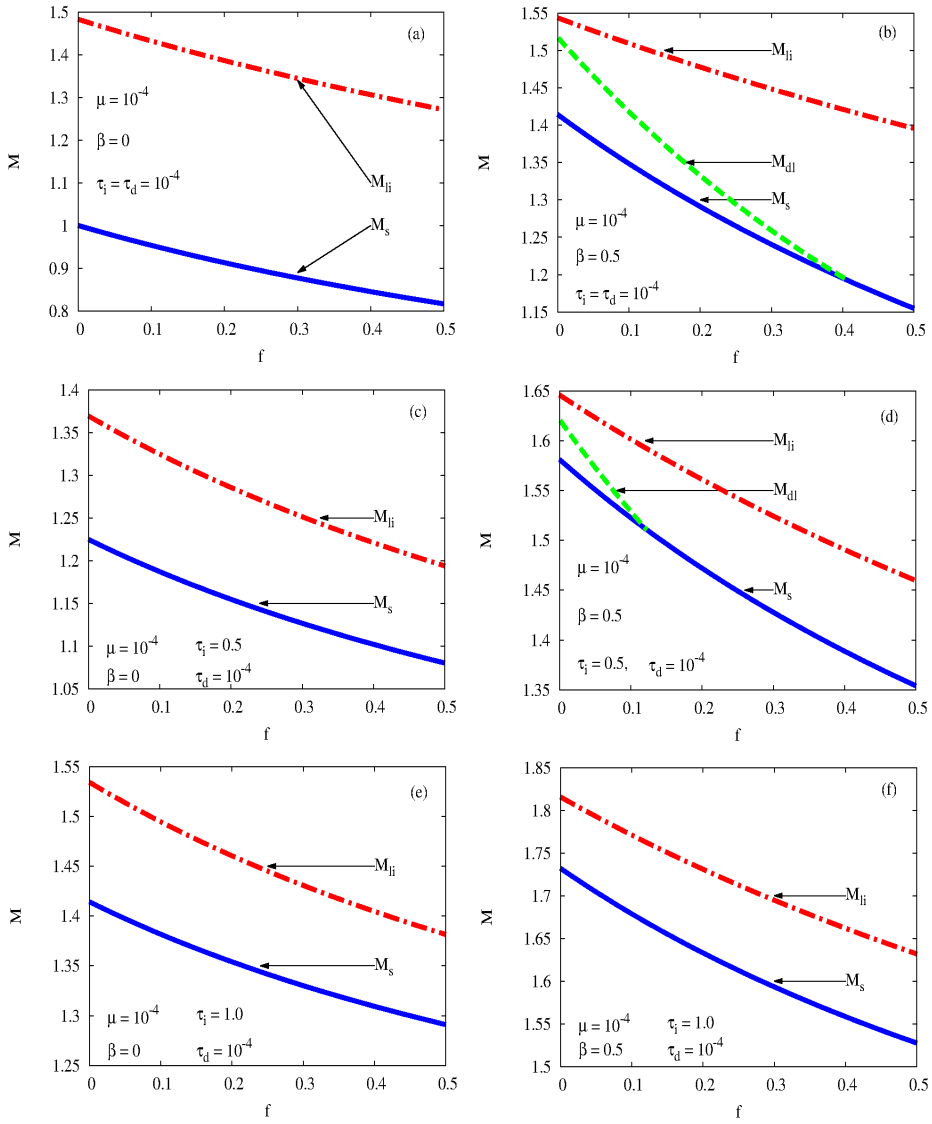

Figure 4.2: (Color online) Existence domains of dust ion acoustic solitary waves and double layers in $\{f, M\}$ space. The left panels $(a), (c)$ and (e) show the effect of increasing the positive ion temperature when the electrons are Maxwellian $(\beta = 0)$, and the right panels $(b), (d)$ and (f) show the same effect when the electrons are strongly non-Maxwellian $(\beta = 0.5)$. The fixed plasma parameters are $\mu = 10^{-4}$ and $\tau_d = 10^{-4}$.

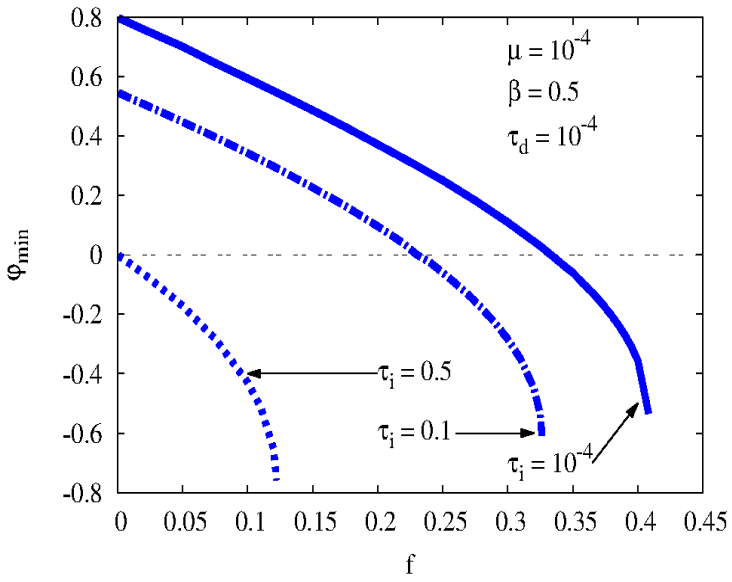

Figure 4.3: (Color online) The variation of the amplitude of the solitons at the acoustic speed φ_{min} as a function of density ratio f for different values of the ion temperature. As the ion temperature τ_i increases, both the critical density f_c at which there is change of polarity and the density f_n at which there is cutoff of negative solitons shift to lower values.

much higher values of f. There is therefore a coexistence of solitons of both polarities within the range $0 < f \lesssim 0.408$.

We note that negative solitons exist for values of the density ratio f beyond the limit f_c predicted by the third derivative of the Sagdeev pseudopotential, and similarly positive solitons exist for the range $f < f_c$ not predicted by the third derivative. This suggests that negative solitons in the range $f_c < f < f_n$ and positive solitons in the range $0 < f < f_c$ are nonKdV in nature. We will show in Section 4.3.2 that for $f < f_c$ there exist positive solitons at the acoustic speed while negative solitons exist at the acoustic speed for $f_c < f < f_n$.

The results presented in panel (d) show that the coexistence region is sensitive to the ion temperature. Also shown in the right panel of Fig. 4.1, this

sensitivity is emphasized in Fig. 4.3, where the amplitude of the soliton at the acoustic speed φ_{min} is plotted against the density ratio f for different values of the ion temperature ratio τ_i. In this figure, the value of f corresponding to $\varphi_{min} = 0$ is the critical density f_c, and the value of f corresponding to the largest negative value of φ_{min} is the negative soliton cutoff density f_n.
When $\tau_i = 10^{-4}$, the critical density $f_c \approx 0.333$ and the negative soliton cutoff density $f_n \approx 0.408$ (solid blue line). As τ_i is increased to 0.1, f_c and f_n shift to lower values, 0.23 and 0.33, respectively (dot dashed blue line). With a further increase of τ_i up to $\tau_i \approx 0.5$, the critical density vanishes $(f_c = 0)$ while the negative soliton cutoff remains finite $(f_n = 0.12)$ (dotted blue line). This means that from the value of $\tau_i \approx 0.5$ and larger, nonKdV negative solitons coexist with KdV positive solitons without change of polarity $(f_c = 0)$. As τ_i approaches 1 the cutoff density ratio f_n goes also to *zero* and the coexistence region disappears completely (panel (f) of Fig. 4.2). Alternatively, the density range supporting the propagation of negative solitons is reduced with an increase in the ion temperature, and only positive solitons survive when the ion thermal effects are significant.

4.3.2 Amplitudes of solitons and double layers

A simple way to check whether the soliton existence domains presented in Fig. 4.2 are free of errors is to plot the pseudopotential for Mach numbers ranging from the minimum value to the maximum value, and for a fixed value of the density ratio. This is illustrated in Fig. 4.4 in which the pseudopotential plots are presented for the case of $\beta = 0.5$, $\tau_i = 10^{-4}$ (left panels) and $\tau_i = 0.5$ (right panels), corresponding to different values of density ratio, f: $f = 0.1$ (upper panels), $f = 0.4$ (middle panels), and $f = 0.5$ (bottom panels).

Clearly, the results show solitons of both polarities, with their coexistence at low values of f ($f \lesssim 0.4$) when the ion thermal effects are moderate (upper and middle panels). The results in panels (a) and (b), obtained for $f = 0.1$ (low value of f), show the existence of a positive soliton with finite amplitude at the acoustic speed $M_s = 1.3484$ (panel (a), blue solid line),

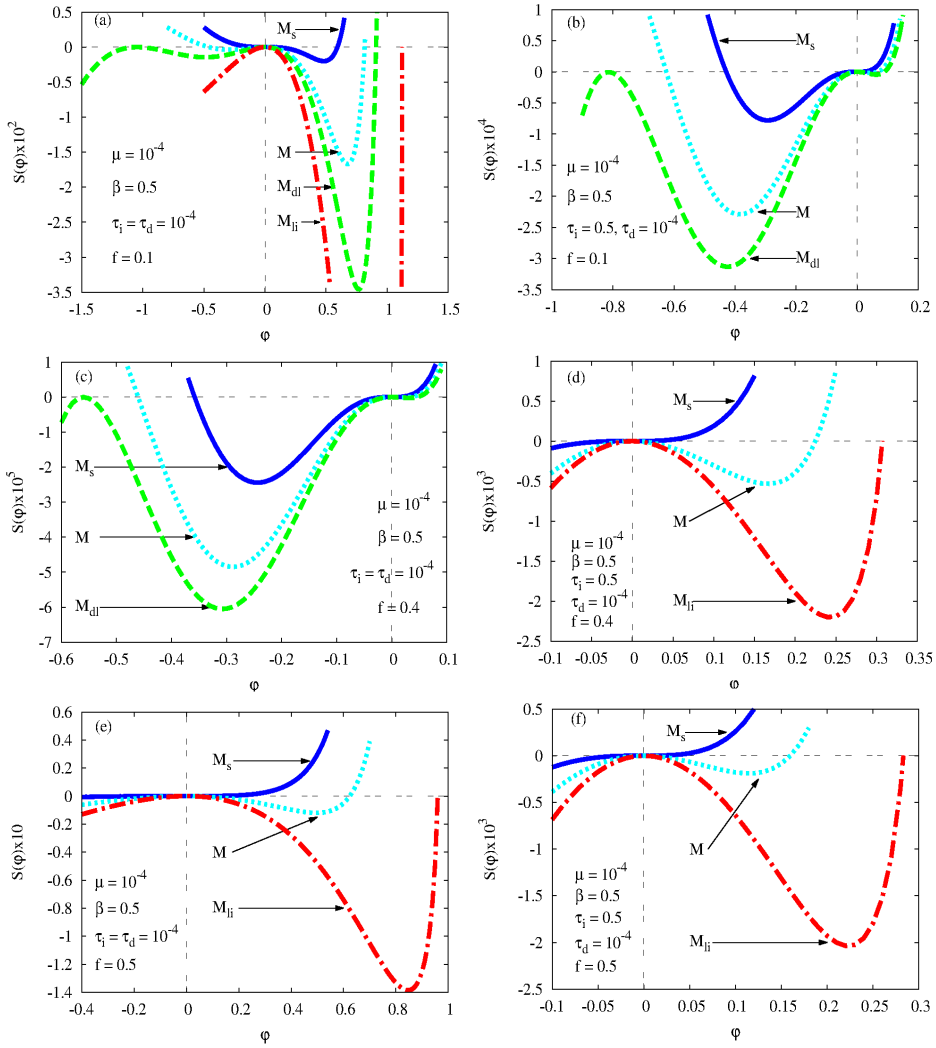

Figure 4.4: (Color online) Sagdeev pseudopotentials for plasma parameter values obtained from the right panels of the existence domains presented in Fig. 4.2 (case $\beta = 0.5$). Moving from the left to right panels, the effect of increasing the value of τ_i is shown considering three different values of the density ratio, f, namely $f = 0.1$ ((a) and (b)), $f = 0.4$ ((c) and (d)), and $f = 0.5$ ((e) and (f)). The values of the Mach numbers used to obtain the plots presented in each panel are discussed in the text.

with a switch of polarity (panel (b), blue solid line plotted at acoustic speed $M_s = 1.5226$) due to an increase in the value of τ_i (i.e. an increase in the ion thermal effects). The coexistence of solitons of both polarities is also shown (dotted cyan lines), limited by the occurrence of a double layer (dashed green lines), as predicted by the corresponding soliton existence domains (panels (b) and (d) of Fig. 4.2). This is in agreement with the conclusion of Verheest et al. [41] who pointed out that the occurrence of a soliton with finite amplitude at the acoustic speed is a pre-requisite for nonlinear structures of both polarities to coexist. However, as we will demonstrate in Section 4.3.3, there are special cases in which nonlinear structures of both polarities may coexist without a soliton with finite amplitude at the acoustic speed.

The results presented in panels (c) and (d) of Fig. 4.4 have been obtained considering a higher value of the density ratio, f, namely $f = 0.4$. For this value of the density ratio, nonlinear structures coexist when the ion species are cold (panel (c)) with a negative soliton at the acoustic speed $M_s = 1.1953$. An increase in the value of τ_i to 0.5 (panel (d)) results in the disappearance of the negative solitons at $f = 0.4$, hence the disappearance of the coexistence region. This suggests that the coexistence of nonlinear structures supported by the plasma model under consideration is possible when the electrons are strongly nonthermal and when the ion thermal effects are low or moderate.
The lower panels (e) and (f) of Fig. 4.4 show KdV-like positive solitons obtained for $f = 0.5$, as predicted by the soliton existence domains (Fig. 4.2). We note a significant decrease in the soliton amplitudes due to an increase in the ion thermal effects.

The ion thermal effects on the soliton amplitudes are further explored in Fig. 4.5. This is a continuation of the interpretation of Fig. 4.1. From the right panel of Fig. 4.1, the case for ion temperature $\tau_i = 10^{-4}$ gives the critical density ratio $f_c = 0.333$. In Fig. 4.5 we discuss ion thermal effects (variation of τ_i) on the amplitudes of solitons at the acoustic speed for values of $f < f_c$ and values of $f > f_c$.

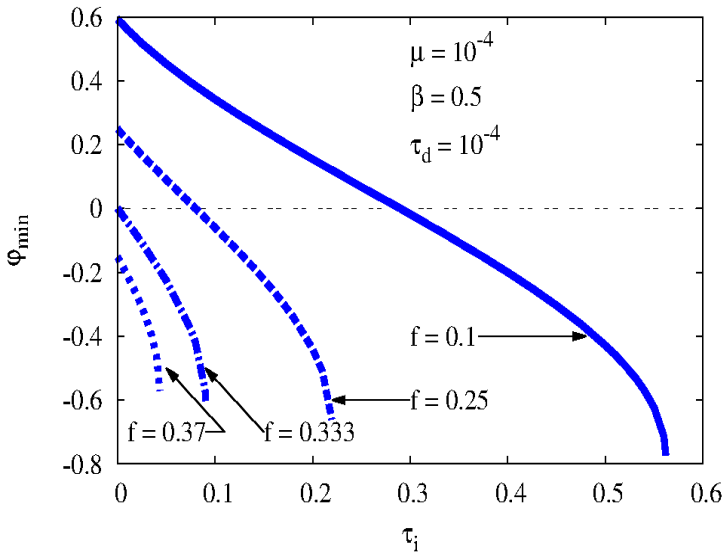

Figure 4.5: (Color online) Soliton amplitude φ_{min} at the acoustic speed versus ion temperature for different values of density ratio f, 0.1 (solid line), 0.25 (dashed line), 0.333 (dot dashed line) and 0.37 (dotted line). φ_{min} vanishes at the critical temperature τ_{ic} and the negative soliton cutoff temperature τ_{in} corresponds to the largest negative value of φ_{min}.

The solid blue line is obtained at $f = 0.1$ smaller than $f_c = 0.333$ when $\tau_i = 10^{-4}$. At these values of plasma parameters, a positive soliton exists at the acoustic speed with amplitude $\varphi_{min} = 0.59$. When the ion temperature increases, this amplitude decreases until it vanishes at a critical ion temperature of $\tau_{ic} \approx 0.28$. For larger values of the ion temperature a negative soliton exists at the acoustic speed and its amplitude increases with increasing ion temperature until at $\tau_{in} \approx 0.56$ a double layer occurs at the acoustic speed, terminating the range of ion temperature supporting nonKdV solitons. When τ_i is larger than τ_{in}, only positive solitons are supported. The same trend is observed for a value of $f = 0.25$ (blue dashed line) larger than 0.1 but smaller than 0.333. However, in this case the vanishing of the positive soliton amplitude and the cutoff of the negative soliton amplitude occur at smaller values of τ_{ic} and τ_{in}, 0.08 and 0.22, respectively. The shift of τ_{ic} and τ_{in} towards lower values continues until at $f_c = 0.333$ (blue dot dashed line)

and $\tau_i = 10^{-4}$ there is no soliton at acoustic speed. For this value, a negative soliton appears at the acoustic speed as τ_i increases beyond 10^{-4} until a cutoff occurs at $\tau_{in} = 0.09$.

For values larger than f_c we have taken the value $f = 0.37$ between $f_c = 0.333$ and $f_n = 0.4$. For $\tau_i = 10^{-4}$, there is a negative soliton with amplitude $|\varphi_{min}| = 0.15$. This amplitude increases with increasing ion temperature until at $\tau_{in} \approx 0.043$, a double layer occurs at the acoustic speed terminating the range of ion temperature supporting nonKdV solitons at $f = 0.37$.

Overall, the amplitudes of positive (negative) solitons at the acoustic speed decrease (increase) with increasing ion temperature. The positive soliton amplitudes vanish at a critical ion temperature τ_{ic} while there is a cutoff of negative soliton amplitudes at τ_{in} at which a double layer occurs at the acoustic speed. For $\tau_i > \tau_{in}$, only positive solitons are supported for the corresponding value of the density ratio f.

4.3.3 Nonlinear structures at the critical density ratio

Having analysed the general features of the nonlinear structures supported by the plasma model under investigation, we now focus on these structures at the critical value of the density ratio, $f_c \approx 0.333$. We present in the left panel of Fig. 4.6 the plots of the pseudopotential obtained for $f_c \approx 0.333$ and Mach numbers ranging from the acoustic speed $M_s = 1.2248$ to the Mach number $M_{dl} = 1.23697$ of the negative double layer. The limiting positive potential associated with the ions is omitted for clarity reasons. This figure clearly shows that the Sagdeev potential at the acoustic speed (blue solid line) does not have the required convexity and does not yield soliton formation. The green dotted line plotted at $M = 1.23 > M_s$ shows the possibility of having solitons of both polarities subjected to the initial conditions. At $M = M_{dl} = 1.23697$ the negative soliton Mach number range is terminated by the occurrence of a double layer (red dashed line). At the

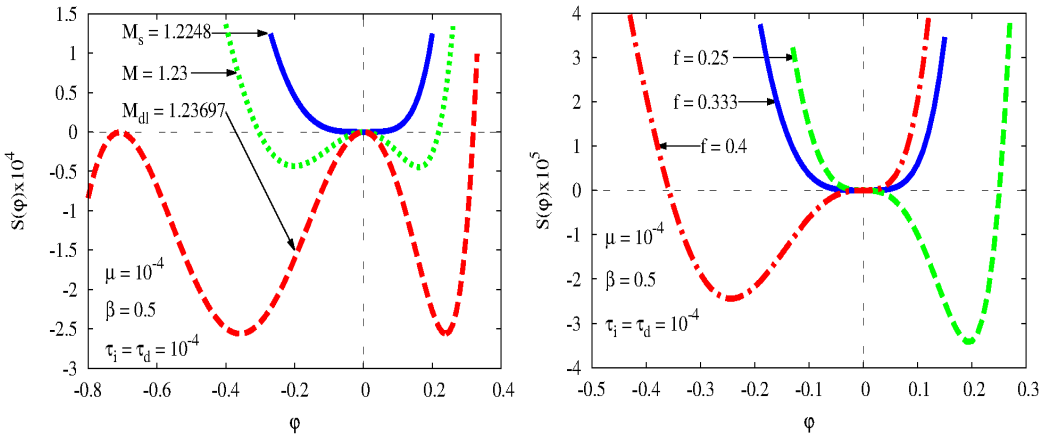

Figure 4.6: (Color online) Left panel: The Sagdeev pseudopotentials at the critical density ratio $f_c = 0.333$ plotted for Mach numbers ranging from the acoustic speed M_s (solid blue line) up to the double layer Mach number M_{dl} (dashed red line). The green doted line is plotted for Mach number $M = 1.23$ larger than M_s and shows the coexistence of solitons of both polarities. The curve corresponding to the limitation associated with the ions is not shown for clarity reasons. Right panel: The Sagdeev pseudopotential at the acoustic speed plotted for different values of the density ratio f: At critical density ratio $f_c = 0.333$ where $M_s = 1.2248$ (solid blue line), at $f = 0.25$ smaller than the critical value f_c with $M_s = 1.265$ (dashed green line) and at $f = 0.4$ larger than the critical value f_c where $M_s = 1.1953$ (dot dashed red line).

critical density ratio f_c, solitons of both polarities coexist, but both are of KdV-like in nature, that is to say, no soliton propagates at the acoustic speed.

For the values of the density ratio, f, that are close to the critical value f_c, positive and negative solitons exist at the acoustic speed. This is shown in the right panel of Fig. 4.6. The dashed line (green colour online) shows a plot of the pseudopotential obtained for $f = 0.25$, a value that is smaller than the critical value f_c. For this value, there is a finite amplitude positive soliton at the acoustic speed with amplitude $\varphi_{min} \approx 0.24$. The figure shows that the soliton amplitude at M_s increases from $\varphi_{min} \approx 0$ at the critical density $f_c \approx 0.333$, to $\varphi_{min} \approx 0.24$ at f= 0.25 and finally to $\varphi_{min} \approx 0.59$ at $f = 0.1$ (not shown in the figure).

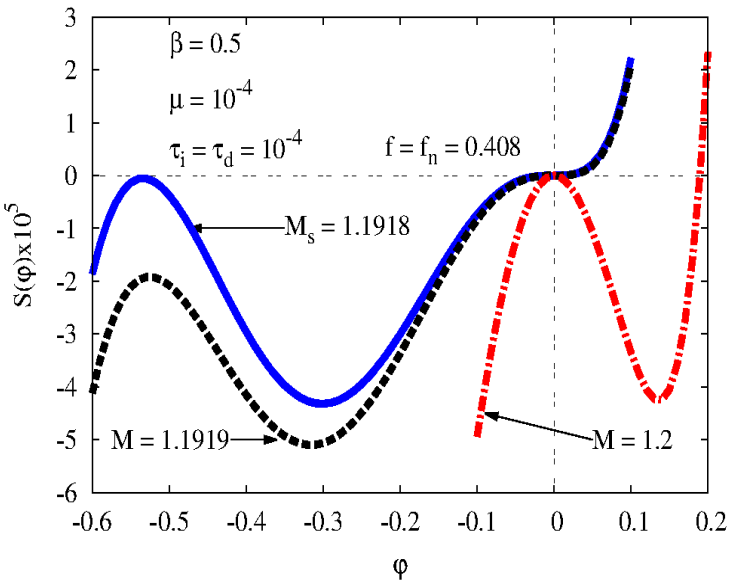

Figure 4.7: (Color online) The Sagdeev pseudopotentials at the negative soliton cutoff density ratio $f_n = 0.408$ when $\tau_i = 10^{-4}$. A double layer occurs at the acoustic speed $M_s = 1.1918$ with amplitude $|\varphi_{dl}| \approx 0.534$ (solid blue line). At a slightly larger Mach number value $M = 1.1919$ (black dashed line) no negative soliton but a positive soliton with small amplitude. The dot dashed red line represents a positive soliton at $M = 1.2 > M_s$.

Considering values of the density ratio, f, greater than f_c we find negative solitons at the acoustic speed, M_s, whose amplitudes increase with increasing f. For $f = 0.34$ the soliton amplitude is $|\varphi_{min}| \approx 0.037$, increasing up to $|\varphi_{min}| \approx 0.358$ for $f = 0.4$. The range of these nonKdV-like negative solitons is ended by the occurrence of a double layer at $f \equiv f_n = 0.408$. This double layer occurs at the acoustic speed, with finite amplitude $|\varphi_{dl}| \approx 0.534$ as is shown in Fig. 4.7 (solid blue line). For Mach number larger than M_s negative solitons do not occur (dashed black line) while positive solitons are supported (dot dashed red line). For $f > f_n$, only positive solitons are supported. This shows that the amplitude of positive solitons at the acoustic speed increases with decreasing density ratio as you move from the critical density ratio (i.e., for $f < f_c$). Similarly, for values of $f > f_c$, amplitudes of negative solitons at

the acoustic speed increase as we increase f. In summary, the soliton amplitude at M_s increases away from the critical density ratio, f_c.

4.4 Summary and conclusion

Using the arbitrary amplitude pseudopotential approach, we have investigated dust ion acoustic solitary waves and double layers in a dusty plasma with adiabatic positive dust, adiabatic positive ion species and Cairns-distributed electrons. While some of our results are qualitatively similar to those found in earlier studies, for example Verheest et al., [41] who studied a plasma composed of two cold positive ion species and Cairns-distributed electrons, there are also some interesting results.

1. This plasma model supports the coexistence of nonlinear structures of both polarities for a range of parameter values, in agreement with earlier findings, [41] for closely related plasma configurations. Results from earlier studies [41] show that the existence of a soliton with finite amplitude at the acoustic speed is a prerequisite for the coexistence of nonlinear structures of both polarities. However, we have found a case in which nonlinear structures of both polarities coexist without a soliton with finite amplitude at the acoustic speed. This occurs at the critical value of the density ratio, at which the third derivative of the Sagdeev pseudopotential changes the sign;.

2. When the electrons are strongly nonthermal with moderate ion temperature, positive nonKdV and negative KdV solitons coexist at low values of density ratio f with switch of polarities at a critical density ratio f_c, at which the third derivative of the Sagdeev pseudopotential vanishes. While positive solitons exist for the whole range of density ratio $0 < f < 1$, negative solitons are cutoff at density ratio f_n at which a double layer occurs at the acoustic speed. Increasing ion thermal effect shifts the coexistence region to lower values of the density ratio, f, leading first to the vanishing of the critical point f_c and therefore to the coexistence of both types of solitons without switch of polarities, and when the ion thermal effects become important, negative solitons disappear and only positive solitons survive.

3. The amplitude of positive solitons at the acoustic speed increases with decreasing density ratio as you move from the critical density ratio (i.e., for $f < f_c$). Similarly, for values of $f > f_c$, amplitudes of negative solitons at the acoustic speed increase as we increase f until a negative soliton cutoff occurs at f_n. Overall the soliton amplitude at M_s increases away from the critical density ratio, f_c.

4. When the ion temperature increases, the amplitude of positive soliton at the acoustic speed decreases at a fixed density ratio until it vanishes at a critical ion temperature τ_{ic}. For larger values of τ_i there are negative solitons at the acoustic speed whose amplitudes increase with increasing ion temperature until at the cutoff of negative solitons, a double layer at the acoustic speed occurs.

Acknowledgements

Financial support from the Swedish International Development Cooperation Agency (SIDA) through the International Science Programme (ISP) to University of Rwanda (UR) through the Rwanda Astrophysics, Space and Climate Science Research Group, Grant No. $ISP/RWA : 01$ is gratefully acknowledged. Part of this work was carried out at Pwani University (Kenya) during a research visit funded by the Royal Academy of Engineering (UK), grant number HEPSSA 1921/3/58, through the Institut d'Enseignement Superieur de Ruhengeri (INES-Ruhengeri, Rwanda). F. Nsengiyumva thanks the Royal Academy of Engineering for this grant and Pwani University for the hospitality.

Data availability

The data that support the findings of this study are available within the article.

4.5 References

[1] P. K. Shukla and A. A. Mamum, *Introduction to Dusty Plasma Physics* (IOP Press, London, 2002).

[2] N. N. Rao, P. K. Shukla and M. Y. Yu, Planet. Space Sci. **3**8, 543 (1990).

[3] P. K. Shukla and V. P. Silin, Phys. Scr. **4**5, 508 (1992).

[4] A. Barkan, R. L. Merlino and N. D'Angelo, Phys. Plasmas **2**, 3563 (1995).

[5] A. Barkan, N. D'Angelo and R. L. Merlino, Planet. Space Sci. **4**4, 239 (1996).

[6] R. L. Merlino, A. Barkan, C. Thompson and N. D'Angelo, Phys. Plasmas **5**, 1607 (1998).

[7] V. E. Fortov, A. P. Nefedov, O. S. Vaulina,*) A. M. Lipaev, V. I. Molotkov, A. A. Samaryan, V. P. Nikitski , A. I. Ivanov, S. F. Savin, A. V. Kalmykov, A. Ya. Solov'ev and P. V. Vinogradov, J. Exp. Theor. Phys. **8**7, 1087 (1998).

[8] M. Horanyi and D. A. Mendis, Astrophys. J. **2**94, 357 (1985).

[9] M. Rosenberg and D. A. Mendis, J. Geophys. Re. **9**7, 14773 (1992).

[10] D. A. Mendis and M. Rosenberg, Annu. Rev. Astron. Astrophys. **3**2, 419 (1994).

[11] R. L. Merlino and J. A. Goree, Physics Today **5**7, 32 (2004).

[12] N.Ya. Kotsarenko, S.V. Koshevaya and A. N. Kotsarenko, Geofísica Internacional **3**7, 71 (1998).

[13] F. Verheest, T. Cattaert and M. A. Hellberg, Phys. Plasmas **1**2, 082308 (2005).

[14] R. L. Merlino, Plasma Physics Applied, 73 (2006).

[15] W. F. El-Taibany and M. Wadati, Phys. Plasmas **1**4, 103703 (2007).

[16] F. Verheest and S. R. Pillay, Phys. Plasmas **1**5, 013703 (2008).

[17] F. Verheest and S. R. Pillay, Nonlin. Processes Geophys. **1**5, 551 (2008).

[18] F. Verheest, M. A. Hellberg and I. Kourakis, Phys. Plasmas **1**5, 112309 (2008).

[19] T. K. Baluku, M. A. Hellberg and R. L. Mace, Phys. Plasmas **1**5, 033701 (2008).

[20] T. K. Baluku and M. A. Hellberg, Phys. Plasmas **1**5, 123705 (2008).

[21] T. K. Baluku, M. A. Hellberg, I. Kourakis and N. S. Saini, Phys. Plasmas **1**7, 053702 (2010).

[22] F. Verheest, M. A. Hellberg and I. Kourakis, Phys. Rev. E **8**7, 043107 (2013).

[23] E. Saberian, A. Esfandyari-Kalejahi and M. Afsari-Ghazi, The Open Plasma Physics Journal **8**, 8 (2015).

[24] A. M. El-Hanbaly, E. K. El-Shewy, M. Sallah and H. F. Darweesh, J. Theor. Appl. Phys. **9**, 167 (2015).

[25] L. L. Yadav, S. V. Singh and R. Bharuthram, J. Plasma Phys. **7**5, 697 (2009).

[26] T. J. Millar, C. Walsh and T. A. Field, Chem. Rev. **1**17, 1765 (2017).

[27] S. K. Maharaj, R. Bharuthram, S. V. Singh and G. S. Lakhina, Phys. Plasmas **2**0, 083705 (2013).

[28] M. Horanyi, Annu. Rev. Astron. Astrophys. **3**4, 383 (1996).

[29] M. Rosenberg D.A. Mendis and D.P. Sheehan, IEEE Trans. Plasma Sci. **2**7, 239 (1999).

[30] R. L. Merlino, J. R. Heinrich, S-H. Kim and J. K. Meyer, Plasma Phys. Control. Fusion **5**4, 124014 (2012).

[31] R. Merlino, Advances in Physics: X **6**, 873859 (2021).

[32] R. K. Shikha, M. M. Orani and A. A. Mamun, Results in Physics **2**7, 104507 (2021).

[33] A. E. Davletov, F. Kurbanov and Ye. S. Mukhametkarimov, Phys. Plasmas **2**5, 120701 (2018).

[34] S. I. Kopnin, I. N. Kosarev, S. I. Popel and M. Y. Yu, Planetary and space Science **5**2, 1187 (2004).

[35] V. E. Fortov, A. P. Nefedov, O. S. Vaulina, O. F. Petrov, I. E. Dranzhevski, A. M. Lipaev and Yu P. Semenov, New J. Phys. **5**, 102 (2003).

[36] M. N. Fomenkova and D. A. Mendis, Astrophys. Space Sci **1**89, 327 (1992).

[37] R. Bharuthram and P. K. Shukla, Planet. Space Sci. **4**0, 973 (1992). .

[38] F. Sayed and A. A. Mamum, Pramana-J. Phys. **7**0, 527 (2008).

[39] M. A. Hellberg, T. K. Baluku and F. Verheest, AIP Conference Proceedings **1**306, 50 (2010).

[40] R. Z. Sagdeev, Rev. Plasma Phys. **4**, 23 (1966).

[41] F. Verheest, M. A. Hellberg and T. K. Baluku, Phys. Plasmas **1**9, 032305 (2012).

[42] R.A. Cairns, A. A. Mamum, R. Bingham, R. Boström, R. O. Dendy, C. M. C. Nairn and P. K. Shukla, Geophys. Res. Lett. **2**2, 2709 (1995).

[43] F. Verheest and M. A. Hellberg, J. Plasmas Phys. **7**6, 277 (2010).

[44] S. Baboolal, R. Bharuthram and M. A. Hellberg, J. Plasma Phys.Phys. **4**4, 1 (1990).

[45] F. Verheest and M. A. Hellberg, Phys. Plasmas **1**7, 102312 (2010).

Chapter 5

Summary and Conclusions

5.1 Summary

The PhD thesis aimed to investigate the existence and propagation of linear and nonlinear ion acoustic waves in some multispecies plasmas, *viz*. in a negative ion plasma (*Chap*. 2 & 3), and in a dusty plasma (*Chap*. 4).

We have first considered a negative ion plasma, composed of adiabatic positive and adiabatic negative ions and nonthermal electrons distributed according to kappa distribution. Also called the generalised Lorentzian distribution, the kappa distributiopn is characterised by the spectral index κ that shows the departure from the Maxwellian distribution. Its values range from $\kappa = 3/2$ up to very large (∞). Very large values indicate an almost Maxwellian distribution. As the spectral index decreases, the amount of nonthermal particles in the distribution increases and values larger but close to $3/2$ indicate a strongly non Maxwellian distribution. Negative ion plasmas are numerous in space, astrophysical and laboratory conditions. Nonthermal distributions of particles have also been identified in many natural environments.

The plasma was treated using the multifluid approach, retaining the ion inertia while electrons contribute via their thermal motion. It is well known that a plasma composed of electrons and two ion species with at least one of them having a finite temperature supports two ion acoustic modes, the fast and the slow modes with the ordering

$$v_{tc} < v_{slow} < v_{th} < v_{fast} < v_{te} \tag{5.1}$$

where v_{tc}, v_{th} and v_{te} are the thermal speeds of cooler ions, hotter ions and electrons respectively while v_{fast} and v_{slow} are the phase speeds of the fast and the slow modes, respectively. We have investigated in details both the fast and the slow modes.

In the linear approximation, the dispersion relation has been derived. This relation determines the possible plane wave phase speed as a function of

plasma parameters. However linearisation does not account for nonlinear behaviour of the plasma which is nonetheless an important aspect. Details of the derivation of the linear dispersion relation are given in appendix A.

Using the reductive perturbation method, we have also derived the KdV equation and obtained the nonlinear and dispersion coefficients as functions of the plasma parameters. The polarity of the KdV solitons is determined by the sign of the nonlinear coefficient, while the dispersion coefficient was found to remain positive for all values of the plasma parameters.

Another important method in the study of nonlinear waves is the Sagdeev pseudopotential method. Using this method, one can investigate the existence and propagation of small and large amplitude nonlinear structures. Furthermore, this method offers the possibility to determine the possible range of phase speeds supporting the propagation of those nonlinear structures. The lower limit of this range coincides with the linear phase speed determined from the linear method or from the reductive perturbation method. The upper limit of the phase speed range arises from the condition that density of inertial species remains real valued function. This condition is equivalent to the requirement that the inertial species reaches its sonic point, at which the flow is choked.

The fast mode is known to support the propagation of only positive solitons when the negative ion density is low, the propagation of negative solitons when the negative ion density is high, and it supports both polarity solitons in what is known as the coexistence region for intermediate values of negative ion density. After confirming this result for cold ions, we have investigated the ion thermal and electron superthermal effects on these soliton existence domains. In particular we have found that when ion thermal effects are important, a negative ion plasma with strongly non Maxwellian electrons supports only negative solitons.

We have based the slow mode on the results obtained by Ichiki et al., *viz*. that

the slow mode can be experimentally observed in a negative ion plasma, if the negative ions are lighter than positive ions. We have found that the slow mode in a negative ion plasma supports three types of nonlinear structures. Standard solitons are supported from low to high values of negative ion density. They are limited by the occurrence of positive ion sonic point for low to intermediate negative ion density, and by double layer for high values of negative ion density. Double layers do not occur only as the limiting factor to the standard soliton amplitude, they appear also as the lower limit to a set of supersolitons for a narrow range of negative ion density. Supersolitons are limited on the lower side either by double layer or the coalescence of two consecutive extrema, and on the upper side by the occurrence of positive ion sonic point or by the coalescence of two consecutive extrema. We have carried out a comprehensive analysis of the effects of ion temperature and electron superthermality on the existence and propagation of these nonlinear structures.

Another multispecies plasma model that has been thoroughly investigated for the existence and propagation of nonlinear structures is a dusty plasma with positively charged cold dust, adiabatic positive ion species and Cairns distributed electrons. Although in many situations the dust in a dusty plasma is negatively charged, It is well known that it can be positively charged by photoionisation mechanism. This plasma configuration supports the propagation and the coexistence of positive and negative dust ion acoustic solitons when electrons are strongly non thermal. Positive solitons are limited by the occurrence of positive ion sonic point while negative solitons are limited by the occurrence of double layer. Coexistence exists at low to intermediate values of dust-to-positive ion equilibrium density ratio f. Non KdV positive and KdV negative solitons coexist up to a critical dust-to-positive ion equilibrium density ratio f_c, at which there is switch of polarity with KdV positive and non KdV negative soliton coexistence for $f > f_C$. There is a density ration f_n such that $f_c < f_n$ at which the coexistence vanishes and only positive solitons are supported. In many situations, the coexistence of opposite polarity solitons is accompanied by the existence of a solitary wave at the acoustic

speed. We have shown that at the critical density ratio f_c, solitons of both polarities coexist although there is no soliton at the acoustic speed. The effects of the dust-to-positive ion density ratio f and ion temperature on the soliton existence domain, amplitude and width have been investigated and reported.

5.2 Future work

Negative ion plasmas are very common in space, laboratory and industrial conditions. The investigation of the wave propagation in theses plasmas is thus vital to human technology to be used in space and on Earth. We have investigated in detail the propagation of the fast and slow ion acoustic electrostatic waves in an unmagnetized negative ion plasma with kappa distributed electrons. However most of space plasmas are magnetised. A further development of our study can therefore focus on the propagation of electromagnetic waves in a negative ion plasmas with superthermal electrons. Furthermore, different other mechanisms like collisions between plasma particles and fluid viscosity leading to the energy dissipation could be considered. Consideration of these and other different aspects can improve our results and bring more light on the nonlinear wave propagation in a negative ion plasma. Regarding the dusty plasmas, our work can be extended by considering the low frequency dust acoustic mode without and in the presence of a magnetic field. Inclusion of the charging currents would also bring new effects that are not studied up to date.

Appendix A

Linear approximation

A.1 Linear approximation

The fluid equations that describe the behaviour of the plasma are nonlinear and their analytical solutions are not easy if not impossible to find. However, information on the plasma behaviour can be found by linearising those nonlinear equation, in which case an analytical solution can be found, or by considering small amplitude waves in which case the system can be reduced to a nonlinear partial differential equation with an exact analytical solution. In appendices *A*, *B* and *C*, we discuss successively the linearised fluid equation, then the small amplitude approximation resulting in KdV equation, and small amplitude approximation from the Sagdeev pseudopotential point of view. For this we consider the fast mode in a negative ion plasma considered in chapter 2. The plasma model consists of a one dimensional (x direction) unmagnetized, collisionless negative ion plasma comprising singly charged negative ions, positive ions and electrons distributed according to kappa distribution [1]. The plasma is treated in the fluid approach, in which it is made of three interpenetrating fluids, a fluid of electrons, a fluid of negative ions and a fluid of positive ions.

We neglect the electron inertial effects and their contribution comes from their thermal motion. Therefore the density of electrons in a electrostatic potential Φ is given by

$$N_e = n_{e0}\left[1 - \frac{2e\Phi}{(2\kappa - 3)T_e}\right]^{-(\kappa - 1/2)}, \tag{A.1}$$

where n_{e0} is the electron equilibrium density, T_e is the electron temperature, expressed in units of energy, Φ is the electrostatic potential, and e is the elementary charge. For the ion species, we retain their inertia and the dynamics of the model is governed by the one dimensional fluid equations of continuity and momentum for both ion species,

$$\frac{\partial N_n}{\partial t} + \frac{\partial\left(N_n U_n\right)}{\partial x} = 0, \tag{A.2}$$

$$N_n m_n\left[\frac{\partial U_n}{\partial t} + U_n\frac{\partial U_n}{\partial x}\right] = -zeN_n\frac{\partial \Phi}{\partial x} - \frac{\partial p_n}{\partial x}, \tag{A.3}$$

$$\frac{\partial N_p}{\partial t} + \frac{\partial \left(N_p U_p\right)}{\partial x} = 0, \tag{A.4}$$

$$N_p m_p \left[\frac{\partial U_p}{\partial t} + U_p \frac{\partial U_p}{\partial x}\right] = -eN_p \frac{\partial \Phi}{\partial x} - \frac{\partial p_p}{\partial x}, \tag{A.5}$$

and the electron and ion densities are coupled by Poisson's equation

$$\varepsilon_0 \frac{\partial^2 \Phi}{\partial x^2} = eN_e - ezN_n - eN_p. \tag{A.6}$$

In these equations, x and t are spatial and time coordinates respectively, $U_n, U_p, T_n, T_p,\ N_n, N_p, n_{n0}, n_{p0}$ are the speed, temperature, density and equilibrium density of negative and positive ion species, respectively, and p_j (j = negative, positive) is the j^{th} ion species thermal pressure. The parameter z introduced in these equations can have values ± 1. When $z = -1$, equations $(A.2)$ to $(A.6)$ model a negative ion plasma, which is the subject of study in *chapters* 2 and 3. When $z = +1$, equations $(A.2)$ to $(A.6)$ model a two positive ion plasma as studied by Nsengiyumva et al. [2].

The system of equations $(A.2)$ to $(A.6)$ is closed by an equation of state, relating the j^{th} ion species thermal pressure to the corresponding ion species density. We have assumed, in Eq.$(A.3)$ and $(A.5)$, negative and positive ions to be adiabatic with polytropic index $\gamma = 3$, and the relation between the fluid thermal pressure of the j^{th} ion species and its density to be of the form

$$p_j \propto N_j^3. \tag{A.7}$$

With this relation, the compression of the j^{th} plasma component in Eqs. $(A.3)$ and $(A.5)$ has the form [3]

$$\frac{\nabla . p_j}{p_j} = \gamma \frac{\nabla . N_j}{N_j}, \tag{A.8}$$

where the unperturbed pressure is defined as $p_{j0} = n_{j0} T_j$.

Equations $(A.2)$ to $(A.6)$ constitute a system of nonlinear partial differential equations. A first insight in the properties of its solution can be obtained by studying the behaviour of small perturbations in the linear approximation. In

this approximation, we first assume that far from the perturbation, the plasma is neutral and in equilibrium. Then near the perturbation, plasma variables can be written in the linear approximation as

$$\begin{aligned} N_j &= n_{j0} + N_{j1}, \\ U_j &= U_{j1}, \\ E &= E_1, \\ \Phi &= \Phi_1, \end{aligned} \tag{A.9}$$

where N_{j1}, U_{j1}, E_1 and Φ_1 are small perturbations of density, velocity, electric field and electrostatic potential, respectively. After replacing $(A.9)$ into $(A.2)$ to $(A.6)$ and restricting to the first order of the perturbation, the system takes the form

$$\frac{\partial N_{n1}}{\partial t} + n_{n0}\frac{\partial U_{n1}}{\partial x} = 0, \tag{A.10}$$

$$N_{n0}m_n\frac{\partial U_{n1}}{\partial t} = -zen_{n0}\frac{\partial \Phi_1}{\partial x} - T_n\frac{\partial N_{n1}}{\partial x}, \tag{A.11}$$

$$\frac{\partial N_{p1}}{\partial t} + N_{p0}\frac{\partial U_{p1}}{\partial x} = 0, \tag{A.12}$$

$$N_{p0}m_p\frac{\partial U_{p1}}{\partial t} = -eN_{p0}\frac{\partial \Phi_1}{\partial x} - T_p\frac{\partial N_{p1}}{\partial x}, \tag{A.13}$$

$$\varepsilon_0\frac{\partial^2 \Phi_1}{\partial x^2} = e(n_{e0} + N_{e1}) - ez(n_{n0} + N_{n1}) - e(n_{p0} + N_{p1}). \tag{A.14}$$

We also assume that these small perturbations are in the form of the plane waves,

$$F_{j1} = \hat{F}_{j1}e^{i(kx-\omega t)}, \tag{A.15}$$

where F_{j1} is any of the perturbed quantities, $\hat{F}_{j1}$ is the corresponding amplitude, k is the wave vector, ω is the wave angular frequency and i is the imaginary unit such that $i^2 = -1$. The plane wave assumption has the advantage of converting the system of differential equations $(A.10)$ to $(A.14)$ into a system of algebraic equations by the replacements $\partial F_{j1}/\partial t = -i\omega F_{j1}$ and $\partial F_{j1}/\partial x = ikF_{j1}$. The negative ion continuity equation $(A.10)$ thus becomes

$$-i\omega\hat{N}_{n1} + ikn_{n0}\hat{U}_{n1} = 0, \tag{A.16}$$

from which the amplitude of the flow velocity is

$$\hat{U}_{n1} = \frac{\omega}{k n_{n0}} \hat{N}_{n1}. \tag{A.17}$$

Replacement of the plane wave ansatz in the negative ion momentum equation $(A.11)$ yields the equation

$$-i\omega\hat{U}_{n1} = -\frac{ze}{m_n} ik\hat{\Phi}_1 - \frac{T_n}{n_{n0} m_n} ik\hat{N}_{n1}, \tag{A.18}$$

Solving for $\hat{N}_{n1}$ in $(A.18)$ with $\hat{U}_{n1}$ given by $(A.17)$ we get

$$\hat{N}_{n1} = \frac{z e n_{n0}}{m_n} \frac{\hat{\Phi}_1}{V^2 - v_{tn}^2}, \tag{A.19}$$

where $v_{tn} = T_n/m_n$ is the negative ion thermal speed and $V = \omega/k$ is the wave phase speed. Similarly from equations $(A.4)$ and $(A.5)$, we get the amplitude of the positive ion density oscillations as a function of the amplitude of the electrostatic potential as

$$\hat{N}_{p1} = \frac{e n_{p0}}{m_p} \frac{\hat{\Phi}_1}{V^2 - v_{tp}^2}, \tag{A.20}$$

where $v_{tp} = T_p/m_p$ is the positive ion thermal speed. To solve the Poisson's equation $(A.6)$, we first expand the electron density $(A.1)$ in powers of the electrostatic potential up to the first order:

$$\hat{N}_e = n_{e0} \left[1 + \frac{2\kappa - 1}{2\kappa - 3} \frac{e}{T_e} \hat{\Phi}_1 \right]. \tag{A.21}$$

Now replacing $(A.19), (A.20)$ and $(A.21)$ in Eq. $(A.6)$, we arrive at the following expression:

$$\begin{aligned} &\varepsilon_0 m_n m_p \left(k^2 + \tfrac{2\kappa-1}{2\kappa-3} \tfrac{1}{\lambda_{De}^2} \right) \tfrac{\omega^4}{k^4} - \tfrac{\omega^2}{k^2} \left[e^2 m_n n_{p0} \right. \\ &\left. + z^2 e^2 m_p n_{n0} + \varepsilon_0 \left(k^2 + \tfrac{2\kappa-1}{2\kappa-3} \tfrac{1}{\lambda_{De}^2} \right) (m_n T_p + m_p T_n) \right] \\ &+ \varepsilon_0 \left[k^2 + \tfrac{2\kappa-1}{2\kappa-3} \tfrac{1}{\lambda_{De}^2} \right] T_n T_p + e^2 T_n n_{p0} + z^2 e^2 T_p n_{n0} \quad = 0, \end{aligned} \tag{A.22}$$

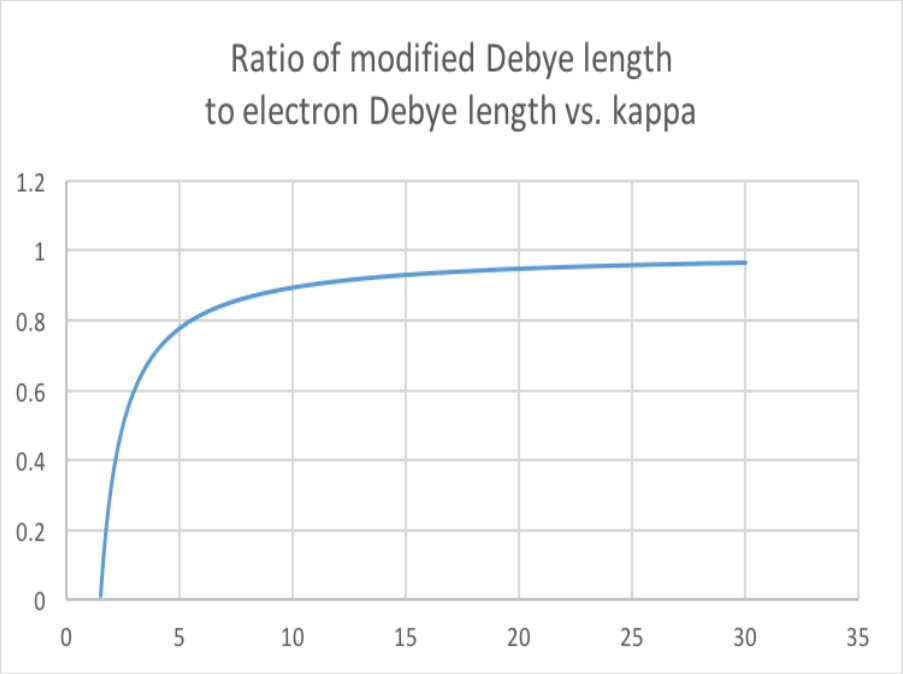

Figure A.1: The ratio $\lambda_{De,\kappa}/\lambda_{De}$ (vertical axis) versus κ (horizontal axis). As the electron superthermality increases, *i.e.* as κ decreases, the modified electron Debye length approaches the electron Debye length.

where $\lambda_{De} = \left(\varepsilon_0 T_e / e^2 n_{e0}\right)^{1/2}$ is the electron Debye length, and

$$\lambda_{De,\kappa} = \frac{2\kappa - 3}{2\kappa - 1}\lambda_{De} \tag{A.23}$$

is the electron Debye length, modified by the electron superthermality. It shows that the superthermal behaviour of electrons increases the plasma shielding by reducing the electron Debye length. Fig. $A.1$ shows the ratio of the modified Debye length to the electron Debye length as a function of the spectral index κ. It shows that when $\kappa \to \infty$, $\lambda_{De,\kappa} \to \lambda_{De}$.

Equation $(A.22)$ is the linear dispersion relation for low-frequency ion-acoustic wave, propagating on a background of uniformly distributed electrons. For $\kappa \to \infty$ (Maxwell distributed electrons) and $z = 1$, it is the same as equation (3.6) of Nsengiyumva et al. [2]. In the superhot approximation, the

electron temperature is much larger than the ion temperatures $T_e \gg T_j$ and we can neglect the ion temperatures $T_n = T_p = 0$. In this case the ion acoustic phase speed is found as

$$\frac{\omega^2}{k^2} = \frac{T_e \left[\frac{n_{p0}}{n_{e0}}\frac{1}{m_p} + \frac{n_{n0}}{n_{e0}}\frac{z^2}{m_n}\right]}{\frac{2\kappa-1}{2\kappa-3} + k^2\lambda_{De}^2}. \tag{A.24}$$

Eq. $(A.24)$ shows that the ion acoustic speed decreases when the electron superthermality increases. The modification of the Debye length by the electron superthermality has thus a direct effect on the propagation of the ion acoustic waves. We note here that in the absence of the electron superthermality $(\kappa \to \infty)$, the decrease of the Debye length leads to an increase of the wave phase speed. In the long wavelength limit, $k\lambda_{De,\kappa} \ll 1$ and the phase wave speed equals the group wave speed

$$\frac{\omega}{k} = \frac{\partial\omega}{\partial k} = \sqrt{\frac{T_e \left[\frac{n_{p0}}{n_{e0}}\frac{1}{m_p} + \frac{n_{n0}}{n_{e0}}\frac{z^2}{m_n}\right]}{\frac{2\kappa-1}{2\kappa-3}}}. \tag{A.25}$$

On the other hand, in the limit of large wave vectors, $k\lambda_{De,\kappa} \gg 1$, and only standing wave oscillations are possible with frequencies

$$\omega_{pi} = \sqrt{\omega_p^2 + z^2\omega_n^2}, \tag{A.26}$$

where $\omega_p^2 = e^2 n_{po}/\varepsilon_0 m_p$ and $\omega_n^2 = z^2 e^2 n_{no}/\varepsilon_0 m_n$ are the positive and negative ion plasma oscillation frequency, respectively. This frequency, which is different from the electron plasma frequency determines the simultaneous oscillations of negative and positive ions in the negative ion plasma.

A.2 References

[1] V. M. Vasyliunas, J. Geophys. Res. **7**3, 2839 (1968).

[2] F. Nsengiyumva, M. A. Hellberg, and R. L. Mace, Phys. Plasmas **2**2, 092304 (2015).

[3] E. Saberian, A. Esfandyari-Kalejahi, and M. Afsari-Ghazi, The Open Plasma Physics Journal **8**, 8 (2015).

Appendix B

Small amplitude approximation: KdV equation

B.1 Derivation of KdV equation

B.1.1 Normalisation of the basic equations

The linear theory ignores the non-linear terms in the linearised equations and therefore does not describe the plasma behaviour arising due to non-linearity. A first step in accounting for non-linearity in fluid equations is to use reductive perturbation theory to study the small amplitude nonlinear structure solution of the model equations. This is better done by considering dimensionless variables. Accordingly Eqs. $(A.2)$-$(A.6)$ have been normalised as follows: The space coordinate x has been normalised by the electron Debye length $\lambda_{De} = (\varepsilon_0 T_e/n_{e0}e^2)^{\frac{1}{2}}$; the time has been normalised by the inverse of the effective ion plasma frequency $\omega_{pi} = (n_{e0}e^2\beta/\varepsilon_0 m_p)^{\frac{1}{2}}$, where $\beta = \frac{\mu+\alpha z^2}{\mu(1+\alpha z)}$; the velocities have been normalised by the ion sound velocity in the mixture $c_s \equiv \omega_{pi}\lambda_{De} = (T_e\beta/m_p)^{\frac{1}{2}}$; the electrostatic potential has been normalised by the thermal potential T_e/e, the densities N_n, N_p, and N_e have been normalised by their respective equilibrium densities n_{n0}, n_{p0}, and n_{e0}. We have also introduced the dimensionless variables: $\mu = m_n/m_p$ is the the negative ion to positive ion mass ratio, $\sigma_j = T_j/T_e$ is the ion-to-electron temperature ratio $(j = n, p)$, and the variable $\alpha = n_{n0}/n_{p0}$ is the negative to positive ion equilibrium density ratio. For a negative ion plasma, $0 < \alpha < 1$. The relation between the variables and their dimensionless counterparts are therefore as following:

$$\begin{cases} x &= \lambda_{D_e} x', \\ t &= \frac{t'}{\omega_p}, \\ U_j &= c_s u_j, \\ \Phi &= \frac{T_e}{e}\varphi, \\ N_j &= n_{j0} n_j. \end{cases} \tag{B.1}$$

Space and time derivatives become

$$\begin{array}{lll} \frac{\partial}{\partial x} &= \frac{\partial}{\partial x'}\frac{\partial x'}{\partial x} &= \frac{1}{\lambda_{D_e}}\frac{\partial}{\partial x'}, \\ \frac{\partial}{\partial t} &= \frac{\partial}{\partial t'}\frac{\partial t}{\partial x} &= \omega_p \frac{\partial}{\partial t'}. \end{array} \tag{B.2}$$

With this normalisation and dropping the primes on the space and time coordinates, the fluid equations take the form

$$\frac{\partial n_n}{\partial t} + \frac{\partial \left(n_n u_n\right)}{\partial x} = 0, \tag{B.3}$$

$$\frac{\partial u_n}{\partial t} + u_n \frac{\partial u_n}{\partial x} = -\frac{z}{\mu\beta}\frac{\partial \varphi}{\partial x} - \frac{3\sigma_n}{\mu\beta} n_n \frac{\partial n_n}{\partial x}, \tag{B.4}$$

$$\frac{\partial n_p}{\partial t} + \frac{\partial \left(n_p u_p\right)}{\partial x} = 0, \tag{B.5}$$

$$\frac{\partial u_p}{\partial t} + u_p \frac{\partial u_p}{\partial x} = -\frac{1}{\beta}\frac{\partial \varphi}{\partial x} - \frac{3\sigma_p}{\beta} n_p \frac{\partial n_p}{\partial x}, \tag{B.6}$$

and the dimensionless Poisson's equation

$$\frac{\partial^2 \varphi}{\partial x^2} = n_e - \frac{\alpha z}{1+\alpha z} n_n - \frac{1}{1+\alpha z} n_p, \tag{B.7}$$

where n_e is the dimensionless density of kappa-distributed electrons [1]

$$n_e = \left[1 - \frac{2\varphi}{2\kappa - 3}\right]^{-\kappa+\frac{1}{2}}. \tag{B.8}$$

In Eqs. $(B.4)$ and $(B.6)$, we have used the adiabatic pressure density relation with polytropic index $\gamma = 3$, that is,

$$p_j n_j^{-3} = p_{j0} n_{j0}^{-3} = constant, \tag{B.9}$$

where the unperturbed pressure of the j^{th} adiabatic species is defined as [2] $p_{j0} = n_{j0} T_j$ and the normalised boundary conditions for localised structures are

$$\begin{cases} u_n(\infty) = u_{n0} = 0; & u_p(\infty) = u_{p0} = 0; \\ n_n(\infty) = n_{n0} = 1; & n_p(\infty) = n_{p0} = 1; \\ \varphi(\infty) = \frac{d\varphi}{dx}(\infty) = \phi_0 = 0. \end{cases} \tag{B.10}$$

B.1.2 Reductive perturbation

To solve the system of equations $(B.3)$ to $(B.7)$, we follow Washimi and Taniuti [3] and introduce the stretched coordinates:

$$\begin{cases} \xi &= \varepsilon^{\frac{1}{2}}(x - M_s t), \\ \tau &= \varepsilon^{\frac{3}{2}} t, \end{cases} \tag{B.11}$$

where M_s is the sound speed in the plasma, normalised by the positive ion sound speed $c_s = (T_e\beta/m_p)^{\frac{1}{2}}$, ε is a small expansion parameter proportional to the amplitude of the perturbation. The derivative relative to these new coordinates are obtained using the chain rule:

$$\begin{aligned} \frac{\partial}{\partial x} &= +\varepsilon^{1/2}\frac{\partial}{\partial \xi}, \\ \frac{\partial}{\partial t} &= -\varepsilon^{1/2} M_s \frac{\partial}{\partial \xi} + \varepsilon^{3/2}\frac{\partial}{\partial \tau}. \end{aligned} \tag{B.12}$$

In the reductive perturbation method, the variables in Eq. $(B.3)$ to $(B.7)$ are expressed as power series of ε as

$$\begin{aligned} n_n &= 1 + \varepsilon n_{n1} + \varepsilon^2 n_{n2} + \varepsilon^3 n_{n3} + \cdots, \\ n_p &= 1 + \varepsilon n_{p1} + \varepsilon^2 n_{p2} + \varepsilon^3 n_{p3} + \cdots, \\ u_n &= \varepsilon u_{n1} + \varepsilon^2 u_{n2} + \varepsilon^3 u_{n3} + \cdots, \\ u_p &= \varepsilon u_{p1} + \varepsilon^2 u_{p2} + \varepsilon^3 u_{p3} + \cdots, \\ \varphi &= \varepsilon \varphi_1 + \varepsilon^2 \varphi_2 + \varepsilon^3 \varphi_3 + \cdots. \end{aligned} \tag{B.13}$$

and the electron density n_e, found after expanding Eq. $(B.8)$ in Taylor series up to the third order of perturbation has the form

$$n_e = 1 + \frac{2\kappa - 1}{2\kappa - 3}\varphi + \frac{(2\kappa-1)(2\kappa+1)}{2(2\kappa-3)^2}\varphi^2 + \frac{(2\kappa-1)(2\kappa+1)(2\kappa+3)}{6(2\kappa-3)^3}\varphi^3. \tag{B.14}$$

We now introduce the stretched coordinates $(B.11)$ and derivatives relative to stretched coordinates $(B.12)$ as well the the expansions $(B.13)$ and $(B.14)$ in normalised equations $(B.3)$ to $(B.7)$. After collecting the coefficients under the same power of the small parameter ε we get the

next system of equations:

The negative ion continuity equation

$$\begin{aligned}
&\varepsilon^{3/2}\left[-M_s\frac{\partial n_{n1}}{\partial\xi}+\frac{\partial u_{n1}}{\partial\xi}\right]\\
&+\varepsilon^{5/2}\left[\frac{\partial n_{n1}}{\partial\tau}+\frac{\partial n_{n1}u_{n1}}{\partial\xi}\ -M_s\frac{\partial n_{n2}}{\partial\xi}+\frac{\partial u_{n2}}{\partial\xi}\right]\\
&+\varepsilon^{7/2}\left[\frac{\partial n_{n1}u_{n2}}{\partial\xi}+\frac{\partial n_{n2}u_{n1}}{\partial\xi}+\frac{\partial n_{n2}}{\partial\xi}\ -M_s\frac{\partial n_{n3}}{\partial\xi}+\frac{\partial u_{n3}}{\partial\xi}\right]+\cdots\ =0.
\end{aligned}\tag{B.15}$$

The negative ion momentum equation

$$\begin{aligned}
&\varepsilon^{3/2}\left[-M_s\frac{\partial u_{n1}}{\partial\xi}+\frac{z}{\mu\beta}\frac{\partial\varphi_1}{\partial\xi}\ +\frac{3\sigma_n}{\mu\beta}\frac{\partial n_{n1}}{\partial\xi}\right]+\varepsilon^{5/2}\left[\frac{\partial u_{n1}}{\partial\tau}\right.\\
&\left.+u_{n1}\frac{\partial u_{n1}}{\partial\xi}\ +\frac{3\sigma_n}{\mu\beta}n_{n1}\frac{\partial n_{n1}}{\partial\xi}\ -M_s\frac{\partial u_{n2}}{\partial\xi}\ +\frac{z}{\mu\beta}\frac{\partial\varphi_2}{\partial\xi}+\frac{3\sigma_n}{\mu\beta}\frac{\partial n_{n2}}{\partial\xi}\right]\\
&+\varepsilon^{7/2}\left[\frac{3\sigma_n}{\mu\beta}n_{n1}\frac{\partial n_{n2}}{\partial\xi}\ +\frac{3\sigma_n}{\mu\beta}n_{n2}\frac{\partial n_{n1}}{\partial\xi}\ +u_{n1}\frac{\partial u_{n2}}{\partial\xi}\right.\\
&\left.+u_{n2}\frac{\partial u_{n1}}{\partial\xi}+\frac{\partial u_{n2}}{\partial\tau}\ -M_s\frac{\partial u_{n3}}{\partial\xi}+\frac{z}{\mu\beta}\frac{\partial\varphi_3}{\partial\xi}\ +\frac{3\sigma_n}{\mu\beta}\frac{\partial n_{n3}}{\partial\xi}\right]+\cdots\ \ =0.
\end{aligned}\tag{B.16}$$

The positive ion continuity equation

$$\begin{aligned}
&\varepsilon^{3/2}\left[-M_s\frac{\partial n_{p1}}{\partial\xi}+\frac{\partial u_{p1}}{\partial\xi}\right]\\
&+\varepsilon^{5/2}\left[\frac{\partial n_{p1}}{\partial\tau}+\frac{\partial n_{p1}u_{p1}}{\partial\xi}\ -M_s\frac{\partial n_{p2}}{\partial\xi}+\frac{\partial u_{p2}}{\partial\xi}\right]\\
&+\varepsilon^{7/2}\left[\frac{\partial n_{p1}u_{p2}}{\partial\xi}+\frac{\partial n_{p2}u_{p1}}{\partial\xi}+\frac{\partial n_{p2}}{\partial\xi}\ -M_s\frac{\partial n_{p3}}{\partial\xi}+\frac{\partial u_{p3}}{\partial\xi}\right]+\cdots\ =0.
\end{aligned}\tag{B.17}$$

The positive ion momentum equation

$$\begin{aligned}
&\varepsilon^{3/2}\left[-M_s\frac{\partial u_{p1}}{\partial\xi}+\frac{1}{\beta}\frac{\partial\varphi_1}{\partial\xi}+\frac{3\sigma_p}{\mu\beta}\frac{\partial n_{p1}}{\partial\xi}\right]+\varepsilon^{5/2}\left[\frac{\partial u_{p1}}{\partial\tau}\right.\\
&\left.+u_{p1}\frac{\partial u_{p1}}{\partial\xi}+\frac{3\sigma_p}{\mu\beta}n_{p1}\frac{\partial n_{p1}}{\partial\xi}-M_s\frac{\partial u_{p2}}{\partial\xi}+\frac{1}{\beta}\frac{\partial\varphi_2}{\partial\xi}+\frac{3\sigma_p}{\mu\beta}\frac{\partial n_{p2}}{\partial\xi}\right]\\
&+\varepsilon^{7/2}\left[\frac{3\sigma_n}{\mu\beta}n_{n1}\frac{\partial n_{n2}}{\partial\xi}+\frac{3\sigma_p}{\mu\beta}n_{p2}\frac{\partial n_{p1}}{\partial\xi}+u_{p1}\frac{\partial u_{p2}}{\partial\xi}\right.\\
&\left.+u_{p2}\frac{\partial u_{p1}}{\partial\xi}+\frac{\partial u_{p2}}{\partial\tau}-M_s\frac{\partial u_{p3}}{\partial\xi}+\frac{1}{\beta}\frac{\partial\varphi_3}{\partial\xi}+\frac{3\sigma_p}{\mu\beta}\frac{\partial n_{p3}}{\partial\xi}\right]+\cdots \qquad =0.
\end{aligned} \tag{B.18}$$

The Poisson's equation

$$\begin{aligned}
&\varepsilon^0\left[1-\frac{\alpha_z}{1+\alpha_z}-\frac{1}{1+\alpha_z}\right]+\varepsilon^1\left[\frac{2\kappa-1}{2\kappa-3}\varphi_1-\frac{\alpha_z}{1+\alpha_z}n_{n1}-\frac{1}{1+\alpha_z}n_{p1}\right]\\
&+\varepsilon^2\left[\frac{2\kappa-1}{2\kappa-3}\varphi_2+\frac{(2\kappa-1)(2\kappa+1)}{2(2\kappa-3)^2}\varphi_1^2-\frac{\alpha_z}{1+\alpha_z}n_{n2}-\frac{1}{1+\alpha_z}n_{p2}-\frac{\partial^2\varphi_1}{\partial\xi^2}\right]\\
&+\varepsilon^3\left[\frac{2\kappa-1}{2\kappa-3}\varphi_3+\frac{(2\kappa-1)(2\kappa+1)}{(2\kappa-3)^2}\varphi_1\varphi_2+\frac{(2\kappa-1)(2\kappa+1)(2\kappa+3)}{6(2\kappa-3)^3}\varphi_1^3\right.\\
&\left.-\frac{\alpha_z}{1+\alpha_z}n_{n3}-\frac{1}{1+\alpha_z}n_{p3}-\frac{\partial^2\varphi_2}{\partial\xi^2}\right]+\cdots \qquad =0.
\end{aligned} \tag{B.19}$$

It s worth mentioning that in Eqs. $(B.15)$ to $(B.19)$, the coefficient of the lowest power of ε, i.e the coefficient of $\varepsilon^0=1$ contains only the equilibrium quantities; the coefficient of the first non-zero power of ε contains only first order perturbed quantities, *e.g.* n_{j1}, u_{j1} and φ_1. Example: the lowest non-zero power of ε is $3/2$ in continuity and momentum equations. The corresponding coefficients for negative ions are successively

$$\begin{aligned}
&-M_s\frac{\partial n_{n1}}{\partial\xi}+\frac{\partial u_{n1}}{\partial\xi},\\
&-M_s\frac{\partial u_{n1}}{\partial\xi}+\frac{z}{\mu\beta}\frac{\partial\varphi_1}{\partial\xi}+\frac{3\sigma_n}{\mu\beta}\frac{\partial n_{n1}}{\partial\xi}.
\end{aligned} \tag{B.20}$$

Only first perturbed quantities enter in these coefficients. The coefficients of the second non-zero power of ε contains both second order

and first order perturbed quantities, that of the third non-zero power of ε contains the first, the second, the third and a combination of the first and second order perturbations. The same applies for higher power of ε. Because ε is a non-zero expansion coefficient, Eqs. $(B.15)$ to $(B.19)$ are verified only if the coefficients under the different powers of ε vanish. Under these cicumstances we can solve successively for the perturbed quantities by first solving for the equilibrium quantities, which enable to solve for the first perturbed quantities under the first non-zero power of ε and so on.

B.1.3 KdV equation derivation

To derive the KdV equation for the negative ion plasma, we successively solve for the perturbed quantities, starting by the zero order perturbation. From the boundary conditions $(B.10)$ and expansion $(B.13)$, it is evident that far from the perturbation $n_{jk}(\infty) = 0$ $(j = n, p; k = 1, 2, 3, ...)$, $u_{jk}(\infty) = 0$ and $\varphi_k(\infty) = 0$.

From the $zero^{th}$ power of ε present only in the Poisson's equation, we get the relation

$$1 - \frac{\alpha z}{1+\alpha z} - \frac{1}{1+\alpha z} = 0. \tag{B.21}$$

This is the charge neutrality condition and tells us that when the plasma is unperturbed the overall charge density is *zero*.

At the first non-zero power of ε in the continuity equations for negative and positive ions, equating their coefficients to *zero* results in two partial differential equations in first order perturbed velocities u_{j1} and first order perturbed densities n_{j1}. Integration of these equations together with boundary conditions yields a relation between u_{j1} and n_{j1}. We then use these relations in equations resulting from consideration of the first non-zero power of ε in the momentum equations for negative and positive ions and obtain partial differential equations whose

solutions yield a dependence of n_{j1} and u_{j1} on the perturbed electrostatic potential φ_1 as

$$n_{n1} = \frac{z}{\mu\beta}\frac{\varphi_1}{M_s^2 - \frac{3\sigma_n}{\mu\beta}}, \tag{B.22}$$

$$u_{n1} = \frac{z}{\mu\beta}\frac{M\varphi_1}{M_s^2 - \frac{3\sigma_n}{\mu\beta}}, \tag{B.23}$$

$$n_{p1} = \frac{1}{\beta}\frac{\varphi_1}{M_s^2 - \frac{3\sigma_p}{\beta}}, \tag{B.24}$$

$$u_{p1} = \frac{1}{\beta}\frac{M\varphi_1}{M_s^2 - \frac{3\sigma_p}{\beta}}. \tag{B.25}$$

Insertion of $(B.22)$ and $(B.24)$ in the equation resulting from the first non-zero power of ε in Poisson's equation yields the dispersion relation

$$\frac{2\kappa-1}{2\kappa-3} - \frac{\alpha z^2}{\mu\beta(1+\alpha z)}\frac{1}{M_s^2 - \frac{3\sigma_n}{\mu\beta}} - \frac{1}{\beta(1+\alpha z)}\frac{1}{M_s^2 - \frac{3\sigma_p}{\beta}} = 0. \tag{B.26}$$

This equation is valid provided the acoustic speed M_s is different from the thermal speeds of positive and negative ions, $\sqrt{3\sigma_p/\beta}$ and $\sqrt{3\sigma_n/\mu\beta}$, respectively. Excluding these values, Eq. $(B.26)$ can be rewritten as

$$M_s^4 - M_s^2\left[\frac{3\sigma_p}{\beta} + \frac{3\sigma_n}{\mu\beta} + \frac{2\kappa-3}{2\kappa-1}\right] + \frac{9\sigma_p\sigma_n}{\mu\beta^2} + \frac{2\kappa-3}{2\kappa-1}\frac{(3\alpha z^2\sigma_p + 3\sigma_n)}{\mu\beta^2(1+\alpha z)} = 0. \tag{B.27}$$

This is a quadratic equation in M_s^2 and can be solved to yield

$$\begin{aligned} M_{s,\pm}^2 \;=\; & \tfrac{3\sigma_p}{2\beta} + \tfrac{3\sigma_n}{2\mu\beta} + \tfrac{2\kappa-3}{2(2\kappa-1)} \pm \tfrac{1}{2}\left\{\left[\tfrac{3\sigma_p}{\beta} + \tfrac{3\sigma_n}{\mu\beta} + \tfrac{2\kappa-3}{2\kappa-1}\right]^2\right. \\ & \left. -4\left[\tfrac{9\sigma_p\sigma_n}{\mu\beta^2} + \tfrac{2\kappa-3}{2\kappa-1}\tfrac{(3\sigma_p\alpha z^2+3\sigma_n)}{\mu\beta^2(1+\alpha z)}\right]\right\}^{1/2}, \end{aligned} \tag{B.28}$$

where in $M_{s,\pm}^2$ the plus sign corresponds to the fast mode and the minus sign corresponds to the slow mode. When the negative ion species is

negligible $\alpha \to 0$, the slow mode disappears and the fast mode Mach number reduces to

$$M_s^2 = 3\sigma_p + \frac{2\kappa - 3}{2\kappa - 1}. \tag{B.29}$$

This is the ion acoustic dispersion relation for a two component plasma with adiabatic positive ions and superthermal electrons, having a generalised Lorentzian distribution. When electrons are Maxwellian, equation $(B.29)$ in dimensional quantities has the form:

$$\frac{\omega^2}{k^2} = \frac{T_p + T_e}{m_p}, \tag{B.30}$$

which is the usual form of ion acoustic Mach number of a two component plasma.

When positive ions are cold equation $(B.29)$ recovers Eq. (21) of Saini2009 et al. [4]

$$M_s^2 = \frac{2\kappa - 3}{2\kappa - 1}, \tag{B.31}$$

who investigated the ion acoustic waves in a two component plasma with cold ions and superthermal electrons.

Equations obtained from the second non-zero power of ε contain second and first order perturbations. For the negative ions continuity and momentum equations, we obtain

$$\frac{\partial n_{n1}}{\partial \tau} + \frac{\partial n_{n1} u_{n1}}{\partial \xi} - M_s \frac{\partial n_{n2}}{\partial \xi} + \frac{\partial u_{n2}}{\partial \xi}, \tag{B.32}$$

and

$$\frac{\partial u_{n1}}{\partial \tau} + u_{n1}\frac{\partial u_{n1}}{\partial \xi} + \frac{3\sigma_n}{\mu\beta} n_{n1} \frac{\partial n_{n1}}{\partial \xi} - M_s \frac{\partial u_{n2}}{\partial \xi} + \frac{z}{\mu\beta}\frac{\partial \varphi_2}{\partial \xi} + \frac{3\sigma_n}{\mu\beta}\frac{\partial n_{n2}}{\partial \xi}. \tag{B.33}$$

These two equations contain three unknown second order perturbations n_{n2}, u_{n2} and φ_2 in addition to known first order perturbations n_{n1} and u_{n1}. As a first step, we eliminate the second order velocity perturbation u_{n2} by multiplying $(B.32)$ by M_s and adding the result to Eq.

$(B.33)$. We obtain an equation with unknown n_{n2} and φ_2:

$$\begin{aligned} & M\frac{\partial n_{n1}}{\partial \tau}+\frac{\partial u_{n1}}{\partial \tau}+\frac{1}{2}\frac{\partial u_{n1}^2}{\partial \xi}+\frac{3\sigma_n}{2\mu\beta}\frac{\partial n_{n1}^2}{\partial \xi}+M\frac{\partial (n_{n1}u_{n1})}{\partial \xi} \\ & +\left[\frac{3\sigma_n}{2\mu\beta}-M^2\right]\frac{\partial n_{n2}}{\partial \xi}+\frac{z}{\mu\beta}\frac{\partial \varphi_2}{\partial \xi} \quad = \quad 0. \end{aligned} \tag{B.34}$$

This is a partial differential equation in unknown second order perturbations n_{n2} and φ_2. We can eliminate $\partial\varphi_2/\partial\xi$ by considering the equation from the second non-zero power of ε in the Poison's equation

$$\frac{2\kappa-1}{2\kappa-3}\varphi_2+\frac{(2\kappa-1)(2\kappa+1)}{2(2\kappa-3)^2}\varphi_1^2-\frac{\alpha z}{1+\alpha z}n_{n2}-\frac{1}{1+\alpha z}n_{p2}-\frac{\partial^2\varphi_1}{\partial\xi^2}. \tag{B.35}$$

After differentiating $(B.35)$ relative to space coordinate x, we find that

$$\begin{aligned} & \frac{\partial \varphi_2}{\partial x}=\frac{2\kappa-3}{2\kappa-1}\frac{\partial^3\varphi_1}{\partial\xi^3}-\frac{2\kappa+1}{2\kappa-3}\varphi_1\frac{\partial\varphi_1}{\partial\xi} \\ & +\frac{\alpha z(2\kappa-3)}{(1+\alpha z)(2\kappa-1)}\frac{\partial n_{n2}}{\partial\xi}+\frac{2\kappa-3}{(1+\alpha z)(2\kappa-1)}\frac{\partial n_{p2}}{\partial\xi} \quad = \quad 0. \end{aligned} \tag{B.36}$$

Plugging $(B.36)$ into $(B.34)$ we get

$$\alpha_n-\left[M_s^2-\frac{2\sigma_n}{\mu\beta}-\frac{\alpha z^2(2\kappa-3)}{\mu\beta(1+\alpha z)(2\kappa-1)}\right]\frac{\partial n_{n2}}{\partial\xi}+\frac{z(2\kappa-3)}{\mu\beta(1+\alpha z)(2\kappa-1)}\frac{\partial n_{p2}}{\partial\xi}=0. \tag{B.37}$$

where α_n depends only on first order perturbation quantities that are known in terms of the first order potential perturbation φ_1. The final expression for α_n has the form

$$\begin{aligned} \alpha_n \quad = \quad & \frac{2M_s z}{\mu\beta(M_s^2-\frac{3\sigma_n}{\mu\beta})}\frac{\partial\varphi_1}{\partial\tau}+\frac{(2\kappa-3)z}{\mu\beta(2\kappa-1)}\frac{\partial^3\varphi_1}{\partial\xi^3} \\ & +\left[\frac{3M_s^2z^2+\frac{3\sigma_n z^2}{\mu\beta}}{\mu^2\beta^2(M_s^2-\frac{3\sigma_n}{\mu\beta})^2}-\frac{(2\kappa+1)z}{\mu\beta(2\kappa-3)}\right]\varphi_1\frac{\partial\varphi_1}{\partial\xi}. \end{aligned} \tag{B.38}$$

Repeating the same process for the positive ion continuity and momentum equations obtained from the second non-zero power of ε, we

get the equation

$$\alpha_p - \left[M_s^2 - \frac{2\sigma}{\beta} - \frac{2\kappa-3}{\beta(1+\alpha z)(2\kappa-1)}\right]\frac{\partial n_{p2}}{\partial \xi} + \frac{\alpha z(2\kappa-3)}{\beta(1+\alpha z)(2\kappa-1)}\frac{\partial n_{n2}}{\partial \xi} = 0. \tag{B.39}$$

where

$$\begin{aligned} \alpha_p &= \frac{2M_s}{\beta(M_s^2-\frac{3\sigma_p}{\beta})}\frac{\partial \varphi_1}{\partial \tau} + \frac{(2\kappa-3)}{\beta(2\kappa-1)}\frac{\partial^3 \varphi_1}{\partial \xi^3} \\ &+ \left[\frac{3M_s^2+\frac{3\sigma_p}{\beta}}{\beta^2(M_s^2-\frac{3\sigma_p}{\beta})^2} - \frac{(2\kappa+1)}{\beta(2\kappa-3)}\right]\varphi_1\frac{\partial \varphi_1}{\partial \xi}. \end{aligned} \tag{B.40}$$

At this level we observe that the dispersion relation can also be written as

$$\begin{aligned} &\left[M_s^2 - \tfrac{3\sigma_n}{\mu\beta} - \tfrac{\alpha z^2(2\kappa-3)}{\mu\beta(1+\alpha z)(2\kappa-1)}\right]\left[M_s^2 - \tfrac{2\sigma}{\beta} - \tfrac{2\kappa-3}{\beta(1+\alpha z)(2\kappa-1)}\right] \\ &\qquad - \tfrac{\alpha z^2(2\kappa-3)^2}{\mu\beta^2(1+\alpha z)^2(2\kappa-1)^2} = 0. \end{aligned} \tag{B.41}$$

This allows to eliminate at the same time the second order perturbations n_{n2} and n_{p2}. This is achieved by adding Eqs. $(B.39)$ and $(B.37)$ after multiplying them respectively by

$$M_s^2 - \frac{3\sigma_n}{\mu\beta} - \frac{\alpha z^2(2\kappa-3)}{\mu\beta(1+\alpha z)(2\kappa-1)},$$

and

$$\frac{\alpha z(2\kappa-3)}{\beta(1+\alpha z)(2\kappa-1)}.$$

The final equation then has the form

$$\alpha_p\left[M_s^2 - \frac{3\sigma_n}{\mu\beta} - \frac{\alpha z^2(2\kappa-3)}{a\mu\beta(1+\alpha z)(2\kappa-1)}\right] + \alpha_n\left[\frac{\alpha z(2\kappa-3)}{\beta(1+\alpha z)(2\kappa-1)}\right] = 0. \tag{B.42}$$

Replacing the expressions of α_n $(B.38)$ and α_p $(B.40)$ in Eq. $(B.42)$ we get a KdV equation

$$\frac{\partial \varphi_1}{\partial \tau} + A\varphi_1 \frac{\partial \varphi_1}{\partial \xi} + B\frac{\partial^3 \varphi_1}{\partial \xi^3} = 0, \tag{B.43}$$

where A is the nonlinear coefficient and B is the dispersion coefficient with

$$A = \frac{a}{b}, B = \frac{1}{b}, \tag{B.44}$$

and

$$a = \frac{1}{\beta^2(1+\alpha z)}\left[\frac{3M_s^2 + \frac{3\sigma_p}{\beta}}{\left(M_s^2 - \frac{3\sigma_p}{\beta}\right)^3} + \frac{\alpha z^3}{\mu^2}\frac{3M_s^2 + \frac{3\sigma_n}{\mu\beta}}{\left(M_s^2 - \frac{3\sigma_3}{\mu\beta}\right)^3}\right] - \frac{(2\kappa-1)(2\kappa+1)}{(2\kappa-3)^2}, \tag{B.45}$$

$$b = \frac{2M_s}{\beta(1+\alpha z)}\left[\frac{1}{\left(M_s^2 - \frac{3\sigma_p}{\beta}\right)^2} + \frac{\alpha z^2}{\mu\left(M_s^2 - \frac{3\sigma_n}{\mu\beta}\right)^2}\right]. \tag{B.46}$$

Equation $(B.43)$ is an evolution nonlinear partial differential equation, describing the propagation of weakly nonlinear solitary waves [3]. The existence of a solitary wave solution to the equation $(B.43)$ is a result of balance between the steepening expressed through the nonlinear coefficient A and the dispersion expressed through the coefficient B. Both coefficients A and B are functions of plasma parameters and change with them.

However, while the dispersion coefficient B is positive for any combination of the plasma parameter values, the nonlinear coefficient A can be negative, zero or positive for some plasma parameter values. The case of vanishing of the nonlinear coefficient A is interesting in that $A = 0$ means equation $(B.43)$ does not account for nonlinear effects, and there is an imbalance between the nonlinear and dispersive effects. To account for nonlinear effects when $A = 0$, we consider higher power of ε, which leads to the modified KdV equation.

B.2 Solutions to the KdV equations

B.2.1 General solution to KdV equation

One of the most important solutions to the KdV equation is the traveling wave solution. To find this solution, we assume that the electrostatic potential φ depends on a combination of variables ξ and τ rather than on each variable separately through the relation

$$\zeta = \xi - \lambda\tau, \tag{B.47}$$

where λ is normalised speed of the solitary wave in a frame co-moving with the ion acoustic wave. This transformation converts the PDE $(B.43)$ into an ODE with one variable ζ. The time and space derivates have now the form

$$\frac{\partial}{\partial\xi} = \frac{\partial\zeta}{\partial\tau}\frac{d}{d\zeta} = \frac{d}{d\zeta}, \tag{B.48}$$

and

$$\frac{\partial}{\partial\tau} = \frac{\partial\zeta}{\partial\xi}\frac{d}{d\zeta} = -\lambda\frac{d}{d\zeta}. \tag{B.49}$$

With the new variable, Eq. $B.43)$ takes the form

$$-\lambda\frac{d\varphi_1}{d\zeta} + A\varphi_1\frac{d\varphi_1}{d\zeta} + B\frac{d^3\varphi_1}{d\zeta^3} = 0. \tag{B.50}$$

The last equation can also be written as

$$\frac{d}{d\zeta}\left\{B\frac{d^2\varphi_1}{d\zeta^2} + \frac{A}{2}\varphi_1^2 - \lambda\varphi_1\right\} = 0. \tag{B.51}$$

This shows that the quantity

$$B\frac{d^2\varphi_1}{d\zeta^2} + \frac{A}{2}\varphi_1^2 - \lambda\varphi_1 = c_1, \tag{B.52}$$

in which c_1 is a constant of integration, is a first integral of the KdV equation in the moving frame. The value of the constant of integration c_1 is found from the boundary conditions. To integrate Eq. $(B.52)$,

we multiply it by the integrating factor $\frac{d\varphi_1}{d\zeta}$ and integrate the resulting equation to get

$$\frac{B}{2}\left(\frac{d\varphi_1}{d\zeta}\right)^2 + \frac{A}{6}\varphi_1^3 - \frac{\lambda}{2}\varphi_1^2 = c_1\varphi_1 + c_2, \tag{B.53}$$

where c_2 is another constant of integration. This equation can be written as

$$\left(\frac{d\varphi_1}{d\zeta}\right)^2 = \frac{A}{3B}G(\varphi_1), \tag{B.54}$$

where $G(\varphi_1)$ is given by

$$G(\varphi_1) = -\varphi_1^3 + \frac{3\lambda}{A}\varphi_1^2 + C_1\varphi_1 + C_2, \tag{B.55}$$

where C_1 and C_2 are constants related to c_1 and c_2 by $C_1 = 6c_1/A$ and $C_2 = 6c_2/A$ respectively. This is an equation with separable variables and integration yields

$$\int \frac{d\varphi_1}{\sqrt{G(\varphi_1)}} = \pm\sqrt{\frac{A}{3B}}\zeta. \tag{B.56}$$

The evaluation of the integral to the left depends on the relationships between the roots of the function $G(\varphi_1)$ whose nature depends on the choice of integration constants C_1 and C_2.

If the polynomial $G(\varphi_1)$ has two complex conjugate and one real root φ_0, then φ' vanishes also at φ_0 and the polynomial $G(\varphi_1)$ is monotonically decreasing and the solution to $(B.54)$ is not bounded. For bounded solutions, $G(\varphi_1)$ must have three real solutions.
Then if ϕ_1, ϕ_2 and ϕ_3 are the three real roots of the polynomial $G(\varphi_1)$ it can be written as the product

$$G(\varphi_1) = -(\varphi - \phi_1)\times(\varphi - \phi_2)\times(\varphi - \phi_3). \tag{B.57}$$

Comparing $(B.55)$ and $(B.57)$, it results that

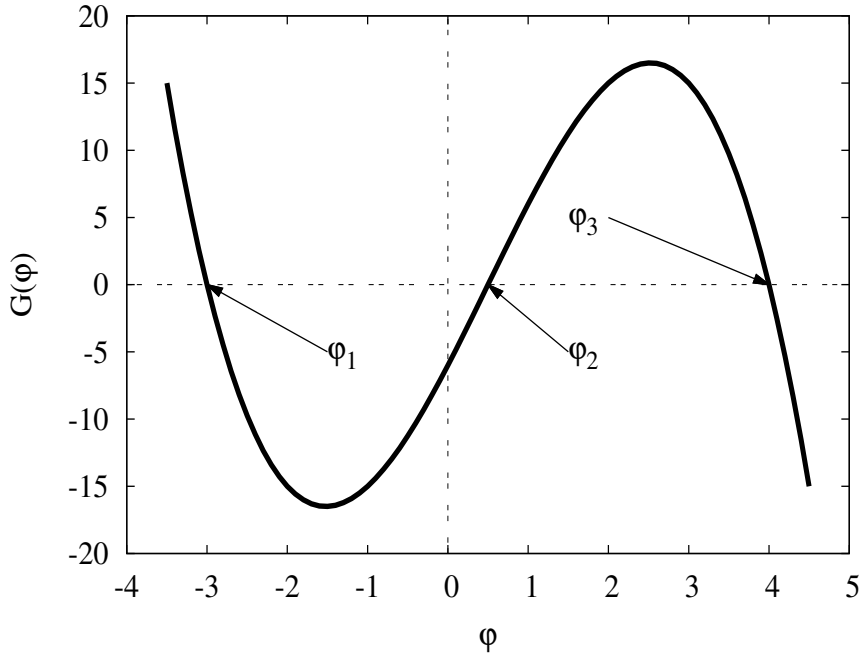

Figure B.1: The function $G(\varphi) = -(\varphi - \phi_1) \times (\varphi - \phi_2) \times (\varphi - \phi_3)$ has 3 real roots, ϕ_1, ϕ_2 and ϕ_3.

$$\begin{aligned} \phi_1 + \phi_2 + \phi_3 &= \tfrac{3\lambda}{A}, \\ \phi_1\phi_2 + \phi_1\phi_3 + \phi_2\phi_3 &= -\tfrac{6C_1}{A}, \\ \phi_1\phi_2\phi_3 &= \tfrac{6C_2}{A}. \end{aligned} \tag{B.58}$$

Assume that $\phi_1 < \phi_2 < \phi_3$. Then for $d\varphi_1/d\zeta$ to be real valued the roots must satisfy the relation $\phi_2 \leqslant \varphi \leqslant \phi_3$ if the nonlinear coefficient A is positive and $\phi_1 \leqslant \varphi \leqslant \phi_2$ if A is negative. This is seen in Fig. $B.1$. Using the change of variable

$$\varphi_1 = \phi_3 - (\phi_3 - \phi_2) sin^2\psi, \tag{B.59}$$

the derivative becomes

$$\frac{d\varphi_1}{d\zeta} = -2(\phi_3 - \phi_2) sin\psi cos\psi \frac{d\psi}{d\zeta}. \tag{B.60}$$

Replacing $(B.59)$ and $(B.60)$ in $(B.54)$ we arrive at the expression

$$\left(\frac{d\psi}{d\zeta}\right)^2 = \frac{A}{12B}(\phi_3-\phi_1)\left[1-\frac{\phi_3-\phi_2}{\phi_3-\phi_1}sin^2\psi\right]. \tag{B.61}$$

Define

$$k^2 = \frac{\phi_3-\phi_2}{\phi_3-\phi_1}, \tag{B.62}$$

with $0 \leqslant k^2 \leqslant 1$. We may then solve implicitly for ψ and obtain

$$\int_0^{\psi(\zeta)} \frac{dt}{\sqrt{1-k^2sin^2t}} = \pm\sqrt{\frac{A}{12B}}\sqrt{\phi_3-\phi_1}\zeta, \tag{B.63}$$

where the right hand side

$$Z(sin(\psi);k) = \int_0^{\psi(\zeta)} \frac{dt}{\sqrt{1-k^2sin^2t}} \tag{B.64}$$

is the incomplete elliptical integral of the first kind, k is the modulus of the elliptic integral and t is a dummy variable of integration. The elliptic integral is thus a function Z of the upper limit ψ and elliptic modulus k: $Z = Z(sin(\psi);k)$. The inverse of the elliptic integrals defines the so called Jacobian elliptic functions. To define two of these functions, let's start by the well known trigonometric functions. We know that

$$\int_0^y \frac{dt}{\sqrt{1-t^2}} = arcsiny, \tag{B.65}$$

where $-1 \leqslant y \leqslant 1$. Therefore the integral to the left can be taken as the definition of the inverse of the trigonometric function "*sine*". If we define the argument θ as

$$\theta(y) = \int_0^y \frac{dt}{\sqrt{1-t^2}}, \tag{B.66}$$

then the trigonometric function "*sine*" is obtained as

$$sin\theta = y. \tag{B.67}$$

And the "*cosine*" function can be defined as $cos\theta = \sqrt{1-sin^2\theta}$.
In a similar procedure, consider the elliptic integral

$$u(sin(\varphi);k) = \int_0^{\varphi} \frac{d\theta}{\sqrt{1-k^2sin^2\theta}}. \tag{B.68}$$

The parameter φ is called the argument of the elliptic integral and $0 \leqslant \varphi \leqslant \pi/2$. We consider this integral as the definition of an inverse function of the Jacobi elliptic function "*sn*" such that

$$sn(u;k) = sin\varphi. \tag{B.69}$$

Since $-1 \leqslant sin(\varphi) \leqslant 1$ we can define the Jacobi elliptic function "*cn*" function as $cn(u;k) = \sqrt{1 - sn^2(u;k)}$.

For extreme cases of the modulus of the elliptic integral of the first kind, we have:

$$\begin{aligned} sn(u;0) &= sinu; \\ sin(u;1) &= tanhu; \\ cn(u;0) &= cosu; \\ cn(u;1) &= sechu. \end{aligned} \tag{B.70}$$

The function "*snu*" is odd while the function "*cnu*" is even and both are periodic with period $4K$ where K is the complete elliptic integral of the first kind

$$K = \int_0^{\pi/2} \frac{dt}{\sqrt{1 - k^2 sin^2 t}}. \tag{B.71}$$

Coming back to Eq. $(B.63)$,

$$Z(sin\psi;k) = \pm\sqrt{\frac{A}{12B}}\sqrt{\phi_3 - \phi_1}\zeta, \tag{B.72}$$

and inverting the Jacobi elliptic integral we get

$$sin\psi = sn\left[\pm\sqrt{\frac{A}{12B}}\sqrt{\phi_3 - \phi_1}\zeta\right]. \tag{B.73}$$

Therefore Eq. $(B.59)$ becomes

$$\varphi_1 = \phi_3 - (\phi_3 - \phi_2)sn^2\left[\sqrt{\frac{A}{12B}}\sqrt{\phi_3 - \phi_1}\zeta\right], \tag{B.74}$$

or in terms of "*cn*" function

$$\varphi_1 = \phi_2 + (\phi_3 - \phi_2) cn^2 \left[\sqrt{\frac{A}{12B}} \sqrt{\phi_3 - \phi_1} \zeta \right]. \tag{B.75}$$

This is the cnoidal analytic solution to the KdV equation. It is a three-parameter family of the KdV solutions.

When the modulus $0 < k < 1$, Eq. $(B.75)$ represents a periodic waves, shown in Fig. $B.2$ upper panel for $k = 0.2$ and middle panel for $k = 0.9$.

When the modulus $k \to 0$, i.e. $\phi_2 \to \phi_3$, $snu = sinu$ and the solution $(B.74)$ tends to a sinusoidal wave. Its mathematical expression can be found by a direct integration of the equation:

$$\varphi_1 = \phi_3 - \phi_0 sin^2 \left[\sqrt{\frac{A}{12B}} \sqrt{\phi_3 - \phi_1} \zeta \right], \tag{B.76}$$

where $\phi_0 = \phi_3 - \phi_2 \ll 1$. We note here that the constants of integration C_1 and C_2 are not zero. When the modulus $k \to 1$ *i.e.* $\phi_2 \to \phi_1$, $cnu = sechu$ and the cnoidal wave changes into a solitary wave with equation

$$\varphi_1 = \phi_1 + (\phi_3 - \varphi_1) sech^2 \left[\sqrt{\frac{A}{12B}} \sqrt{\phi_3 - \phi_1} \zeta \right]. \tag{B.77}$$

The hyperbolic secant function is vanishingly small as its argument $|x| \to \infty$. This means that the solitary waves are localised structures in agreement with the boundary condition $\varphi_1 \to 0$ for $\zeta \to \pm\infty$ and the constants of integration C_1 and C_2 in Eq. $(B.53)$ take a value of *zero*. Under these conditions, the solution to the system of equations $(B.58)$ yields $\phi_1 = \phi_2 = 0$ and the only nonzero parameter is $\phi_3 = 3\lambda/A$. With these parameters the solitary wave equation takes the form

$$\varphi_1(\zeta) = \frac{3\lambda}{A} sech^2 \left[\sqrt{\frac{\lambda}{4B}} \zeta \right]. \tag{B.78}$$

It represents a soliton moving to the right. The solution $(B.78)$ is written in a frame moving with the solitary wave. Going back to the laboratory frame in which variables (x,t) were stretched (Eq. $(B.11)$), we

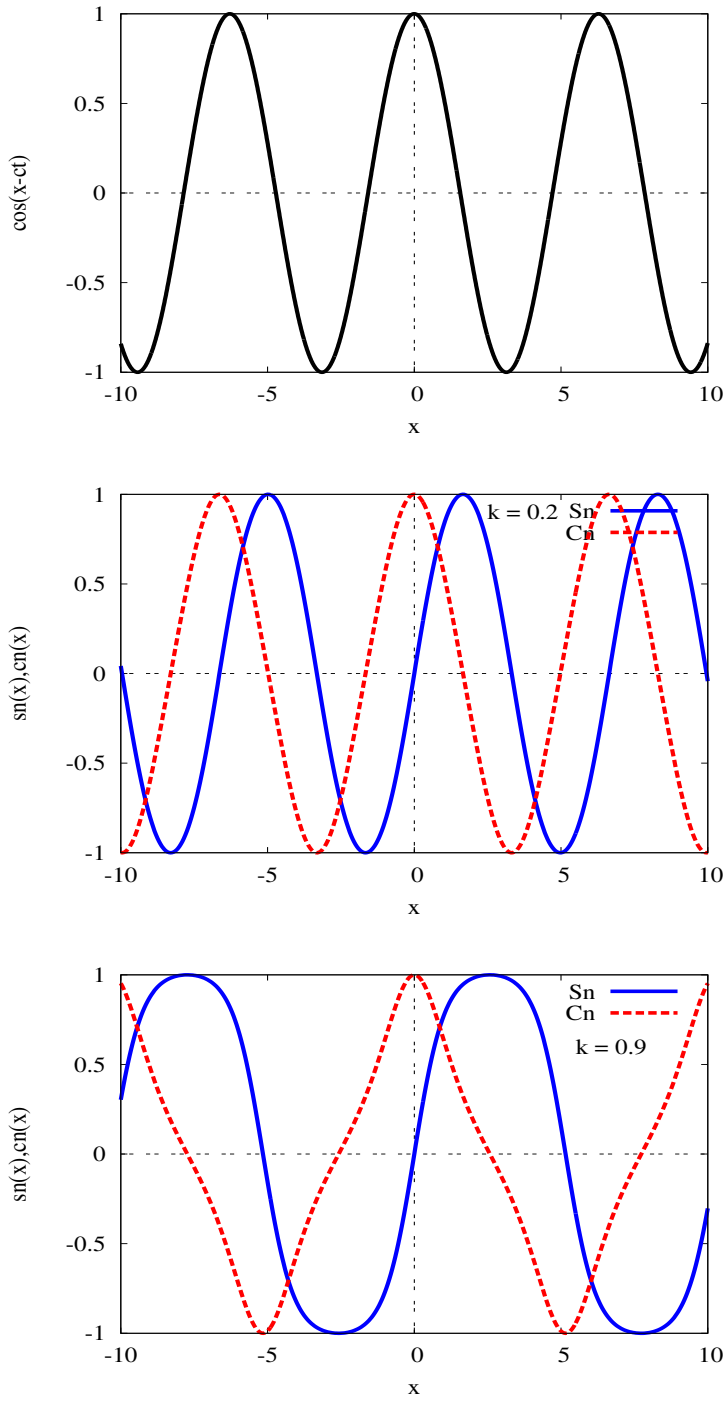

Figure B.2: Periodic solutions of the KdV equation. For $k = 0$ the sinusoidal wave is a solution (upper panel). For $0 < k < 1$ the cnoidal waves are the periodic solutions ($k = 0.2$ in the middle panel and $k = 0.9$ in the lower panel).

find that the argument ζ/w of the hyperbolic secant function becomes

$$\sqrt{\frac{\lambda\varepsilon}{4B}}\left[x-(M_s+\varepsilon\lambda)t\right]. \tag{B.79}$$

The variable $M = M_s + \varepsilon\lambda$ is the normalised speed of the soliton in the laboratory frame. We can use this relation to define a small quantity: $\delta M = M - M_s = \varepsilon\lambda$ which is the difference between the solitary wave speed and the sound speed in the plasma. Furthermore considering the expansion $(B.13)$, the electrostatic potential in this first approximation is $\varphi \approx \varepsilon\varphi_1$. Therefore the electrostatic potential in the laboratory frame takes the form

$$\varphi(x,t) = \varphi_m sech^2\left(\frac{x-Mt}{w}\right), \tag{B.80}$$

where the wave amplitude

$$\varphi_m = \frac{3\delta M}{A}, \tag{B.81}$$

and the wave width

$$w = \sqrt{\frac{4B}{\delta M}}. \tag{B.82}$$

It is now obvious that for the width to be real the fraction $4B/\delta M$ must be positive. But the dispersion coefficient B and the expansion parameter are both positive whatever the values of the plasma parameters. This means that for real solitons, λ is also positive and $M > M_s$ implying that solitary waves are supersonic.

Expression $(B.81)$ shows that the soliton amplitude is a linear function of the soliton speed λ in the stationary frame. When λ tends to *zero*, or in other words when the soliton Mach number M tends to the acoustic Mach number M_s the amplitude also vanishes. Solitons whose amplitude vanishes at the acoustic speed were called KdV soliton.

The soliton amplitude and width satisfy the relation [5]

$$\phi_m w^2 = \frac{12}{A}. \tag{B.83}$$

Because the factor A is independent of λ, the product $\varphi_m w^2$ does not change when λ is varied with other plasma parameter values held fixed. In these conditions, an increase in the amplitude of KdV solitons is accompanied with a decrease of the soliton width. This conclusion can be drawn also by looking at the equation $(B.80)$. This equation shows that the soliton amplitude is of the order ε while its width is of the order $\varepsilon^{-1/2}$.

With λ and dispersion coefficient B being positive, the sign of the KdV soliton amplitude is determined by the nonlinear coefficient A. When A is positive, positive potential or hump like solitons exist in the plasma while negative potential or deep like solitons exist for negative values of A. There exist therefore two regimes, a regime characterised by plasma parameter values admitting the propagation of positive solitons, and a regime admitting the propagation of negative solitons, the two being separated by the vanishing of the coefficient A. When $A = 0$, the coefficient of the nonlinear term vanishes and the KdV equation is no longer a valid equation associating balance between nonlinearity and dispersion. In this situation a higher order non-linearity is to be considered. This leads to higher order KdV equations.

But before the solutions to higher order KdV equations are given without any proof, we mention that a third type of solution for KdV equation exists: it is the multisoliton solution. An example of two soliton soliton solution has the form

$$\varphi(x,t) = \frac{(A_2 - A_1)\left[A_1 sech^2(\theta_1(x,t)) + A_2 csch^2(\theta_2(x,t))\right]}{\left[\sqrt{A_1} tanh(\theta_1(x,t)) - \sqrt{A_2} coth(\theta_2(x,t))\right]^2}. \tag{B.84}$$

Fig. $B.3$ shows the multisoliton solution at different values of time t. It shows that taller solitons move faster and overtake smaller ones. More over, when the two solitons interact they recover their shapes and amplitude after the collision. This is the particle property of solitons.

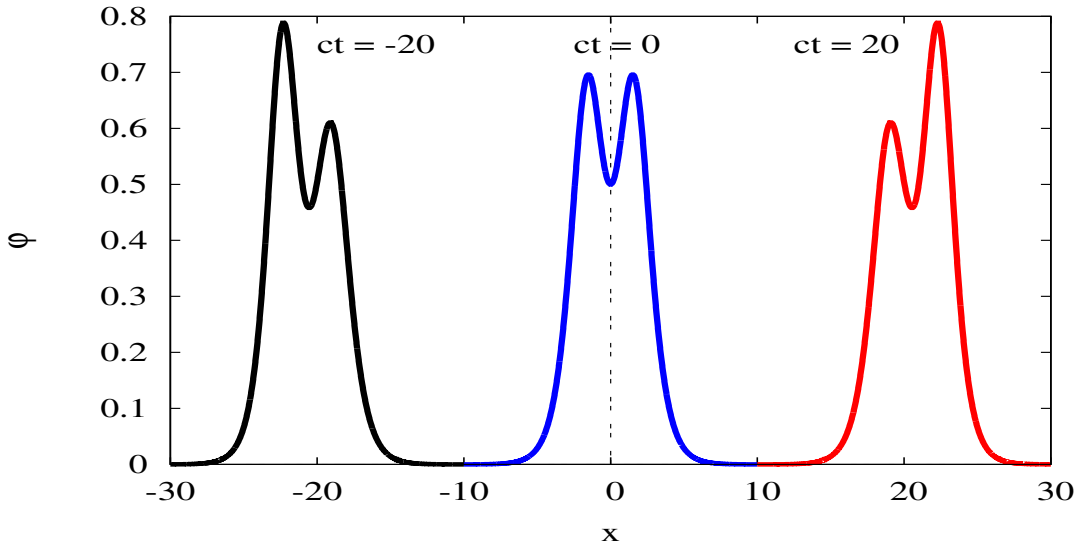

Figure B.3: Multisoliton solution.

B.2.2 Solution to the modified KdV and mixed modified KdV

The mixed modified KdV equation for φ_1 was found to be of the form:

$$\frac{\partial \phi}{\partial \tau} + A\phi\frac{\partial \phi}{\partial \xi} + C\phi^2\frac{\partial \phi}{\partial \xi} + B\frac{\partial^3 \phi}{\partial \xi^3} = 0. \tag{B.85}$$

To look for a unidirectional travelling wave solution with permanent shape, we first transform Eq. $(B.85)$ to a moving frame using $(B.47)$ to $(B.49)$ and integrate the resulting equation with boundary conditions $(B.10)$. We then reduce Eq. $(B.85)$ to an energy like equation

$$\frac{1}{2}\left(\frac{d\varphi_1}{d\zeta}\right)^2 - \frac{\lambda}{2B}\varphi_1^2 + \frac{A}{6B}\varphi_1^3 + \frac{C}{12B}\varphi_1^4 = 0. \tag{B.86}$$

Modified KdV

For a modified KdV, the second order nonlinear coefficient $A = 0$. The resulting equation can be written as

$$\frac{d\varphi_1}{\varphi_1\sqrt{\frac{6\lambda}{C} - \varphi_1^2}} = \pm\sqrt{\frac{C}{6B}}d\zeta. \tag{B.87}$$

The right hand side can be integrated easily and the left hand side can be integrated using a change of variable $\varphi_1 = \sqrt{6\lambda/C}sech t$. The soliton solution to Eq. $(B.85)$ in the moving frame is found as

$$\varphi_1 = \pm\sqrt{\frac{6\lambda}{C}}sech\left[\sqrt{\frac{\lambda}{B}}\zeta\right]. \tag{B.88}$$

Mixed modified KdV

For a mixed modified KdV, the second order nonlinear coefficient $A \neq 0$. The resulting equation can be written as

$$\frac{d\varphi_1}{\varphi_1(\frac{6\lambda}{A} - \varphi_1)} = \pm\sqrt{\frac{-C}{6B}}d\zeta. \tag{B.89}$$

Both left and right hands can be integrated exactly to give the solution

$$\varphi = \frac{\varphi_m}{2}\left[1 \pm tanh\left(\frac{\zeta}{\Lambda}\right)\right], \tag{B.90}$$

where the double layer amplitude φ_m is given by

$$\varphi_m = -\frac{A}{C}, \tag{B.91}$$

and the double layer width

$$\Lambda = \left[\frac{\varphi_m}{2}\sqrt{\frac{-C}{6B}}\right]^{-1}. \tag{B.92}$$

B.3 References

[1] T. K. Balukuand M. A. Hellberg, Phys. Plasmas **1**5, 123705 (2008).

[2] F. Verheest and M. A. Hellberg, J. Plasma Phys. **7**6, 277 (2010).

[3] H. Washimi and T. Taniuti, Phys. Rev. Lett. **1**7, 996 (1966).

[4] N. S. Saini, I. Kourakis and M. A. Hellberg, Phys. Plasmas **1**6, 062903 (2009).

[5] E. Saberian, A. Esfandyari-Kalejahi and M. Afsari-Ghazi, Open Plasma Phys. J. **8**, 8 (2015).

Appendix C

Small amplitude from the Sagdeev potential

C.1 Small amplitude from the Sagdeev potential

We have derived the Sagdeev pseudopotential that we used to investigate the existence and propagation of fast mode solitons with arbitrary large amplitude in a negative ion plasma. The objective of this section is to show that when the electrostatic perturbation is small, we can expand the Sagdeev pseudopotential in powers of the electrostatic potential and obtain the KdV equation as expected.

The Sagdeev pseudopotential for a negative ion plasma $(z=-1)$ was found to be of the form

$$\begin{aligned} S(\varphi,M) &= 1-\left(1-\tfrac{2\varphi}{2\kappa-3}\right)^{-\kappa+3/2} \\ &\quad +\tfrac{\alpha\mu\beta}{6(1+\alpha z)}\sqrt{\tfrac{\mu\beta}{3\sigma_n}}\left\{2\left(\tfrac{3\sigma_n}{\mu\beta}\right)^{3/2}+6M^2\left(\tfrac{3\sigma_n}{\mu\beta}\right)^{1/2}\right. \\ &\quad -\left[\left(M+\sqrt{\tfrac{3\sigma_n}{\mu\beta}}\right)^2-\tfrac{2z\varphi}{\mu\beta}\right]^{3/2} \\ &\quad \left.+\left[\left(M-\sqrt{\tfrac{3\sigma_n}{\mu\beta}}\right)^2-\tfrac{2z\varphi}{\mu\beta}\right]^{3/2}\right\} \\ &\quad +\tfrac{\beta}{6(1+\alpha z)}\sqrt{\tfrac{\beta}{3\sigma_p}}\left\{2\left(\tfrac{3\sigma_p}{\beta}\right)^{3/2}+6M^2\left(\tfrac{3\sigma_p}{\beta}\right)^{1/2}\right. \\ &\quad \left.-\left[\left(M+\sqrt{\tfrac{3\sigma_p}{\beta}}\right)^2-\tfrac{2\varphi}{\beta}\right]^{3/2}+\left[\left(M-\sqrt{\tfrac{3\sigma_p}{\beta}}\right)^2-\tfrac{2\varphi}{\beta}\right]^{3/2}\right\}. \end{aligned} \tag{C.1}$$

Expansion of $C.1$ in a Taylor series around $\varphi=0$ up to the third

power gives:

$$S(\varphi,M) \approx S(0,M) + \frac{\partial S}{\partial \varphi}(0,M)\varphi + \frac{1}{2!}\frac{\partial^2 S}{\partial \varphi^2}(0,M)\varphi^2 + \frac{1}{3!}\frac{\partial^3}{\partial \varphi^3}(0,M)\varphi^3, \tag{C.2}$$

where $S(0,M) = \partial S/\partial\varphi(0,M) = 0$ for the function $S(\varphi)$ to yield a solitary wave solution. A direct replacement of the value $\varphi = 0$ in the Sagdeev expression $(C.1)$ shows that the condition $S(0,M) = 0$ is satisfied for all values of the Mach number M.

The first derivative has the form:

$$\begin{aligned}
\frac{\partial S(\varphi,M)}{\partial \varphi} &= -\left(1-\frac{2\varphi}{2\kappa-3}\right)^{-\kappa+1/2} \\
&\quad + \frac{\alpha z}{2(1+\alpha z)}\sqrt{\frac{\mu\beta}{3\sigma_n}}\left\{\left[\left(M+\sqrt{\frac{3\sigma_n}{\mu\beta}}\right)^2 - \frac{2z\varphi}{\mu\beta}\right]^{1/2}\right. \\
&\quad \left. - \left[\left(M-\sqrt{\frac{3\sigma_n}{\mu\beta}}\right)^2 - \frac{2z\varphi}{\mu\beta}\right]^{1/2}\right\} \\
&\quad + \frac{1}{2(1+\alpha z)}\sqrt{\frac{\beta}{3\sigma_p}}\left\{\left[\left(M+\sqrt{\frac{3\sigma_p}{\beta}}\right)^2 - \frac{2\varphi}{\beta}\right]^{1/2}\right. \\
&\quad \left. - \left[\left(M-\sqrt{\frac{3\sigma_p}{\beta}}\right)^2 - \frac{2\varphi}{\beta}\right]^{1/2}\right\}.
\end{aligned} \tag{C.3}$$

Far from the disturbance, where the plasma is undisturbed, $\varphi = 0$ and this expression reduces to the plasma quasineutrality condition, i.e.

$$\frac{\partial S(\varphi,M)}{\partial \varphi}(0,M) = -1 + \frac{\alpha z}{1+\alpha z} + \frac{1}{1+\alpha z} = 0. \tag{C.4}$$

The second derivative has the form

$$\begin{aligned}\frac{\partial^2 S(\varphi,M)}{\partial\varphi^2} &= -\frac{2\kappa-1}{2\kappa-3}\left(1-\frac{2\varphi}{2\kappa-3}\right)^{-\kappa-1/2} \\ &\quad -\frac{\alpha z^2}{2\mu\beta(1+\alpha z)}\sqrt{\frac{\mu\beta}{3\sigma_n}}\left\{\left[\left(M+\sqrt{\frac{3\sigma_n}{\mu\beta}}\right)^2-\frac{2z\varphi}{\mu\beta}\right]^{-1/2}\right. \\ &\quad \left.-\left[\left(M-\sqrt{\frac{3\sigma_n}{\mu\beta}}\right)^2-\frac{2z\varphi}{\mu\beta}\right]^{-1/2}\right\} \\ &\quad -\frac{1}{2\beta(1+\alpha z)}\sqrt{\frac{\beta}{3\sigma_p}}\left\{\left[\left(M+\sqrt{\frac{3\sigma_p}{\beta}}\right)^2-\frac{2\varphi}{\beta}\right]^{-1/2}\right. \\ &\quad \left.-\left[\left(M-\sqrt{\frac{3\sigma_p}{\beta}}\right)^2-\frac{2\varphi}{\beta}\right]^{-1/2}\right\}.\end{aligned} \tag{C.5}$$

Let $C(M)=\partial^2 S(\varphi,M)/\partial\varphi^2(0,M)$ be the second derivative of the Sagdev pseudopotential calculated far from the solitary wave where the electrostatic potential vanishes and for an arbitrary Mach number in the soliton existence domain. From $(C.5)$,

$$C(M)=\frac{2\kappa-1}{2\kappa-3}-\frac{\alpha z^2}{\mu\beta(1+\alpha z)}\frac{1}{M^2-\frac{3\sigma_n}{\mu\beta}}-\frac{1}{\beta(1+\alpha z)}\frac{1}{M^2-\frac{3\sigma_p}{\beta}}. \tag{C.6}$$

Although the right hand side of Eq. $(C.6)$ is similar to the left hand side of Eq. $(B.26)$, the Mach number M in this equation is different from the ion acoustic Mach number M_s in Eq. $(B.26)$. For KdV solitons, $M=M_s+\delta M$ where $\delta M \ll M_s$ and $C(M)=C(M_s+\delta M)$. Expansion of $C(M_s+\delta M)$ in powers of δM up to the first order gives

$$C(M)\approx C(M_s)+\frac{\partial C}{\partial\delta M}(M_s)\delta M \tag{C.7}$$

with $C(M_s)=0$ from the KdV theory. $C(M)$ takes the form

$$C(M) = -\frac{2M_s}{\beta(1+\alpha z)}\left\{\frac{\alpha z^2}{\mu(M^2-\frac{3\sigma_n}{\mu\beta})^2}+\frac{1}{(M^2-\frac{3\sigma_p}{\beta})^2}\right\}\delta M. \tag{C.8}$$

The coefficient of δM is the inverse of the dispersion coefficient $C(M)=1/B$ in Eq. $(B.53)$ in the KdV theory.

The third derivative

$$\begin{aligned}\frac{\partial^3 S(\varphi,M)}{\partial\varphi^3} &= -\frac{(2\kappa-1)(2\kappa+1)}{(2\kappa-3)^2}\left(1-\frac{2\varphi}{2\kappa-3}\right)^{-\kappa-3/2} \\ &\quad -\frac{\alpha z^3}{2(\mu\beta)^2(1+\alpha z)}\sqrt{\frac{\mu\beta}{3\sigma_n}}\left\{\left[\left(M+\sqrt{\frac{3\sigma_n}{\mu\beta}}\right)^2-\frac{2z\varphi}{\mu\beta}\right]^{-3/2}\right. \\ &\quad \left.-\left[\left(M-\sqrt{\frac{3\sigma_n}{\mu\beta}}\right)^2-\frac{2z\varphi}{\mu\beta}\right]^{-3/2}\right\} \\ &\quad -\frac{1}{2\beta^2(1+\alpha z)}\sqrt{\frac{\beta}{3\sigma_p}}\left\{\left[\left(M+\sqrt{\frac{3\sigma_p}{\beta}}\right)^2-\frac{2\varphi}{\beta}\right]^{-3/2}\right. \\ &\quad \left.-\left[\left(M-\sqrt{\frac{3\sigma_p}{\beta}}\right)^2-\frac{2\varphi}{\beta}\right]^{-3/2}\right\}.\end{aligned} \tag{C.9}$$

At $\varphi=0$, it reduces to

$$\begin{aligned}\frac{\partial^3 S(\varphi,M)}{\partial\varphi^3}(0,M) &= -\frac{(2\kappa-1)(2\kappa+1)}{(2\kappa-3)^2}+\frac{\alpha z^3}{(\mu\beta)^2(1+\alpha z)}\frac{3M^2+\frac{3\sigma_n}{\mu\beta}}{(M^2-\frac{3\sigma_n}{\mu\beta})^3} \\ &\quad +\frac{1}{\beta^2(1+\alpha z)}\frac{3M^2+\frac{3\sigma_p}{\beta}}{(M^2-\frac{3\sigma_p}{\beta})^3}.\end{aligned} \tag{C.10}$$

As $\delta M \ll M_s$ we can keep the zeroth order after developing this expression in powers of δM. In this case, expression $(C.10$ is

the same as the factor A of the nonlinear coefficient in the KdV equation. Putting all together for small amplitudes, the Sagdeev potential reduces to the potential $V(\varphi)$ in the KdV theory. Thus for small amplitude, the Sagdeev approach gives the same results as the KdV approach.